TrypanoFluidique : compartimentation, culture et analyse de la microfluidique de gouttes de Trypanosoma brucei

Simone Oldenburg

université de BORDEAUX

THÈSE PRÉSENTÉE
POUR OBTENIR LE GRADE DE

DOCTEUR DE L'UNIVERSITÉ DE BORDEAUX

ECOLE DOCTORALE DES SCIENCES CHIMIQUES

Physico-Chimie de la Matière Condensée

Par **Simone Helene Oldenburg**

TrypanoFluidics: Compartmentalization, cultivation and analysis of *Trypanosoma brucei* by droplet-based microfluidics

---

Sous la direction de : **Jean-Christophe BARET** & **Loïc RIVIÈRE**

le 12 novembre 2021

Membres du jury :

M. Nicolai SIEGEL	Ludwig-Maximilians-Universität (Germany)	Rapporteur
M. Tom ROBINSON	Max Planck Institutes (Germany)	Rapporteur
Mme. Cécile ZAKRI	Université de Bordeaux (France)	Président du jury
M. Axel HOCHSTETTER	Life on a Chip (Germany)	Examinateur
M. Loïc RIVIÈRE	Université de Bordeaux (France)	Examinateur
M. Jean-Christophe BARET	Université de Bordeaux (France)	Directeur

Thesis presented for obtaining the degree of

Doctor of Philosophy

of The Univeristy of Bordeaux

Doctoral School of Chemical Sciences

TrypanoFluidics: Compartmentalization, cultivation and analysis of *Trypanosoma brucei* by droplet-based microfluidics

by **Simone Helene Oldenburg**

Supervised by: **Jean-Christophe BARET** & **Loïc RIVIÈRE**

November 12th 2021

Acknowledgements

This thesis project could not have been done without the support of many people to whom I would like to express my deepest gratitude. I would first of all like to thank my jury members; Nicolai Siegel and Tom Robinson for accepting being reviewers of my thesis, and Axel Hochstetter and Cécile Zakri for accepting the role of my examiners.

I send my deepest gratitude to my supervisors Jean-Christophe Baret and Loïc Rivière. I am truly grateful for you to give me this opportunity of working with you both in the two best teams of Bordeaux! Thank you for your consistent guidance and support whenever needed.

Thank you to all of the SMS team members, especially to Thomas Beneyton and Mathias Girault for all the help you have given, not only inside the lab but also with the complicated french administration. Thank you to Lionel Buisson for contributing with our specialised setup and teaching me how to operate it. A big thanks to the "old" team members Laura Chacon, Aurelie Vigne and Deniz Pekin for welcoming me so nicely in the team. Especially to Deniz I am extra grateful, for everything she has done for me and easing my first months in France.

I would like to thank everyone in CRPP who always greets me with a smile and make me feel welcome in the lab, despite the small language barrier. A big thank you to my running team, Les poulettes avec coach Ahmed. Thank you for the great motivation and keeping me physically and mentally in shape during all these years including a pandemic.

I would further like to send a very warm gratitude to all the iMet team members, Fred Bringaud, Coco, Nico, Manu, Erika, Yoann, Mag and Pauline. Thank you for all the good discussions during team meetings and the much needed help and teaching about trypanosomes. Thank you to the rest of MFP for always being friendly and helpful whenever needed. A special thanks to Nico L. for helping me use the fluorescence microscopes. A big thank you to Rija, Chloé and Magamba for taking care of me at MFP with a few TGIF/M/T/W/T and for forcing me to learn french! A special thanks to Sarah and Oriana for all the great moments, trips and parties, you truly

have become my family!

And to the rest of my "french" family; Ale, Arantza, Flavia, David, Petra, Kate, Cian, Fernando, Mayte, Raj and Armand, you have all been a special part of my journey in Bordeaux and I am forever grateful for all the amazing moments we have shared! You all deserve more than this sentence, but honestly, no-one is going to read it anyway ;) Thank you Fred, for getting me through the final but hardest times of my PhD, and for not giving up on me halfway.

To the best year in the history of CRPP; Etienne, Manu, Maeva, Lachlan and Rajam, I cannot express enough my gratitude for sharing this journey with you guys! And a special thanks to Rajam for always being there with a glass (or bottle) of wine, when PhD life became too much.

A huge thank you to all my friends in Denmark who stayed around for my 4 years of absence and took the time to come and visit. For that I am more grateful than I can describe with words. Special thanks to Pat and Osteabe for being right by the phone whenever needed.

Lastly, I send the biggest acknowledgements to my family! I could not have completed this crazy but amazing journey without your support and love. Thank you.

Abstract

Keywords: Droplet-based microfluidics, *Trypanosoma brucei*, single-cell analysis, enzyme secretion

Trypanosoma brucei are protozoan parasites infecting mammals in Sub-Saharan Africa causing the disease known as Sleeping sickness. The parasites are transmitted between the mammal hosts through bites of an insect vector. The transmission from insect to mammal is one out of many steps in a complex life cycle causing numbers of metabolic and physiological changes. While the majority of a population is preparing to reenter the insect vector, a fraction of the population continuously adapt to the immune system of the host, showing a heterogeneous pattern within the population. Though numerous analytical methods for studying single cells are continuously developed, little is still know of *T. brucei* on a single-cell level. Droplet-based microfluidics is a high-throughput tool for single cell analysis emerging within the last decades. We here developed an analytical method for quantitative measurements at the single cell level based on encapsulation and cultivation of *T. brucei* in microcompartment droplets. We described a microfluidic system for single-cell encapsulation and analysis based on fluorescence measurements. We first showed the survival of *T. brucei* for several hours to days in droplets with influence on both survival and growth by the droplet size. We unraveled various growth patterns within a population, and found that droplet cultivation of trypanosomes revealed highly dividing cell variants with 10-fold higher cell densities compared to standard cultivation techniques. We further combined the encapsulation of *T. brucei* with an enzymatic detection assay to study protease secretion. Using a fluorescence based substrate allowed detection of protease activity secreted from single cells. Lastly, we tested the setup in two additional applications both used on single-cell *T. brucei*. Conclusively, droplet-based microfluidics have shown promising as an analytical tool for trypanosome cultivation and analysis with a further potential for high-throughput single-cell analysis.

Résumé

Mots-clés : Microfluidique en gouttes, *Trypanosoma brucei*, analyse de cellules uniques, sécrétion d'enzymes

Trypanosoma brucei est un parasite protozoaire infectant les mammifères en Afrique subsaharienne et provoquant la maladie connue sous le nom de maladie du sommeil. Les parasites sont transmis entre les hôtes mammifères par les piqûres d'un insecte vecteur. La transmission de l'insecte au mammifère est l'une des nombreuses étapes d'un cycle de vie complexe provoquant de nombreux changements métaboliques et physiologiques. Alors que la majorité d'une population se prépare à réintégrer l'insecte vecteur, une fraction de la population s'adapte en permanence au système immunitaire de l'hôte, montrant un schéma hétérogène au sein de la population. Bien que de nombreuses méthodes analytiques soient continuellement développées pour étudier les cellules individuelles, on sait encore peu de choses sur *T. brucei* au niveau cellulaire. La 'microfluidique en gouttes' est un outil à haut débit pour l'analyse de cellules uniques qui a émergé au cours des dernières décennies. Nous avons développé ici une méthode analytique pour les mesures quantitatives au niveau de la cellule unique basée sur l'encapsulation et la culture de *T. brucei* dans des gouttes agissant comme des microcompartiments. Nous avons décrit un système microfluidique pour l'encapsulation et l'analyse de cellules individuelles basées sur des mesures de fluorescence. Nous avons d'abord montré la survie de *T. brucei* pendant plusieurs heures à plusieurs jours dans des gouttelettes avec une influence à la fois sur la survie et la croissance par la taille des gouttelettes. Nous avons observé divers modèles de croissance au sein d'une population et avons découvert que la culture par gouttes de trypanosomes révélait des variants cellulaires à division élevée avec des densités cellulaires 10 fois plus élevées que les techniques de culture standard. Nous avons en outre combiné l'encapsulation de *T. brucei* avec un test de détection enzymatique pour étudier la sécrétion de protéase. L'utilisation d'un substrat basé sur la fluorescence a permis la détection de l'activité protéase sécrétée par des cellules individuelles. Enfin, nous avons testé la configuration

dans deux applications supplémentaires, toutes deux utilisées sur *T. brucei* unicellulaire. En conclusion, la microfluidique en gouttes s'est révélée prometteuse en tant qu'outil analytique pour la culture et l'analyse des trypanosomes avec un potentiel supplémentaire pour l'analyse unicellulaire à haut débit.

Centre de Recherce Paul Pascal - UMR 5031
115, Avenue du Dr Albert Schweitzer, 33600 Pessac, France

Laboratoire de Microbiologie Fondamentale et Pathogenicité - UMR5234
146, Rue Leo Saignat, 33076 Bordeaux Cedex, France

Contents

List of Figures

List of Tables

List of abbreviations

AAT	Animal African Trypanosomiasis
APOL-1	Apolipoprote L1
BBB	Blood-brain barrier
BSF	Bloodstream form
BF	Band pass filter
BS	Beam splitter
CAD	Computer-aided design
CATT	Card agglutination test for trypanosomiasis
CNS	Central nerve system
DAQ	Data acquisition card
DM	Dichronic mirror
ER	Endoplasmic reticulum
FACS	Fluorescence-activated cell sorting
FP	Flagellar pocket
GFP	Green fluorescent protein
HAT	Human African Trypanosomiasis
IMDM	Iscove's Modified Dulbecco's Medium
mtp	microtiter plate
NF	Notch filter
OD	Optical density
P	Pinhole
PAD1	Protein associated with differentiation 1
PCF	Procyclic form
PDMS	Polydimethylsiloxane
PLA2	Phospholipase A2
PLC	Phospholipase C
PMT	Photo multiplier tube
RBC	Red blood cell
RFU	Relative fluorescence unit
SIF	Stumpy induction factor
VSG	Variant surface glycoprotein
2D	Two-dimensional
3D	Three-dimensional

Résumé de projet

Contexte du projet

Les trypanosomes sont des parasites protozoaires pathogènes infectant les mammifères dans les pays d'Afrique subsaharienne. *T. b. rhodesiense* et *T. b. gambiense* sont responsables de la trypanosomose humaine africaine (THA) plus connue sous le nom de maladie du sommeil [1], tandis que *Trypanosoma congolense*, *T. vivax* et *T. b. brucei* sont retrouvés chez les animaux et conduisent à la trypanosomose animale africaine (TAA) ou Nagana [2, 3]. Ces parasites sont transférés entre les hôtes à partir de piqûres d'un insecte vecteur. Ce cycle évolutif nécessite des modifications physiologiques et métaboliques permettant de s'adapter dans chacun des hôtes [4]. Un exemple d'adaptation à l'intérieur de l'hôte mammifère est bien décrit : il s'agit du phénomène de variation antigénique. Alors qu'une large proportion de parasites est détruite par l'hôte, certains font varier leurs protéines variables de surface (VSG) dupant ainsi le système immunitaire et échappant ainsi à la réponse adaptative innée [5, 6]. Ces mécanismes indiquent un comportement hétérogène au sein d'une population et mettent en évidence l'importance de la variabilité dans une population de trypanosomes. Alors que la plupart des analyses de *T. brucei* sont basées sur des mesures de population ou de sous populations, on sait encore peu de choses sur le parasite à l'échelle d'une seule cellule. Il y a donc un besoin de développer des méthodes analytiques qui fournissent une mesure quantitative du comportement cellulaire avec une résolution de « cellule unique », permettant de caractériser les fluctuations et variations dans de grandes populations.

La microfluidique est l'étude de la manipulation et du traitement de la fluidique de petit volume qui fournit les capacités de multiplexer des tests biochimiques à haut débit jusqu'à obtenir des données de réponse à l'échelle de la cellule unique [7, 8, 9, 10, 11, 12]. La microfluidique a été utilisée dans des études rapporter dans la littérature pour étudier des trypanosomes individuels. Mais ces études ont un faible débit ce qui

restreint l'étude à des faibles nombres et de ce fait ne peut pas représenter l'ensemble des fluctuations de comportements. La lyse immédiate des cellules pendant l'analyse empêche égallement dans certains cas de comprendre la dynamique des cellules. [13, 14, 15, 16]. La microfluidique en gouttes est une branche importante du domaine microfluidique permettant une analyse à haut débit de cellules individuelles vivantes confinées dans des gouttelettes de microcompartiments et apporte ainsi des données cellulaires quantitatives à haute-résolution.

L'étude des trypanosomes en « cellule unique » est d'une grande importance pour acquérir une connaissance des mécanismes hétérogènes au sein d'une population et ainsi obtenir une compréhension plus approfondie de la dynamique de l'infection. Dans cette thèse, j'ai utilisé un système de microfluidique en gouttes comme outil analytique pour étudier les trypanosomes. L'objectif était de développer un système permettant d'étudier l'hétérogénéité de cellule à cellule en étudiant la dynamique de croissance et les activités enzymatiques au niveau d'une seule cellule.

Techniques expérimentales

Nous avons développé une plateforme microfluidique pour créer et contrôler des gouttelettes que nous utilisons comme microcompartiments d'analyse. Cette plateforme a été construite à partir d'un microscope inversé permettant l'imagerie en champs clair conventionelle couplé avec un système de mesure de fluorescence : des composants optomécaniques guident un laser à travers l'objectif du microscope focalisé sur les gouttes. La fluorescence émise par les gouttes est détectée dans un mode épifluorescence et collectée par un tube photomultiplicateur, interfacé avec un système d'acquisition de données. L'ensemble du système a été calibré et optimisé pour la détection de gouttelettes et la mesure de la fluorescence de chaque microcompartiment individuel, permettant donc des analyses unicellulaires. Nous avons fabriqué les dispositifs microfluidiques pour la production de gouttelettes en utilisant des techniques de lithographie douce. Le matériau polymère PDMS a été moulé à partir d'une conception spécialisée et collé à une lame de verre microscopique. Les trous d'entrée et de sortie ont permis l'injection des fluides non miscibles créant nos gouttes. Le débit fluidique était contrôlé par des pompes à seringue basse pression connectées et contrôlées à partir d'un ordinateur portable. Nous utilisons une phase aqueuse et une phase huileuse pour la production de gouttelettes stabilisées avec des molécules de tensioactifs. Des dispositifs de collecte et d'incubation supplémentaires ont été fabriqués pour le stockage

à long terme des gouttes.

La plateforme permet donc l'imagerie, la mesure de fluorescence, l'acquisition de données haut-débit, la production de gouttes pour l'encapsulation, la réinjection de gouttes, l'ensemble étant optimisé pour l'encapsulation et l'analyse unicellulaire de *T. b. brucei*.

Culture de *T. b. brucei* en gouttes

Les travaux de cette section ont donné lieu à une publication dans Scientific Reports (2021). L'article final est présenté dans le chapitre 3. Pour l'analyse quantitative de la cellule unique *T. b. brucei*, nous avons d'abord testé la compatibilité de l'encapsulation et de la culture de cellules de trypanosomes uniques dans des gouttelettes. L'encapsulation des trypanosomes suivait une distribution de Poisson comme pour tout type de particule dispersée aléatoirement dans un échantillon de départ. Nous avons ensuite montré que le trypanosome au stade mammifère était capable de survivre de plusieurs heures à plusieurs jours dans des gouttelettes. Ici, la taille des gouttelettes a une influence à la fois sur la survie et la croissance avec des gouttes plus grosses conduisant à une survie plus longue et un nombre de cellules plus élevé par goutte, mais des gouttes plus petites conduisaient à une densité cellulaire plus élevée (nombre de cellules par volume). Nous avons identifié des comportements hétérogènes en terme de croissance au sein d'une population. Certaines gouttes contenaient des variantes cellulaires à division élevée, tandis que d'autres contenaient des cellules à croissance très lente ou ne divisant plus du tout. La culture en gouttelettes des trypanosomes a en outre entraîné des densités cellulaires 10 fois plus élevées des cellules qui se divisent le plus par rapport aux techniques de culture standard. Certains variantes ont atteint des titres cellulaires finaux à l'intérieur des gouttelettes plus proches de ce qui est observé dans la nature par rapport aux cultures standard. Nous avons montré ainsi ici une bonne compatibilité pour l'encapsulation de cellules individuelles dans des gouttes de microcompartiments avec une utilisation prometteuse pour l'analyse des variabilités cellulaires au sein d'une population.

Sécrétion enzymatique par unicellulaire *T. b. brucei*

Lorsqu'ils infectent un hôte mammifère, les trypanosomes sont exposés à un environnement hostile confronté en permanence aux attaques des cellules immunitaires de

l'hôte. Une partie du mécanisme de défense des trypanosomes est la libération de phospholipase et de protéase supposées avoir des propriétés pathogènes [17, 18, 19]. La sécrétion de plusieurs classes de protéases à partir de trypanosomes vivants a été identifiée et rapportée dans la littérature, notamment la cystéine peptidase, l'oligopeptidase et la métallopeptidase [19, 20, 21, 22]. De par leurs rôles pathogènes dans l'infection par les trypanosomes, les enzymes sécrétées sont de bons candidats pour le ciblage de médicaments. Cependant, avec la perspective d'un comportement hétérogène au sein d'une population, comme nous l'avons également observé au chapitre 3 sur la division, des méthodes analytiques sont nécessaires pour les mesures quantitatives des enzymes sécrétées à l'échelle d'une seule cellule.

Nous développons ici un test de sécrétion pour la détection de l'activité enzymatique par des mesures de fluorescence sur une seule cellule *T. b. brucei* en utilisant la microfluidique en gouttes. Nous avons identifié un certain nombre d'enzymes possiblement liées à la virulence des trypanosomes et sélectionné trois candidats. La compatibilité avec les mesures en microfluidique de trois kits commercialisés pour mesurer nos candidats enzymatiques a été évaluée. Nous avons finalement choisi un test d'activité de protéase basé sur la fluorescence adapté à une utilisation en gouttes. En co-encapsulant un substrat de protéase et *T. b. brucei*, nous avons pu détecter une sous-population de gouttes avec une fluorescence plus élevée que le bruit de fond des gouttes vides, indiquant une sécrétion de protéase à partir de trypanosomes uniques. En comparant la fluorescence moyenne détectée à partir des cellules encapsulées avec une courbe standard de trypsine, nous proposons une estimation de la protéase sécrétée équivalente à la trypsine de 1-3 $\mu g\,mL^{-1}$. Pour s'assurer que la fluorescence que nous avons détectée provient réellement de la protéase sécrétée, nous avons testé l'effet d'inhibiteurs de protéase sur le signal mesuré. Nous avons observé ici une activité plus faible dans les gouttes avec des inhibiteurs par rapport à celles sans, couplant la fluorescence mesurée à l'activité de la protéase. Ces résultats soulignent l'utilisation prometteuse d'un système microfluidique en gouttes pour étudier la sécrétion d'enzymes à partir de trypanosomes monocellulaires.

Analyse unicellulaire par la microfluidique en gouttes

Après le développement de notre plate-forme microfluidique en gouttes, nous avons effectué une série d'expériences préliminaires mais prometteuses impliquant une analyse de *T. b. brucei* en « cellule unique ». Nous avons déjà étudié la dynamique de crois-

sance lors de l'encapsulation de gouttelettes. Dans la première partie de ce chapitre, nous avons élargi l'étude de la dynamique de croissance et analysé la différenciation des formes élancées aux formes trapues dans des conditions de culture en présence de glycérol. Pour cela, nous avons utilisé ici une lignée cellulaire rapporteur GFP:PAD1$_{utr}$ exprimant la GFP lorsque les cellules sont différenciées en la forme trapue ne se divisant pas [23]. Nous avons testé la survie et la dynamique de croissance de la lignée cellulaire rapporteur dans trois tailles de gouttelettes différentes et avons trouvé que la taille optimale pour la croissance était de 0,75 nL . Nous avons en outre analysé les niveaux de croissance et d'expression de la GFP lorsqu'ils étaient cultivés dans du glucose, du glycérol et un mélange 50:50 des deux. Comme prévu, d'après les observations précédentes dans notre laboratoire, la culture en présence de glycérol a entraîné des taux de croissance lents et une augmentation de l'expression de la GFP, indiquant une augmentation de la différenciation en formes trapues. Au contraire, les cellules en culture avec du glucose ont montré un taux de croissance plus élevé avec une expression nulle ou très faible de la GFP. En présence de glycérol, nous avons en outre observé des cellules en division exprimant encore la GFP, confirmant l'existence d'une forme intermédiaire ou spéciale comme suggéré dans des études rapportées dans la littérature [24, 23, 25]. Nous avons décrit ici l'approche basée sur les gouttelettes pour l'analyse de la corrélation entre la croissance et la différenciation en forme trapue dans des conditions de culture en présence de glycérol. Bien qu'un développement supplémentaire soit nécessaire, la microfluidique en gouttes s'est révélée utile pour étudier la dynamique de croissance et de différenciation au niveau d'une seule cellule.

Dans le chapitre 4, nous avons utilisé notre configuration de gouttelettes pour analyser la sécrétion d'enzymes par des cellules uniques. La deuxième partie de ce chapitre a été consacrée à l'analyse de l'interaction directe avec l'hôte entre les globules rouges (GR) et la *T. b. brucei* sous forme de gouttelettes. Nous avons développé une approche pour étudier l'interaction cellulaire en mesurant l'hémolyse des globules rouges. La membrane des GR se compose de nombreux lipides et protéines dont la composition spécifique varie entre les différentes espèces de mammifères [26, 27, 28]. Dans ce travail, nous avons utilisé des globules rouges de mouton et avons d'abord testé la tolérance membranaire à l'hémolyse osmotique. Nous avons découvert une tolérance élevée de ces globules rouges comparée à d'autres mammifères selon les données de la litérature. Pour visualiser l'hémolyse en gouttes, nous avons utilisé un kit commercial pour enrober les globules rouges de protéines fluorescentes. Ici, nous avons découvert que l'hémolyse n'a pas conduit à une rupture complète des globules rouges, mais au lieu

de cela, les cellules ont conservé leur forme intacte. Bien qu'il ne soit pas adapté à la détection par fluorescence, ce test offre la possibilité d'analyser l'hémolyse sur la base d'une analyse d'image. Enfin, nous avons testé la compatibilité de la co-encapsulation de GR et de *T. b. brucei*, entraînant la survie et la croissance en gouttes de 0,2 nL pendant au moins 8 heures d'incubation. L'ajustement de la taille des gouttelettes et du rapport des globules rouges et des trypanosomes semble être nécessaire pour prolonger la survie et optimiser l'interaction entre cellules mais une approche basée sur l'encapsulation en goutte permettra probablement d'étudier les interactions entre cellules individuelles de manière quantitative.

Conclusion et perspectives

Dans cette thèse, nous avons exploré la compartimentation, la culture et l'analyse de cellules uniques de *T. b. brucei* en utilisant la microfluidique en gouttes. Nous avons décrit la conception et la mise en place d'une plateforme de microfluidique en gouttes, permettant une analyse à haut débit de cellules individuelles. En encapsulant *T. b. brucei* en gouttes, nous avons observé une survie cellulaire de plusieurs heures à plusieurs jours, et avons démêlé des comportements hétérogènes en termes de croissance entre les cellules d'une population. Une suite intéressante serait la sélection de gouttes avec des variantes se divisant plus que la moyenne. Une mise en œuvre d'un module de criblage sélectionnant pour une biomasse élevée, nous permettrait de collecter ces variantes. Une optimisation supplémentaire du système pourrait être envisagée en automatisant le processus d'imagerie pour une collecte de données plus rapide. L'association de l'encapsulation unicellulaire avec un substrat enzymatique nous a permis d'étudier *T. b. brucei* sécrétion de protéase à partir de cellules individuelles. Les tests commerciaux disponibles se sont avérés peu quantitatif pour une étude plus approfondie de la variabilité de la protéase sécrétée. Cela laisse une suite évidente pour trouver d'autres approches pour la détection des gouttelettes de l'activité de la protéase permettant d'étudier ces variabilités de virulence. Les stratégies de détection de la variabilité pourraient inclure l'étude des schémas de nage ou la surveillance d'autres composés ou métabolites sécrétés. Nous avons en outre étudié la corrélation entre l'expression de la protéine associée à la différenciation, PAD1, et l'arrêt de la croissance au niveau d'une seule cellule. L'identification des cellules en division exprimant encore PAD1, a souligné la nécessité d'une analyse plus approfondie de la dynamique de croissance et de différenciation. Enfin, nous avons testé une approche pour analyser l'interaction di-

recte entre les globules rouges et les trypanosomes basée sur l'hémolyse. Nos résultats préliminaires ont montré la possibilité de marquer les globules rouges avec des protéines fluorescentes pour une observation visuelle. Nous avons en outre montré une bonne compatibilité de co-encapsulation de *T. b. brucei* et les globules rouges à des temps d'incubation allant jusqu'à 24 heures. Cette approche s'est révélée prometteuse pour l'analyse future de l'interaction des trypanosomes avec les globules rouges et pour mesurer davantage l'activité enzymatique sécrétée au niveau d'une seule cellule.

Dans cette thèse, nous avons montré que la microfluidique en gouttes est un outil efficace pour l'encapsulation de cellules uniques et l'analyse de *T. b. brucei*. pour des mesures quantitatives de trypanosomes isolés. Ces technologies 'cellules uniques' sont d'un grand intérêt pour de nombreuses applications faisant progresser l'exploration de l'hétérogénéité de cellule à cellule. Cela permettra avant tout de mieux comprendre la dynamique complexe des trypanosomes et peut in fine conduire à l'identification de nouvelles cibles médicamenteuses contre la maladie.

Introduction

For decades, the golden standards of conventional biological research have been extracting information on population levels assuming equal contribution from every cell or neglecting variability. Developments of a variety of single cell technologies have led to an awareness of cell-to-cell heterogeneity in seemingly isogenic populations. Heterogeneity within populations are often used as survival strategies against environmental changes and is already well characterized in bacteria and yeast [29, 30, 31, 32].

The protozoan parasite *Trypanosoma brucei* is an interesting example of an isogenic cell population exhibiting an heterogeneic life style [33]. Trypanosomes are infecting mammals in African countries and are transmitted between hosts through bites of an insect vector. In prior to transmission, the majority of the population differentiate into a pre-adapted stage ready to reenter the insect vector, while a fraction of the population stay adapted to the mammal host [4]. The fraction of non-differentiated cells staying in the host continuously adapt to escape the host's immune system through multiple cycles of antigenic variation [5]. Though the mammalian stage of the parasites are defined as *bloodstream forms*, they eventually start invading the host and adapt to different tissues [23]. These mechanisms of host transmission, antigenic variation and tissue adaptation reveal the importance of heterogeneic behaviours in trypanosome parasites. Here, single cell studies are of great interest for systematic characterization of the mechanisms of trypanosome heterogeneity. Though numerous analytical methods for single-cell study are continuously developed, little is known of trypanosomes at the single cell level, calling for the development and use of new technologies.

Droplet-based microfluidics is a prominent branch in the microfluidic field of controlling and manipulating small volumes of fluids. Encapsulation of individual cells in microcompartment droplets allows for high-throughput analysis of single cells [34, 35]. Therefore droplet-based microfluidics is a promising tool for quantitatively studying heterogeneity in trypanosomes population with a single cell resolution.

Aim of project

Studying single cell trypanosomes is of great importance for gaining knowledge of the heterogeneic mechanisms and thereby obtaining a deeper understanding of the dynamics of infection.

In this thesis I developed and used a droplet-based microfluidic system as an analytical tool to study single cell trypanosomes. The aim was to develop a droplet-based microfluidic method and system allowing for the investigation of cell-to-cell heterogeneity by studying growth dynamics and enzymatic activities at the single-cell level.

In **Chapter 1**, I introduce the trypanosome parasite which is the biological model used in this work. I clarify the standard techniques used for studying single cell trypanosomes and present the microfluidic techniques used to date. Hereafter, I introduce droplet-based microfluidics, its characteristics and current use in single-cell analysis.

The microfluidic techniques used in this thesis for studying single-cell trypanosomes are presented in **Chapter 2**. Here, I describe the setup and its functions used to create microcompartment droplets.

I further use this setup to encapsulate and cultivate trypanosomes and finding the optimal settings for future analysis. These results have been published in Scientific Reports and are presented in **Chapter 3** as the final paper. After establishing the single-cell encapsulation approach I further investigated single-cell enzyme secretion.

In **Chapter 4**, I first test the compatibility of our droplet system with different fluorescence-based commercialized kits for enzymatic activity detection. I select a protease candidate for co-encapsulation with trypanosomes to detect the level of secretion and validate the detected activity.

With an established droplet-microfluidic setup I further investigated the dynamics of single-cell trypanosome behaviours by a series of preliminary yet interesting experiments. In the first part of **Chapter 5**, I investigate the correlation between growth dynamics and cell differentiation. In the second part of **Chapter 5**, I design a droplet-based approach for studying the interaction between red blood cells and trypanosome by analysing hemolysis. I then test the compatibility of co-encapsulating red blood cells with trypanosomes to ensure *in vitro* survival. Finally, in **Chapter 6**, I conclude on the work performed in this thesis and discuss future perspectives of where this work can bring us.

This work was funded by a University of Bordeaux fellowship (interdisciplinary call 2017). Additional funding in the lab was provided by the French Government 'Investments for the Future' Program, the University of Bordeaux Initiative of Ex-

cellence (ANR-10-IDEX-03-02), the 'Region Nouvelle Aquitaine', the Institute Universitaire de France and the Labex Parafrap. I extend my gratitude to Emulseo (`https://www.emulseo.com/`) for kindly providing all the surfactant used in this thesis.

1 Background

In this chapter, I present the *Trypanosoma brucei* parasite, the biological model used in this thesis. I shortly describe the cell taxonomy, disease dynamics, life cycle, cellular structure and introduce the interest of analysing single cells in the context of parasite infection. I clarify the current techniques used for studying single *Trypanosoma brucei* cells, and present the microfluidic tools today used for single-cell analysis of *Trypanosoma brucei*. Lastly, I describe the characteristics of droplet-based microfluidics, the main technique used in this thesis, and highlight the relevance of extracting new information of *Trypanosoma brucei* at the single cell level.

1.1 Trypanosomes

Trypanosomes are single-cell flagellate parasites of the order Trypanosomatida belonging to the kinetoplastids (Kinetoplastea class). The kinetoplastids are characterized by the presence of a single and unique structure containing a dense mass of mitochondrial DNA named the kinetoplast [36]. The Trypanosomatida order is one out of four orders, including the well-studied pathogenic parasites from the *Trypanosoma* and *Leishmania* genus (Fig. 1.1). The remaining of the kinetoplastid orders are the Bodonoids predominately being the free-living species of Eubodonida, Parabodonida and Neobodonida [37, 38, 39, 40].

The single family Trypanosomatidae of the Trypanosomatida order consists of a varity of parasites with a broad repertoire of vertebrate, invertebrate and plant hosts, including the three parasites *Leishmania*, *Trypanosoma cruzi* and *Trypanosoma brucei* each responsible for a neglected tropical disease (Leishmaniasis, Chagas disease and Human African Trypanosomiasis (HAT)) [41]. The members of the *Trypanosoma* genus are overall distinguished in between two groups based on their mode of transmission. The *Stercoraria* group includes parasites transmitted through excrements of their insect vector represented by *T. cruzi*. The other group, the *Salivaria*, comprise parasites transmitted in saliva from bites of an insect vector [42]. This group is represented

by the medical relevant species *T. brucei*, *T. vivax* and *T. congolense*. The *T. brucei* subspecies *T. b. gambiense* and *T. b. rhodesiense* are transmitted by the tsetse fly (*Glossina* genus) and are infecting livestock and humans being the causative agents of HAT [43]. Contrary, the subspecies *T. b. brucei*, also transmitted by the tsetse fly, are only capable of infecting wild and domestic mammals and are together with *T. vivax* and *T. congolense* the dominating infectious agents of Animal African Trypanosomiasis (AAT) [2, 3].

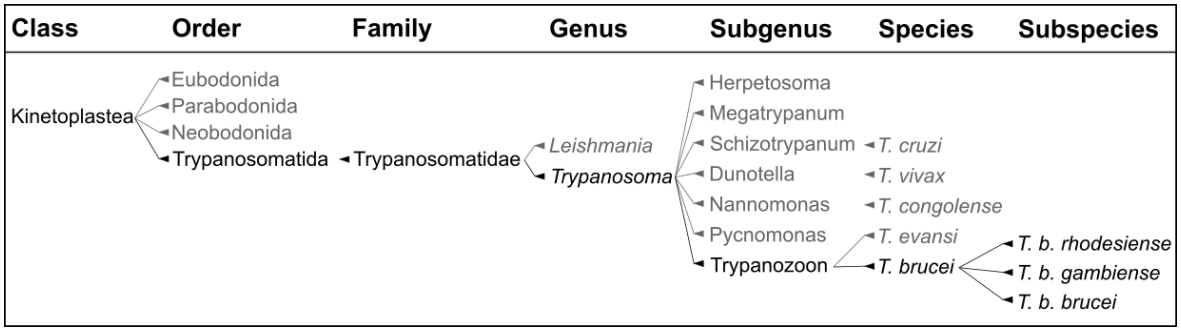

Figure 1.1: Overview of *Trypanosoma* classification. Schematic representation of the main classification for the *Trypanosoma* species. The figure is created with inspiration from Simpson *et al.* [39] and Baral *et al.* [44].

1.1.1 Human African Trypanosomiasis

HAT, commonly referred as Sleeping sickness, is a neglected tropical disease widespread in Sub-Saharan African countries. *T. b. gambiense* are responsible for slowly progressive infections in central and west Africa being accountable for 98% of all cases. While *T. b. rhodesiense* only are responsible for 2% of all cases spread in eastern and southern Africa, *T. b. rhodesiense* are causing a fast progressing and severe illness [43, 45, 41]. Both HAT forms have two stages of the disease and are lethal if not treated. In the first and early stage, the parasites are multiplying in the blood and lymphatic system and patients can experience mild non-specific symptoms as headache, fever or fatigue. In the second and later stage, parasites have crossed the blood-brain barrier (BBB) infecting the central nervous system, giving rise to more severe symptoms as neuropsychiatric disorders, sleep disturbance (hence the name Sleeping sickness) and entering coma.

Diagnosis of HAT mainly relies on serodiagnostic tests for detection of trypanosome-specific antibodies followed by the confirmation of parasites present in the blood. Card agglutination test for trypanosomiasis (CATT) is the most abounded used test for the last 40 years where new rapid tests have started to emerge within the last decade

[1, 46, 47]. While serodiagnostic tests only exist for *T. b. gambiense*, diagnosis of *T. b. rhodesiense* relies on parasite detection in blood. The state of the disease is finally determined by examination of the cerebrospinal fluid [41].

Until recently, five drugs were available for treatment of HAT. For *T. b. gambiense*, pentamidine was used as first-stage treatment, where a combination therapy of nifurtimox and eflornithine were used as second-stage treatment. For infections with *T. b. rhodesiense*, suramin and melarsoprol were used as first and second-stage treatment, respectively [48, 41, 1]. The latest addition of treatments against HAT is the drug fexinidazole. Contrary the previous treatments, fexinidazole is only administered orally eliminating the need of systematic hospitalization and leads to reduction of treatment cost. Additionally, fexinidazole has shown effective as both first and second-stage treatment [49, 50, 41]. While resistance towards melarsoprol is the only example of widespread drug resistance in patients, potential resistance of nifurtimox and fexinidazole have been shown *in vitro* and *in vivo* [51, 52]. Years with extensive surveillance and treatment have lead to a significant decrease in HAT cases over the last decade, where in 2018 less than 1000 cases were reported (Fig. 1.2). WHO has targeted the elimination of HAT as health problem by 2020 and a full interruption of transmission by 2030 [53].

1.1.2 Animal African Trypanosomiasis

AAT is the animal version of Sleeping sickness also called Nagana and derive from infections of *T. congolense*, *T. vivax* and in less extent *T. b. brucei* [2, 3]. The disease is transmitted through bites of the tseste fly (*Glossina* genus), the same vector as for HAT. *T. vivax* can furthermore be transmitted mechanically by other insect vectors as horseflies (*Tabanus* spp.) and stable flies (*Stomoxys* spp.), having allowed the spread of *T. vivax* outside the tsetse area in Africa [54]. Contrary the human infectious species, AAT *Trypanosoma* species are incapable of establishing human infections, though a few rare cases have shown otherwise [55]. *T. b. gambiense* and *T. b. rhodesiense* each express a resistance protein incapacitating the human-specific serum apolipoprotein L1 (APOL-1) with trypanolytic activity. In *T. congolense*, *T. vivax* and *T. b. brucei* APOL-1 are endocytosed through the coupling of a high-density lipoprotein particle. Upon storage in the parasitic lysosomes the acidic environment induce conformation changes of APOL-1 creating membrane pores which induce lysis and cell death [56, 57].

AAT is widely spread in sub-Sahara Africa with a broad range of hosts. Besides many wild mammals working as natural reservoirs, valuable domestic livestock as cat-

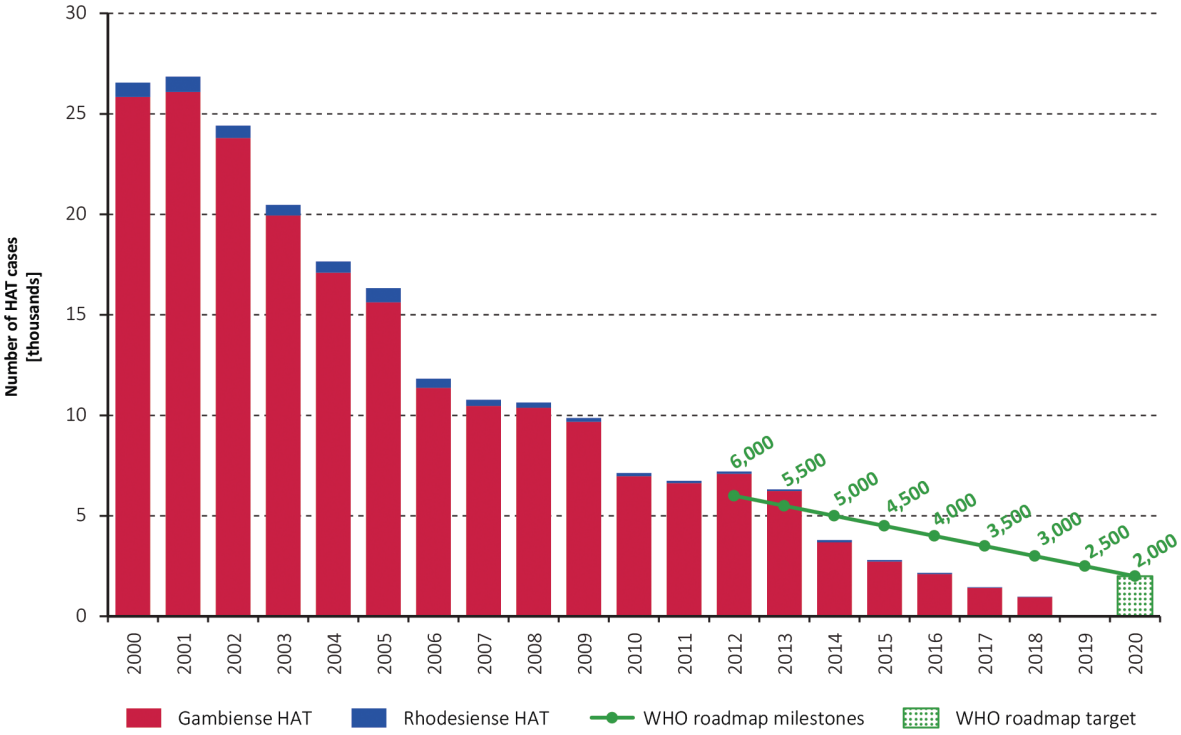

Figure 1.2: Reported cases of HAT from 2000-2018. Graphic presentation of the progression in elimination of HAT (gambiense and rhodesiense) for the last 20 years. The green bar and line are the target and milestones defined by WHO [41]. The figure is reproduced from Franco *et al.* [53].

tle, horses, sheep and goats are affected [3]. Other *Trypanosoma* species affecting valuable livestock are *T. evansi* and *T. equiperdum*. *T. evansi* are infecting mammals as horses, cattle, camels and buffalo causing the disease Surra, where *T. equiperdum* mainly infect horses leading to the Dourine diesease. Both trypanosome species are believed to derive from *T. brucei* by partially or fully losing their kinetoplast DNA, blocking them from adaptation to the insect vector [58].

Many symptoms from AAT infections are similar to those of HAT in humans, but the most common in animals are anemia leading to weakness, heart failure and death if not treated. However, the specific symptoms are varying a lot between the type of animal and the stage of the disease. For treating AAT, the main trypanocidal drugs used are diminazene aceturate, ethidium bromide and isometamidium chloride. Due to high usage of these trypanocides cases of drug resistance have been reported since the 1960s [59, 60]. Since drug treatment for big herds of livestock can be both challenging and expensive, other strategies for controlling the disease, also used for HAT cases, are targeting the insect vectors instead of the parasites. Insecticides can be distributed from air covering large area of landmass or they can be applied directly on the animals. Another more complicated technique involves the production of sterile male tsetse flies

for outnumbering the wild males and stopping the reproduction in a tsetse population [61].

With the widespread livestock herds and large wildlife reservoirs, surveillance and control of AAT are challenging and lead to great economic consequences in the affected areas. Farmers are directly affected in the meat and diary production from sicken animals and their need for extensive medical treatment. However, dying or weakened livestock also have an indirect impact on the crop production by the many integrated crop-livestock systems. It is estimated that the total cost of AAT is more than one billion dollars annually. However, it is further estimated that this number can be significantly decreased with improved tsetse control [62, 63].

1.1.3 Life cycle of *T. b. brucei*

T. b. brucei is an optimal model organism closely related to the two human-infecting subspecies and is the model organism used in this thesis. The use of multiple hosts makes the life cycle of *T. b. brucei* complex being well adapted to both vector and host (Fig. 1.3). The parasites are entering the tsetse fly by a blood meal from an infected host animal. When entering the insect vector the trypanosomes are differentiating into a proliferating procyclic form (PCF) when reaching the mid-gut of the insect.

From here, the trypanosomes continue their journey inside the insect reaching the proventriculus, a part of the intestine system, where they undergo asymmetric differentiation into long and short epimastigotes. Continuing through the mouth regions the epimastigotes end up in the salivary glands, where short epimastigotes are attaching to the epithelial cells of the glands. Here they replicate and differentiate into the non-dividing metacyclic form. The metacyclic forms, pre-adapted for the mammal host, detach from the salivary glands and are ready for transmission back into a mammal host to establish a new infection [65, 66, 67, 64].

By injection from the tsetse fly, adapted metacyclics enter the bloodstream of the mammal host. In the blood, the metacyclic forms are differentiating into long and slender proliferating bloodstream forms (BSF). Here, the BSF trypanosomes are highly proliferating and spreading throughout the entire circulatory system. The parasite will continue spreading to several other tissues as, adipose tissue, the skin, spleen, liver and eventually the central nerve system (CNS) and brain [45, 68, 23, 69, 70]. A part of the pre-adaption step in the late metacyclic form is the expression of variant surface glycoproteins (VSG). The mechanism of VSG allows adaptation of the trypanosomes to the host's immune response. Upon attack from immune cells, a small part of the

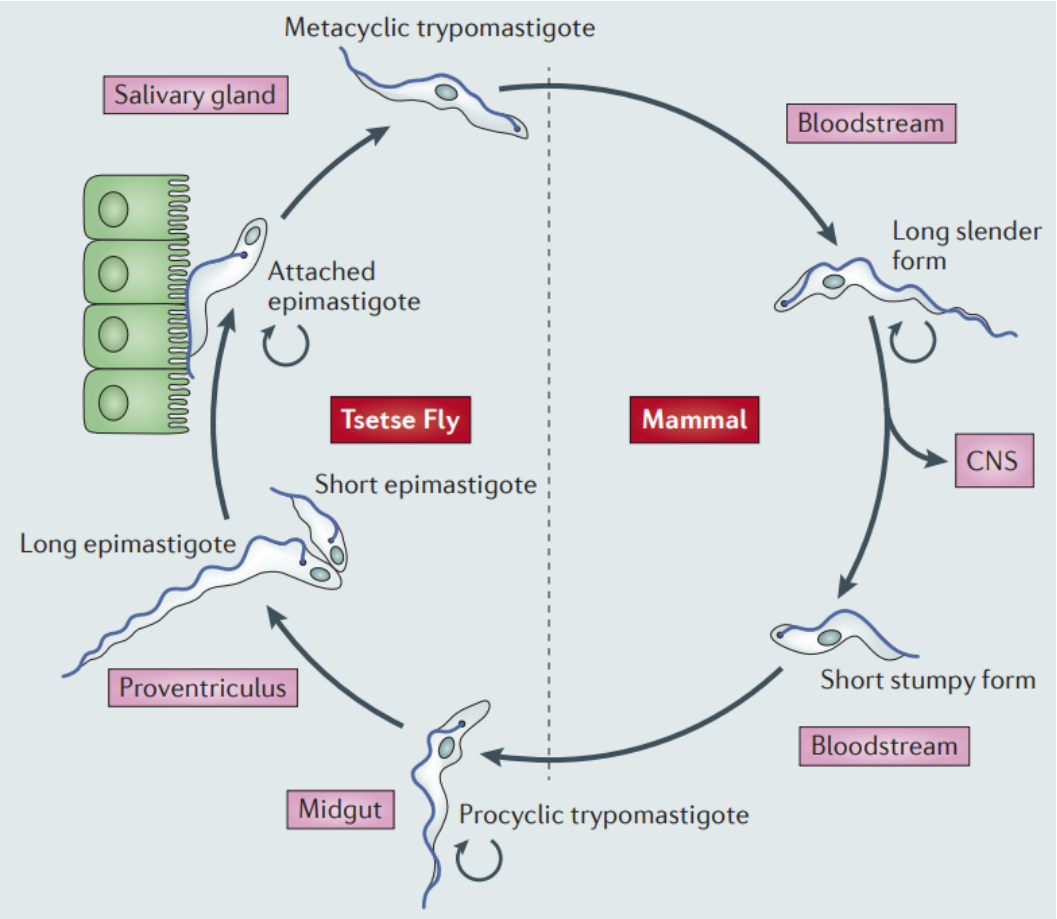

Figure 1.3: Life cycle of *T. b. brucei*. Schematic representation of the major stages in the life cycle of *T. b. brucei* in the insect vector and the mammal host. The circled arrows present the capacity to proliferate. The figure is reproduced from Langousis and Hill [64].

trypanosome population will change their VSG coat hiding them from the immune system. This action, known as antigenic variation (Fig. 1.4), allows a small part of the population to continuously re-adapt to new immune responses at multiple cycles during infection [65, 5, 6]. Though, only one VSG is expressed at a time, the cells contain an estimate of 300 fully functionally VSG genes and more than 2000 partial or incomplete genes [71]. Activation of VSG expression includes transcriptional activation and inactivation of the VSG expression site and homologous recombination of active VSGs or between active and inactive expression sites [72]. The vast part of the population not performing antigenic variation is differentiating into the short non-dividing stumpy form being adapted to re-enter the insect vector. During the peak in parasitaemia, accumulation of stumpy induction factor (SIF) triggers the differentiation into stumpy forms by a quorum sensing mechanism [73, 4, 74]. Stumpy forms are now ready for transmission back into the tsetse fly during the next blood meal, where the stumpy forms left in the mammal host will be targeted and cleared by the immune system. The

exact actions behind antigenic variation or differentiating into stumpy forms are not fully understood. However, these adaptation mechanisms indicate variability within a population linked to cell-to-cell heterogeneity [33].

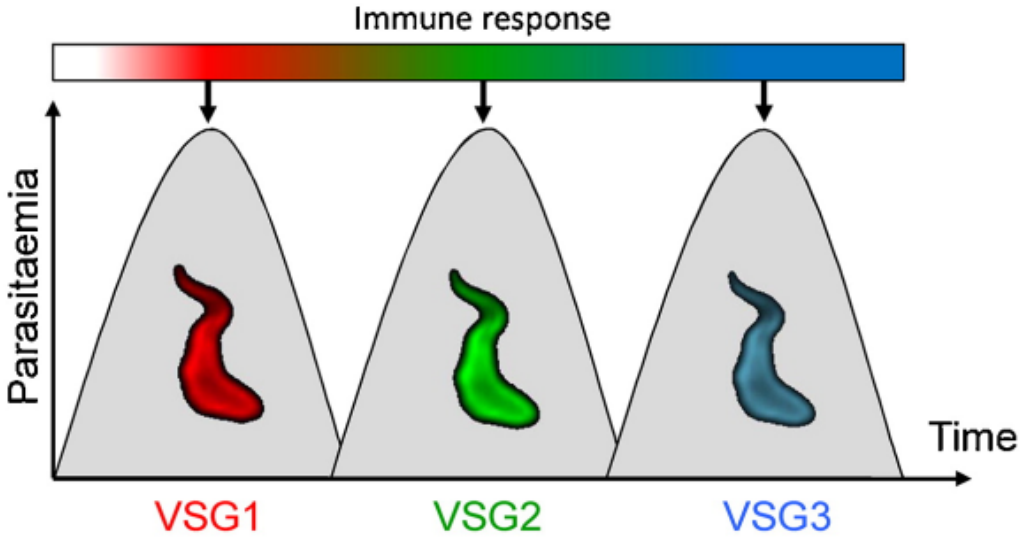

Figure 1.4: Antigenic variation in *T. b. brucei*. The switching of VSG expression over time during an infection causes cycled peaks in the parasitaemia level. The immune response's elimination of parasites with one type of VSG gives rise to parasites with another type of VSG. The figure is reproduced from Horn *et al.* [72].

1.1.4 Cellular structure

Like other kinetoplastids, *T. b. brucei* carry the single-copy organelles; golgi complex, endoplasmic reticulum (ER), nucleus and the kinetoplast (Fig. 1.5) [75]. The kinetoplast contains the mitochondrial genome which is composed of a dense mass of DNA circles [36]. It is located inside the mitochondrion, extending through the entire cell body. The kinetoplast is connected to the flagellum inside the flagellar pocket (FP) in the posterior end of the cell. The flagellum is extended outside the cell attached alongside the membrane ending free from the cell at the anterior end [64]. Flagellum movement is foremost essential for cell survival in the many different host environments and tissues. It has furthermore shown to facilitate the clearance of VSG bound antibodies from the cell surface [76]. In addition to being the exit point of the flagellum, the FP has many important cellular functions. It is the only site for endo- and exocytosis for sorting and recycling compounds by endosomes and lysosomes [77, 78], and is involved in processes as cell division and cell polarity [79, 80]. In addition, *T. b. brucei* contain numerous peculiar organelles named glycosomes. Glycosomes are peroxisome-related and their contents are involved in glycolysis and other important metabolic

pathways. The specific content of the glycosomes changes together with the cell when changing between insect vector and mammal host [81]. The shape and stability of the entire cell body is defined by the cytoskeleton, composed of a subpellicular microtubule array [82]. In BSFs, the outer cell membrane is coated with VSGs, where in PCFs the surface is cleared from VSG and covered by the surface proteins procyclins, adapting the cell for the environment of the insect [83].

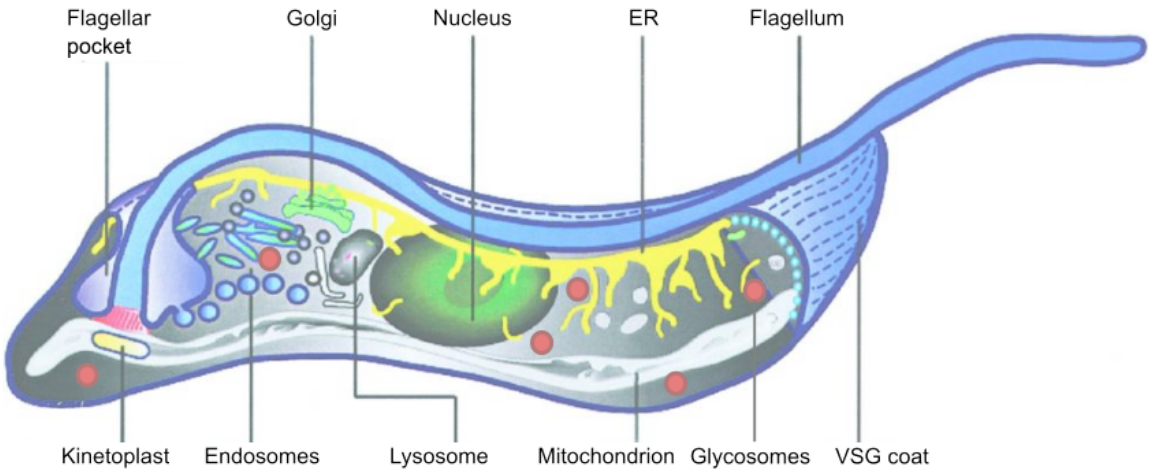

Figure 1.5: Cellular structure of *T. b. brucei*. A simplified schematic presentation of the major compartments in a *T. b. brucei* cell. The figure is adapted from Grünfelder *et al.* [77].

1.2 Single-cell study of Trypanosomes

T. brucei is a well studied organism where both the insect stage and the mammal stage can be cultivated in laboratory settings *in vitro* and *in vivo* [84, 85, 86, 87]. A variety of gene editing tools as transfection and transcriptional regulation are well established for gene function analysis in *T. brucei*, but also new technologies like the CRISPR-Cas9 system have shown successful [88, 89, 90]. Where most *T. brucei* research are based on partial or whole population measurements like in any conventional microbiological research, little is yet known of the parasite at the single cell level. The main methods commonly used for analysing single trypanosome cells are based on microscopy imaging techniques. Organelle specific dyes are used to visualize locations and structures of the organelles in individual cells. Other techniques such as immunofluorescence microscopy using fluorescent antibodies or fluorescence gene-tagging give information on presence or expression of specific proteins [91, 92, 93]. Most microscopy imaging requires fixation of the cells, although a few techniques have been developed for analysing the motility of single cells on cultivation gels [94], isolated in microfluidic compartments

[14] or within optical traps [13]. Though imaging techniques are ideal for visualizing organelle location or protein expression, it is a low-throughput method and highly time consuming for quantitative analysis. For a higher throughput, analysis of single-cell trypanosomes involving fluorescence-activated cell sorting (FACS) have successfully been tested [95, 96]. Though, FACS is a well establish method permitting sorting by specific properties, data collection is only from a single time point and does not permit monitoring of living cells over time.

The well established field of microfluidics have for years been widely used for single-cell analysis of various cell types and organisms including bacteria [97, 98], yeast [99], multicellular organisms [100] and human cells [101, 102]. Microfluidics is the study of manipulation and processing of fluidics in the scale of nano- to attoliters. These extremely small volumes come with a range of advantages including the usage of lesser quantities of reagents, high sensitivity and fast analysis [7, 9, 103]. Despite a broad range of single-cell applications, only a handful of have yet been used on single-cell trypanosomes which will be described in the following sections.

1.2.1 Motility assay

In 2012, Heddergott *et al.* developed a microfluidic device consisting of regularly aligned polydimethylsiloxane (PDMS) pillars to study the speed of *T. brucei* [104]. The conditions were set in order to simulate the flow dynamics of red blood cells (RBCs) inside the bloodstream as much as possible (Fig. 1.6a). With pillar diameters of 8 µm and spacing of 4 µm, trypanosomes showed the highest proportion of cells having faster and directional motion compared to other array conditions (Fig. 1.6b-c). The trypanosomes showed less tumbling (non-directional motion) and a maximum velocity almost 8 times higher of the mean population in standard cell cultures. Bargul *et al.* (2016) later used similar devices showing how different species of trypanosomes (*T. brucei*, *T. evansi*, *T. congolense* and *T. vivax*) showed diverse velocities [105]. They extended the original array and measured the cellular velocities at different sizes of pillar diameter and spacing (Fig. 1.6d). All the trypanosome species showed diverse velocities in the different conditions compared to each other. Furthermore, by using this microfluidic array simulating the bloodstream dynamics, most of the trypanosome species reached higher maximum velocities compared to measurements performed in a viscosity medium and still blood samples.

Other studies of trypanosome motility have focused on motion behaviors in various flow velocities. Uppaluri *et al.* showed that cells in low velocities exhibited specific

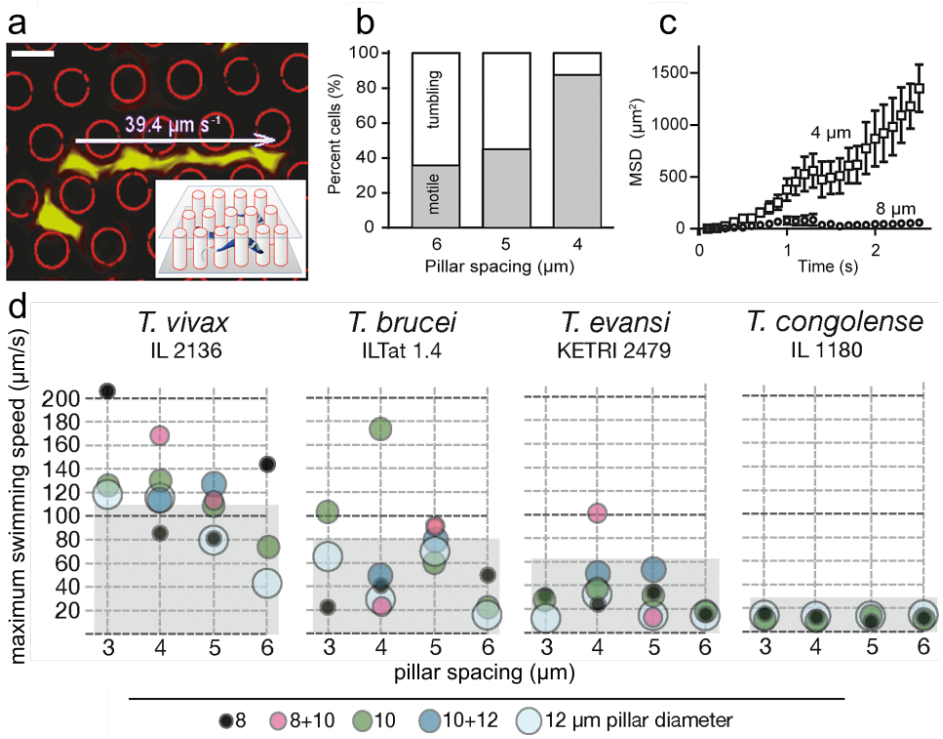

Figure 1.6: Motility measurements among obstacles mimicking the bloodstream. (**a**) Fluorescent-labeled trypanosome (green) moving in a pillar array with 4 μm spacing. Inset: Illustration of the experimental design. (**b**) Percentage of persistently swimming trypanosomes in surroundings with different pillar spacing (n = 150). (**c**) The net directional movement represented by the mean squared displacement (MSD) plotted over the observation time in pillar arrays of 4 and 8 µm spacing (n = 12; mean and SEM). (**d**) Measurements of motile trypanosomes by different arrays of obstacles mimicking the environment of the bloodstream. Persistently swimming cells were measured and maximum velocities were determined (n $\geq$ 200/ species). Grey shaded area indicate the swimming speeds measured by other experimental methods, i.e. in high viscosity media or wet blood films. The figure is adapted from Heddergott *et al.* [104] and Bargul *et al.* [105].

swimming pattern with sine like waves in an upstream orientation of the flow, while cells in the opposite orientation tumbled around in a streamline [106]. When increasing the flow velocities the pattern became less frequent and more tumbling for the upstream orientated as well. This study indicated that self-propulsion is important to the swimming pattern of trypanosomes even in flow velocities higher than their own swimming speed.

In a more recent approach Sun *et al.* (2018) tested the importance of a well functional flagellum for cell motility [107]. They designed a microfluidic device enabling the investigation of *T. brucei* motility focusing on the flagellum beating (Fig. 1.7). A PDMS-on-glass device was designed consisting of constrictions with small slits of 1.4 µm, equivalent to half the width of a normal trypanosome parasite. Two different

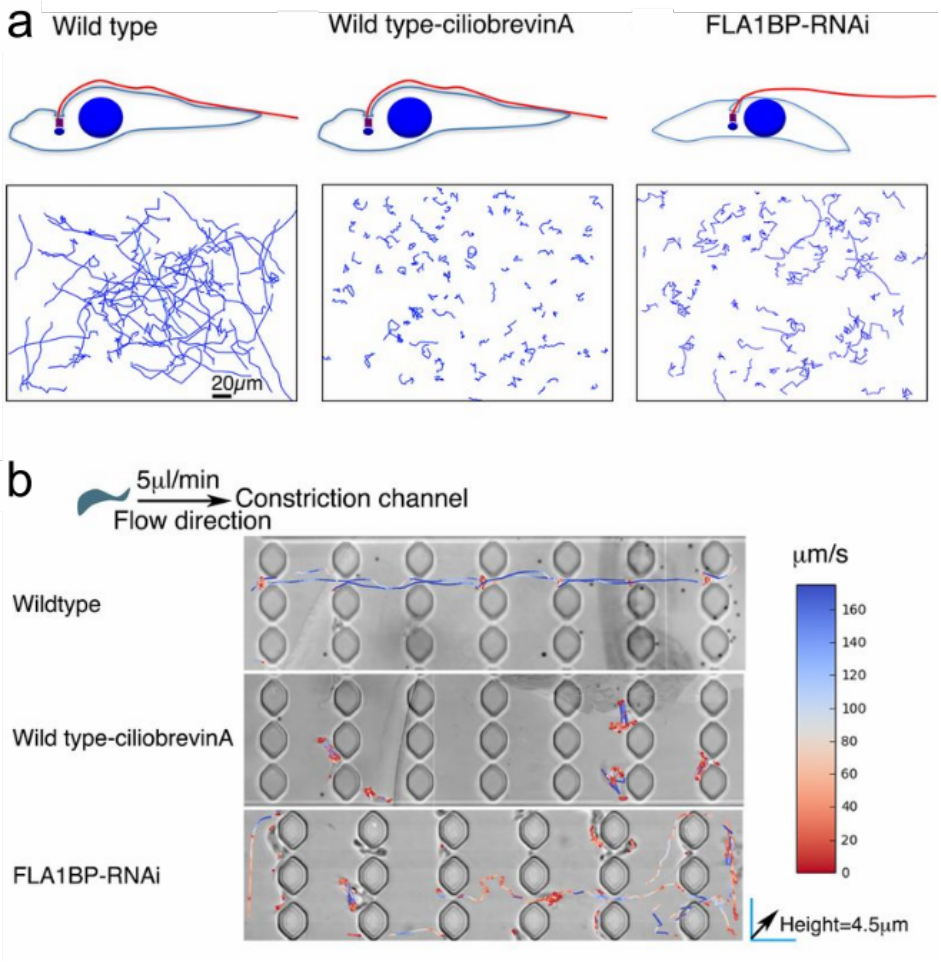

Figure 1.7: Flagellum-based movement easing cell deformation. (**a**) Three different cell conditions (wild-type, FLA1BP-RNAi, and ciliobrevin A-treated) differing in flagellum attachment and motility used for swimming measurements (n $\sim$ 90 for each). (**b**) Microfluidic device where the cells of the three conditions are passed through constriction channels with slit sizes of 1.4 µm at a constant flow rate. Cell movement are shown overlaying the device, with colors representing the velocities. The figure is adapted from Sun *et al.* [107].

conditions were tested together with wild type cells. In one condition, flagellum beating was inhibited by ciliobrevin A, where the other mutants had a flagellum detached from the cell bodies (Fig. 1.7a). When running through the microfluidic device by applying a small flow, they observed that wild type cells moved by great ease through the small slits, despite their much larger body size. Meanwhile the two cell types with flagellum deficiencies struggled in the same settings (Fig. 1.7b). The majority of the wild type trypanosomes managed to swim through numerous obstacles in a limited amount of time, where those cells with flagellum deficiencies, which succeeded the obstacles, showed a significant slower swimming speed than the wild types. This strongly indicates that functional flagella are highly essential for the movement of the trypanosomes inside the host. They suggested that by flagellum beating the cells could deform their

bodies enabling to move through tight openings more narrow than the cell itself.

1.2.2 Single-cell trapping

Analysing motility of single-cell trypanosomes in more confined surroundings was achieved using optical trapping [108, 13]. Optical trapping or optical tweezers is the act of focusing a laser beam on an object creating a force from the scattering of photons and was first used on cells in 1987 [109]. Stellamanns *et al.* (2014) combined optical tweezers with a microfluidic platform to investigate motility patterns and force generation by the flagellum in *T. brucei* [13]. Later, in 2015, together with Hochstetter *et al.* they presented a single-cell viability assay using optical trapping [14]. After trapping the cells by optical tweezers, they were loaded into small connected chambers (Fig. 1.8a).

When placed in the chambers, different compounds were loaded from the sides creating chemical gradients throughout the system. Here, they succeeded in testing the effect on trypanosome motility and viability at different concentrations of chemical compounds as glutaraldehyde commonly used for cell fixation (Fig. 1.8b). They further tested the commonly used drug for treating early stage HAT, suramin. By filling the chambers with suramin, they observed two different responses on the cells. Among most of the cells, paralysis was observed when the concentration of suramin reached a critical level. When removing the drug by flushing the device with normal culture medium the cells regained their motility when low concentrations were used. However, for most cells the drug had lethal effects causing the trypanosomes to disintegrate even after the suramin was flushed out of the device.

A microfluidic device has also been used in combination with microscopy imaging, immobilizing living cells allowing live image-based measurements. *T. brucei* cells were immobilized using a commercialized microfluidic device enabling live imaging and time lapse videos of viable cells [110]. The device consisted of chambers made by PDMS on glass in different heights, creating a gradually decrease of space which permitted the trapping of trypanosomes based on their size (Fig. 1.9). When the cells were trapped, the device was used as a buffer exchanging system, allowing investigation of the dynamic responses to environmental changes. Here, they monitored changes in cytosolic glucose levels of single cells at different extracellular glucose concentrations using cytosolic glucose biosensors. All responses from the trapped but living cells could be measured and recorded by time-lapse microscopy images. Both the mammalian BSFs (Fig. 1.9b) and the insect PCFs (Fig. 1.9c) were trapped and maintained alive at a duration of 48 hours, while cell division could still take place.

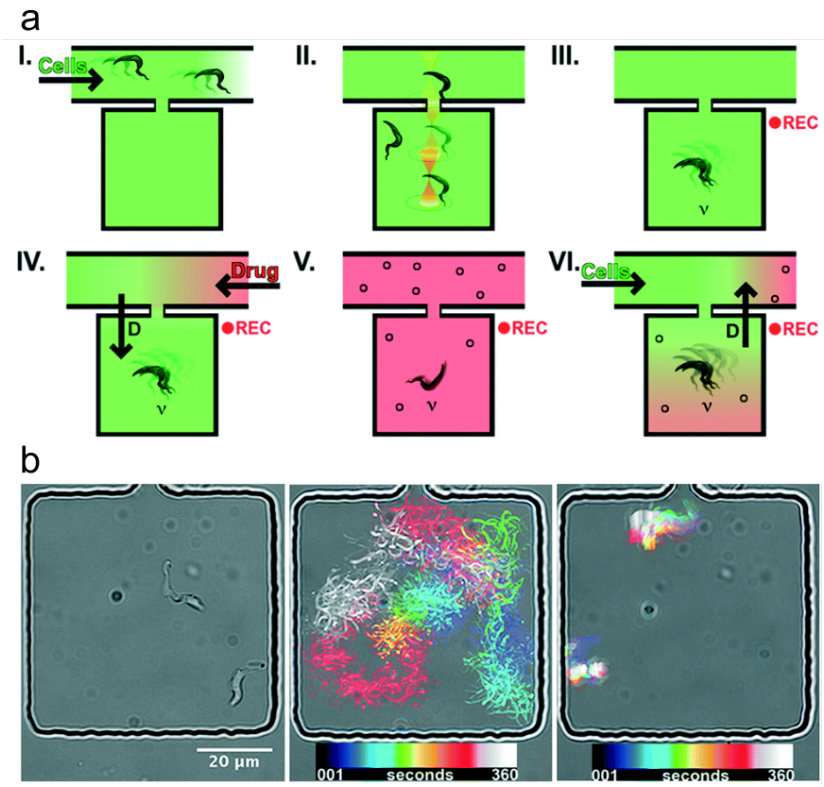

Figure 1.8: Drug effect on trypanosome motility by optical trapping. (**a**) Schematic representation of the microfluidic device and the procedure starting by loading the device with cells and medium (I), then cells are trapped by optical tweezers and placed inside the microchambers (II) where their displacement is recorded (III). A solution of a chosen drug is pumped through the main channel and diffuses into the microchambers (IV) until equilibrium is reached (V). The procedure is reversed with pumping in normal culture medium and the drug concentration decreases inside the microchambers (VI). (**b**) Bright-field micrographs of two trypanosomes confined in a microchamber (left). Overlaid color-coded time lapse trajectories of trypanosomes over 6 min in normal culture medium (middle). Time-lapse trajectories over 6 min after addition of glutaraldehyde normally used for fixation (right). The figure is adapted from Hochstetter *et al.* [14].

1.2.3 Single-cell sequencing

The most recent attempts on studying single-cell trypanosomes are sequencing of single-cell RNA based on the well established microfluidic technique, droplet-based microfluidics. Droplet-based microfluidics allows the generation of thousands of multiplex micro systems and will be further elaborated in the next section (1.3). Three studies have successfully used a single-cell RNA sequencing approach on insect forms and BSF trypanosomes by a droplet-microfluidic system (Fig. 1.10). In brief, barcoded micro beads are individually encapsulated with single cells and the required reagents for sequencing (Fig. 1.10a). Each cell is now designated to a unique barcode released from the bead which will be attached to the cells RNA (Fig. 1.10b). By reverse transcription

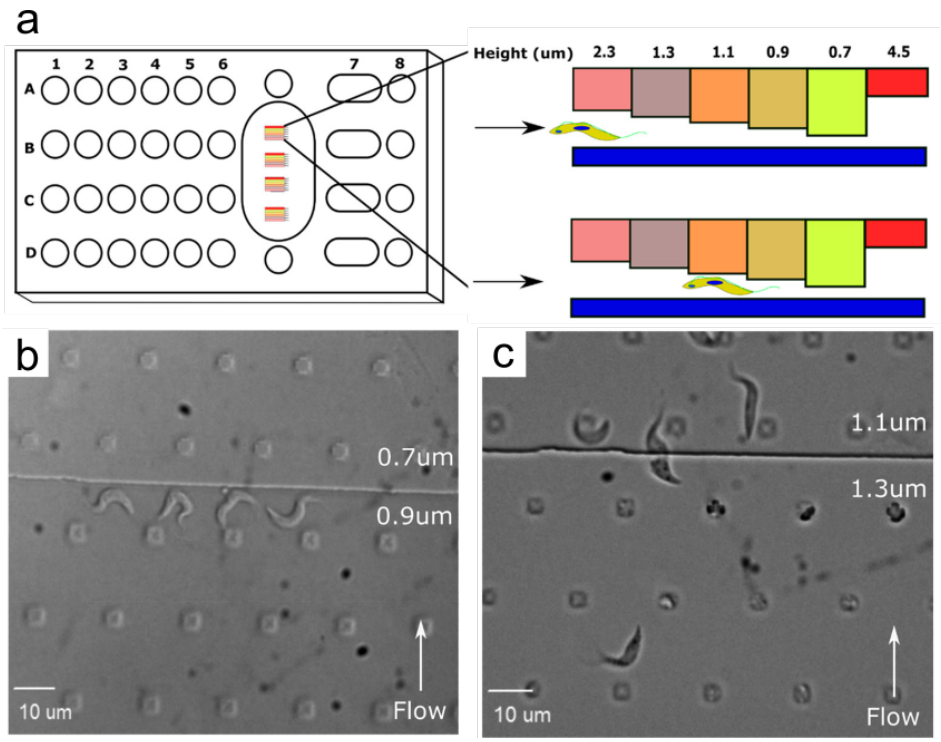

Figure 1.9: Trypanosome trapping for single-cell real-life imaging. (**a**) Representation of commercialized microfluidic device (left) with colored strips representing the different heights of the compartments. By applying flow, cells are pushed from the left side through the device until they are trapped between the bottom glass (blue bar) and the different ceiling heights (right). Based on size difference the cells are trapped in different areas of the device. (**b**) Representative DIC microscopic images of BSF and (**c**) procyclic trypanosomes immobilized in the microfluidic trapping device. The trapping heights are shown on the images along with the direction of flow. The figure is adapted from Voyton *et al.* [110]

and PCR, the unique barcoding is incorporated to the cells mRNA, and the specific RNA sequence from the cell can now be identified from thousands of other cells (1.10c) [111]. This method was first used on *T. b. brucei* isolated from the tsetse fly in 2020. Vigneron *et al.* used a commercialized droplet system, 10x genomics [112], where they extracted cells from the salivary glands of the tsetse fly. They identified three major clusters representing the epimastigotes and the pre- and mature metacyclics. The metacyclics showed a diverse pool of expressed VSG, but with each cell only expressing one type of VSG [16]. Later, Hutchinson *et al.* (2021) confirmed the singular expression of VSG in mature metacyclics using the inDrop system described by Zilionis *et al.* (2016) [111]. They further analysed the developmental program in the salivary glands, and revealed that pre-metacyclics express multiple VSG genes before the expression of only one in the mature metacyclic stage [113]. Briggs *et al.* (2020) also used the commercialized system 10x genomics but on *T. brucei* BSF to model the asynchronous differentiation from long slender to short stumpy. They captured the transcriptomes

of 9000 individual cells and found the gene ZC3H20 essential for differentiation with a temporary high expression at the transition point between slender and stumpy [114].

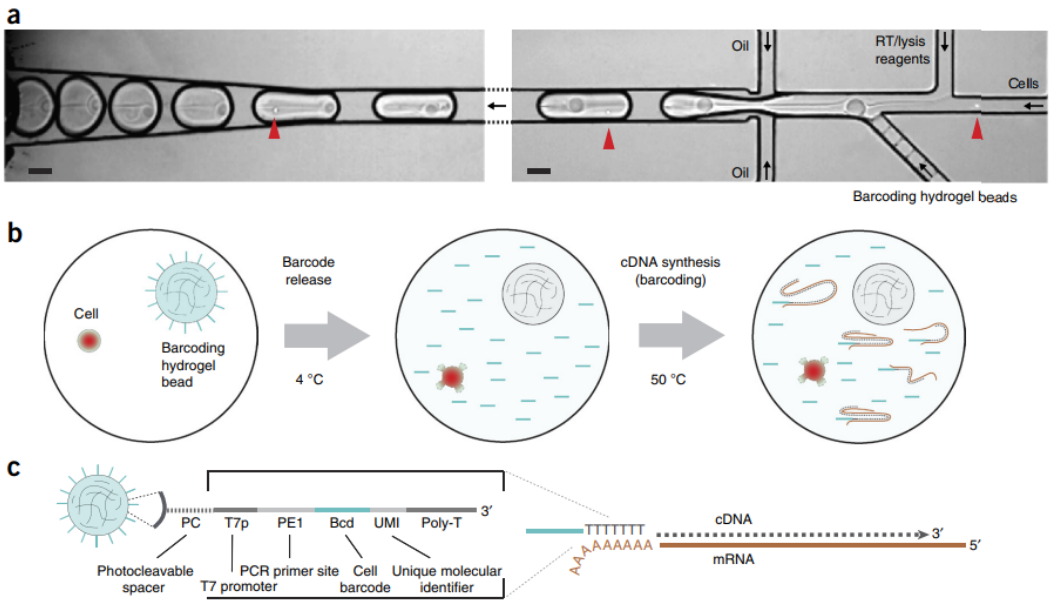

Figure 1.10: Barcoding in single cells for sequencing. Example of the process for single-cell RNA sequencing used in all three studies described. (**a**) Coencapsulation of barcoded microbeads, cells (red arrows) and reverse-transcription lysis reagents in microfluidic droplets. (**b**) Schematic representation of single-cell barcoding steps including release of cDNA from microbeads and attachment to the cells mRNA. (**c**) Representation of the barcoding structure on the microbead. The figure is reproduced from Zilionis *et al.* [111]

While these techniques have shown promising in isolating single parasites from the total population, they exhibit a relatively low throughput for analysis of living cells. To obtain better quantitative measurements representing a total population including possible cell variability herein, a system for higher throughput of single cell analysis is needed. The single-cell sequencing approach presented here relies on cell lysis shortly after encapsulation to access the genomic content of the cells. However, the droplet-based microfluidic system they use holds all the needed qualities for high-throughput analysis of confined single cells, and is therefor the main technique used in this thesis.

1.3 Droplet-based microfluidics

Droplet-based microfluidics is the technology of creating and manipulating microcompartment droplets commonly by controlled mixing of two immiscible fluids inside micro channels. This allows a high-rate generation of monodispersed droplets with sizes ranging from femto- to nanoliters [7, 115, 116, 117]. For biological and chemical analysis, droplet-microfluidics brings several advantages making it a prominent tool in

research. The small volumes of the droplets produced open the possibility of molecular or single-cell analysis in miniaturized assays significantly decreasing the use of reagents. Furthermore, the full compartmentalisation of reagents permits independent manipulation, making each drop working as individual mircoreactors. Finally, the high monodispersity between drops in a high-throughput manner, provides a qualitative and quantitative analysis platform for parallel and continuous processing of drops [117, 34, 118, 35].

1.3.1 Dynamics of droplet-based microfluidics

Droplet-microfluidic systems are based on the use of two immiscible liquid phases. A continuous phase is coflown with a disperse phase, thereby creating the droplets. In general, the droplet generation is controlled by the geometries of the microfluidic channels, the flow rates and the density and viscosity of the used fluids. Four types of forces control the droplet generation; inertial force, viscous force, gravity and capillary force. Their relative importance is characterized by dimensionless numbers which determine the droplet production properties as volume, frequency and dispersity [116, 119, 120].

The ratio of internal to viscous stress gives the Reynolds number, Re, related by the density ρ, the velocity u, the viscosity η and the characteristic dimension of the system L.

$$Re = \frac{\rho u L}{\eta} \tag{1.1}$$

In microfluidics, Re is usually characterized by values lower than 1 due to the small sizes of the micro systems. The inertial stress is thereby dominated by the viscous stress yielding laminar flow over turbulent (Fig. 1.11a-b) [115, 116, 120].

For droplet production, the most important dimensionless number is the Capillary number, Ca, describing droplet deformation. Ca is the ratio of viscous stress to capillary pressure relating the viscosity η and velocity u to the interfacial tension, γ.

$$Ca = \frac{\eta u}{\gamma} \tag{1.2}$$

Low Ca numbers lead to a droplet production controlled by the geometry of the micro channels. A droplet is pinched off from the continuous phase squeezing the disperse phase after a rise in pressure from obstruction of its flow (Fig. 1.11c). When increasing Ca the droplet production enters first the dripping regime before turning into jetting when viscous forces dominate over interfacial tension (Fig. 1.11d-e). In

droplet-microfluidics Ca typically ranges between 10^{-3} to 10 [121, 119, 120].

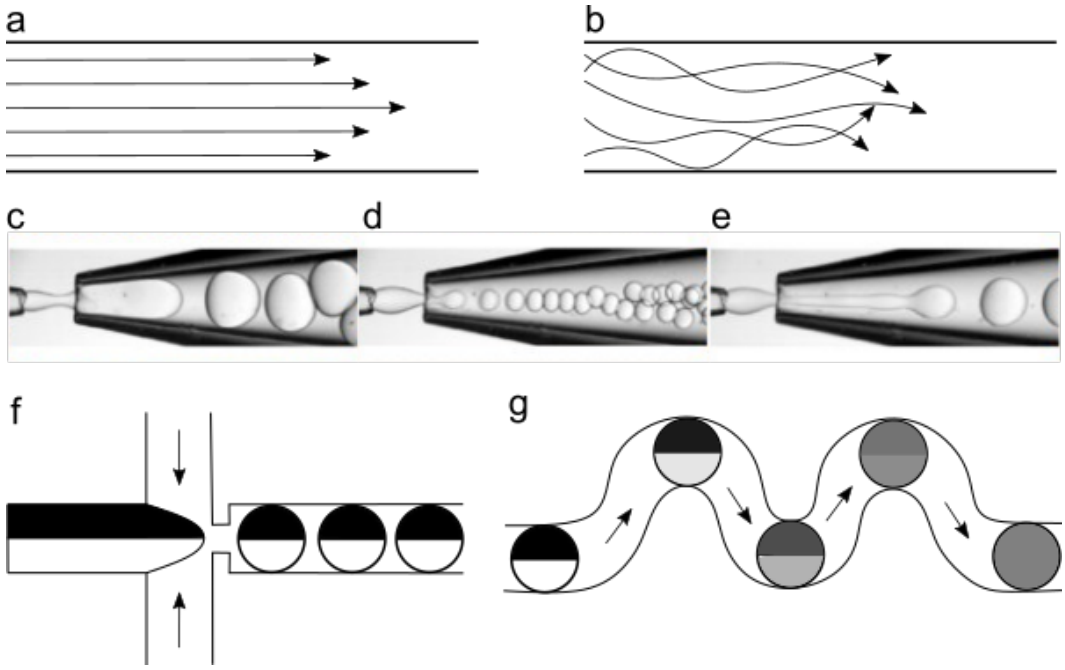

Figure 1.11: Flow dynamics in micro channels. Characteristics of laminar flow at Re smaller than 1 (**a**) and turbulent flow at Re larger than 1 (**b**). The different break-up regimes when increasing Ca, starting from squeezing (**c**) moving to dripping (**d**) and eventually jetting (**e**). (**c-e**) are adapted from Zhu *et al.* [120]. Mixing of a multi-dispersed phase in laminar flow (**f**) are dominated by convection and require specialized geometries (e.g. zig-zag) for proper mixing (**g**). Black arrows are indicating flow directions.

When working in laminar flow, which is typical for droplet-mircofluidics, the mixing of components are characterized by the Péclet number, Pe. Pe is the relative importance of convective and diffusive transport, relating the velocity u, the dimensions of the system L and the diffusion coefficient D.

$$Pe = \frac{Lu}{D} \tag{1.3}$$

In most droplet-microfluidic systems yielding laminar flow, Pe is usually larger than 1 indicating convective transport dominating over diffusion (Fig. 1.11f). For using drops as microreactors proper mixing of components is important and can be overcome by introducing special geometries in the micro system (Fig. 1.11g) [122, 123].

Working with two phases like in droplet-microfluidics the relative importance of gravity to capillary pressure can be described as the Bond number, Bo. Here the density difference $\Delta\rho$ of the two phases is related to the gravitational acceleration g,

the characteristic dimension of the system L and the the interfacial tension, γ.

$$Bo = \frac{\Delta\rho g L^2}{\gamma} \tag{1.4}$$

When the two phases used are liquid-liquid, like water-in-oil emulsions, $\Delta\rho$ becomes very small together with the size scale of the systems. These small values make the importance of the gravity force negligible for droplet formation in most droplet-microfluidic systems [116, 120].

1.3.2 Droplet formation

Droplet formation in microfluidic devices can be performed by passive or active methods. Where active methods involve additional energy-input by external elements, passive methods only rely on pressure-driven flow derived from syringe or pressure pumps. In passive droplet formation the dispersed phase is introduced into the continuous phase in a microfluidic device. Three main device geometries are characterized as cross-flow, co-flow and flow focusing [116, 120].

The first creation of monodispersed microcompartment droplets in a microfluidic device was performed by Thorsen *et al.* in 2001 using a T-junction cross-flow break-up model [115]. In cross-flow droplet breakup the dispersed phase typically meets the continuous phase at an angle on the main channel from a T-junction structure (Fig. 1.12a). Other geometric structures represent cross-flow droplet break-up, but are all in common characterized by one inlet for each of the liquid phases [120].

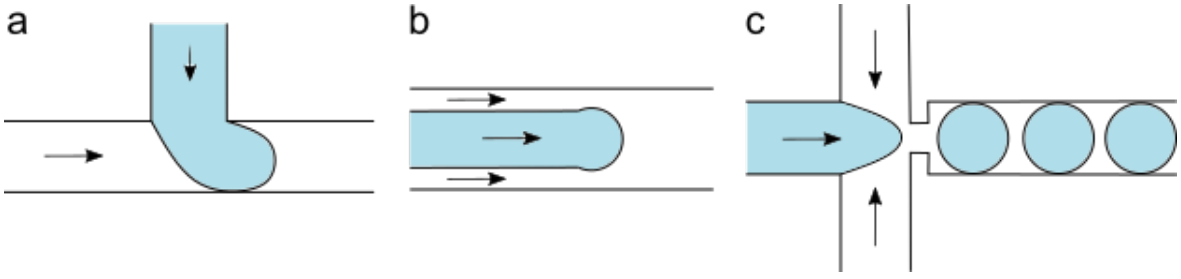

Figure 1.12: Droplet break-up models. Schematic representation of the three major break-up models for droplet formation. (**a**) Cross-flow break-up in a T-junction structure. (**b**) Co-flow break-up by parallel flow of the dispersed and continuous phase. (**c**) Break-up by flow-focusing where the dispersed phase is squeezed between two opposite-directional flows of the continuous phase. Black arrows are indicating the flow directions of the dispersed phase (blue) and the continuous phase (white).

The co-flow break-up model has a simple geometry of two concentric micro channels with the dispersed phase flowing in the inner channel, and the continuous phase

flowing in parallel in the outer channel (Fig. 1.12b). Emulsions created by co-flow was first performed by Umbanhowar *et al.* in 2000 [124], and was later implemented in a microfluidic context by Cramer *et al.* (2004) [125]. Droplet production by a co-flow module can be configured both in quasi-two-dimensional (2D) and three-dimensional (3D) systems [120].

Droplet break-up by flow focusing was first demonstrated in a microfluidic device by Anna *et al.* (2003) [126]. In flow focusing droplet production the dispersed phase is squeezed by a counter flow of two streams of the continuous phases (Fig. 1.12c). Both phases flow through a contraction region generating an elongation field eventually leading to droplet break-up [116].

1.3.3 Systems for droplet manipulation

Some of the benefits of using droplet-microfluidics are the ability of manipulating and controlling droplets after production, and thereby using them as micro reactors for biological and chemical applications. For this reason, micro systems are continuously under development. One important aspect in biochemical assays is mixing of reagents allowing chemical synthesis, kinetic studies and organic reactions. In these cases, controlled merging of individual droplets are crucial for initiating reactions [127, 117]. Adding reagents into drops is characterized through passive merging, active merging and picoinjection. Passive drop merging is controlled by specified geometries of the micro channels. Structures like temporary channel expansions (Fig. 1.13a) or micro pillars have shown to induce coalescence of two drops flowing in series [128, 129]. Active drop merging involves applying external forces to the system and can be necessary for merging when droplets are stabilized by surfactants. A commonly used method for active drop merging is applying an electric field to the system (Fig. 1.13b) [130, 131, 132]. Other techniques shown to induce drop merging are thermally triggered coalescence controlled by a laser or local heating in the device [133, 134]. A great advantage of the above mentioned active merging techniques is controlled activation on demand.

Another way of adding reagents to stabilized droplets without the complexity of synchronizing flows of multiple drops is by picoinjection [135]. Here, an adjoining channel is introduced to a flow of drops where the liquid phase is held by a constant pressure (Fig. 1.13c). Droplets can pass by the adjoined liquid phase without coalescing due to surface stabilization. When an electric field is applied the droplet interface is disrupted and the liquid is injected into the passing droplets.

In addition, some applications require breaking up droplets for reduced volumes

[136]. Droplet splitting is the division of drops into smaller daughter drops. Like for droplet merging, the splitting process can be both passive and active. The most straight forward method is using a bifurcated channel like a T-junction split (Fig. 1.14a). Multiple series of dividing channels can be added to further divide the drops into smaller sizes [137, 138]. Active drop splitting can be activated by surface acoustic waves or pneumatic valve actuation [139, 140].

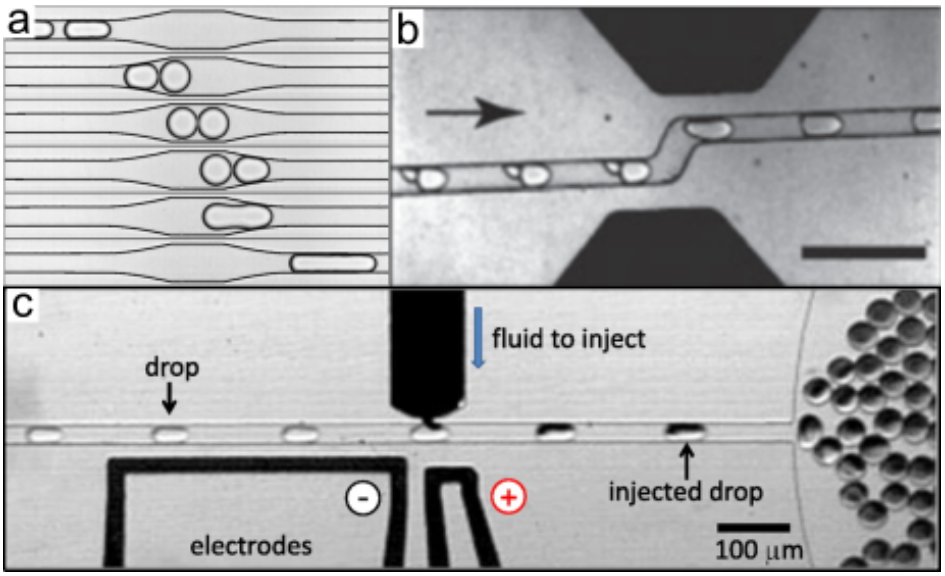

Figure 1.13: Microfluidic systems for droplet merging and picoinjection. (**a**) Passive droplet merging by temporary channel expansion. The picture is reproduced from Bremond *et al.* [128]. (**b**) Active droplet merging induced by applying an electric field. The picture is reproduced from Mazutis *et al.* [131]. (**c**) System for adding reagents into the drops by picoinjection, activated by applying an electric field. The picture is adapted from Abate *et al.* [135].

In biological assays, selection of cells in a population based on special activities or unusual behaviours are of great interest. In the following part, I briefly present different sorting methods used in the literature, where the specific use of sorting systems for single-cells will be presented later (section 1.3.4). Like in many other droplet manipulation systems, droplet sorting can be either passive or active. Passive sorting is based on the hydrodynamic interactions of the channel geometries and the droplet proportions. Smaller droplets can be guided away from the main flow of bigger drops through adjoining channels [141, 142]. Active droplet sorting is controlled by applying external forces as an electrical field in an asymmetric device [143]. Droplets will tend to follow the route with lower resistance until an electric field is applied. This technique have further been coupled with laser detection in fluorescence activated sorting (Fig. 1.14b). This method is highly used in single-cell analysis where cell-containing

drops can be selected based on fluorescence using fluorogenic substrate or live-dead cell assays [97, 103, 144]. Active sorting can furthermore be growth-dependent and controlled by optical detection, allowing selection of droplets based on cellular growth [145, 146].

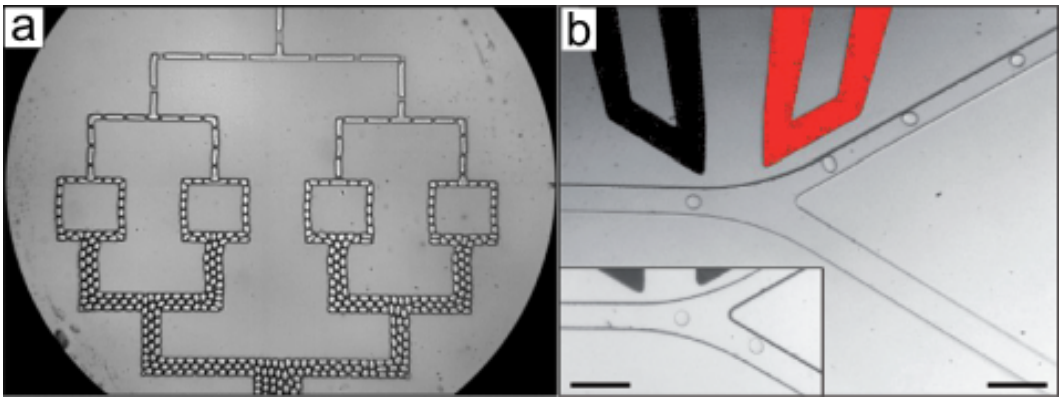

Figure 1.14: Microfluidic modules for splitting and sorting. (**a**) Microfluidic device for passive splitting of droplets in series. The picture is reproduced from Link *et al.* [137]. (**b**) Active droplet sorting induced by an applied electrical field activated by fluorescence. The picture is reproduced from Baret *et al.* [97].

Chemical and biological application assays often require incubation times ranging from few minutes to several hours. For scaling down such assays into droplet systems, proper storage of the drops is needed. One design enabling droplet incubation on-chip was performed by Huebner *et al.* (2009). A microfluidic device was constructed with multiple small traps where drops could be stored for optical monitoring over periods of time and released after use (Fig. 1.15a) [147]. For quantitatively better droplet analysis, special flow designs as the delayline have been developed [148, 103]. A delayline device typically consists of several small chambers connected with narrow channels allowing high-throughput droplet measurements at different time points (Fig. 1.15b). These microsystems can be designed as needed with incubation times ranging from a few minutes [149, 150] up to an hour [151, 152]. For some applications, longer incubation times at special conditions are however necessary. In these situation, a variety of different off-chip incubation strategies have been developed. The most simple collection systems are directly using classical laboratory equipment as Eppendorf tubes and Pasteur pipettes [144, 146, 8]. A more advanced collection system have been developed by Mahler *et al.* where the collection device are connected to a pumping unit continuously oxygenating the collected drops (Fig. 1.15c). This enabled longer storage and increased biomass from different species of encapsulated cells [153]. Incubation in temperature controlled incubators are essential for longtime storage of most microor-

ganisms. A simple chamber for monolayer droplet collection and storage have been fabricated by Eyer *et al.*, enabling continuously monitoring of a large number of drops (∼40.000) over time (Fig. 1.15d) [154]. Though such an incubation device do not permit reinjection on-chip for further analysis like the devices mentioned before, it is an interesting tool for easy monitoring and imaging of single cells.

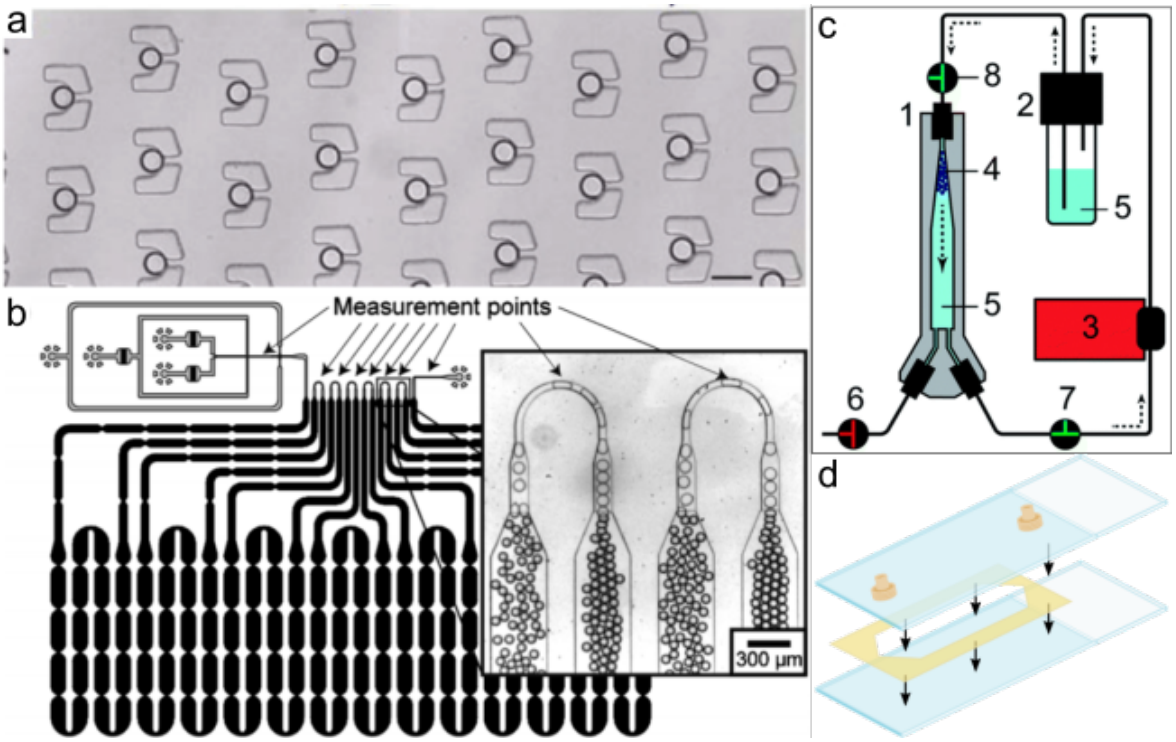

Figure 1.15: Microfluidic systems for droplet trapping and incubation. (**a**) Device for trapping individual drops for on-chip incubation. The picture is reproduced from Huebner *et al.* [147]. (**b**) Delayline system permitting droplet incubation and measurements in a time scale ranging from a few minuets to an hour. The picture is reproduced from Frenz *et al.* [148]. (**c**) Off-chip collection device for long-time storage and oxygenation of system. The picture reproduced from Mahler *et al.* [153]. (**d**) Schematic representation of off-chip incubation chamber for optical monitoring of monolayer drops during long-time storage. The illustrated chamber is recreated from Eyer *et al.* [154].

1.3.4 Droplet-based microfluidics with single cells

Analysis of cellular behaviour at a single-cell level have led to the discovery of cell-to-cell heterogeneity in seemingly isogenic populations. Along with an increasing availability and improvement of single-cell technologies, biological fields are showing raised interest on single cell studies. Despite the recognition of heterogeneity within isogenic populations, many cell studies are still based on bulk average measurements with assumptions of an equal contribution from each cell [155, 30, 32, 156, 157]. With total compart-

mentalization of single cells, droplet-based microfluidics are overcoming the misleading results from bulk experiments [34, 9]. Where bulk analysis are based on a population average, droplet-based microfluidics enable the analysis of every single cell in a population (Fig. 1.16). For adequate single-cell analysis in confined droplets, efficient cell encapsulation and viability is a requisite.

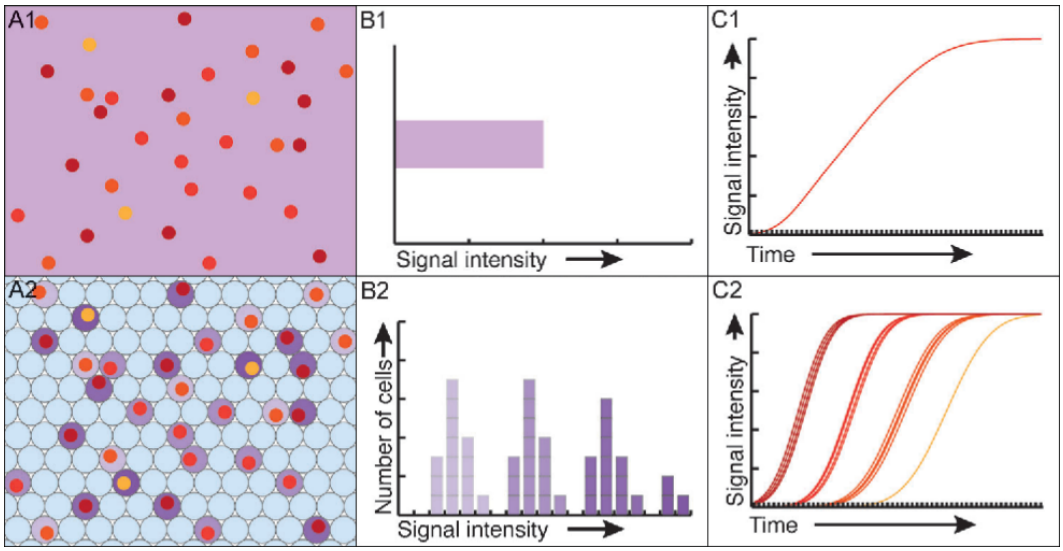

Figure 1.16: Bulk vs. single cell analysis. An illustration of the differences between in-bulk analysis (**A1**) and single-cell analysis (**A2**). Analysis of in-bulk populations will yield the average of cellular activities or behaviours (**B1,C1**), where single-cell analysis can characterize a variety of different activities and behaviours within a population (**B2,C2**). The figure is adapted from Joensson and Svahn[34].

Emulsification of a cell population follows the Poisson distribution given by;

$$f(\lambda, n) = \frac{\lambda^n e^{-\lambda}}{n!} \tag{1.5}$$

where n is the actual cell occupation number and λ is the average cell number per droplet volume [158]. To ensure a droplet occupation of no more than one cell per drop, the production of empty drops will by far dominate the production of single-cell containing drops. However, with the high-throughput in droplet production this is in most cases not an issue in single-cell studies [159]. Higher quantities of cell-containing drops can be achieved by coupling of additional techniques such as pre-encapsulation cell ordering [160, 161] or post-encapsulation droplet sorting [162].

Multiple types of single cells and even multicellular organisms have successfully been used in a droplet-based platform [9, 34] including bacteria [97, 159], yeast [99], algae [163], *C. elegans*, mammalian and human cells [101, 103]. Droplet-microfluidics provides means to encapsulate these cells in suitable micro environments with equal

access to respiratory gasses. These benefits not only permit sufficient survival time for carrying out long experiments but also enable cell proliferation over longer periods of time from several hours to days [97, 164, 163]. Several studies have taking advantages of complete isolation of cells e.g. for detection of protein expression [147] and screening of various cell-secreted compounds as antibodies [165, 144], cytokines [151, 166] or enzymes [167, 168]. A coupling with additional sorting modules further provide beneficial platforms in research of directed evolution. Encapsulating single cells with enzyme-specific substrate allow detection of active cell variants. By fluorescent activated sorting, highly active variants have successfully been selected to further use in more rounds of selection or to break-up the emulsion for re-cultivating the cells [97, 149].

A key application of droplet-based microfluidics is the characterisation of heterogeneity within populations. Variability between cells can be defined in multiple ways including those described above. One way described earlier, is the performance of single-cell transcriptomic analysis and sequencing [16, 169, 112]. Where these procedures however require cell lysis for release of genomic content, other studies have analysed population variability on living cells. Boediciker *et al.* (2009) not only revealed a heterogeneous pattern in quorum sensing between cells confined in different drops, but also between the cells confined within the same drop. As exemplified in Fig. 1.17, three drops each contained two cells at the beginning of an experiment. After eight hours of incubation all drops showed similar growth, but the cells of one drop did not initiate quorum sensing. Additionally, another drop contained cells both with and without initiated quorum sensing indicating a heterogeneous pattern within the population [170]. In another study, Del Ben *et al.* (2016) described a system exploiting the increase of lactate secretion from cancer cells (Fig. 1.17d-f). The presence of lactate was measured both directly and indirectly from an assay inducing fluorescence from lactate or from a change in pH. This enabled the detection of sick cancer cells from a population of healthy cells [171].

These studies are merely exemplifying the promising yet significant use of droplet-microfluidics for revealing heterogeneous dynamics in cell populations. With the ability to detect both the presence and activity of various secreted compounds, we here have a tool for identifying and selecting special cell variants. This brings deeper insight of the cellular dynamics on an individual and population level and can further give us important information in prominent areas as drug development and diagnostics.

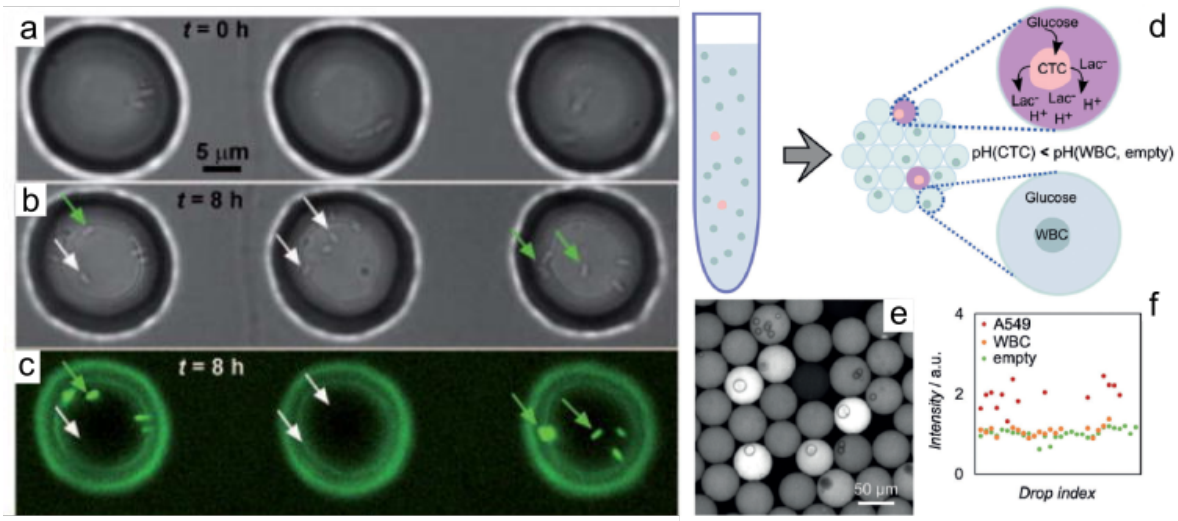

Figure 1.17: Cellular heterogeneity within populations. Detection of quorum sensing between droplet-confined cells (**a**). After eight hours of incubation the cells have proliferated equally (**b**), where some cells have initiated quorum sensing (green arrows) and others have not (white arrows) (**c**). The picture is adapted from Boedicker *et al.* (2009) [170]. Detection of cancer cells based on lactate secretion (**d**). Increased fluorescence from drops containing cancer cells and not from healthy cells (**e**). Quantification of fluorescence between empty drops, drops with healthy cells and drops with cancer cells (**f**). The picture is reproduced from Del Ben *et al.* (2016) [171].

1.4 Thesis objectives

In this thesis, I aim to combine the main parts presented in this chapter by studying the *T. b. brucei* parasite on a single-cell level using droplet-based microfluidics.

Trypanosomes are organisms going through a complex life cycle involving different hosts and adaptation mechanisms to many different environments. While still very little is known on a single cell level, I here investigate the dynamics of single trypanosome cells. For the compartmentalization of single cells, we designed, assembled and used a homemade setup. I first present the main techniques used for encapsulation and analysis of cells. Then, I describe the compatibility of implementing trypanosome cultivation in a droplet-based microfluidic platform. I then use the platform to analyse the activity of secreted enzymes from single cells. Finally, I test the system in different applications all involving the analysis of dynamic behaviours of *T. b. brucei* on a single-cell level.

2 Experimental techniques for droplet-based microfluidics

In this chapter, I introduce the development and implementation of the microfluidic techniques used throughout the work presented in this thesis. I describe the setup we designed and constructed and its functions used to perform all experiments performed in a droplet-based microfluidics format. I present the main methods for droplet production and measurements together with the fabrication of the microfluidic devices. The specific methodologies for each experiment are elaborated further in the individual chapters.

2.1 Microfluidic setup

For production, observation and fluorescence measurement of microcompartment droplets, I use a home-made microfluidic setup by adapting an inverted microscope (Axiovert 135, Carl Zeiss). Fluorescence is excited by a continuous laser at 473 nm (Cobolt 06-MLD, Cobolt AB) attenuated through a reflective optical density filter (OD) (Thorlabs). The laser is guided by an optomechanical mirror (M) and a dichronic mirror (DM) (Thorlabs) through the observation objective of the microscope (Zeiss LD Achroplan 40×/0.6 Korr Ph2 for laser measurements) focused on the drops (Fig. 2.1). All other optical observations are through a 10×/0.25 Ph1 objective (Zeiss Achroplan). The laser is enclosed by black sheets of hardboard, with exception of the outlet hole for the laser beam and a small passage for power cables, to reduce noise from background light. Emitted fluorescence from the sample is guided back through a notch filter (NF) and a beam splitter (BS). One beam is filtered by a band pass filter (BF) at 525 nm and 50 nm width (525/50 BrightLine HC) and collected through a pinhole (P) by a photo multiplier tube (PMT) (H10723, Hamamatsu Photonics K.K.) at 10 kHz with a NI data acquisition card (DAQ) (NI USB 6008). The other beam is directed to a Blackfly®S USB3 high-speed camera (FLIR Systems) mounted on the top camera port

of the microscope where the ocular piece have been removed. Fluorescence collection is performed in confocal configuration to reduce background noise. The entire setup is fixed on an aluminium platform with vibration dampening feet to reduce vibration noise from the surroundings. All flow rates of fluids in the sample devices are controlled by three low pressure neMESYS syringe pumps (CETONI) connected and controlled by a laptop, from where all data are collected.

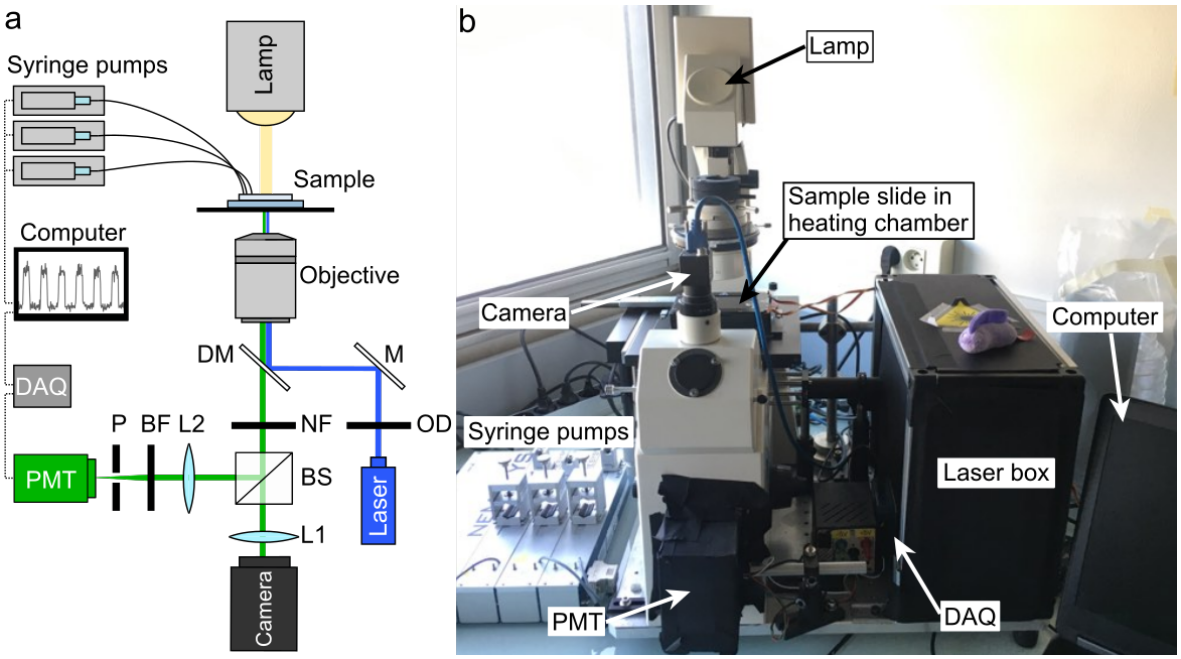

Figure 2.1: Illustration of homemade microfluidic setup. (**a**) Schematic representation of the microfluidic setup, (**b**) and a real photo of the setup in the lab. The setup is constructed by implementing the following components to an inverted microscope; syringe pumps, computer for control and acquisition, data acquisition (DAQ) card, photomultiplier tube (PMT), pinhole (P), band pass filter (BF), PMT lens (L2), dichroic mirror (DM), notch filter (NF), beam splitter (BS), camera lens directly from microscope (L1), mirror (M) and optical density filter (OD). Illustration is created in Inkscape (`https://inkscape.org`).

2.1.1 Laser and sensor calibration

All fluorescence measurements are recorded by the PMT as the voltage U and are transformed into relative fluorescence unit (RFU) by rescaling with the gain G: $RFU = U/G^{8.7}$. This allows us to compare data obtained at different gain values. The exponent 8.7 are given by the manufacturer of the PMT and depends on the PMT types. The PMT value is here experimentally verified from a number of measurements of fluorescent samples recorded with different gain values (Fig. 2.2). Droplets containing fluorescein concentrations of $0.05\,\mu g\,mL^{-1}$, $0.1\,\mu g\,mL^{-1}$, $0.5\,\mu g\,mL^{-1}$, $1\,\mu g\,mL^{-1}$ and $5\,\mu g\,mL^{-1}$ are recorded with gain values fitting the respective concentrations. For each

concentration I use four different gain values (Table 2.1). When the data are plotted as log(recorded signal/fluorescein conc.) as a function of log(gain value), the PMT value is found as the slope of the linear fit.

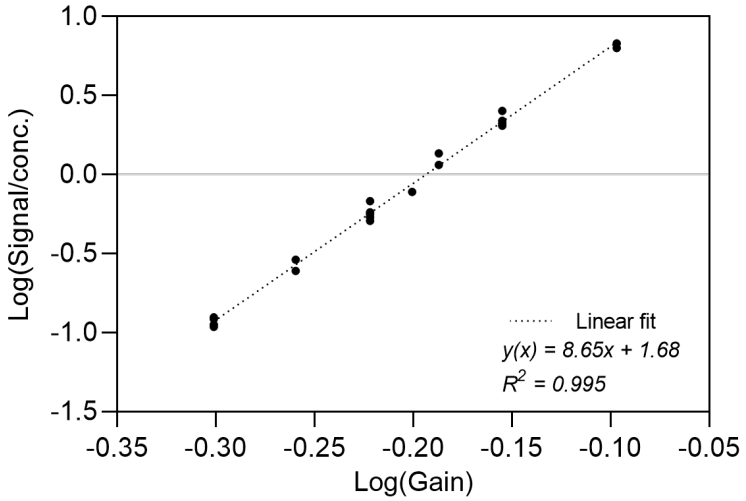

Figure 2.2: Verification of PMT value. The exponent for the PMT is found as the slope of the linear fit by plotting the logarithmic values of the recorded signals over the fluorescein concentrations as a function of the gain values. The exponent 8.65 is consistent with the supplier datasheet.

To ensure a good sensitivity for detection of low fluorescence, two different OD filters are tested. By changing from a ND20A (1% transmission) to a ND10A (10% transmission) filter, the detected RFU is expected to increase by a factor 10. I measure fluorescence from droplets containing fluorescein concentrations as used above and recorded by the same gain settings. For the ND20A filter I use fluorescein concentrations of $0.1\,\mu g\,mL^{-1}$, $0.5\,\mu g\,mL^{-1}$, $1\,\mu g\,mL^{-1}$, $5\,\mu g\,mL^{-1}$ and $10\,\mu g\,mL^{-1}$ recorded with gain values fitting the respective concentrations (Table 2.1). RFU values are plotted as a function of fluorescein concentrations, where each data point is the mean RFU of four different gain values for each fluorescein concentration (Fig. 2.3a). We observe that the recorded RFU with OD filter ND10A has indeed increased by a factor 10. This is seen by the upward shift of the fitted plot at the y-axis intersection. The equations of the best fitted lines are presented in Table 2.2. We furthermore observe that the detected background only have increased by a factor 2, confirming the improved sensitivity of the system.

As the setup was build in one location (CRPP lab) and later moved to another (MFP lab), the sensitivity of the laser is checked again after transfer. The same fluorescein concentrations and gain settings are used as for the ND10A measurements above. The

Table 2.1: Gain settings for fluorescence detection. The different gain settings used for each fluorescein concentration in the experiments of PMT exponent verification and sensitivity of setup presented in Figure 2.2 and 2.3.

Fluorescein conc. ($\mu g\,mL^{-1}$)	Gain settings (PMT ver. and ND10A)	Gain settings (ND20A)
0.05	0.55	-
	0.6	-
	0.65	-
	0.7	-
0.1	0.5	0.85
	0.6	0.9
	0.7	0.95
	0.8	1
0.5	0.5	0.6
	0.6	0.7
	0.7	0.8
	0.8	0.9
1	0.5	0.6
	0.6	0.7
	0.65	0.8
	0.7	0.9
5	0.5	0.5
	0.55	0.6
	0.6	0.7
	0.63	0.8
10	-	0.5
	-	0.6
	-	0.7
	-	0.75

measured RFU for the droplets and their backgrounds are plotted for the two different locations as a function of fluorescein concentrations, where RFU is the mean value detected from four different gain settings (Fig. 2.3b). We see no difference between the detected RFU of the droplets from each location, where only a small insignificant difference is observed for the background RFU (Table 2.2). I thereby manage to keep the good sensitivity after movement demonstrating the portability of the setup.

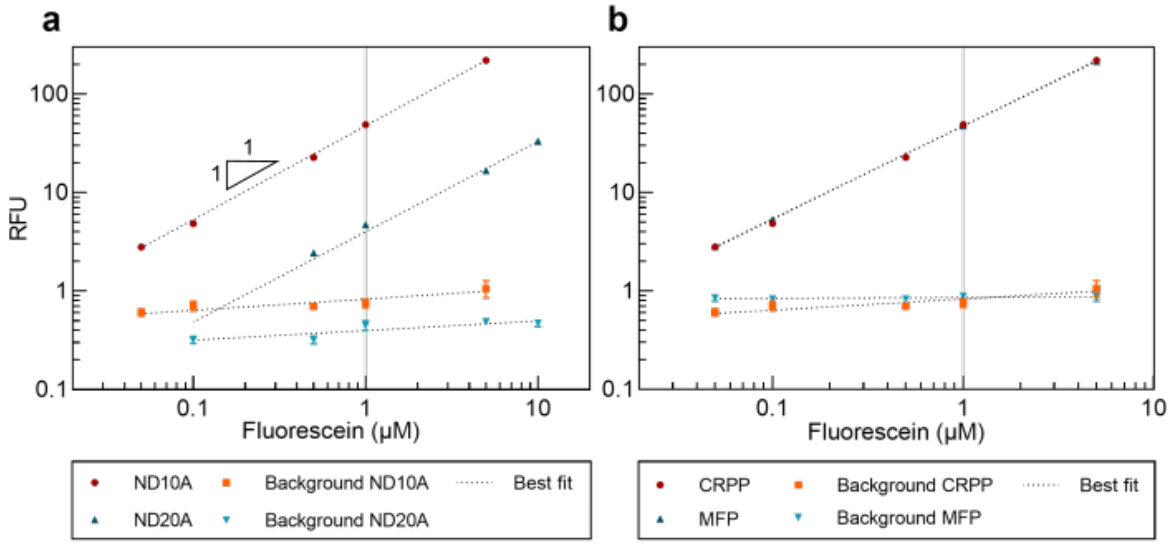

Figure 2.3: Sensitivity of microfluidic setup. (**a**) Sensitivity was tested with two different optical density filters, ND10A and ND20A. Fluorescence measurements of fluorescein-containing droplets and the respective background values are plotted as RFU as a function of fluorescein concentrations. (**b**) The optimal sensitivity was verified for the final setup by repeating the experiment with the same conditions after change of location from one lab (CRPP) to another (MFP). Equations of the fitted plots are presented in Table 2.2 for all the graphs.

Table 2.2: Fitted values of sensitivity plots. Equations and goodness of fit for the fitted lines of the plotted data points ND10A, ND20A, and their backgrounds before and after movement of setup presented in Figure 2.2 and 2.3.

	Data set	$y(x) =$	$R^2 =$
CRPP	ND10A	$47.64x^{0.95}$	0.999
	ND20A	$4.01x^{0.92}$	0.998
	Background ND10A	$0.83x^{0.11}$	0.614
	Background ND20A	$0.40x^{0.10}$	0.667
MFP	ND10A	$47.21x^{0.94}$	0.999
	Background ND10A	$0.86x^{0.01}$	0.044

2.2 Microfabrication

For production of the microfluidic devices used in this work, I use standard photo- and soft lithography techniques [172, 173, 174, 175]. The designs of the different devices are created with the computer-aided design (CAD) software (Autocad, Autodesk Inc.) and printed on transparent photomasks (CAD/Art Services, Inc., SELBA S. A. for high-resolution printing (50800 dpi)) (Fig. 2.4a). A silicon wafer is poured with negative photoresist SU-8 3050 (SU8-3000, MicroChem Corp.) and spin-coated according to the wanted heights of the devices for 30 sec. (Table 2.3). After the negative photoresist have been equally distributed on the wafer, it is soft baked at 95°C for 15-30 min. After the wafer is cooled down, it is exposed to UV light through the customized photomask using a MJB4 mask aligner (SUSS MicroTec) for 30 sec. Following UV exposure the master mold is post baked at 95°C for 5 min before treatment with SU-8 developer (MicroChem) until all non exposed photoresist leftovers are removed. After development the mold is washed with isopropanol and placed at 180°C for 5 min. The final heights of the molds are verified by a 3D optical profilometer (ContourGT, Bruker) (Table 2.3).

Table 2.3: Settings for SU8 spin-coating. The specific settings used to obtain the different heights of the microfluidic devices from negative photoresist.

Device	Target height (µm)	Measured height (µm)	Rotation speed (rounds/min)
Classic	60	63±2	2700
Co-flow	60	60±1	2700
Dual	60	66±1	2700
Classic	80	85±2	1500
Classic	100	95±2	1000

The fabricated microfluidic devices are made from PDMS (Sylgard 184). PDMS comes with are large range of advantages [175, 174] including; device specificalities on a micron scale through molding techniques, transparent material allowing observation by microscopy and high compatibility with fluorescence detection techniques, and good biocompatibility being non-toxic and permeable to CO_2 and O_2 [175]. Finally, PDMS is a cheap and easy material to work with [174, 176].

A mixture of PDMS and a curing agent 10% (w/w) (Sylgard 184 kit) is poured on the molds, degassed in a vacuum chamber and cured at 70°C for at least 2 hours (Fig. 2.4b). The PDMS is peeled from the molds and cut into separate slabs for each

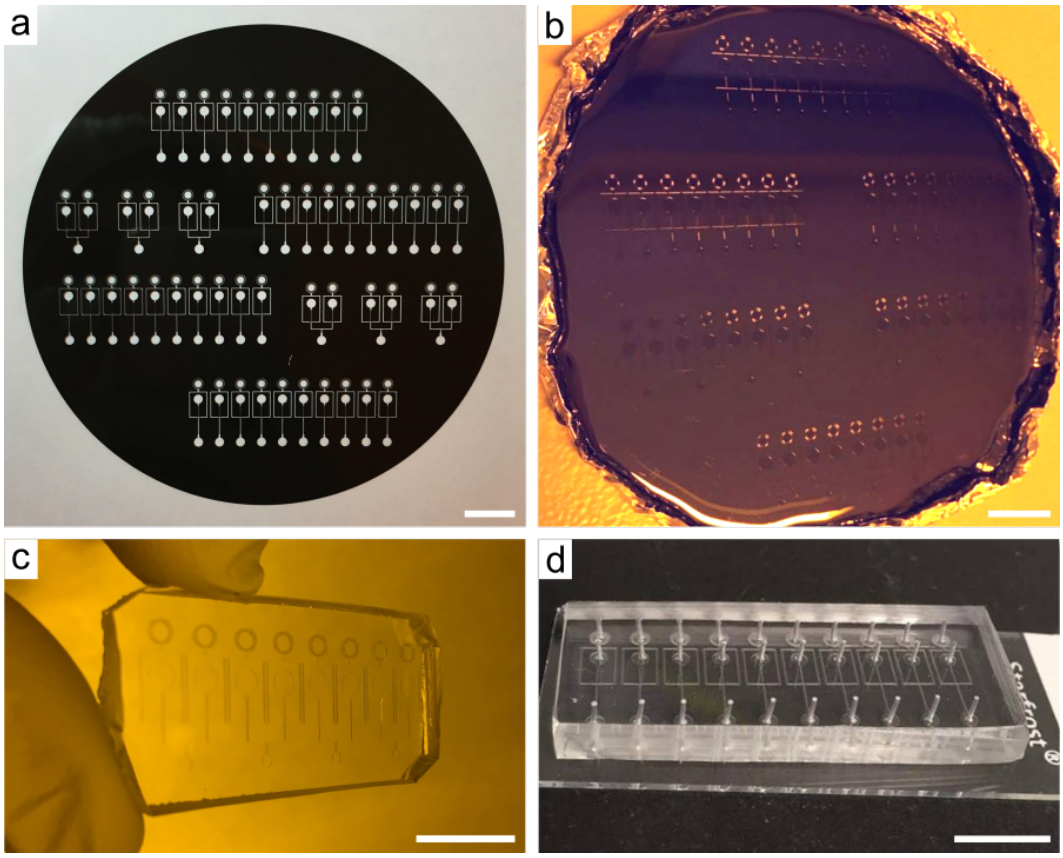

Figure 2.4: Examples of photo- and soft lithography techniques. (**a**) Customized photomask created by the designing CAD software. (**b**) Wafer with a master mold made from hardened negative photoresist poured with PDMS. (**c**) PDMS slab with imprinted designs. (**d**) Final device after punched holes and bonding with microscope glass slide. All scale bars are 1 cm.

design pattern (Fig. 2.4c) and inlet and outlet holes are punched with a 0.75 mm-diameter puncher. Prepared PDMS slabs and microscope glass slides are cleaned with isopropanol and dried prior to oxygen-plasma treatment (PICO Low pressure plasma system, Diener electronic). After surface treatment by plasma, the PDMS and glass slide are bonded by pressing the two components together and post incubated at 70°C for 15-20 min (Fig. 2.4d). The surface of the microfluidic channels are treated with fluoro-silane (Aquapel, PPG Industries) making them fluorophilic prior to use. All devices are flushed with argon before and after Aquapel treatment.

For all experiments in this work, I used different versions of the flow focusing technique for droplet production. The channel dimensions of the devices described in the following sections are varying according to the desired droplet sizes for the individual experiments.

2.2.1 Classic production device

For standard droplet production, I use a standard flow focusing device (Fig.2.5.). Fluorinated oil containing surfactant pinches of a flow of sample suspension, creating equal sized droplet microcompartments (Fig.2.5: Insert 1.). The devices consist of two inlets for oil and sample suspension, of where the oil-inlets have small constructions working as filters, and one outlet used for droplet collection or waste. The flow focusing devices are furthermore used for reinjection of droplets after the initial collection. The drops are reinjected through the sample suspension inlet lacking the filter constructions (Fig.2.5: Insert 2).

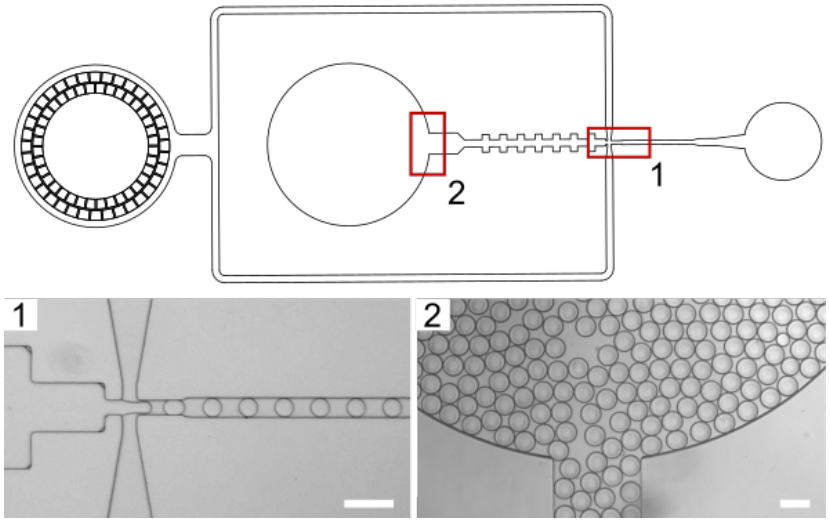

Figure 2.5: Classic droplet production device. Droplet production device based on flow focusing of two immiscible fluids (insert 1). The device consists of an oil inlet with filter constructions, a sample inlet also used for reinjection of drops after collection (insert 2) and an outlet for drop collection or trash. Scale bars are 100 µm.

2.2.2 Dual production device

For simultaneous production and collection of two different droplet populations, I use a dual production device. The device consists of two standard production devices in parallel with individual sample suspension inlets but with a joined oil inlet and collection outlet (Fig.2.6). The total droplet frequency f is found as the joined frequency from each of the parallel devices: $f_1 + f_2 = f$.

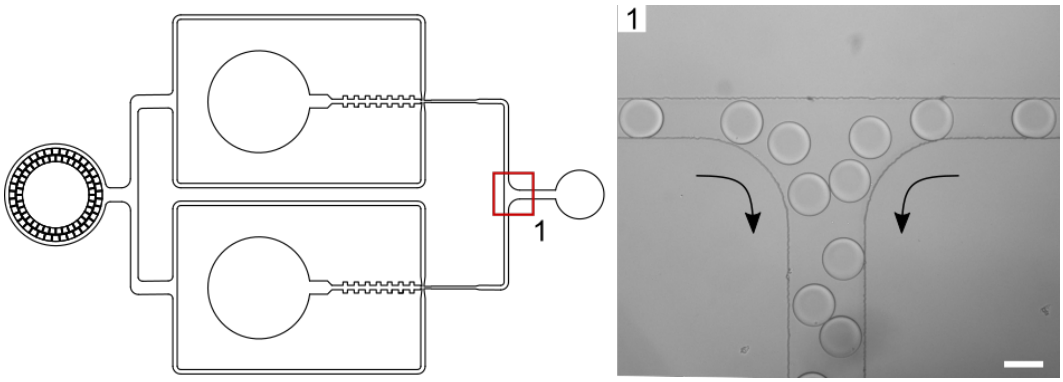

Figure 2.6: Dual droplet production device. Dual device consisting of two classic production devices in parallel with separate sample inlets and a joined oil inlet and joined droplet collection (insert 1). Scale bar 100 µm.

2.2.3 Co-flow production device

For working with enzymatic reactions starting on-chip, I use a co-flow device with two sample inlets for mixing reagents just in prior to droplet production. The two sample inlets are joined in a Y-shape junction just before the flow focusing of the oil creates the droplet compartments (Fig.2.7). In this device the total aqueous flow rate Q_{aq} are defined as $Q_{aq1} + Q_{aq2} = Q_{aq}$ with Q_{aq1} and Q_{aq2} being the individual flow rates for the two sample inlets.

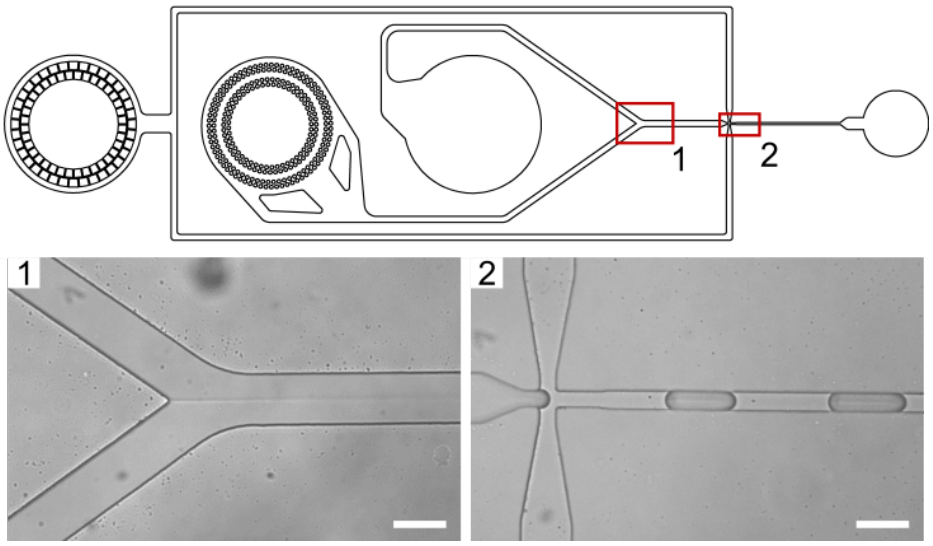

Figure 2.7: Co-flow production device. Co-flow device consisting of two sample inlets joined before drop making (insert 1). At drop making the two separate fluidic phases are still observed and will be mixed by diffusion over time (insert 2). Scale bars are 100 µm.

2.2.4 2D collection device

To observe drops as a two dimensional (2D)-array for longer periods of time, an incubation chamber was fabricated allowing movement for longer storage. The chamber is fabricated as previously described [154]. Glass microscopy slides are used as top and bottom covers (76×25×1 mm). Two holes are created in the top glass slide by micro-sandblasting (Fig.2.8). Both slides are cleaned using soap, water and ethanol and dried at 70°C. The desired chamber design is cut in a 60μm thick double-sided bonding tape (1375, SDAG, Adhesif) using a Graphtech cutting plotter (CE6000-40). The two cleaned microscope slides are then attached to each other using the bonding tape. 10-32 NanoPort^{TM} assembled with NanoTight^{TM} fittings (IDEX Health and Science) are glued on the inlet holes with UV curing glue (Loctite 3529, Henkel). The inner dimension of the incubation chamber is appx. 1×3 cm and 60 µm in depth corresponding to a volume of 18 µL and therefore provides multiplex measurement of over 10^4 droplets. The chamber is treated with Aquapel and dried with argon prior to use. The chamber is reused multiple times and cleaned between each experiment by flushing fluorinated oil. The incubation chamber can be connected to the outlet of the encapsulation device by external tubings. After filling, the incubation chamber can be detached from the encapsulation device and completely sealed. This enables transfer of the chamber to a cell incubator or a microscope when needed.

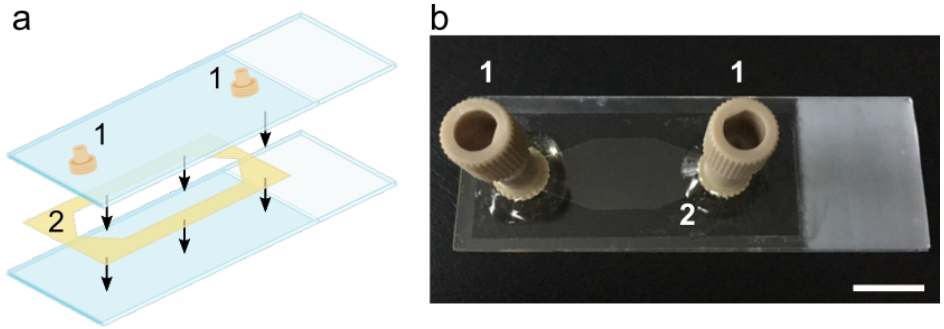

Figure 2.8: 2D incubation chamber. Schematic representation (**a**) and real presentation (**b**) of 2D incubation chamber. The chamber is build from two microscope glass slides, the top one joined with inlet assemblies for droplet access (1), bonded with a doubled-sided bonding tape. The tape is cut in a desired shape giving the actual dimensions of the chamber (2). Scale bar is 1 cm. The chamber is recreated from Eyer *et al.* [154].

2.2.5 3D collection device

For high-throughput fluorescence measurements of droplets over time, I use three-dimensional (3D) collection vials capable of containing 10^6 droplets or more, depending

on the size of the droplets and the vial. Two different vials are used, a plastic vial with an integrated micro insert of 400 µL and a glass vial with a volume of 2 mL (CARL ROTH) (Fig. 2.9a,b). The vials are closed with screw caps with holes sealed by silicone PTFE-coated blockers (CARL ROTH). In the silicone blockers two holes are punched for tubing in- and outlets allowing secure droplet filling and re-injection of the vials. The vials can be connected to the droplet production devices by external tubings to the outlet hole of the device. After collection, the vials can be detached and blocked for long term storage or incubation. For reinjection of the droplets, the opposite tube than used for collection can be attached to a syringe to apply flow directed back into the droplet device (Fig. 2.9c).

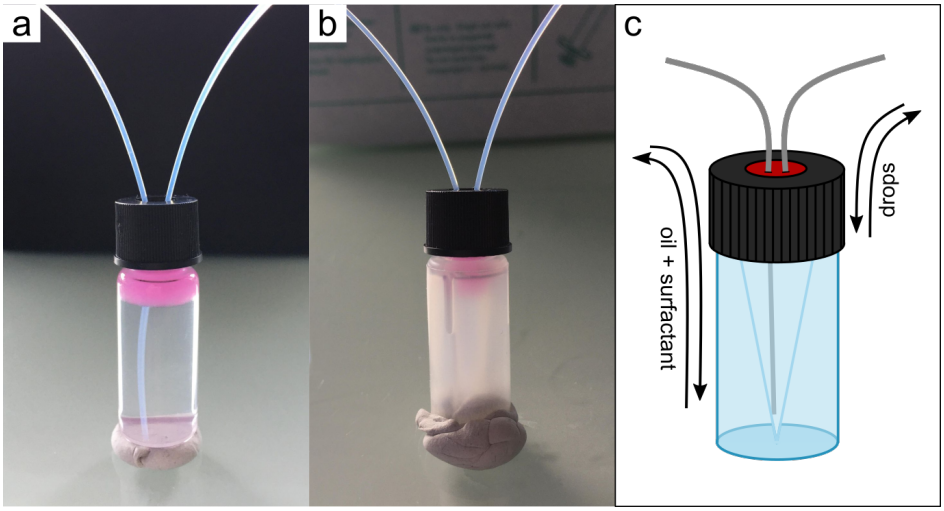

Figure 2.9: 3D collection vials. Two collection vials were assembled for droplet collection; a glass vial with an internal volume of 2 mL (**a**) and a plastic vial with an internal volume of 400 µL (**b**). (**c**) A schematic representation of the plastic vial showing the micro insert of 400 µL and the respective flow directions of oil and drops during collection and reinjection.

2.3 Emulsification

An emulsion is created when two immiscible liquids are mixed leading to a suspension of drops. Such a dispersion is unstable as drops will coalesce. In order to stabilize an emulsion of droplets as a collection of individual microcompartments, one need to ensure good stability, biocompatibility and a tight control of exchange between droplets [177]. To implement these parameters, using surface active agents, surfactants, are indispensable. A surfactant molecule is amphiphilic and is here used to stabilise water-in-oil emulsions by creating droplets as an inverse emulsion (Fig. 2.10).

In this work I use the fluorinated surfactant FluoSurf^{TM} for all experiments. The

surfactant is produced and sold by Emulseo located in Pessac, France, who kindly provided for us when needed. Emulseo is a startup company created in 2018 as a result of a technology transfer project from the CRPP lab. The surfactant is synthesized, purified and formulated by Emulseo (`https://www.emulseo.com/`).

To create our droplet microcompartments, I coflow an aqueous phase, in our case a sample solution, with 2.5% surfactant (v/v) diluted in HFE-7500 fluorinated oil (NovecTM) in our microfluidic devices. Using a fluorinated oil together with the fluorinated surfactant ensures a high biocompatibility allowing easy transport of the essential respiratory gasses, CO_2 and O_2, in the oil and between the droplets. In addition, the fluorinated oil is highly compatible with the material of our microfluidic devices [178, 179].

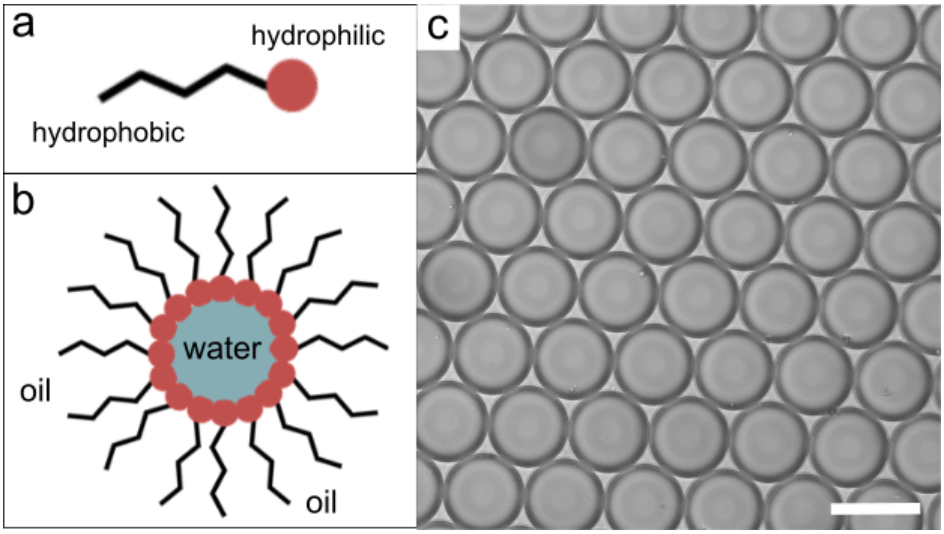

Figure 2.10: Emulsion stabilizer. (**a**) Surfactant molecule used as emulsion stabilizer showing the hydrophobic and hydrophilic ends. (**b**) Micelle with an aqueous core created from multiple surfactant molecules in oil. (**c**) Micrographic presentation of droplets made from water-in-oil emulsion stabilized by FluoSurf^{TM} surfactant. Scale bar is 80 µm.

2.4 Droplet measurements

For all droplet measurements, the droplet fluorescence is collected by the PMT with a DAQ, interfaced with a homemade LabVIEW program. The laser point is positioned in the middle of the production device channel just after droplet production. In prior to all fluorescence measurements the LED light of the microscope is turned off together with the light in the room of the setup. The droplets are measured as fluorescence over time and is recorded during production and reinjection. A two minute recording corresponds to an average of 25.000-50.000 drops depending on the specific droplet

sizes. Each drop is detected as one peak where the RFU of the individual drops is determined as the mean RFU value within one peak (Fig 2.11).

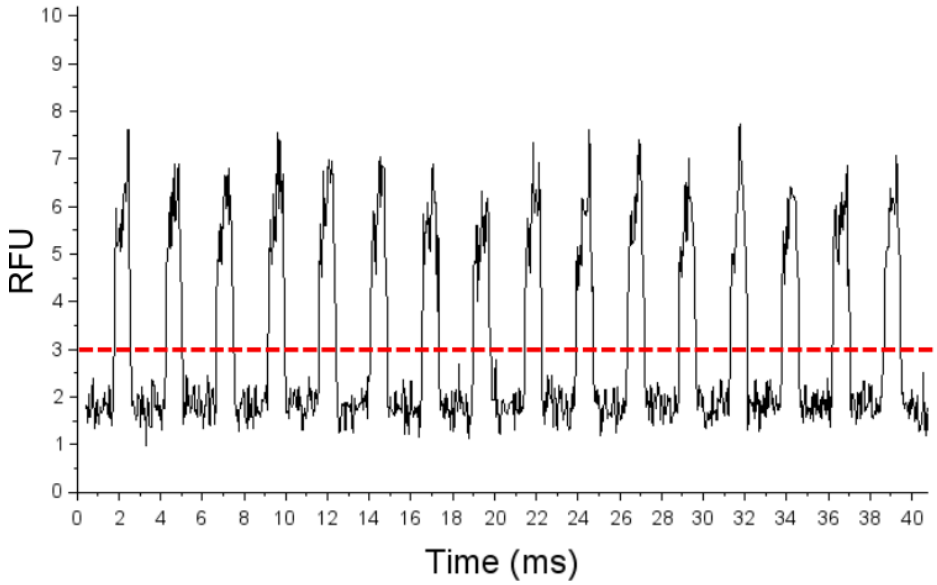

Figure 2.11: Peak detection for size measurements. Recorded data from drops are transferred into a peak diagram with RFU as a function of time for size determination.

From the peaks, I define a threshold line distinguishing the droplet RFU from the background RFU. Mean RFU values detected for each droplet peak are plotted in a histogram as number of drops (droplet counts) with corresponding RFU values. In addition, the measured drops are presented in a heat map showing the droplet size vs. RFU distribution for each drop (Fig 2.12). The droplet sizes shown in the heat map is defined as the width of a peak and is therefore an indirect measurement of the droplet size. The size corresponds to the required time for a whole droplet to cross the laser point. Slower or faster reinjection can thereby change the recorded size according to the speed. We can however use this size measurement as an estimate for size dispersion revealing the fraction of droplets that broke or coalesced during reinjection.

The droplet sizes are controlled by the flow rates Q_{oil} and Q_{aq} of the oil and aqueous phases together with the dimensions of the respective devices. The volumes are determined as $V_{drops} = Q_{aq}/f$ where Q_{aq} is controlled in $\mu L\,h^{-1}$ and f is the droplet frequency. The droplet frequency is calculated from the RFU measured by the laser as $f = N_{drops}/\Delta t$. Counting a given number of drops, N_{drops}, in a certain time span, Δt, thereby gives us the droplet frequency and allow us to calculate the average droplet volumes.

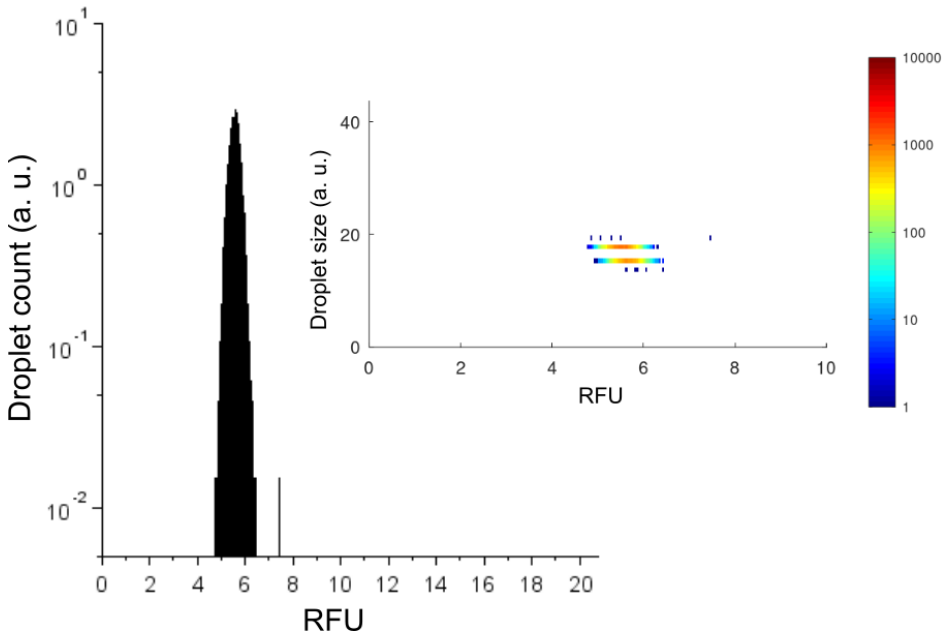

Figure 2.12: Detection of droplet count and fluorescence. Mean RFU values from the peak diagram are transferred into a histogram displaying droplet count over RFU. Insert: Heat map presenting the histogram data as droplet size over RFU.

2.5 Conclusion

In this chapter, I have described the home build optical setup used for performing droplet-based microfluidics. The incorporation of a continuous laser, the PMT and all the other components enable high-throughput detection and collection of fluorescent droplets together with on-chip monitoring from the high speed camera. The sensitivity of the setup was optimized and maintained after movement to another location. I have further presented the fabrication and description of the microfluidic devices optimal for single-cell encapsulation, collection and analysis.

The system presented here allows us to perform high-throughput analysis of single-cell *T. b. brucei* by encapsulation in microcompartment droplets. The setup constitutes the technical and methodical foundation of all the work carried out in this thesis.

2.6 Summary

In this chapter, I have described the development of the microfluidic techniques used in this thesis.

- I have described and assembled a fluorescence setup for droplet-based microfluidics and transferred it to the MFP lab.
- Laser and sensor calibration have been optimized for droplet detection and single cell analysis.
- I have presented the manufacturing of the microfluidic devices and described their functionally.
- The device designs are compatible with encapsulation and visualization of single trypanosomes for quantitative analysis.

3 | *T. b. brucei* cultivation in drops

In this chapter, I study single cell trypanosomes using droplet-based microfluidics and further investigate cell variability within a population. I encapsulate single-cell *T. b. brucei* in microcompartment droplets and test the effect of different droplet sizes on the survival and growth of the cells. The results of these studies have been published in Scientific Reports and are here presented as the final paper. The supplementary information of the paper are presented directly after. Some parts will be repetitions of sections in the background in Chapter 1 and the experimental technique in Chapter 2. An additional experiment, not presented in the publication, is described in the last section of this chapter. All experiments, data collection and analysis was performed by myself. The final paper was written together with my supervisors Jean-Christophe Baret and Loïc Rivière with valuable contributions from all the authors.

3.1 Publication

scientific reports

Check for updates

OPEN

Confining *Trypanosoma brucei* in emulsion droplets reveals population variabilities in division rates and improves *in vitro* cultivation

Simone H. Oldenburg[1,2], Lionel Buisson[1], Thomas Beneyton[1], Deniz Pekin[1], Magali Thonnus[2], Frédéric Bringaud[2], Loïc Rivière[2]✉ & Jean-Christophe Baret[1,3]✉

Trypanosome parasites are infecting mammals in Sub-Saharan Africa and are transmitted between hosts through bites of the tsetse fly. The transmission from the insect vector to the mammal host causes a number of metabolic and physiological changes. A fraction of the population continuously adapt to the immune system of the host, indicating heterogeneity at the population level. Yet, the cell to cell variability in populations is mostly unknown. We develop here an analytical method for quantitative measurements at the single cell level based on encapsulation and cultivation of single-cell *Trypanosoma brucei* in emulsion droplets. We first show that mammalian stage trypanosomes survive for several hours to days in droplets, with an influence of droplet size on both survival and growth. We unravel various growth patterns within a population and find that droplet cultivation of trypanosomes results in 10-fold higher cell densities of the highest dividing cell variants compared to standard cultivation techniques. Some variants reach final cell titers in droplets closer to what is observed in nature than standard culture, of practical interest for cell production. Droplet microfluidics is therefore a promising tool for trypanosome cultivation and analysis with further potential for high-throughput single cell trypanosome analysis.

Trypanosomes are pathogenic protozoan parasites infecting mammals in Sub-Saharan African countries. *T.b. rhodesiense* and *T.b. gambiense* sspp. are the causative agents of Human African Trypanosomiasis (HAT) better known as Sleeping sickness[1], while *Trypanosoma congolense*, *T. vivax* and the *T.b. brucei* ssp. are the infectious agents in animal hosts leading to Animal African Trypanosomiasis (AAT) also known as Nagana[2,3]. Current treatments are complex and causing a variety of undesirable side effects, while *T.b.* infections being lethal if not treated. An extensive surveillance is required to decrease HAT cases[4,5] which all adds up to large economic consequences in the affected areas[6,7].

It is well known that trypanosomes are transmitted between hosts through bites of the tsetse fly (*Glossina* spp.). The repetitive switch between the insect vector and the mammal host causes a number of physiological and metabolic changes in the life cycle of the parasites[8] such as cell cycle arrest, preparing the parasites to enter the insect vector[9]. Within the host, a well described mechanism is sudden changes of variant surface glycoproteins (VSGs) allowing adaptation to the immune system of the host. This action, known as antigenic variation, allows a small part of the population to continuously re-adapt to new immune system responses[10,11]. Both aspects require an heterogeneous behavior within the population and highlight the importance of variability in a cell population of trypanosomes. There is therefore a need for analytical methods that provide quantitative measurements of the cell response with a single cell resolution to identify variants potentially responsible for fast adaptation of the population to external changes. Microfluidics provide the capabilities to multiplex biochemical assays at high-throughput down to the single cell[12–17]. Previous studies have used microfluidic tools to study

[1]Université de Bordeaux, Centre National de la Recherche Scientifique, Centre de Recherche Paul Pascal, Unité Mixte de Recherche 5031, 33600 Pessac, France. [2]Université de Bordeaux, Centre National de la Recherche Scientifique, Microbiologie Fondamentale et Pathogénicité, Unité Mixte de Recherche 5234, 33076 Bordeaux, France. [3]Institut Universitaire de France, 75231 Paris, France. ✉email: loic.riviere@u-bordeaux.fr; jean-christophe.baret@u-bordeaux.fr

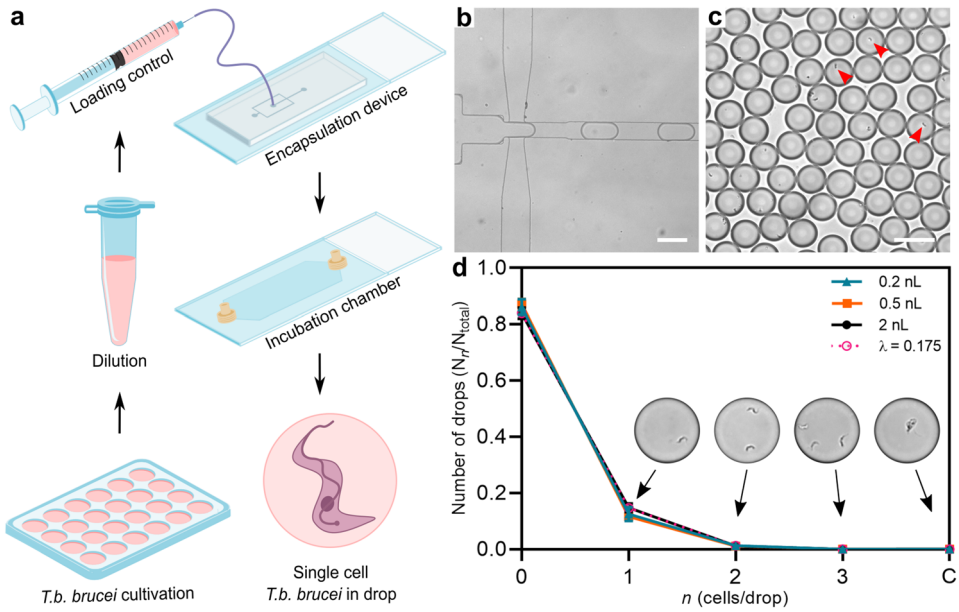

Figure 1. Single cell encapsulation of *T.b. brucei*. (**a**) Overview of experimental procedure. Starting from a classical cell culture, *T.b. brucei* cells are diluted to match the respective drop sizes used. After, the cell suspensions are loaded into syringes enabling connection to microfluidic devices. From encapsulation, the drops are loaded into an incubation chamber where visualization of encapsulated *T.b. brucei* takes place. (**b**) Microscopic image of drop-making process in personalized encapsulation device visualized through ×10 microscopic objective (Fig. S2a). (**c**) Fixed droplets containing encapsulated cells displayed in an incubation chamber visualized through ×10 microscopic objective. Red arrows highlight examples of encapsulated cells. (**d**) Poisson distribution of three different sizes of drops together with the predicted statistic values with a cell distribution of 0.175 cells per drop. All data are presented as mean values ±SD made as biological replicates (n = 3). Inserted images show examples of drops containing one, two, or three cells and an uncountable quantity defined as 'clumps' (C) using a ×20 microscopic objective. All scale bars are set to 100 μm. Images displayed in **a** are used directly or modified in Inkscape (https://inkscape.org) from SMART (Servier Medical Art), licensed under a Creative Common Attribution 3.0 Unported License (https://smart.servier.com).

the *Trypanosoma* parasite. Using optical tweezers, single-cell trapping of trypanosomes coupled to the creation of chemical gradients, provided means to analyse the effect of drugs on the parasite[18,19]. More recently, Voyton *et al.* (2019) designed a trapping system to immobilize cells for single cell- imaging[20]. While promising, these techniques isolate single parasites from the total population where the relative low throughput of the analysis does not necessarily provide measurements representative of the variability observable in a large population. Droplet-based microfluidics enable compartmentalization of single cells allowing to study heterogeneity in a given group[21–23], to quantitatively assess the effect of drugs at the single-cell level[13] and to possibly isolate extraordinary variants[24,25]. It has shown to be relevant as culture platforms for cells and cell populations of bacteria[26–28], yeast[29,30], and mammalian cells[23].

Here we describe a droplet-based microfluidic approach for encapsulation and cultivation of single *T.b. brucei* parasites in the drops of a water-in-oil emulsion. The droplets of controlled sizes serve as microreactors for the growth of parasites from single cells. We demonstrate the viability and the proliferation of the cells within the compartments over days. Interestingly, the variability of the division shows that a large population indeed contains highly dividing variants which would rapidly dominate the population in a bulk culture and possibly be responsible for drifts in culture. We also show that the final titer of the parasite in droplets exceed the maximal titer in standard cultures. Emulsion cultivation therefore appears to be a powerful cultivation method for trypanosomes in droplets leading to titer closer to the titers found *in vivo*, without the need for complicating infrastructure or animal vectors.

Results

Drop encapsulation of *T.b. brucei*. Bloodstream forms of *T.b. brucei* are cultivated in 24-microwell plates. All survival and growth experiments are initiated from the same starting culture to reduce population variation between different stock cultures. Growth in standard bulk culture is monitored as a control at the beginning and the end of the experiments, to ensure that the observed differences are not caused by unstable growth from an aging or drifting population (Fig. S1).

We use two devices to respectively encapsulate and incubate single cell *T.b. brucei* and quantify their growth in nL volume microcompartments (Fig. S2). Cell suspensions are loaded into syringes in prior to injection in the microfluidic devices (Fig.1a). For drop production, we use a dual flow device with fluorinated oil containing

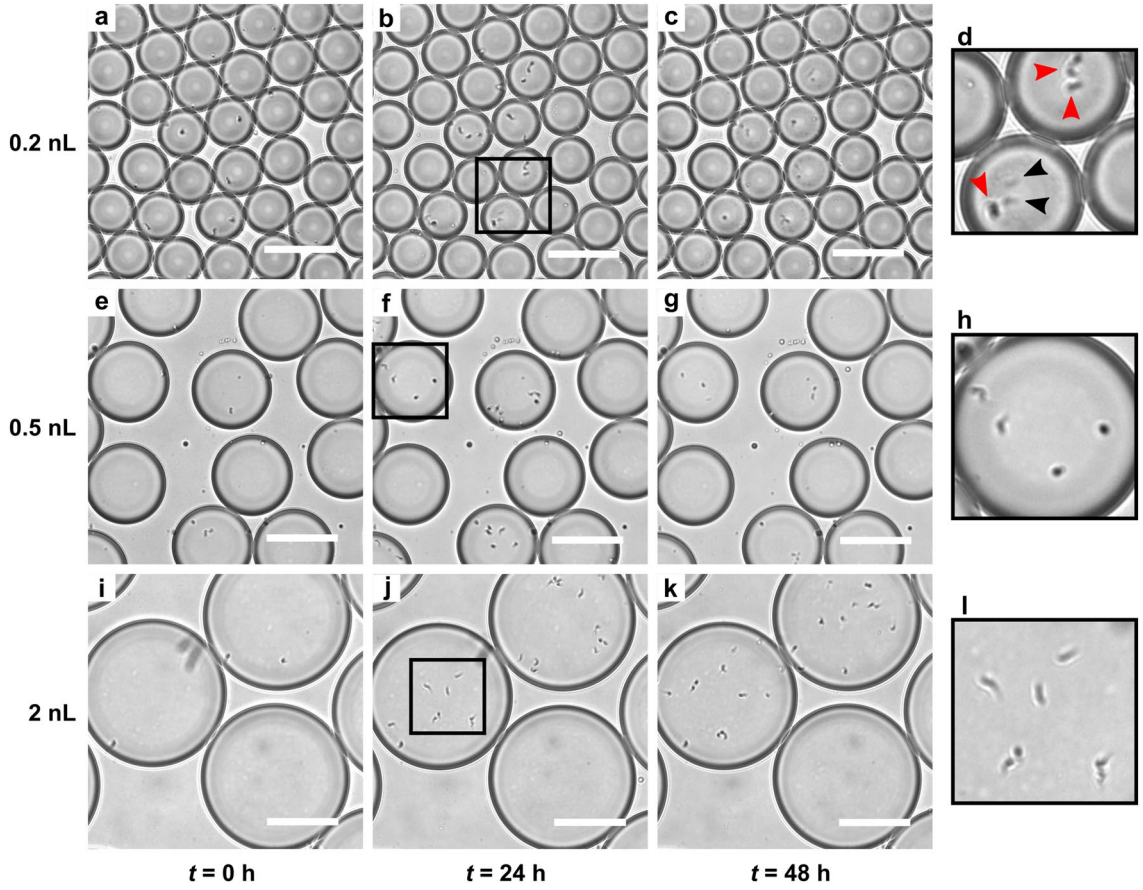

Figure 2. Impact of drop size on trypanosome survival. The figure display snapshots of encapsulated *T.b. brucei* cells just after encapsulation, after 24 h of incubation and after 48 h of incubation in drop sizes of 0.2 nL (**a–c**), 0.5 nL (**e–g**) and 2 nL (**i–k**), visualized in incubation chamber through a x10 microscopic objective. Examples of living cells (red arrows) and dead cells (black arrows) are seen in the close-up snapshot (**d**) at 24 h. In the snapshots (**h**, **l**) all cells are alive. All scale bars are 100μm. For snapshots **a–c**, **e–g** and **i–k**, the corresponding original movies, showing survival based on motion of the trypanosomes, are provided as supplementary (Movie S1–S9).

surfactant pinching the cell suspension flow creating equal sized microcompartments in the form of drops (Fig. 1b, Fig. S2a). The flow rates of the oil and cell suspension together with the dimension of the nozzle in the respective devices are controlling the drop sizes to reach final drop volumes V_{drops} of 0.2 nL ±1.80%, 0.5 nL ±1.84% and 2 nL ±2.61%. For incubation, the drops are collected in an incubation chamber stabilizing the drops in a monolayer display allowing the exact same drops to be analysed over periods of time, as described previously (Fig. 1c)[25]. The incubation chamber is connected to the outlet of the encapsulation device by external tubings and has a volume of approximately 18 μL (Fig. S2b). One incubation chamber therefore provides multiplex measurement of over 10^4 droplets. After filling, the incubation chamber is detached from the encapsulation device and completely sealed enabling the transfer of the chamber to a cell incubator or a microscope when needed.

In order to investigate cell survival upon isolation, we optimized the number of drops containing only single cells, while keeping the number of drops containing more than one cell at a minimum, by dilution of the encapsulated cell suspensions (in the range $C = 0.875 - 8.750 \cdot 10^5$ cells/mL). The cells being randomly distributed in the bulk suspension, the cell distribution is expected to follow a Poisson distribution: $f(\lambda; n) = \lambda^n e^{-\lambda}/n!$, where n is the actual number of cells in the drops and λ is the average number of cells per drop[23]. λ relates directly to the cell density C in the culture as $C = \lambda/V_{drops}$. Using an occupation factor $\lambda = 0.175$, we recover cell distributions consistent with a Poisson distribution for the three sizes of drops (Fig. 1d). We obtain ~ 11–15% drops containing single cells in drop sizes of 0.2 nL, 0.5 nL and 2 nL. For all three sizes, less than 1.5% of drops contain more than one cell. In few of the drops we observe a cluster of several cells clumping together (Fig. 1d), referred to as clumps (C). This is a common event in *in vitro* cultures when populations are reaching high cell densities. Except for these rare events, the encapsulation of trypanosomes is reliable and equivalent to the encapsulation of any type of particles randomly distributed in the initial volume.

Survival and growth of *T.b. brucei* in drops. We first determine the survival of cells in droplets as a function of droplet sizes (Fig. 2, supporting Movie S1–S6). Droplets containing cells are collected in the incubation chamber in which 200–400 cell-containing drops are counted. All counting experiments are performed in triplicates for each experimental condition. The cells are counted directly from the incubation chamber by eye

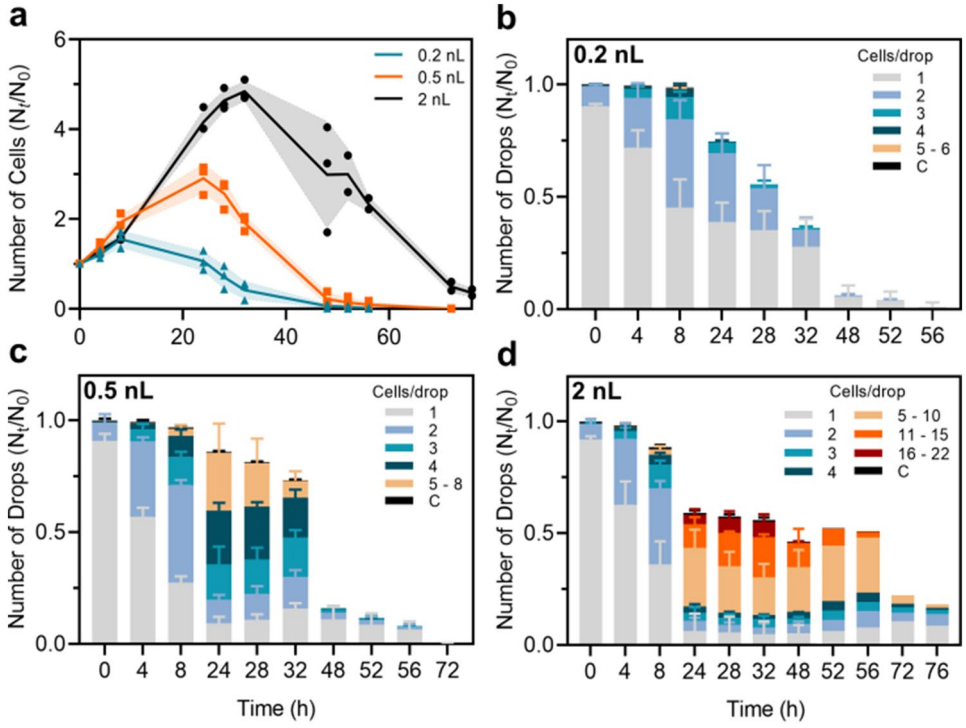

Figure 3. Survival and growth of encapsulated *T.b. brucei*. (**a**) Comparison of cell survival, defined as normalized total cell number, between droplet sizes of 0.2 nL (blue), 0.5 nL (orange) and 2 nL (black) over time. Supporting the cell survival data is the presentations of growth over time defined as normalized number of drops containing a given number of cells in 0.2nL drops (**b**), 0.5 nL drops (**c**) and 2nL drops (**d**). All results are presented as mean values ±SD. Experimental data from 0.2 nL, 0.5 nL and 2 nL drops (0–48 h) are made as biological replicates (n = 3). For 2 nL drops at time 52 to 76 h n = 2. Significance values supporting the survival differences observed in (**a**) are presented in Table 1, 2 and 3.

every 4 h during daytime until death occurs and the experiments are repeated for each drop size (Fig. 2a–k). Cell death is determined when no movement is observed in a time period of 2–3 min. In the micrographs, a dead cell is identified as cell debris appearing as fainted traces (black arrows Fig. 2d).

We analyze the influence of the drop size on survival and growth of encapsulated *T.b. brucei* (Fig. 3). In the 0.2 nL drops, the total cell number increases by a factor of 1.5 during the first 8 h of incubation to reach a maximum. After 24 h, the total cell number has reached down to the initial level and further decreased until all cells have died (after 56 h, Fig. 3a,b). In the 0.5 nL drops, the total cell number increases by a factor of 3 with a maximum at 24 h. All cells are dead after 72 h (Fig. 3a,c). Finally, in the 2 nL drops, the total cell number has increased by a factor of 5 at the maximum after 32 h of incubation. After 76 h when the experiment is terminated, a small fraction of cells remains alive (50% of the initial count, Fig. 3a,d). The initial growth dynamics is similar for all volumes over the first 8 h of incubation. For larger incubation times the growth dynamics strongly depends on the droplet size. From 8 to 32 h of incubation we observe a significant difference in growth between all the drop sizes, with bigger drops reaching a higher total cell number (Table 1, 2 and 3).

We have shown that single cell *T.b. brucei* is indeed able to survive and grow upon isolation in a time span of hours to days, with longer survival and higher cell number per droplet measured in larger droplets.

Growth variability between drops. We have focused on the survival and growth between different sizes of drops. A further analysis of the data reveals three general types of growth behaviours regardless of drop size (Fig. 4a). By tracking the individual drops over time, we observe a minor part of the drop populations containing cells dying within the first 8 h of encapsulation. In 2 nL drops, early death is observed in 11.58% of the drop population, where in 0.2 nL and 0.5 nL drops early death is seen in 1.27% and 3.03% of the populations, respectively. In a huge fraction of the drop populations, surviving cells do not undergo cell division at any time during their lifetime occurring in 14% to 34% of the cases (Fig. 4a). The majority of the drop populations contain cells undergoing minimum one cycle of cell division with doubling times varying from > 10 h to < 5.5 h after 8 and 24 h of incubation (Fig. 4a,b). At 8 h, all drop sizes have similar growth where 40–50% of the populations contain cells with doubling times in the range of 8 h, and 10–20% of the drop populations contain cells with doubling times in the range of 5 h or less (Fig. 4b (left)). At 24 h of incubation, the remaining living cells of 0.2 nL drops and the majority of the 0.5 nL drops have doubling times higher than 10 h. The doubling times in the 2 nL drops are about evenly distributed, in the range from 6 h up to 10 h and higher (Fig. 4b (right)). In the fast growing drops, the maximum cell densities reached are 22, 8 and 6 cells per drop in respectively 2 nL, 0.5 nL and 0.2 nL drops. In order to compare the droplet conditions, we calculate the cell volume density. The maximum cell den-

Time (h)	*P* value	Significance	Effect size (*g*)
4	0.34665	ns	0.87
8	0.01795	*	3.16
24	0.00741	**	4.09
28	0.00083	***	7.39
32	$5.25 \cdot 10^{-5}$	****	14.94
48	0.01597	*	3.28
52	0.00283	**	8.28
56	0.00024	***	19.17
72	0.00658	**	6.18
76	–	–	–

Table 1. Difference in cell survival between 2 nL and 0.5 nL drops. Statistical differences are presented as *P* values. Two-sided Student's *t* test was used to find significance values. Effect sizes were calculated as Hedges' *g*[57]. $P > 0.05$ = non significant (ns), $P \leq 0.05$ = *, $P \leq 0.01$ = **, $P \leq 0.001$ = *** and $P \leq 0.0001$ = ****.

Time (h)	*P* value	Significance	Effect size (*g*)
4	0.38852	ns	0.79
8	0.84538	ns	0.17
24	0.00011	***	12.36
28	$4.26 \cdot 10^{-5}$	****	15.75
32	$1.34 \cdot 10^{-5}$	****	21.05
48	0.01305	*	3.48
52	0.00233	**	8.85
56	–	–	–
72	–	–	–
76	–	–	–

Table 2. Difference in cell survival between 2 nL and 0.2 nL drops. Statistical differences are presented as *P* values. Two-sided Student's *t* test was used to find significance values. Effect sizes were calculated as Hedges' *g*[57]. $P > 0.05$ = non significant (ns), $P \leq 0.05$ = *, *P*, ≤ 0.01 = **, $P \leq 0.001$ = *** and $P \leq 0.0001$ = ****.

Time (h)	*P* value	Significance	Effect size (*g*)
4	0.07137	ns	2.00
8	0.05461	ns	2.20
24	0.00126	**	6.62
28	0.00144	**	6.39
32	0.00057	***	8.12
48	0.15578	ns	1.43
52	0.20194	ns	1.25
56	–	–	–
72	–	–	–

Table 3. Difference in cell survival between 0.5 nL and 0.2 nL drops. Statistical differences are presented as *P* values. Two-sided Student's *t* test was used to find significance values. Effect sizes were calculated as Hedges' *g*[57]. $P > 0.05$ = non significant (ns), $P \leq 0.05$ = *, $P \leq 0.01$ = **, $P \leq 0.001$ = *** and $P \leq 0.0001$ = ****.

sity in the 2 nL drops reaches a maximum of 8–11 cells/nL, in 0.5 nL drops 10–16 cells/nL and in 0.2 nL drops reaching a maximum of 15–30 cells/nL (Table 4).

We plot growth curves corresponding to the growth observed in the drops reaching the maximum cell densities and compare with growth from standard in bulk techniques (Fig. 4c). In the standard growth curves two different starting concentrations are used and cells are counted every 4 h during daytime until cell densities start decreasing. In classic growth curves the maximum cell densities reach $4–5 \cdot 10^6$ cells/mL, with the lowest starting concentration reaching the highest density. The average of the maximum cell densities reached in drop cultivation is $2 \cdot 10^7$ cells/mL in 0.2 nL drops, $1 \cdot 10^7$ cells/mL in 0.5 nL drops and $8 \cdot 10^6$ cells/mL in 2 nl drops.

We have here measured a large variability in division within populations of *T.b. brucei* and shown higher maximum cell densities in droplet cultivation over standard in bulk techniques for the highly dividing fraction of cells.

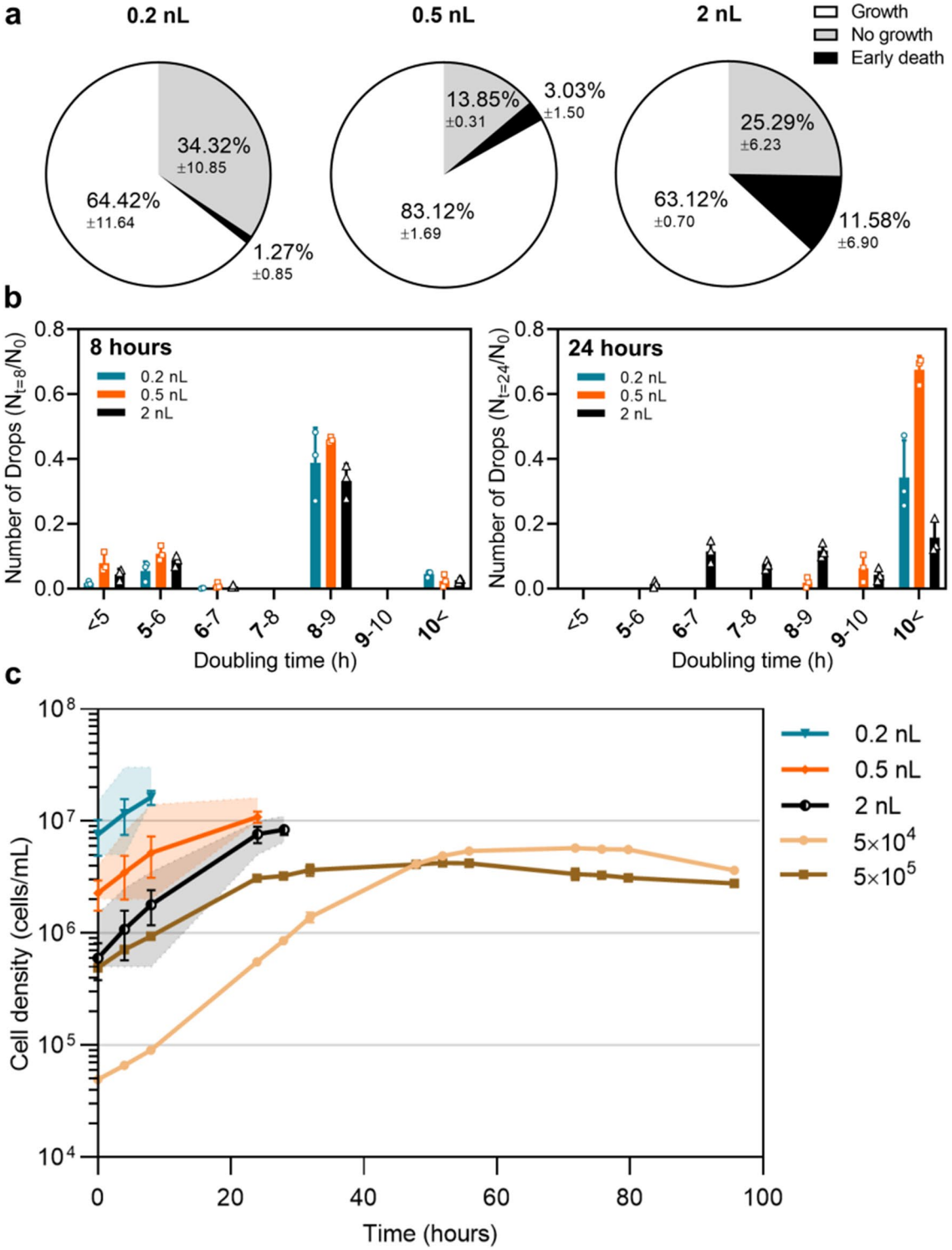

Figure 4. Growth variabilities within drop populations. (**a**) Divisions of the total populations in three main behaviors; normal growth (white), survival for more than 8 h without division (grey) and early death occurring before 8 h (black) in 0.2 nL, 0.5 nL and 2 nL drops. (**b**) Comparison of doubling times at 8 h and 24 h between 0.2nL drops (blue), 0.5nL drops (orange) and 2 nL drops (black). Doubling times represented by bold values are included in the respective group. (**c**) Comparison of growth curves between drop cultivation (blue, orange and black lines) and standard cultivation (brown lines) techniques. Droplet growth curves represent the fastest growing populations in 0.2 nL, 0.5 nL and 2 nL droplets. The shaded areas show the lower and upper limits of the cell numbers. Standard growth curves are initiated from respectively $5 \cdot 10^4$ and $5 \cdot 10^5$ cells/mL. Results in (**a**) and (**b**) are presented as mean values of biological triplicates ±SD. Results in (**c**) are presented as mean values ±SD of biological or technical triplicates for respectively drop- and standard cultivation curves.

Droplet size (nL)	Max. cell number per drop	Max. cell number per nL
0.2	3–6	15–30
0.5	5–8	10–16
2	16–22	8–11

Table 4. Maximum cell numbers reached in droplet cultivation. Overview of maximum cell number (cells per drop) reached in the three drop sizes and the respective cell volume densities (cells per volume).

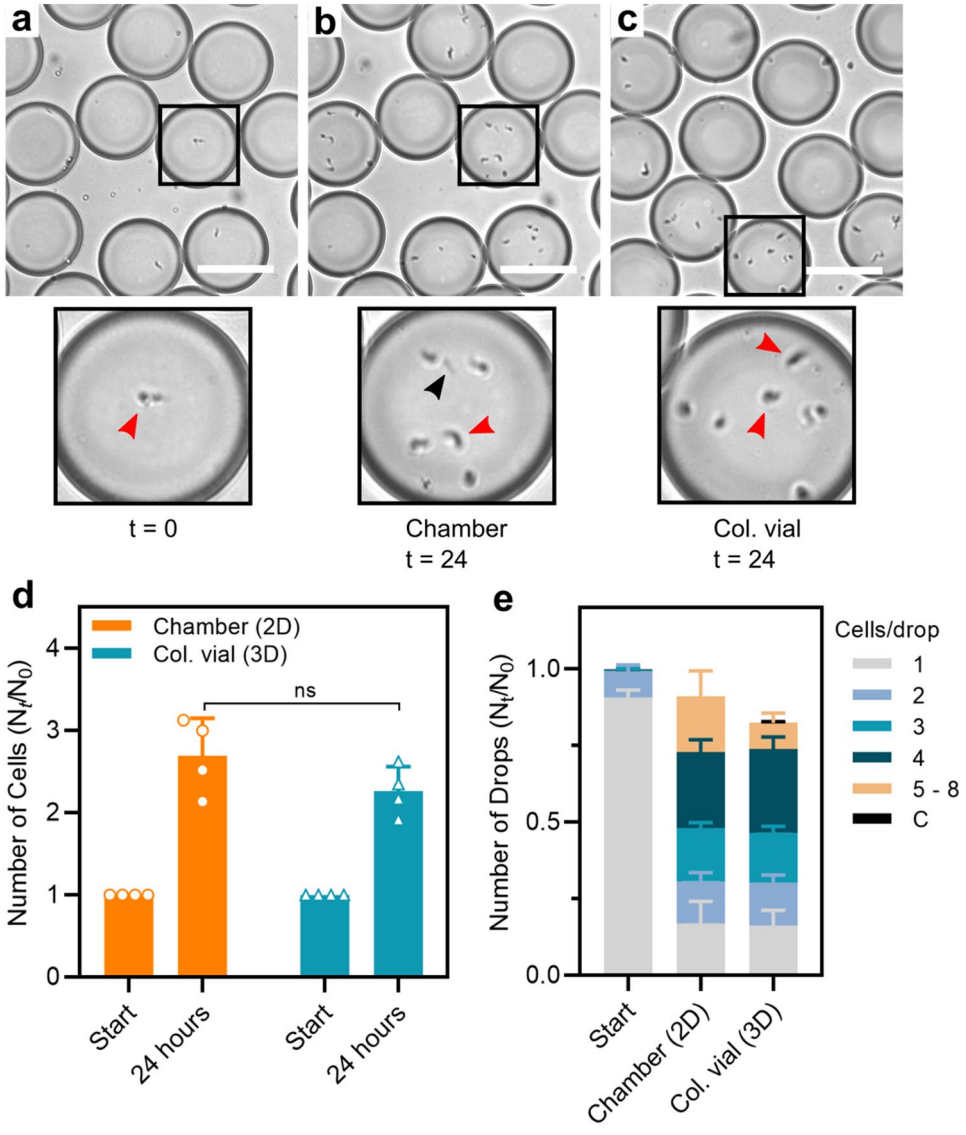

Figure 5. Collection and incubation of 0.5 nL drops in chamber vs. collection vial. (**a**) Snapshots of encapsulated *T.b. brucei* cells at beginning of incubation, (**b**) after 24 h of incubation in chamber and (**c**) after 24 h of incubation in collection vial, visualized through a x10 microscopic objective. Micrographs display close-up examples of encapsulated trypanosomes in drops of the respective collection devices. (**d**) Comparison of cell survival as normalized values after collection and 24 h of incubation in incubation chamber and collection vial. (**e**) Supporting cell survival data is the presentations of growth after 24 h as normalized number of drops containing a given number of cells in the different collection devices. All data are presented as mean values ±SD made as biological replicates (n = 4). Two-sided Student's *t* test were used to find significance value ($P = 0.16$) in (**d**).

Up-scaling of drop yield. After establishing encapsulation and cultivation of single-cell trypanosomes in microcompartment droplets, we analyse the potential of up-scaling the final drop yield (Fig. 5). *T.b. brucei* are encapsulated in 0.5 nL drops and collected for 15 min. off-chip in a 200 μL plastic vial providing a collection of $> 10^5$ droplets, allowing multiple usage of the drops by re-injection from the collection vial. After collection, the inlet tubing is detached and closed and the vial is moved to incubation. For control, drops are simultaneously collected in the incubation chamber, where an estimate of 300 cell containing drops are counted, functioning as time zero for both collection devices (Fig. 5a). After 24 h of incubation the cell-containing drops are counted in the incubation chamber (Fig. 5b) where drops from the collection vial subsequently are re-injected and counted (Fig. 5c).

We analyse how the survival and growth of *T.b. brucei* in drops are influenced by collection and incubation in the larger collection device. After 24 h of incubation the total cell number increases by a factor around 2.5 in both collection devices (Fig. 5d). A small non-significant increase in total cell number is seen in the incubation chamber compared to the collection vial ($P = 0.16$). The cell densities inside the individual drops are likewise similar between growth in the incubation chamber and the collection vial (Fig. 5e). In comparison with the previous survival and growth results of encapsulated *T.b. brucei* in 0.5 nL drops, we furthermore obtain almost identical results between the two experiments emphasizing good experimental repetitiveness (Fig. S3).

We have shown that drop production can easily be up-scaled to achieve a higher drop yield without influencing survival and growth of the trypanosomes. We also emphasize the reproducibility of the survival and growth assays executed with several months in between.

Discussion

We have here developed a droplet-based microfluidic system for creation of microcompartment droplets to successfully encapsulate and cultivate the *T.b. brucei* parasite on a single-cell level (Fig. 1, Fig. 2). We have shown how encapsulated trypanosomes survive in micron-sized droplets from several hours to days (Fig. 3). The droplet sizes are found to positively correlate with the survival time of the encapsulated cells, making larger droplets preferred for long-term experiments.

During trypanosome infection the parasitemia level of the infected mammal is varying from 10^7 cells/mL up to 10^9 cells/mL with large fluctuations during the time period of the infection[31–33]. However, in *in vitro* cultivation the obtained titters of the *T.b. brucei* bloodstream forms are much lower. By standard laboratory techniques cell densities reach a maximum of $4–5 \cdot 10^6$ cells/mL[34–36]. Different techniques involving continuously medium refreshment have previously been described to improve the poor yield of *in vitro* trypanosome cultivation[35,37]. However, by cultivating trypanosomes in drops we here reach cell densities 10-fold higher than by standard cultivation without the need of medium or nutrition replacement. Interestingly, while bigger drops have the longest survival, we observed that smaller drops lead to a higher cell density. With a maximum density of $1.1 \cdot 10^7$ cells/mL in 2 nL drops, 0.2 nL drops reached a max density 3 times higher with $3 \cdot 10^7$ cells/mL (Fig. 4, Table 4). A similar correlation has previously been observed, where survival time of encapsulated human cells showed an inverse correlation with the cell density[23]. Worth noting, by simply increasing the starting concentration in standard cultivation techniques we did not observe a higher final cell density (Fig. 4). Thus, cultivation in droplets seem to benefit the trypanosome parasite, not because of a higher starting cell density but possibly due to the small confined volumes.

By cultivating single *T.b. brucei* cells in drops, we show that droplets of the same size do not promote identical growth (Fig. 4). Where in standard cell-based research, we assume that average activities from a population represent the typical cell, we here reveal various cellular growth patterns within a population. Worth emphasizing is the existence of various growth patterns in standard culture condition as well as in droplet cultures. However, in standard conditions fast growing cells are likely to quickly dominate a population and hide the slower growth rates that we here reveal in drops. While some cells reach doubling times as seen in bulk, most cells exhibit slower or none growth ranging from around 6–24 h after droplet encapsulation. Those cells would be out-competed in a bulk experiment showing how a small fraction of fast dividing cells might quickly become dominant in the bulk culture and a possible reason of adaptation in the population. Heterogeneity in monoclonal populations is a well known phenomena derived from events as stochastic switching or noise present in both prokaryotic and eukaryotic cells[38–40]. In the protozoan parasites *Leishmania* and *Trypanosoma cruzi*, belonging to the same taxonomic family as *T.b. brucei*, cell to cell variation has been shown by stochastic DNA amplification and clonal variation in stress-related responses[41,42]. Variabilities within *T.b. brucei* populations have already been shown to occur during adaptation from the insect vector to the mammal host and back again[8,10,11]. These transitions, causing a number of physiological and metabolic changes, indicate a heterogeneous behaviour inside the populations. Single-cell analytical methods like microfluidics are therefor highly desirable to further study these heterogeneous behaviors and to discover new variabilities or behaviors. Although other studies have already coupled microfluidic approaches to study trypanosomes on a single-cell level[18–20], no successful attempts have been reported on isolating a single trypanosome in enclosed compartments. In this work, droplet-based microfluidics show promising for single-cell compartmentalisation and cultivation of the trypanosome parasite. By moving from a two-dimensional collection chamber to a three-dimensional collection vial, we maintained the same survival and growth patterns in an environment allowing continual usage of the collected drops by reinjection (Fig. 5).

A next step to investigate population variability is a further analysis of the highest dividing variants. Coupling our droplet-cultivation approach with additional sorting modules will allow us to select droplets containing the most dividing cell variants. Such systems have previously been shown to successfully screen and select drops based on content densities[43–45]. Other well described approaches are using fluorescence-based sorting for high-throughput analysis of cellular activities on a single cell level[23,46–48]. Using fluorescence-based assays is another promising tool to study population variability by analysing enzymatic activities between individual cells. Finally,

obtaining genetic information of variants with prominent division rate or enzymatic activity in populations of trypanosomes is of great interest. Droplet-based sequencing allow the acquisition of genetic profiling of individual cells[49–51] and can possibly lead to the identification of new drug targets against the disease.

Conclusion

We have here established a system for encapsulation and growth of *T.b. brucei* in microcompartment droplets at the single-cell level. We have shown that trypanosomes survive from several hours to days being sufficient time for several cycles of cell division. We see that differences in droplet size influence the survival and division: qualitatively, cells survive longest in the largest drops (2 nL) reaching higher total cell numbers per drop, but simultaneously the highest cell densities (cells per volume) is reached in the smallest droplets (0.2 nL). We observed an heterogeneous pattern of growth behavior between the individual cells within a population, indicating that some cell variants divide more efficiently while others divide slower than the average. Cultivating trypanosomes in droplets also resulted in 10-fold higher cell densities among the fastest dividing variants compared to standard cultivation techniques. This improvement is achieved in drops without the need of additional maintenance methods and is potentially interesting to optimize cultivation techniques of the parasite. Finally, these effects quantitatively characterized in two-dimensional microfluidic systems is shown robust. The same improvement in cell densities is obtained for incubation of the cells in a three-dimensional macroscopic emulsion.

Our results demonstrate the interest to cultivate single cell trypanosomes in microcompartment droplets, and represent a future opportunity to develop a droplet-based microfluidic platform to investigate behaviors and activities on a single cell level. Further adaptation of our system can lead to numerous applications as droplet sorting and screening to advance the exploration of new drug candidates against the trypanosome parasite.

Methods

Cell preparation. Cells are cultivated using standard cultivation protocols[34]. In brief, monomorphic *Trypanosoma brucei brucei* 427 90-13 bloodstream form (BF) were grown in Iscove's Modified Dulbecco's Medium (IMDM) (Life Technologies) supplemented with 10% (v/v) heat-inactivated fetal calf serum (FCS), 0.2 mM β -mercaptoethanol, 36 mM $NaHCO_3$, 1 mM hypoxanthine, 0.16 mM thymidine, 1 mM sodium pyruvate, 0.05 mM bathocuprone, 1.5 mM L-cysteine, 40μg $\cdot$ mL^{-1} streptomycin and 40U $\cdot$ mL^{-1} penicillin. *T.b. brucei* BF were maintained as one-mL cultures in 24-well Nunc plates (Thermo Fischer Scientific) at 37° C with 5% CO_2. Every 2 or 3 days cultures were sub-cultured with a 1.000 or 10.000 fold dilution, respectively. In prior to all encapsulation steps, cells are counted in a Guava easyCyte Flow cytometer (EMD Millipore). All doubling times, d_t, for bulk and droplet cultivation are calculated as $d_t = (t_2 - t_1) \cdot (log(2)/log(\frac{q_2}{q_1}))$, where t_1 and t_2 is the time of the beginning and the end of the time span for the wanted doubling times, and q_1 and q_2 are the start and the end cell numbers for the respective time span.

Device design and fabrication. Microfluidic encapsulation devices were made of poly-(dimethylsiloxane) (PDMS, Sylgard 184) from SU8-3000 negative photoresists (MicroChem Corp) molds produced using standard soft lithography techniques[52]. Briefly, negative photo resist SU-8 3050 or SU-8 3025 were spin-coated on silicon wafers (Brand) and exposed to UV light through customized patterned transparent photomasks (CAD/Art Services, Inc., SELBA S. A. for high-resolution printing (50800 dpi)) using a MJB4 mask aligner (SUSS MicroTec). After UV exposure the molds are developed by SU-8 developer (MicroChem). A mixture of PDMS/curing agent (10% w/w, Sylgard 184 kit) was poured on the molds, degassed in a vacuum chamber and cured at 70°C for at least 2 h. The PDMS was peeled from the molds and inlet and outlet holes were punched with a 0.75mm-diameter puncher. Prepared PDMS slabs and microscope glass slides were cleaned, dried and exposed to oxygen-plasma treatment (Pico Low pressure plasma system, Diener electronic) in prior to bonding by pressing the two components together. The surface of the microfluidic channels were treated using fluoro-silane (Aquapel, PPG Industries) before use. All devices were flushed with argon before and after Aquapel treatment. Devices for encapsulation were fabricated in three different sizes according to the desired size of drops. For drop production with sizes of 0.2 nL, the channel depths of the devices were 30 μm and nozzle widths 50 μm. For sizes of 0.5 nL, channel depths were 85 μm and nozzle widths 50 μm. For drops of 2 nL, channel depths were 95 μm and nozzle widths 100 μm. To observe drops as a 2D-array, an incubation chamber was fabricated as previously described[25]. Glass microscopy slides were used as top and bottom covers (76×25×1mm). Two holes were created in the top glass slide by micro-sandblasting. Both slides were cleaned using soap, water and ethanol and dried at 70°C. The desired chamber design was cut in a 60 μm thick double-sided bonding tape (1375, SDAG, Adhesif) using a Graphtech cutting plotter (CE6000-40). The two cleaned microscope slides were attached to each other using the bonding tape. 10-32 NanoPort assembled with NanoTight fittings (IDEX Health and Science) were glued on the inlet holes with UV curing glue (Loctite 3529, Henkel)(Fig. S2b). The inner dimension of the incubation chamber was appx. 1×3 cm and 60 μm in depth corresponding to a volume of 18 μL. The chamber was treated with fluoro-silane (Aquapel, PPG Industies) and dried with argon prior to use. The chamber was reused multiple times and cleaned between each experiment by flushing fluorinated oil.

Optical setup. For drop observation and size measurements, we used a homemade laser-induced epifluorescence setup, implemented on an inverted microscope (Axiovert 135, Carl Zeiss) (Fig. S4). Fluorescence was excited by a continuous laser at 473 nm (Cobolt 06-MLD, Cobolt AB) focused directly on the drops by the observation objective (Zeiss LD Achroplan 40x/0.6 Korr Ph2). Fluorescence was filtered by a band pass filter at 525 nm and 50 nm width (525/50 BrightLine HC) and collected by a photo multiplier tube (PMT) (H10723, Hamamatsu Photonics K.K.) at 10kHz with a NI acquisition card (NI USB 6008), which was controlled by a homemade LabVIEW program. Fluorescence collection was done in confocal configuration to reduce background noise.

A Blackfly S USB3 camera (FLIR Systems) was mounted on the top camera port of the microscope where the ocular piece have been removed. The entire setup was fixed on an aluminium platform with vibration dampening feet to reduce vibration noise from the surroundings.

Cell encapsulation and incubation. Cells were grown to a density of 1.2–3×10^6 cells· mL^{-1} in prior to each experiment. The cell suspensions were further diluted to a value corresponding to 0.175 cells/drop in each of the wanted drop sizes. Upon drop formation, cell suspensions were emulsified using HFE-7500 fluorinated oil (3MTM Novec) stabilized by FluoSurf surfactant (emulseo) with a final concentration of 2.5% (v/v). Cell suspension and fluorinated oil were separately loaded into 1 mL Omnifix-F syringes (B Braun) with 0.4×19 mm needle tips (Terumo) and pumped into the drop making device by low pressure neMESYS syringe pumps (CETONI GmbH) with flow rates corresponding to the wanted drop sizes. The drop sizes were determined as $V_{drops} = Q/f$, where Q was flow rate of the cell suspension in μL/h and f was the drop frequency calculated from laser measurements (Fig. S4 text). For 0.2 nL drops and 0.5nL drops the flow rates of the fluorinated oil were 300 μL· h^{-1} and 850 μL· h^{-1} and for the cell suspension 280 ± 10 μL· h^{-1} and 250 ± 20 μL· h^{-1}, respectively. For 2 nL drops, the flow rate of the fluorinated oil was 750 μL· h^{-1} and 330 ± 20 μL· h^{-1} for the cell suspension. Syringes were connected with microfluidic devices by polyethene tubing (Adtech) in dimensions of 0.3 mm inner diameter and 0.76 mm outer diameter. After drop making, the emulsion was collected off-chip in an incubation chamber or a collection vial. After collection, the emulsion-containing collection device was incubated at 37°C with 5% CO_2 until further use. All cell counting were performed by eye directly from the incubation chamber containing the emulsified cells during a time span of 30–45 min. For all drop and cell counting upon fixation the in incubation chamber, a microscope incubator (Okolab) was used set at 37°C.

Statistical analysis. Statistical analyses were performed between all drop sizes at each time point during the survival assay (Fig. 3a) in order to find the significance values presented in Table 1, 2 and 3. We used a Student's t test (parametric, unpaired, two-tailed analysis) to determine significance between the mean survival of the different drop sizes[53,54]. Supplementary we calculated the effect size for each analysis, which previously has been recommended when working with small sample sizes[55–57]. T tests were performed in Microsoft Excel (Microsoft Corporation) and by GraphPad prism version 8 (GraphPad Software) supporting the findings. Effect sizes were found using the online tool Effect Size Calculator for tests (https://www.socscistatistics.com/effectsize/default3.aspx). Alpha level for all analyses were 0.05.

Data availability

All relevant data are available from the corresponding author upon request.

Received: 31 March 2021; Accepted: 30 July 2021
Published online: 14 September 2021

References

1. Büscher, P., Cecchi, G., Jamonneau, V. & Priotto, G. Human African trypanosomiasis. *The Lancet***390**, 2397–2409 (2017). https://linkinghub.elsevier.com/retrieve/pii/S0140673617315106
2. Giordani, F., Morrison, L. J., Rowan, T. G., DE Koning, H. P. & Barrett, M. P. The animal trypanosomiases and their chemotherapy: a review. *Parasitology* **143**, 1862–1889 (2016).
3. Ulienberg, G. A field guide for the diagnosis, treatment and prevention of African animal trypanosomosis (1998). http://www.fao.org/3/x0413e/x0413e00.htm.
4. Legros, D. *et al.* Treatment of human African trypanosomiasis—present situation and needs for research and development. *Lancet Infect. Dis.***2**, 437–440 (2002). https://linkinghub.elsevier.com/retrieve/pii/S1473309902003213.
5. World Health Organization. *WHO interim guidelines for the treatment of gambiense human African trypanosomiasis* (2019). https://www.ncbi.nlm.nih.gov/books/NBK545514/. OCLC: 1135360434.
6. Kristjanson, P. M., Swallow, B. M., Rowlands, G. J., Kruska, R. L. & de Leeuw, P. N. Measuring the costs of African animal trypanosomosis, the potential benefits of control and returns to research. *Agric. Syst.***59**, 79–98 (1999). http://www.sciencedirect.com/science/article/pii/S0308521X98000869.
7. Swallow, B. M. *Impacts of trypanosomiasis on African agriculture* (PAAT Technical and Scientific Series, FAO, 2000). https://www.cabdirect.org/cabdirect/abstract/20003010139.
8. Rico, E. *et al.* Bloodstream form pre-adaptation to the tsetse fly in Trypanosoma brucei. *Front. Cell Infect. Microbiol.***3**, (2013). https://www.ncbi.nlm.nih.gov/pmc/articles/PMC3827541/.
9. Vassella, E., Reuner, B., Yutzy, B. & Boshart, M. Differentiation of African trypanosomes is controlled by a density sensing mechanism which signals cell cycle arrest via the cAMP pathway. *J. Cell Sci.***110**, 2661–2671 (1997). https://jcs.biologists.org/content/110/21/2661.
10. David Barry, J. & McCulloch, R. Antigenic variation in trypanosomes: Enhanced phenotypic variation in a eukaryotic parasite. In *Advances in Parasitology*, vol. 49, 1–70 (Academic Press, 2001). http://www.sciencedirect.com/science/article/pii/S0065308X01490373.
11. Blum, M. L. *et al.* A structural motif in the variant surface glycoproteins of Trypanosoma brucei. *Nature***362**, 603–609 (1993). http://www.nature.com/articles/362603a0.
12. Whitesides, G. M. The origins and the future of microfluidics. *Nature***442**, 368–373 (2006). http://www.nature.com/articles/nature05058.
13. Baret, J.-C., Beck, Y., Billas-Massobrio, I., Moras, D. & Griffiths, A. D. Quantitative cell-based reporter gene assays using droplet-based microfluidics. *Chem. Biol.* **17**, 528–536 (2010).
14. Yin, H. & Marshall, D. Microfluidics for single cell analysis. *Curr. Opin. Biotechnol.***23**, 110–119 (2012). https://linkinghub.elsevier.com/retrieve/pii/S0958166911007130.
15. Seah, Y. F. S., Hu, H. & Merten, C. A. Microfluidic single-cell technology in immunology and antibody screening. *Mol. Aspects Med.* **59**, 47–61 (2018).
16. Svensson, C.-M. *et al.* Coding of experimental conditions in microfluidic droplet assays using colored beads and machine learning supported image analysis. *Small***15**, 1802384 (2019). https://onlinelibrary.wiley.com/doi/abs/10.1002/smll.201802384.

17. Kulesa, A., Kehe, J., Hurtado, J. E., Tawde, P. & Blainey, P. C. Combinatorial drug discovery in nanoliter droplets. *PNAS***115**, 6685–6690 (2018). https://www.pnas.org/content/115/26/6685.
18. Stellamanns, E. *et al.* Optical trapping reveals propulsion forces, power generation and motility efficiency of the unicellular parasites Trypanosoma brucei brucei. *Sci Rep***4**, (2014). https://www.ncbi.nlm.nih.gov/pmc/articles/PMC4180810/.
19. Hochstetter, A. *et al.* Microfluidics-based single cell analysis reveals drug-dependent motility changes in trypanosomes. *Lab on a Chip***15**, 1961–1968 (2015). http://xlink.rsc.org/?DOI=C5LC00124B.
20. Voyton, C. M. *et al.* A microfluidic-based microscopy platform for continuous interrogation of trypanosoma brucei during environmental perturbation. *Biochemistry***58**, 875–882 (2019). https://pubs.acs.org/doi/10.1021/acs.biochem.8b01269.
21. Jönsson, H. & Svahn, H. A. Droplet microfluidics—a tool for single-cell analysis. *ANGEW CHEM INT EDIT***51**, 12176–12192 (2012). https://orbit.dtu.dk/en/publications/droplet-microfluidicsa-tool-for-singlecell-analysis.
22. Köster, S. *et al.* Drop-based microfluidic devices for encapsulation of single cells. *Lab Chip* **8**, 1110–1115 (2008).
23. Clausell-Tormos, J. *et al.* Droplet-based microfluidic platforms for the encapsulation and screening of mammalian cells and multicellular organisms. *Chem. Biol.***15**, 427–437 (2008). http://www.sciencedirect.com/science/article/pii/S1074552108001506.
24. Agresti, J. J. *et al.* Ultrahigh-throughput screening in drop-based microfluidics for directed evolution. *PNAS***107**, 4004–4009 (2010). https://www.pnas.org/content/107/9/4004.
25. Eyer, K. *et al.* Single-cell deep phenotyping of IgG-secreting cells for high-resolution immune monitoring. *Nat. Biotechnol.***35**, 977–982 (2017). http://www.nature.com/doifinder/10.1038/nbt.3964.
26. Mahler, L. *et al.* Enhanced and homogeneous oxygen availability during incubation of microfluidic droplets. *RSC Adv.***5**, 101871–101878 (2015). https://pubs.rsc.org/en/content/articlelanding/2015/ra/c5ra20118g.
27. Lalanne-Aulet, D. *et al.* Multiscale study of bacterial growth: experiments and model to understand the impact of gas exchange on global growth. *Phys. Rev. E***92**, 052706 (2015). https://link.aps.org/doi/10.1103/PhysRevE.92.052706.
28. Scheler, O. *et al.* Droplet-based digital antibiotic susceptibility screen reveals single-cell clonal heteroresistance in an isogenic bacterial population. *Sci. Rep.***10**, 3282 (2020). https://www.nature.com/articles/s41598-020-60381-z.
29. Boitard, L. *et al.* Monitoring single-cell bioenergetics via the coarsening of emulsion droplets. *PNAS***109**, 7181–7186 (2012). https://www.pnas.org/content/109/19/7181.
30. Woronoff, G. *et al.* Metabolic cost of rapid adaptation of single yeast cells. *PNAS***117**, 10660–10666 (2020). https://www.pnas.org/content/117/20/10660.
31. Black, S. J. *et al.* Regulation of Parasitaemia in mice infected with Trypanosoma brucei. *Curr. Top. Microbiol. Immunol.* **117**, 93–118 (1985).
32. Magez, S., Stijlemans, B., Caljon, G., Eugster, H.-P. & De Baetselier, P. Control of experimental trypanosoma brucei infections occurs independently of lymphotoxin-α induction. *Infect. Immun.***70**, 1342–1351 (2002). https://www.ncbi.nlm.nih.gov/pmc/articles/PMC127790/.
33. Trindade, S. *et al.* Trypanosoma brucei Parasites occupy and functionally adapt to the adipose tissue in mice. *Cell Host Microbe* **19**, 837–848 (2016).
34. Hirumi, H. & Hirumi, K. Continuous cultivation of Trypanosoma brucei blood stream forms in a medium containing a low concentration of serum protein without feeder cell layers. *J. Parasitol.* **75**, 985–989 (1989).
35. Hesse, F., Selzer, P. M., Mühlstädt, K. & Duszenko, M. A novel cultivation technique for long-term maintenance of bloodstream form trypanosomes in vitro. *Mol. Biochem. Parasitol.***70**, 157–166 (1995). http://www.sciencedirect.com/science/article/pii/016668519500027X.
36. Schuster, F. L. & Sullivan, J. J. Cultivation of clinically significant hemoflagellates. *Clin. Microbiol. Rev*. **15**, 374–389 (2002). https://www.ncbi.nlm.nih.gov/pmc/articles/PMC118086/.
37. Ajoko, C. & Steverding, D. A cultivation method for growing bloodstream forms of Trypanosoma brucei to higher cell density and for longer time. *Parasitol. Res.* **114**, 1611–1612 (2015).
38. Elowitz, M. B., Levine, A. J., Siggia, E. D. & Swain, P. S. Stochastic gene expression in a single cell. *Science* **297**, 1183–1186 (2002).
39. Acar, M., Mettetal, J. T. & van Oudenaarden, A. Stochastic switching as a survival strategy in fluctuating environments. *Nat. Genet.* **40**, 471–475 (2008).
40. Spencer, S. L., Gaudet, S., Albeck, J. G., Burke, J. M. & Sorger, P. K. Non-genetic origins of cell-to-cell variability in TRAIL-induced apoptosis. *Nature***459**, 428–432 (2009). https://www.nature.com/articles/nature08012.
41. Ubeda, J.-M. *et al.* Genome-wide stochastic adaptive DNA amplification at direct and inverted DNA repeats in the parasite leishmania. *PLoS Biol***12**, (2014). https://www.ncbi.nlm.nih.gov/pmc/articles/PMC4028189/.
42. Merrin, J. Frontiers in microfluidics, a teaching resource review. *Bioengineering***6**, 109 (2019). https://www.mdpi.com/2306-5354/6/4/109.
43. Cao, Z. *et al.* Droplet sorting based on the number of encapsulated particles using a solenoid valve. *Lab Chip***13**, 171–178 (2012). https://pubs.rsc.org/en/content/articlelanding/2013/lc/c2lc40950j.
44. Zang, E. *et al.* Real-time image processing for label-free enrichment of Actinobacteria cultivated in picolitre droplets. *Lab Chip***13**, 3707–3713 (2013). https://pubs.rsc.org/en/content/articlelanding/2013/lc/c3lc50572c.
45. Liu, X. *et al.* High-throughput screening of antibiotic-resistant bacteria in picodroplets. *Lab Chip***16**, 1636–1643 (2016). https://pubs.rsc.org/en/content/articlelanding/2016/lc/c6lc00180g.
46. Baret, J.-C. *et al.* Fluorescence-activated droplet sorting (FADS): efficient microfluidic cell sorting based on enzymatic activity. *Lab Chip***9**, 1850–1858 (2009). https://pubs.rsc.org/en/content/articlelanding/2009/lc/b902504a.
47. Brouzes, E. *et al.* Droplet microfluidic technology for single-cell high-throughput screening. *Proc. Natl. Acad. Sci. U.S.A.* **106**, 14195–14200 (2009).
48. Mazutis, L. *et al.* Single-cell analysis and sorting using droplet-based microfluidics. *Nat. Protoc.***8**, 870–891 (2013). http://www.nature.com/articles/nprot.2013.046.
49. Klein, A. M. *et al.* Droplet barcoding for single-cell transcriptomics applied to embryonic stem cells. *Cell***161**, 1187–1201 (2015). http://www.sciencedirect.com/science/article/pii/S0092867415005000.
50. Macosko, E. Z. *et al.* Highly parallel genome-wide expression profiling of individual cells using nanoliter droplets. *Cell***161**, 1202–1214 (2015). http://www.sciencedirect.com/science/article/pii/S0092867415005498.
51. Zheng, G. X. Y. *et al.* Massively parallel digital transcriptional profiling of single cells. *Nat. Commun.***8**, 14049 (2017). https://www.nature.com/articles/ncomms14049.
52. Duffy, D. C., McDonald, J. C., Schueller, O. J. A. & Whitesides, G. M. Rapid prototyping of microfluidic systems in poly(dimethylsiloxane). *Anal. Chem.* **70**, 4974–4984. https://doi.org/10.1021/ac980656z (1998).
53. Student. The Probable error of a mean. *Biometrika***6**, 1–25 (1908). https://www.jstor.org/stable/2331554.
54. Zabell, S. L. On student's 1908 Article "The Probable Error of a Mean". *J. Am. Stat. Assoc.***103**, 1–7 (2008). https://doi.org/10.1198/016214508000000030.
55. Fritz, C. O., Morris, P. E. & Richler, J. J. Effect size estimates: current use, calculations, and interpretation. *J. Exp. Psychol. Gen.* **141**, 2–18 (2012).
56. de Winter, J. C. F. Using the student's t-test with extremely small sample sizes. *Practical Assess. Res. Eval.***18**, 1–12 (2013).
57. Hedges, L. V. Estimation of effect size from a series of independent experiments. *Psychol.Bull.***92**, 490–499 (1982). https://www.scholars.northwestern.edu/en/publications/estimation-of-effect-size-from-a-series-of-independent-experiment.

Acknowledgements
This project has received funding from the French Government 'Investments for the Future' Program, University of Bordeaux Initiative of Excellence (ANR-10-IDEX-03-02) and from the 'Région Nouvelle Aquitaine'. S.H.O. acknowledges the support of the Univ. Bordeaux for her PhD fellowship. Emulseo (www.emulseo.com), startup launched with the financial support of the European Research Council (ERC) under the European Union's Horizon 2020 research and innovation program (grant agreement No. 727480), kindly provided the surfactant used in the study.

Author contributions
S.H.O. performed the experiments and analyzed the data, L.B. contributed analytical tools with the setup of the optical system, T.B. contributed analytical tools for the microfluidic encapsulation and analysis, D.P. and M.T. performed preliminary experiments on the viability of cells in drops. L.R and J.C.B conceived and supervised the project with contribution of F.B. and analyzed the data. S.H.O., L.R. and J.C.B wrote the manuscript with contributions from all authors. All authors reviewed the manuscript.

Competing interests
J.-C. B. is the founder of Emulseo developing the surfactant formulation used in the manuscript. All other authors do not have any competing interest to declare.

Additional information
Supplementary Information The online version contains supplementary material available at https://doi.org/10.1038/s41598-021-97356-7.

Correspondence and requests for materials should be addressed to L.R. or J.-C.B.

Reprints and permissions information is available at www.nature.com/reprints.

Publisher's note Springer Nature remains neutral with regard to jurisdictional claims in published maps and institutional affiliations.

Confining *Trypanosoma brucei* in emulsion droplets reveals population variabilities in division rates and improves *in vitro* cultivation

Simone H. Oldenburg,[1,2] Lionel Buisson,[1] Thomas Beneyton,[1] Deniz Pekin,[1] Magali Thonnus,[2] Frédéric Bringaud,[2] Loïc Rivière,[2] and Jean-Christophe Baret[1,3]

[1] *Université de Bordeaux, Centre National de la Recherche Scientifique, Centre de Recherche Paul Pascal, Unité Mixte de Recherche 5031, Pessac, 33600, France*

[2] *Université de Bordeaux, Centre National de la Recherche Scientifique, Microbiologie Fondamentale et Pathogénicité, Unité Mixte de Recherche 5234, Bordeaux, 33076, France*

[3] *Institut Universitaire de France, Paris, 75231, France*

Supplementary text

Growth stability

To ensure that any observed variability was not caused by changed or unstable growth from age differences or population drifting, we made growth curves of the starting bulk cultures (Fig. S1). During the first and the last two weeks of the of the experimental time span, the cells were counted every day and diluted back to the initial densities where doubling times were calculated from the cumulative cell numbers.

Microfluidic devices

Two microfluidic devices were used for respectively cell encapsulation and droplet incubation (Fig. S2). Cell encapsulation devices are made from negative photoresists molds by standard soft lithography techniques [1]. The two-dimensional incubation chamber are fabricated as described in the main text [2].

Long term repetition

After testing the possibility of up-scaling the drop yield (main text Fig. 5), we compared the results between the up-scaling growth experiment with the initial survival and growth experiments (main text Fig. 3) both from incubation in the two-dimensional chamber. Up-scaling experiment are here referred to as 'New data' where the initial survival and growth experiments are referred to as 'Previous data' (Fig. S3). The Previous data and the New data were made with a eight month gab, where all material conditions were renewed. With the use of new batches of cells, culture medium and surfactant, no significant difference (P = 0.53) was observed in survival and growth between encapsulated *T.b. brucei* in 0.5 nL droplets after 24 hours of incubation.

Optical setup

All experiments were executed on a homemade laser-induced epifluorescence setup build on an inverted microscope (Fig. S4). Syringe pumps were controlling the flows of the devices which together with excited fluorescence by a continuous laser (473 nm) were used to calculate the exact droplet volumes. The laser was passed by an optical density filter (OD) and focused directly on the drops through the microscope objective directed by a mirror (M) and a dichronic mirror (DM). Fluorescent signal was directed back through the DM, a notch filter (NF) and split by a beam splitter (BS). One beam was directed to the camera, where the other was filtered by a band pass filter (BF) and collected by the PMT with a NI acquisition card (DAQ). The fluorescent signal acquisition was controlled on the computer by a LabVIEW program. To reduce background noise fluorescence collection was done in confocal configuration through a pinhole (P).

Droplet volumes

Droplet volumes were determined as $V_{drops} = Q/f$ with Q as the cell suspension flow rates in $\mu L/h$ and f as droplet frequency. The droplet frequency were calculated from the signals obtained by the laser measurements as $f = N_{drops}/\Delta t$. Background fluorescence from the cell culture medium made it possible to record signals for the individual drops as fluorescence signal over a period of time, where one peak equals one drop (Fig S4 Insert).

Counting a given number of drops N_{drops} in a certain time span Δt allowed us to find the droplet frequency and calculate the exact droplet volumes.

Supplementary movies

Movie S1. Start of incubation (t= 0) for encapsulated trypanosomes in 0.2 nL droplets.

Movie S2. 24 hours of incubation for encapsulated trypanosomes in 0.2 nL droplets.

Movie S3. 48 hours of incubation for encapsulated trypanosomes in 0.2 nL droplets.

Movie S4. Start of incubation (t= 0) for encapsulated trypanosomes in 0.5 nL droplets.

Movie S5. 24 hours of incubation for encapsulated trypanosomes in 0.5 nL droplets.

Movie S6. 48 hours of incubation for encapsulated trypanosomes in 0.5 nL droplets.

Movie S7. Start of incubation (t= 0) for encapsulated trypanosomes in 2 nL droplets.

Movie S8. 24 hours of incubation for encapsulated trypanosomes in 2 nL droplets.

Movie S9. 48 hours of incubation for encapsulated trypanosomes in 2 nL droplets.

[1] D. C. Duffy, J. C. McDonald, O. J. A. Schueller, and G. M. Whitesides, Anal. Chem. **70**, 4974 (1998), ISSN 0003-2700, URL `https://doi.org/10.1021/ac980656z`.

[2] K. Eyer, R. C. L. Doineau, C. E. Castrillon, L. Briseño-Roa, V. Menrath, G. Mottet, P. England, A. Godina, E. Brient-Litzler, C. Nizak, et al., Nature Biotechnology **35**, 977 (2017), ISSN 1087-0156, 1546-1696, URL `http://www.nature.com/doifinder/10.1038/nbt.3964`.

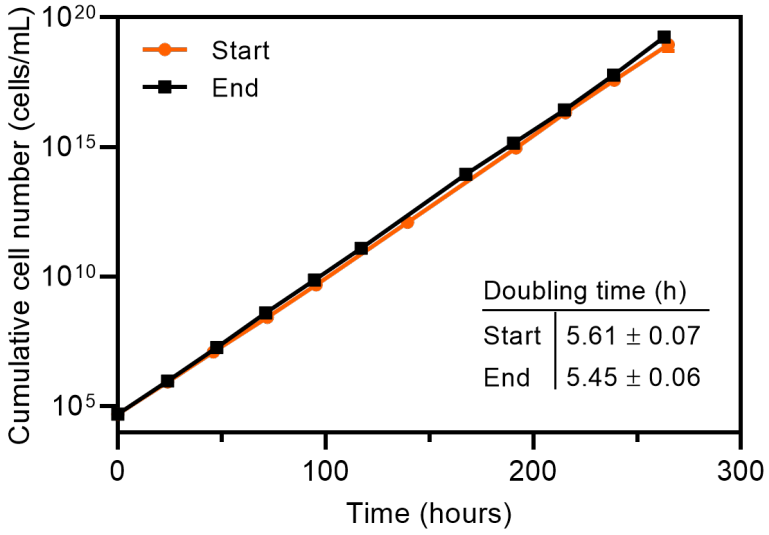

FIG. S1: Growth curves of *T.b. brucei* in bulk culture. Growth curves are presented as logarithmic accumulated cell number over time during a two-week period. Cells are counted at the beginning (orange) and the end (black) of the survival and growth experiments. Inserted table shows the respective doubling times from the start and the end measurements. All data are represented as mean values ±SD of technical replicates (n = 3).

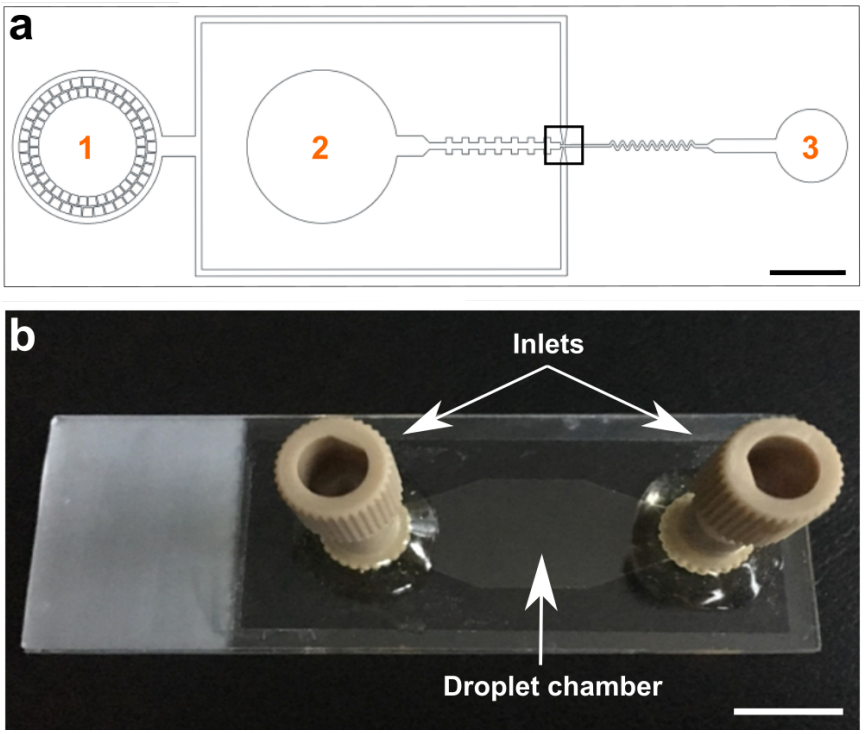

FIG. S2: Microfluidic devices for *T.b. brucei* encapsulation and incubation. (**a**) CAD design of a drop maker for single-cell encapsulation consisting of the oil inlet (1), the cell suspension inlet (2) and the collection outlet (3). The black square represents the microscopic image presented in Fig. 1b. Scale bar is 1 mm. (**b**) Incubation chamber enabling mono dispersed arrangement of drops adapted from Eyer *et al.* (2017)[2]. Scale bar is 12 mm.

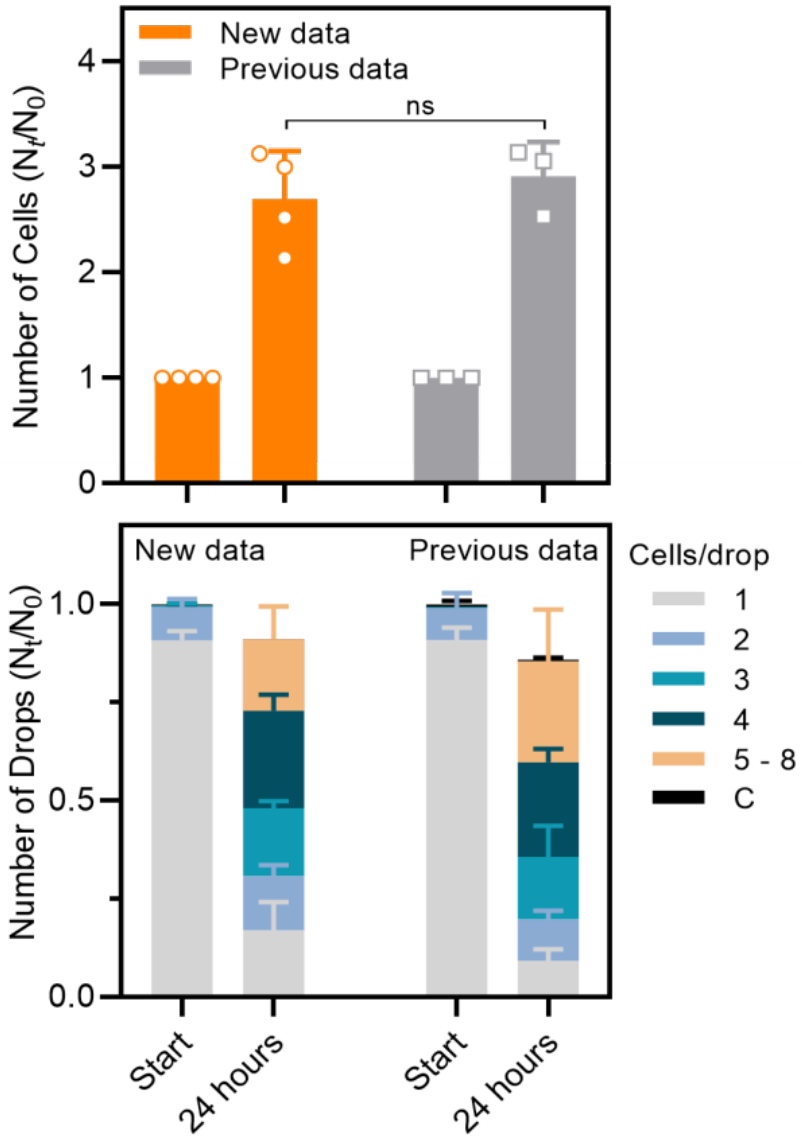

FIG. S3: Collection and incubation of *T.b. brucei* in 0.5 nL drops. Comparison of Previous data and New data of cell survival as normalized values after collection and 24 hours of incubation in two-dimensional incubation chamber (upper). Supporting cell survival data is the presentations of growth after 24 hours as normalized number of drops containing a given number of cells (lower). All data are presented as mean values ±SD. Two-sided Student's t-test were used in the upper graph to find significance value ($P = 0.53$) with $n = 3$ in Previous data and $n = 4$ in New data as biological replicates.

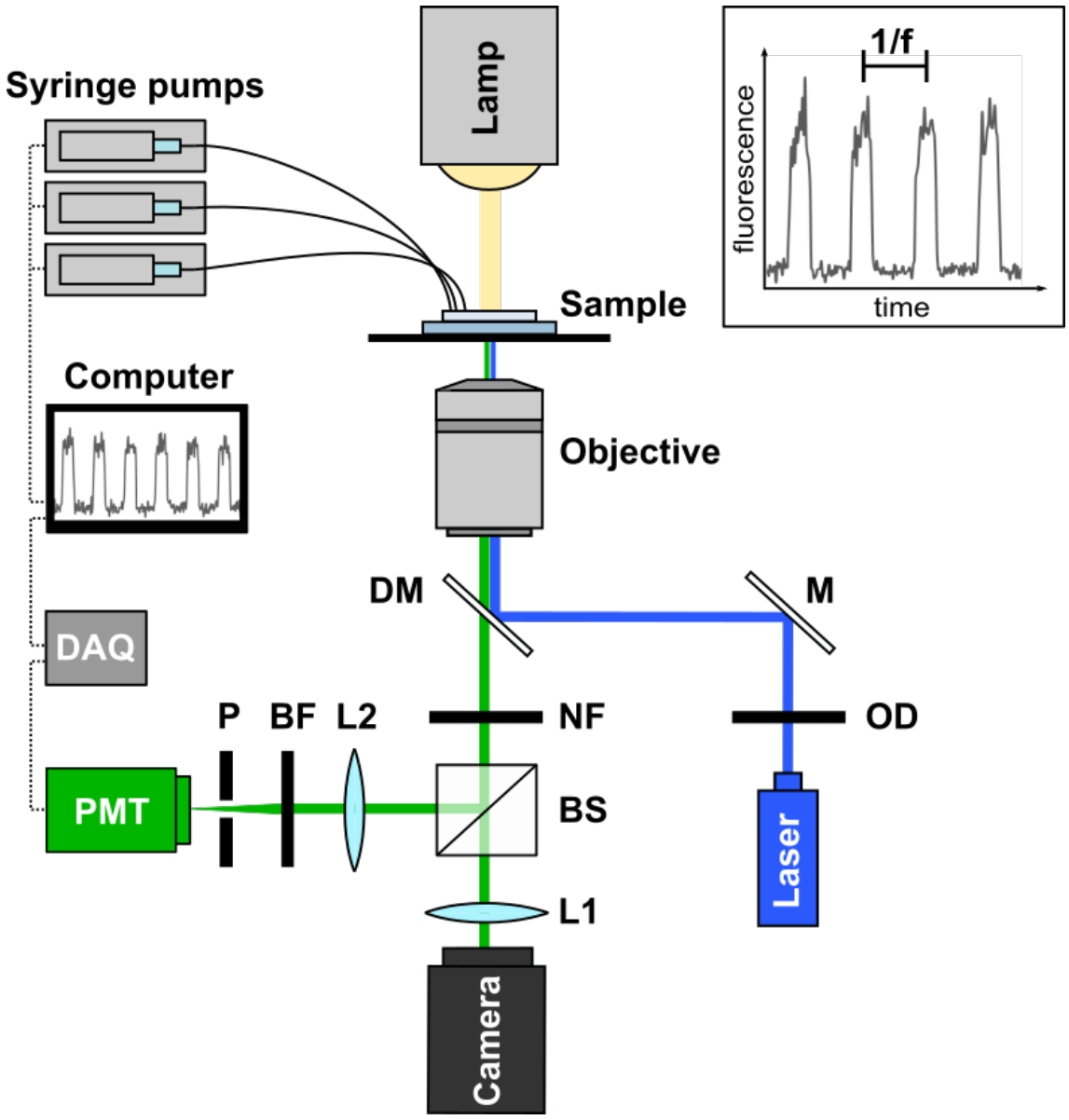

FIG. S4: Illustration of microfluidic setup used for all experiments. The setup is constructed by implementing the following components to an inverted microscope; syringe pumps, computer for control and acquisition, data acquisition (DAQ) card, photomultiplier tube (PMT), pinhole (P), band pass filter (BF), PMT lens (L2), dichroic mirror (DM), notch filter (NF), beam splitter (BM), camera lens directly from microscope (L1), mirror (M) and optical density (OD). Inset: Example of recorded signal from the drops used to calculate the droplet sizes. Illustration is created in Inkscape (https://inkscape.org).

3.2 Additional data

3.2.1 Survival deficiencies in aged cultures

In the work presented in this chapter, the cells were continuously sub-cultured for a maximum period of two months. After two months the cells were trashed and a fresh batch of cells was de-frozen and prepared for use. In our preliminary tests of cell encapsulation and survival, I did not give much attention to the time span of the sub-culturing. This resulted in encapsulation tests on cells continuously sub-cultured for appx. six months. When comparing the six months sub-cultivation (Old) with the two month sub-cultivation (New) in 0.5 nL drops, we observe significant differences in survival and growth (Fig. 3.1a and Table 3.1). The total cell number from the old culture only increase by a small fraction during the first eight hours of incubation, where the total number from the new cell culture increase by a factor of two. While the new culture reach a maximum cell number after 24 hours of incubation, the total number of cells in the old culture have decreased to half of the initial cell number at this time. Total cell death is observed after 48 hours. In addition, for the old sub-culture we observe that half of the drops or more only contain one cell during the experiment, where most of the growth were represented by two cells (Fig. 3.1b). In the new sub-culture, the majority of the drops contain growing cells at eight hours and forth, with most of the growth represented by more than two cells from 24 hours and forwards (Fig. 3.1c). These results suggest deficiencies in survival and growth of cells in long-term maintained cultures. Repetitive sub-culturing of trypanosomes could be a burden for the population with a decrease in growth dynamics in later generations. This could be a side effect of *in vitro* cultivation where natural environments most likely benefit the population on the long-term. All experimental procedures are the same as described in the publication above.

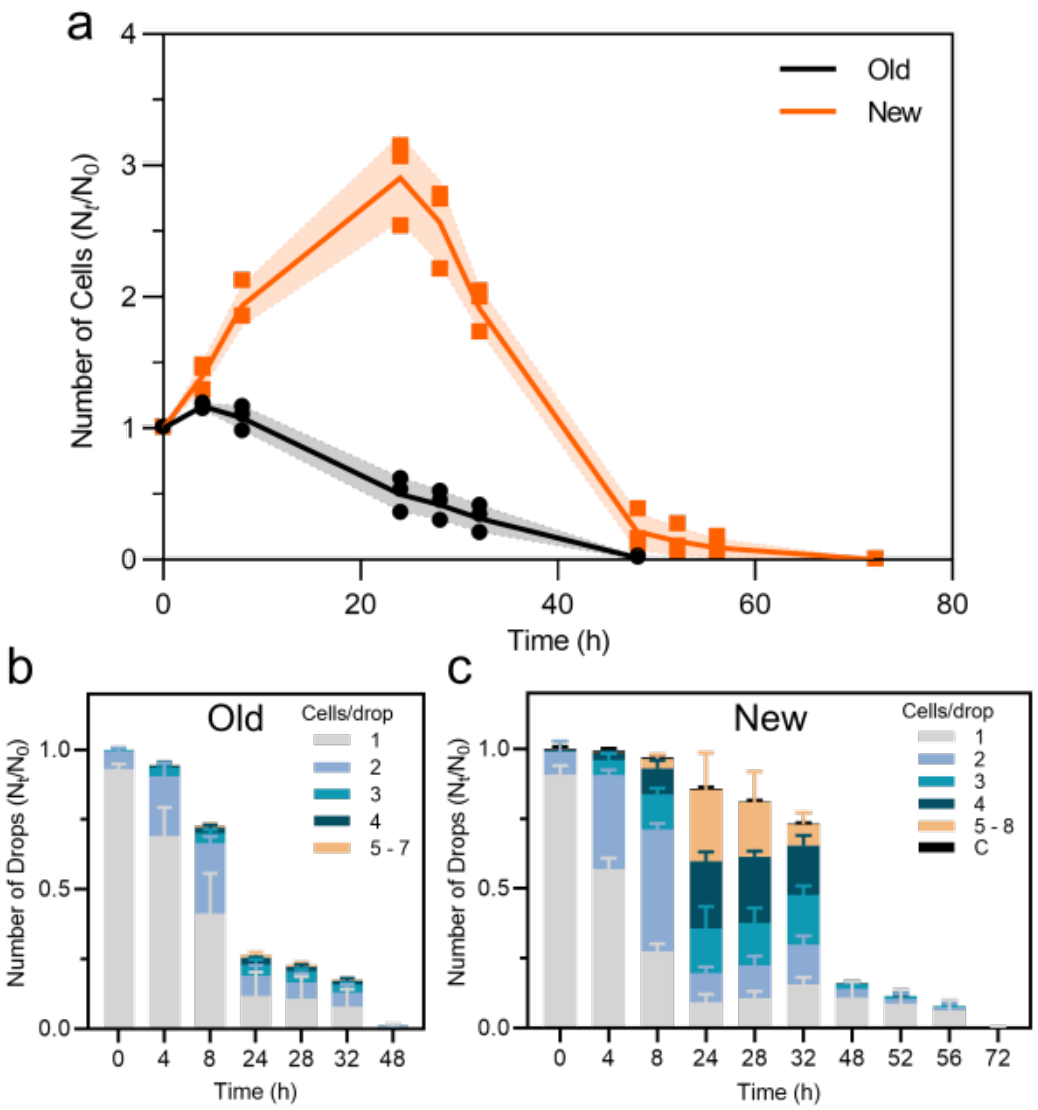

Figure 3.1: Survival and growth in 0.5 nL drops. (**a**) Comparison of cell survival, defined as normalized total cell number, between an old (black) and a new (orange) cell culture over time in 0.5 nL drops. The data are presented as mean values ±SD and all the individual data points. Supporting the cell survival data is the presentations of growth over time defined as normalized number of drops containing a given number of cells for the old cell culture (**b**) and the new cell culture (**c**). The data are presented as mean values ±SD. All experimental data are made as biological replicates (n = 3). Significance values supporting the survival differences observed in (**a**) are presented in Table 3.1.

Time (hours)	P-value	Significance	Effect size (g)
4	0.01790	*	3.16
8	0.00123	**	6.66
24	0.00030	***	9.61
28	0.00038	***	9.02
32	0.00015	****	11.45
48	0.07186	*	1.99
52	-	-	-

Table 3.1: Difference in cell survival between old and new sub-cultures in 0.5 nL drops. Statistical differences are presented as P-values. Two-sided Student's t-test was used to find significance values. Effect sizes were calculated as Hedges' g [180]. P>0.05 = non significant (ns), P≤0.05 = *, P≤0.01 = **, P≤0.001 = *** and P≤0.0001 = ****.

3.3 Summary

I have here tested the compatibility of encapsulating and cultivating single cell trypanosomes in microcompartment droplets.

- I showed the reliability of single cell encapsulation by following the Poisson distribution as for any type of particle.
- I discovered that big droplet volumes led to longer survival and higher cell numbers, where small volumes led to higher cell densities (cells per volume)
- From cultivation in drops, I revealed various growth patterns within the same droplet volumes, indicating heterogeneous growth behaviours between cells in a population.
- I demonstrated the possibilities of up-scaling the droplet yield without changing the growth dynamics, by using a collection device with a larger volume.
- Lastly, I discovered possible age deficiencies from long-term sub-cultivation, showing a significant decrease in growth from an old cell culture.

4 Enzyme secretion by single-cell *T. b. brucei*

In this chapter, I investigate the dynamics of enzyme secretion from *T. b. brucei* at the single-cell level. I first test the compatibility of different commercialized kits for detection of enzyme activity for the use in droplet-based microfluidics. I select the best candidate for encapsulation with *T. b. brucei* for detection of secreted enzymes in micro-compartment droplets and validate the detected activity.

4.1 Introduction

When infecting a mammal host, trypanosomes are exposed to an hostile environment continuously facing attacks of host immune cells. A part of the trypanosome defence mechanism is the release of various pathogenic factors when a majority of the infecting cells are facing trypanolysis. Infected mammals have been recorded suffering from severe anemia during the recovery phase of the parasitemia cycle, where dying cells release compounds as phospholipase and protease with pathogenic properties [17, 18, 19]. Later studies have further identified secretion of several protease classes from living trypanosomes including cysteine peptidase, oligopeptidase and metallopeptidase [19, 20, 21, 22]. Cysteine peptidases are considered to play a crucial role during trypanosome infections. They have been proposed to play a direct role in crossing the BBB (blood-brain barrier) in the late stage infection and to protect the cells from lysis of the host serum [19, 20, 181, 182]. The activity of oligopeptidases have been the suggested mechanism of penetrating the endothelium layer promoting cell proliferation outside the vascular system as well as the crossing of the BBB [22, 181]. Other oligopeptidases identified in the secretome of trypanosomes are the metallopeptidases whose activities are involved in blood coagulation and inflammation [183]. With the many pathogenic roles in trypanosome infection, secreted enzymes like protease make good candidates for drug targeting. However, with the prospective of a heterogeneous behaviour within

a population, as we also observed in chapter 3, analytical methods are needed for quantitative measurements of secreted enzymes on a single-cell level.

Droplet-based microfluidics have shown advantageous in detecting secreted compounds from single cells. Several studies have focused on immune responses where some have detected antibody secretion from single cells [165, 144, 154, 159], while others have focused on detection of secreted cytokines from immune cells like T-cells and dendritic cells [151, 166, 184]. Other studies have used droplet-microfluidics for successful detection of cell-secreted enzymes and measured the enzymatic activity on a single-cell level [168, 185, 167]. Although these studies are using different procedures for detection single-cell secretion, all in common they depend on emitted fluorescence for enabling detection. With the potential of coupling sorting modules for fluorescence-based selection of active drops, droplet-microfluidics makes a perfect tool for analysing enzyme secretion on single-cell trypanosomes.

I here develop an in-drop secretion assay for detection of enzyme activity by fluorescence measurements on single cell *T. b. brucei* (4.1). I identified a number of enzymes possibly related to trypanosomes virulence. Table 4.1 summarize a list of enzymes, their possibilities for activity detection and the best candidates to use in drops for single cell measurements. Trypanosomes and enzyme substrate will be mixed on-chip prior to encapsulation creating numerous mono-dispersed droplets working as bioreactors (4.1a). In order to ensure encapsulation of single cells, the majority of the droplets will be empty only containing enzyme substrate. Collected drops will be reinjected after sufficient time of incubation, where fluorescence are measured to detect activity of secreted enzymes (4.1b).

Table 4.1: Overview of secreted protease from *T. b. brucei*. A presentation of enzyme candidates for single-cell detection, available detection methods and compatibility with laser detection.

Enzyme	Assay	Detection method	Type	Laser detection (473 nm)
Phospholipase	Commercial	Fluorometric (505/515 nm)	PLA2	✓
		Fluorometric (509/516 nm)	PLC	✓
Protease	Commercial	Fluorometric (505/513 nm)	Various protease classes	✓
Glycolytic enzymes	Commercial	Fluorometric (535/587 nm)	Enolase	-
		Fluorometric (535/587 nm)	Hexokinase	-

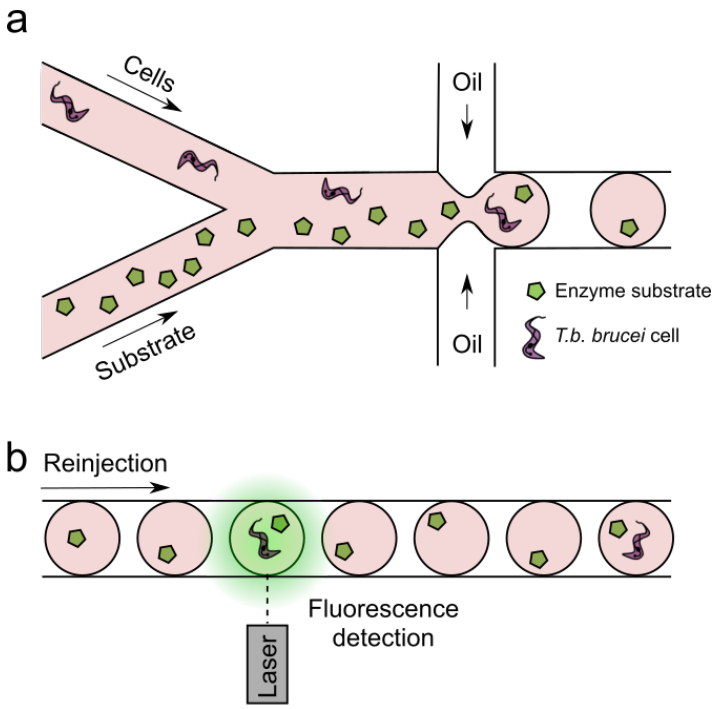

Figure 4.1: Overview of our single-cell enzyme assay. (**a**) Encapsulation process of trypanosomes and enzyme substrate in co-flow device following collection of drops.(**b**) After incubation the collected drops are reinjected where enzyme activity is detected as fluorescent drops by laser measurements.

4.2 EnzChek enzyme activity kits

Before starting the analysis of enzymatic secretion from single-cell trypanosomes, I test different commercialized enzyme activity kits to ensure a good compatibility with droplet-based microfluidics. I test three different kits, two for detecting phospholipase activity of phospholipase A2 (PLA2) and phospholipase C (PLC), and one for the detection of protease activity. The substrates of the phospholipase activity kits are based on the fluorescent molecule BODIPY^{TM}FL being attached to the second fatty acid tale (sn-2) of a phospholipid (Fig. 4.2.). For the PLA2 substrate an additional BODIPY^{TM}FL molecule is attached to the first fatty acid tail (sn-1) working as a FRET acceptor prior to cleavage. This allow us to also measure activity as a change in the emission ratio upon cleavage.

The protease substrate is based on a casein derivative protein which allows detection of a broad range of proteases including a number of serine proteases and metalloprotease. The substrate is highly labeled with BODIPY^{TM}FL molecules resulting in quenched fluorescence prior to cleavage. When a protease is present the substrate protein will be cleaved into smaller fragments, resulting in a continuous increase of

fluorescence over longer periods of time (Fig. 4.3).

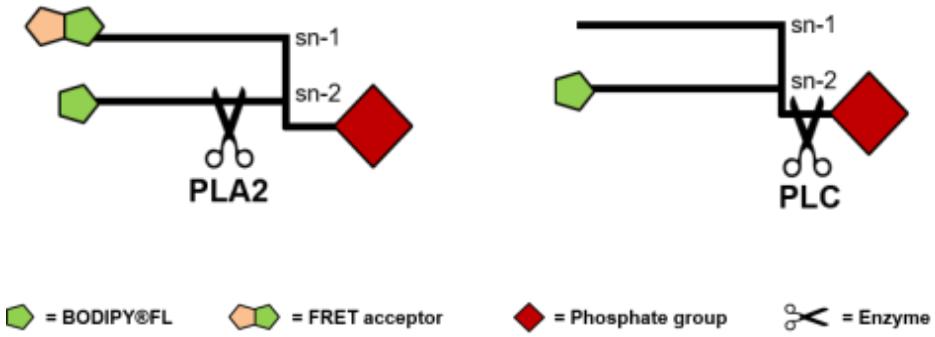

Figure 4.2: Substrates of phospholipase A2 and phospholipase C. The phospolipase substrates consists of a phospholipid with a fluorescent BODIPY^{TM}FL molecule attached to the second fatty acid tail (sn-2). In co-presence of PLA2 and PLA2 substrate, the sn-2 is cleaved and fluorescence is emitted from both sn-1 and sn-2 detectable at different wavelengths (left). For PLC substrate the presence of PLC cleaves the dye-labeled diacylglycerol from the rest of the phospholipid releasing fluorescence (right).

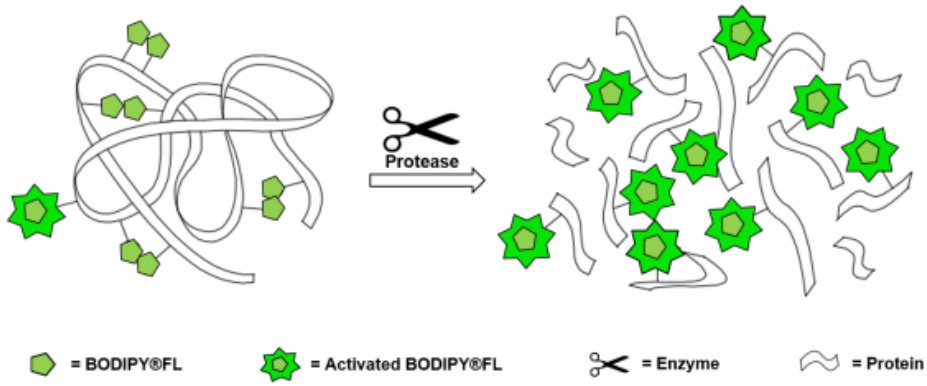

Figure 4.3: Substrate for protease detection. In the presence of a protease the quenched substrate is cleaved and fluorescence will gradually increase over time. The figure is modified from the manufacture's protocol.

4.2.1 Phospholipase compatibility test

I first test the compatibility of the PLA2 substrate with droplet-microfluidics. Two populations of drops are made in a dual production device. One population contain the end product from a two hour enzymatic reaction of 3 µM PLA2 substrate and 4 U mL^{-1} PLA2. The other drop population is empty and contain only dilution buffer. After production, the drops are collected in a collection vial and a 2D incubation chamber. After one hour of incubation the drops are either reinjected for fluorescent detection by laser measurements or observed under a fluorescence microscope when

fixed in an incubation chamber. By laser measurements of the reinjected droplets, only one population is detected indicating leakage of the fluorescent product between the drops (Fig. 4.4).

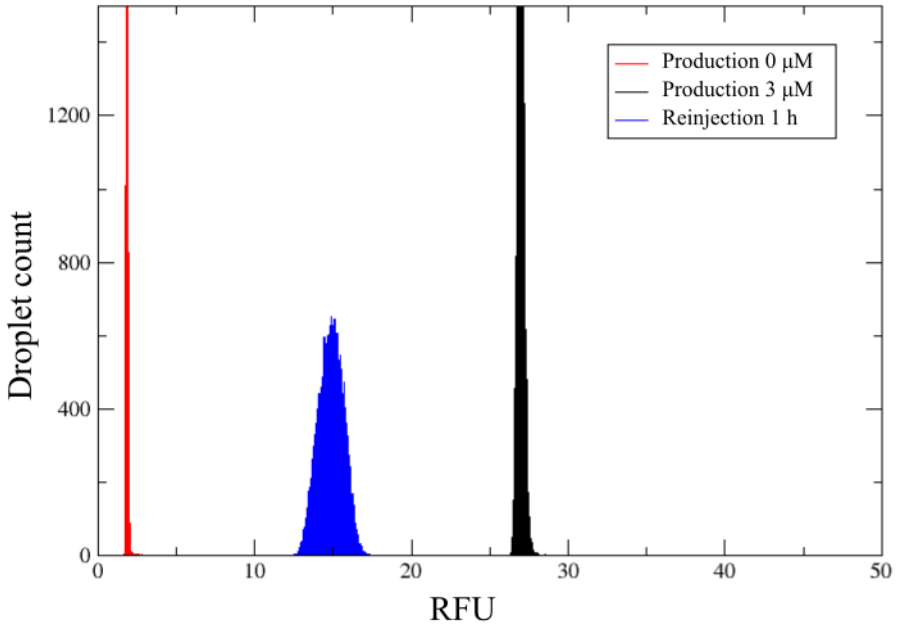

Figure 4.4: PLA2 activity measurements in drops. Fluorescence measurements of droplet production of empty drops (red) and drops containing the PLA2 enzyme reaction (black) and the reinjection of both populations after one hour of incubation (blue).

The observations by fluorescence microscopy support the indications of fluorescent leakage. After one hour of incubation fluorescence is appearing in the population of empty drops (Fig. 4.5). I further measure the change in intensity ratio between the two fluorescent molecules after cleavage, where leakage also is observed. The PLA2 kit is therefore discarded for further use due to high substrate leakage between the droplets.

Next I test the PLC substrate for compatibility with droplet-microfluidics, where the end product is a bigger compound and thereby holds the opportunity to remain inside the drops. Two droplet populations are made in a dual production device with the end reaction of 1X substrate and $1\,\mathrm{U\,mL^{-1}}$ enzyme in one population and dilution buffer in the other population. The drops are collected and reinjected for laser measurements like for the PLA2 tests. After only half an hour of incubation a high degree of leakage is observed between the drops, where only one main peak appears at reinjection (Fig. 4.6).

When observing the PLC reaction in drops by fluorescence microscopy we see a very high degree of leakage. After one hour of incubation no difference is seen between the two drop population (Fig.4.7). Furthermore, at observation immediately after col-

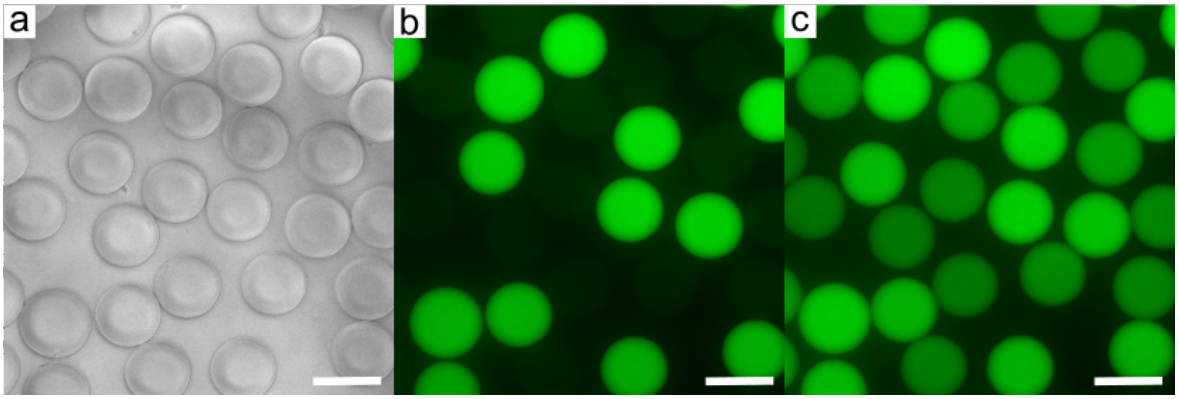

Figure 4.5: PLA2 fluorescence observation in drops. Images from fluorescence microscopy of the two droplet population through a 10× objective directly after collection with phase contrast (**a**) and fluorescence (**b**) and after one hour of incubation with fluorescence (**c**). All scale bars are 100 µm.

lection in the incubation chamber, only a very little difference is seen. We here identify the population containing the enzyme reactions by the presence of small aggregations of fluorescent compounds (Fig.4.7b: Insert). In addition, it appears that the fluorescent molecules have leaked out to the surrounding oil. The PLC activity kit is likewise discarded for further use due to high leakage issues. The leakage observed from the two phospholipase assay kits are likely a result of highly hydrophobic products. High hydrophobicity of organic molecules have shown to mediate leakage from and between drops [186, 187].

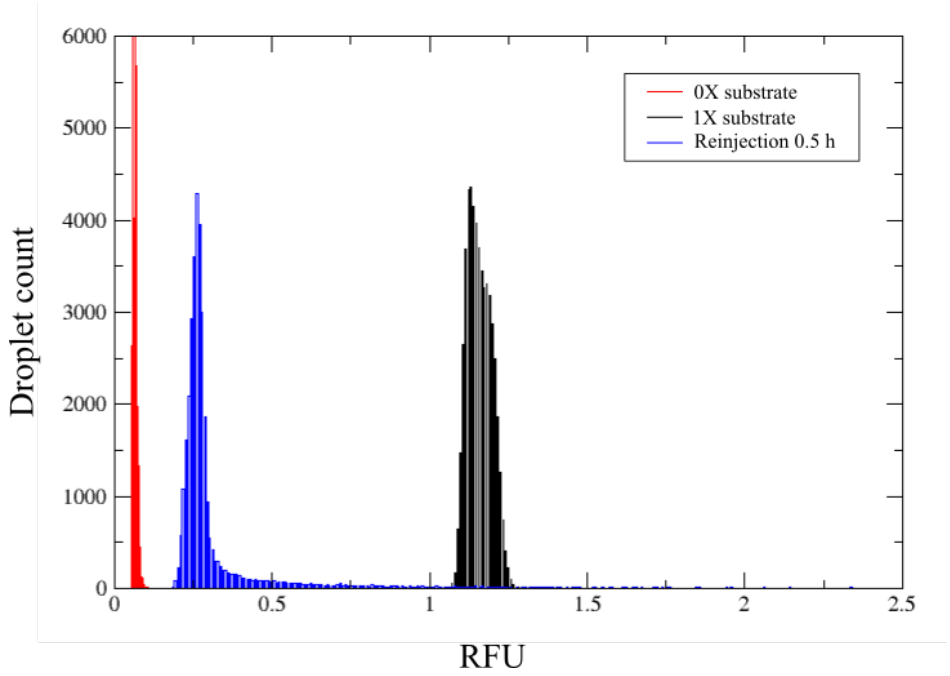

Figure 4.6: PLC activity measurements in drops. Fluorescence measurements of droplet production of empty drops (red) and drops containing the PLC enzyme reaction (black) and the reinjection of both populations after half an hour of incubation (blue).

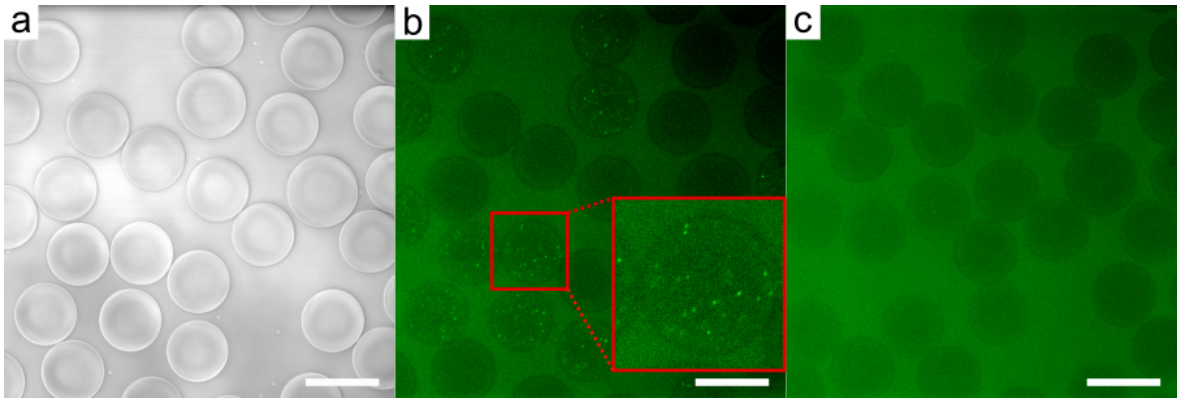

Figure 4.7: PLC fluorescence observation in drops. Images from fluorescence microscopy of the two droplet population through a 10× objective, directly after collection with phase contrast (**a**) and fluorescence (insert: close-up micrograph of aggregations in drop) (**b**) and after one hour of incubation with fluorescence (**c**). All scale bars are 100 µm.

4.2.2 Protease compatibility test

To test compatibility of the protease activity kit with our droplet system, I make two populations of drops from end products of a 2-3 hours reaction. In this work, I use the protease trypsin as our control protease. One population contain 10 µg mL^{-1} substrate and 3 µg mL^{-1} trypsin where the other population contain 1 µg mL^{-1} substrate and 3 µg mL^{-1} trypsin. Drops are made in a dual production device and collected in a collection vial. After one hour of incubation the drops are reinjected prior to laser measurements. Contrary to the phospholipase kits we here observe two distinct droplet populations (Fig. 4.8). Furthermore, after one day of incubation two distinct populations are still observed indicating no signs of product leakage between the drops.

In addition, droplets are produced where both populations contain 10 µg mL^{-1} substrate but only one population contain 3 µg mL^{-1} trypsin. Here, the droplets are collected in an incubation chamber for observation by fluorescence microscopy. After 24 hours of incubation we still observe two distinct droplet populations confirming that the fluorescent end-product did not leak (Fig. 4.9). Showing a good compatibility with droplet-based microfluidics, I select the protease activity kit for further use for trypanosome secretion analysis.

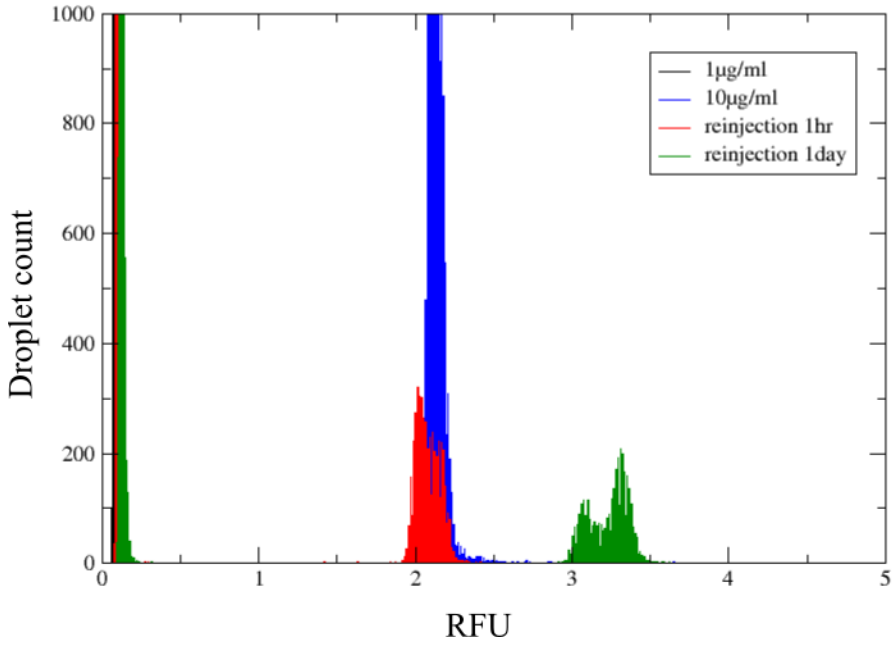

Figure 4.8: Protease activity measurements in drops. Fluorescence measurements of droplet production with drops containing protease enzyme reaction with 1 µg mL^{-1} substrate (black) and 10 µg mL^{-1} substrate (blue) and the reinjection of both populations after one hour (red) and 24 hours (green) of incubation.

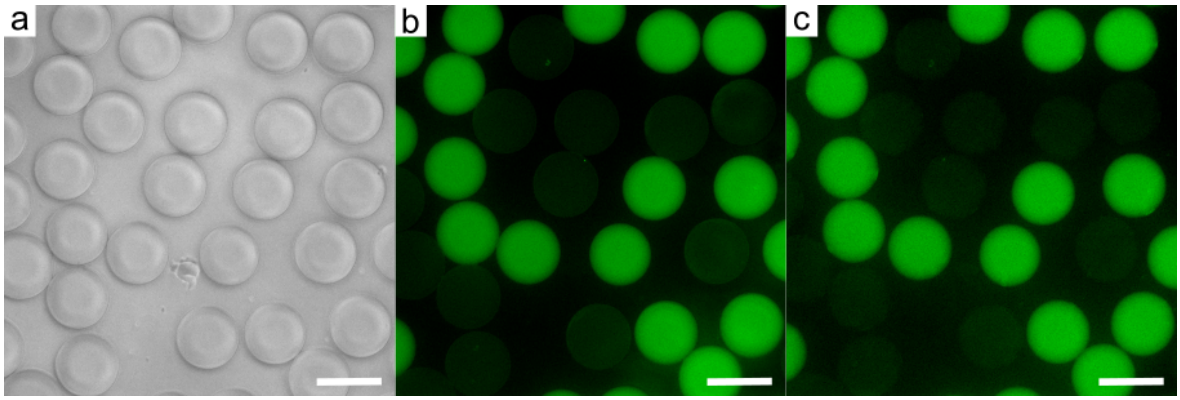

Figure 4.9: Protease fluorescence observation in drops. Images from fluorescence microscopy of the two droplet population through a 10× objective, directly after collection with phase contrast (**a**) and fluorescence (**b**) and after 24 hours of incubation with fluorescence (**c**). All scale bars are 100 µm.

4.3 *T. b. brucei* protease secretion

4.3.1 *T. b. brucei* protease secretion in bulk

Measurements of secreted *T. b. brucei* protease activity are made in bulk to estimate the average protease secretion from a population of trypanosomes. At first, I follow a secretion protocol to determine the activity of secreted enzyme [188]. After 2.5 hours of incubation in a secretion medium stressing the cells, the cells are removed from the medium now containing secreted compounds. The medium is either concentrated 30 folds or non-concentrated. The cell-free medium is then mixed with protease substrate and the activity is detected as emitted fluorescence in a plate reader together with a trypsin control (Fig. 4.10a).

In the non-concentrated samples, I detect a protease activity close to the equivalent of $0.2\,\mu g\,mL^{-1}$ trypsin (Fig. 4.10a open symbols). After concentration, the activity measured from the secretion medium is detected in the same level as $0.5\,\mu g\,mL^{-1}$ trypsin (Fig. 4.10a closed symbols). The fluorescence detection from the cell medium confirms the presence of secreted protease from the cells when incubated in secretion medium.

However, for single-cell *T. b. brucei* measurements in drops, we cannot follow the same procedure of removing the cells and concentrate the secretion medium from the individual drops. Measurements will instead be performed while the cells are still encapsulated in the drops and with longer incubation times between the measurements. Furthermore, the starting cell concentration will be lower to ensure the correct cell

number inside the drops. I therefor made a new in bulk assay to measure protease activity while mimicking the droplet experiments as much as possible. *T. b. brucei* are washed and diluted in secretion medium and mixed with protease substrate to a final concentration of 1.5×10^6 cells mL^{-1}. Protease activity is determined by endpoint fluorescence measurements after four, eight and 24 hours of incubation (Fig. 4.10b). A standard curve of trypin is prepared together with the cell samples.

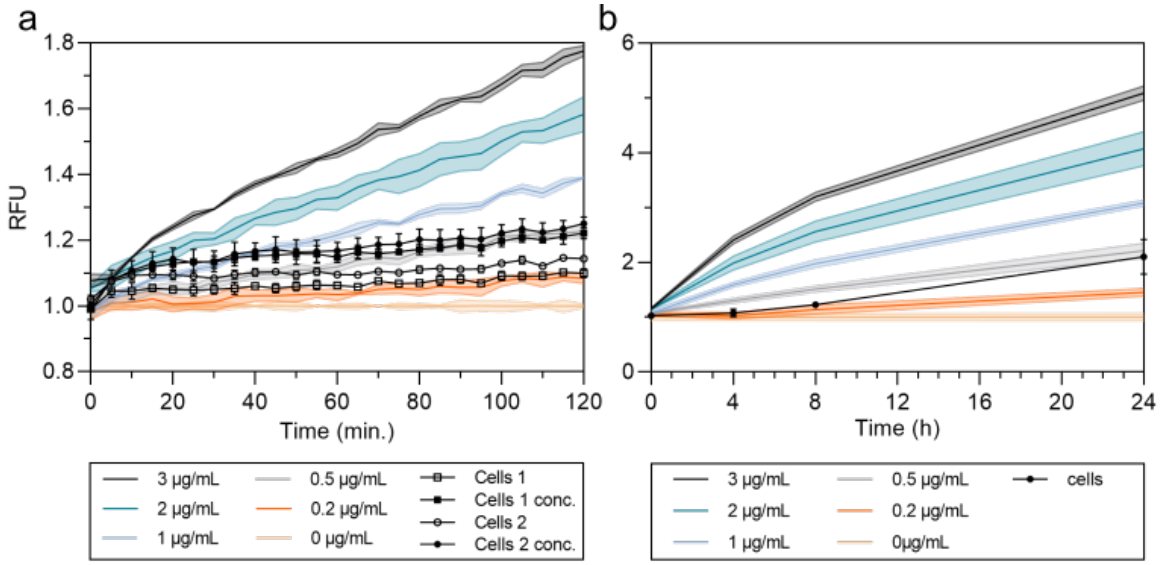

Figure 4.10: In bulk protease activity. (**a**) Protease activities from cell populations and trypin in mtp. (**b**) Endpoint measurements of protease activity after four, eigth and 24 hours from cell populations and trypin in mtp. Trypsin was used for all standard curves with concentrations ranging from 0 to 3 µg mL^{-1}.

After 4 hours of incubation the activity detected from the secretion medium is in the range of 0 to 0.2 µg mL^{-1} of trypsin. After eight hours of incubation the activity slightly increase being closer to 0.2 µg mL^{-1} trypsin. At 24 hours of incubation we observe that the detected activity is reaching same range as 0.5 µg mL^{-1} of trypsin. The high fluorescence detected after 24 hours of incubation are most likely from intracellular protease released upon cell death. The secretion medium is stressing the cells by starvation and the they can in most cases not survive for 24 hours.

The activity I detect from the bulk measurements are means of the total population. It is a common assumption that in population measurements, each cell contribute equally to the detected activity. However, we cannot rule out that some cells have a much higher activity while others have little or none at all. Therefore, it was in our interest to further investigate the secreted protease activity at the single-cell level using droplet-based microfluidics.

4.3.2 Protease assay control in drops

Prior to initiating the protease activity measurements on single cells, a positive control is performed in drops to be used as a droplet standard curve. I use a concentration of 20 µg mL^{-1} protease substrate and 2 µg mL^{-1} trypsin as a first control. Trypsin solutions of 2 and 0 µg mL^{-1} are emulsified with protease substrate in a co-flow encapsulation device, mimicking the same encapsulation process that will be used for *T. b. brucei* measurements. Drops of 0.2 nL are collected for both trypsin concentrations in the same collection vial and incubated at 37°C until further use. After four, eight and 24 hours of incubation fluorescence is measured. After four hours of incubation we foremost see a large variance in fluorescence (Fig.4.11).

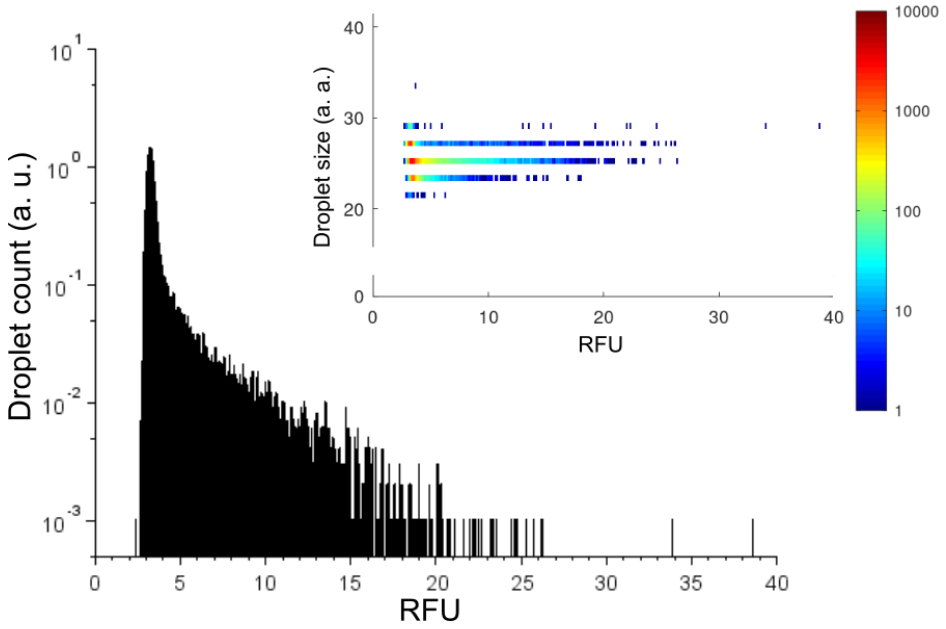

Figure 4.11: Positive control with empty drops. Reinjection of two droplet population with 2 and 0 µg mL^{-1} trypsin and 20 µg mL^{-1} substrate after four hours of incubation. Insert: Heatmap of droplet size vs. RFU.

We would expect two separate populations represented as two peaks for each of the trypsin concentrations. Here we observe one main peak around 3-4 RFU with the rest of the drops showing varying RFU values stretching from 4 all the way up to 20 and in a few drops even higher. Due to the large variability in fluorescence observed in Fig 4.11 we cannot distinguish the two droplet populations containing 0 or 2 µg mL^{-1} from each other. After eight and 24 hours of incubation we see the same large variability in detected fluorescence but with slightly higher mean fluorescence values (Table 4.2, Fig. A.1 and A.2). Two additional replicates are performed all showing a similar variability pattern in detected fluorescence.

Table 4.2: Control of protease assay in drops. Mean RFU values±SD of detected fluorescence over time for raw and normalized data.

	4 hours	8 hours	24 hours
Mean (RFU±SD)	7.05±3.23	7.52±3.75	8.08±4.11
Normalized mean (RFU±SD)	2.13±0.99	2.29±1.14	2.57±1.30

I repeat the assay using only a positive droplet population containing both protease substrate and trypsin, encapsulated in the same manner as before. After four hours of incubation we observe the same large variability of fluorescence (Fig. A.3)

These results are complicated to use as a standard curve to further estimate the degree of secreted protease from *T. b. brucei*, since it will be difficult to distinguish the different mean values from each other when using multiple trypsin concentrations. Due to this large variability when reactions were mixed on chip, I make a standard curve from off chip enzymatic reactions. Trypsin and protease substrate are mixed off chip to final concentrations of 0-3 $\mu g\,mL^{-1}$ trypsin and 20 $\mu g\,mL^{-1}$ substrate. After four, eight and 24 hours of incubation, endpoint reactions are emulsified to 0.2 nL droplets and fluorescence is measured (Fig. 4.12).

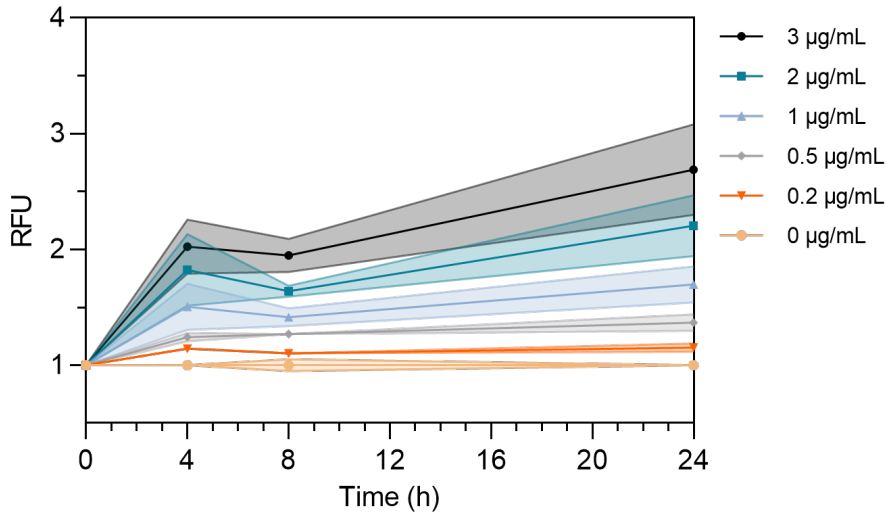

Figure 4.12: Trypsin standard curve at 37° in drops. 0-3 $\mu g\,mL^{-1}$ of trypsin and 20 $\mu g\,mL^{-1}$ protease substrate encapsulated in drops and incubated at 37°C.

We observe a small decrease in fluorescence for all the conditions after eight hours of incubation, with RFU values close to or lower than the fluorescence detected after four hours of incubation. The protocol of the protease activity kit recommends to incubate samples at room temperature. When following these recommendations we both observe

nicer shapes of the curves with the predicted increase over time and a general higher fluorescence for all the conditions (Fig. A.4). The deterioration of the standard curves when incubated at 37°C might be due to a negative effect on the protease substrate at high temperatures. Though incubation at room temperature resulted in better standard curves, I will be using the standard curve at 37°C as comparison to have the same conditions as needed for *T. b. brucei*.

4.3.3 Single-cell protease secretion

T. b. brucei cells and protease substrate are co-emulsified in a 50:50 ratio by a co-flow encapsulation device into 0.2 nL droplets, giving a final concentration of 20 µg mL^{-1} substrate and 1.5×10^6 cells mL^{-1}. This cell density equals an occupation factor $\lambda = 0.3$ corresponding to a theoretical occupation of around 26% when following a Poisson distribution (Fig. A.5). Drops are collected and incubated at 37°C until further use. After four, eight and 24 hours of incubation the drops are then reinjected and fluorescence is measured. Cell occupation and survival are estimated at start and after each fluorescence measurement (Fig. 4.13).

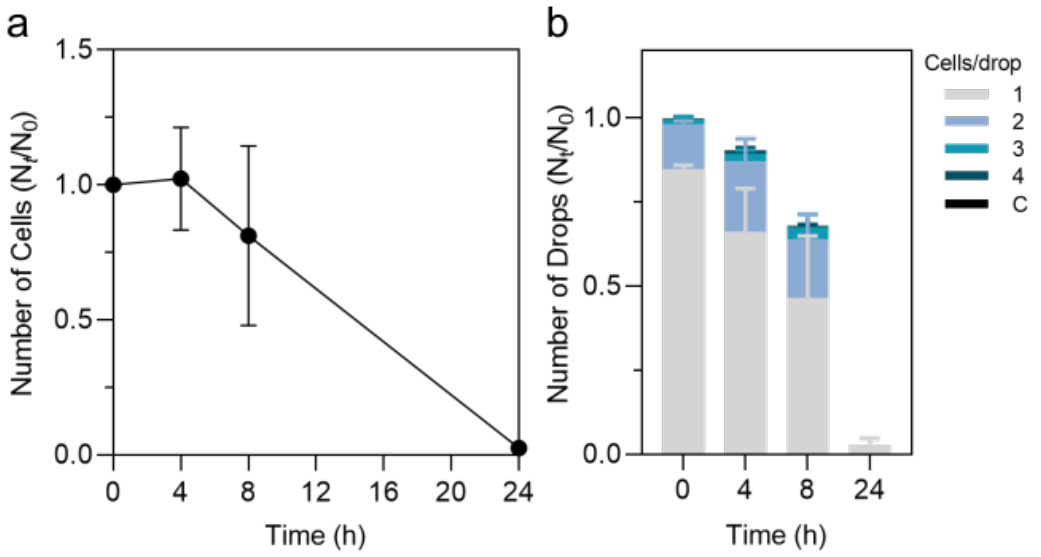

Figure 4.13: Cell survival and occupation. (**a**) Cell survival after encapsulation with protease substrate as normalized cell numbers. (**b**) Cell occupation in drops during encapsulation time as normalized droplet number.

We first observe that the cells are dying faster than compared to droplet incubation using standard cell medium as used in chapter 3 (Fig. 4.13a). Additionally, no or very little growth is observed during the first eight hours (Fig. 4.13b), and after 24 hours of incubation, almost all cells have died. This decline in survival and growth are expected

from using the specialised secretion medium. The cells are starved in order to trigger release of protease as a stress response.

From fluorescence measurements we observe a sub population with higher RFU values than the main population after four hours of incubation (Fig. 4.14a). We assume this sub population to be drops containing protease secreted from cells and the main population to be empty drops. The gray lines and squares represent the threshold I set, separating the empty and active drops. After eight and 24 hours of incubation the mean fluorescence of the sub population increase, as seen by a shift towards the right and a larger spread of variance (Fig. 4.14b,c). Mean values and standard deviations of the measured drops are presented in Table 4.3 together with the fraction of active drops and drops containing living cells.

Table 4.3: 1. replicate - Overview of secreted protease from encapsulated *T. b. brucei*. Mean RFU values±SD of detected fluorescence and the respective fractions of active drops and cell occupation for each condition over time.

	Start	4 hours	8 hours	24 hours
Mean (RFU±SD)	5.99±0.17	4.89±0.97	7.83±2.63	18.01 ±12.73
Normalized mean (RFU±SD)	1.00±0.03	1.56±0.31	2.35±0.79	4.91±3.47
Active drops (%)	-	15.89	18.03	22.41
Cell occupation (%)	17.72	18.94	16.51	0.40

In two additional replicates, less active droplets are detected than in the previous tests (Table 4.4 and Fig. A.6; Table 4.5 and Fig.A.7). The decrease in activity between replicates could be related to the time difference of two weeks between the execution of each replicate. This could have led to a change of fitness in the cell culture. In addition, the cells are taken from the bulk population roughly within the same range of their growth phase (2.47×10^6 cells mL^{-1} ; SD = 0.6). The small difference in fitness between cells taken from the lower range or the higher range of the growth curve, could have a substantial impact on the change of activity. This could both directly affect the survival of the cells themselves but also affect the stress response and thereby the release of protease.

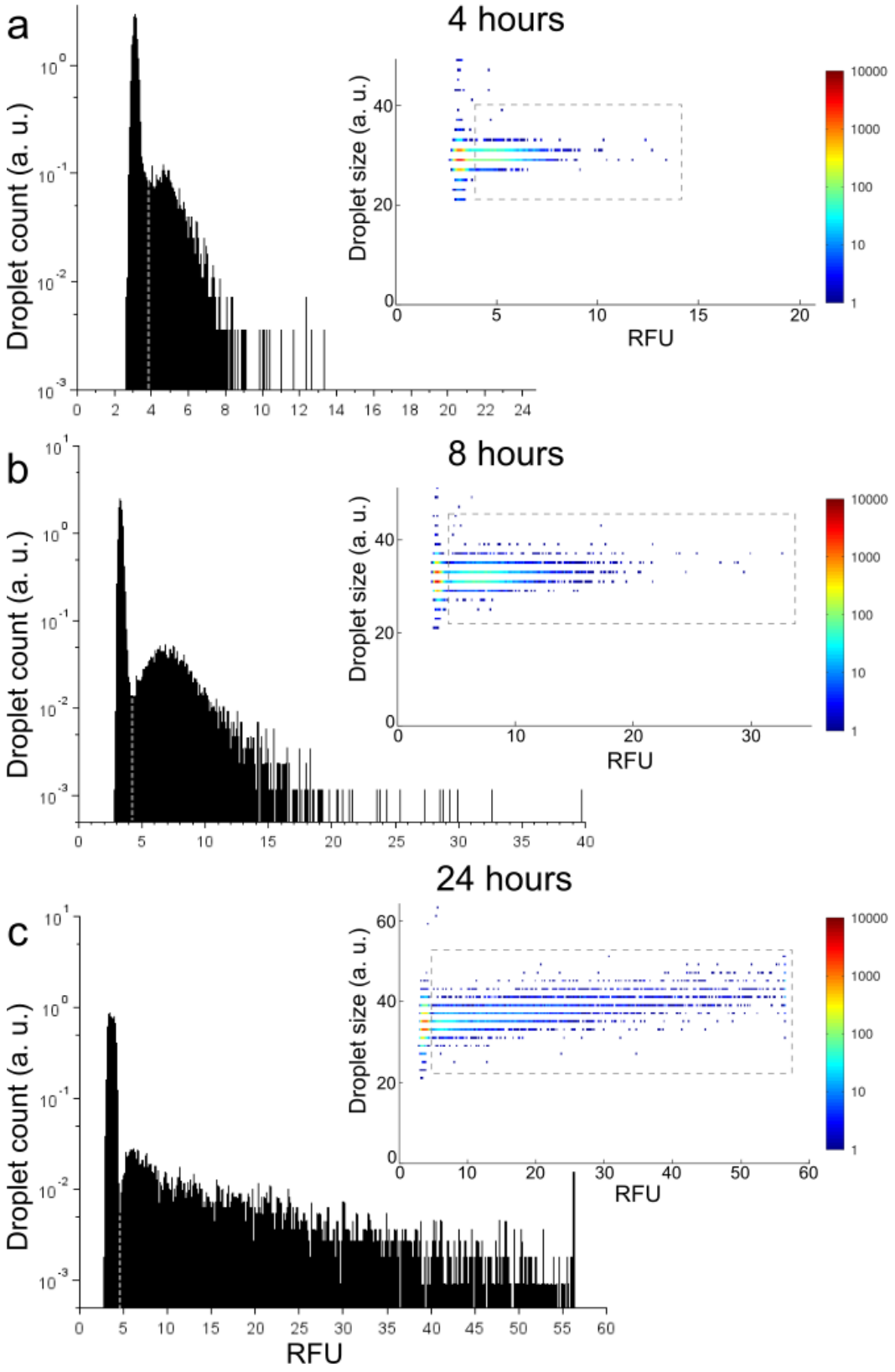

Figure 4.14: Fluorescence of encapsulated *T. b. brucei*. Fluorescence measurements of reinjected *T. b. brucei* encapsulated with protease substrate after four hours (**a**), eight hours (**b**) and 24 hours (**c**) of incubation, presented as droplet numbers at different RFU values. Inserts: Heat maps of droplet size vs. RFU for the respective reinjections.

Table 4.4: 2. replicate - Overview of secreted protease from encapsulated *T. b. brucei*. Mean RFU values±SD of detected fluorescence and the respective fractions of active drops and cell occupation for each condition over time

	Start	4 hours	8 hours	24 hours
Mean (RFU±SD)	7.08±0.23	5.78±2.04	6.49±2.74	15.04 ±10.31
Normalized mean (RFU±SD)	1.00±0.03	1.61±0.57	1.83±0.77	4.69±3.21
Active drops (%)	-	4.47	8.02	13.87
Cell occupation (%)	19.71	15.61	8.60	0.99

Table 4.5: 3. replicate - Overview of secreted protease from encapsulated *T. b. brucei*. Mean RFU values±SD of detected fluorescence and the respective fractions of active drops and cell occupation for each condition over time

	Start	4 hours	8 hours	24 hours
Mean (RFU±SD)	8.15±0.26	5.60±0.85	7.26±3.96	13.68 ±12.78
Normalized mean (RFU±SD)	1.00±0.03	1.39±0.21	1.83±1.00	3.25±3.04
Active drops (%)	-	0.12	1.63	7.80
Cell occupation (%)	17.00	14.44	11.43	0.27

To ensure that the fluorescence from active droplets are coming from cell-secreted protease, I do fluorescent microscopy to confirm the occupation of cells in active drops. I compare the fluorescence with phase contrast images to see the presence of cells inside the droplets (Fig. 4.15; Fig. A.8, black arrows). The fluorescence detected by laser measurements is much lower than the detection limit of the fluorescence microscope. This means that longer incubation times for more than 16 hours were needed to visually observe fluorescent droplets. In addition, we observe a high background fluorescence from empty drops, which might have covered up the droplets with lower fluorescence expected after shorter incubation times. After the required incubation time, cell survival is very low and I had difficulties to verify the presence of cells. Most fluorescent droplets contain easy detectable cells or cell fragments (Fig. 4.15b:1,3,4; A.8a). Some fluorescent drops contain very small or weak fragments which origin from cells could be questioned (Fig. A.8b:2-4), while others have unusual-shaped fragments (Fig. A.8b:1) and some seeming visually empty (4.15b:2; Fig. A.8c). Though we cannot see cells or cell fragments in the "empty" droplets, it does not necessarily mean that they did not contain cells. The structure and dimensions of the incubation chamber did not fit to the large objectives of the non-inverted fluorescence microscope, hence I could only use

a 10× objective. Due to the low magnification and a need to focus on the drop itself, cell fragments might have been lost in the poor resolution.

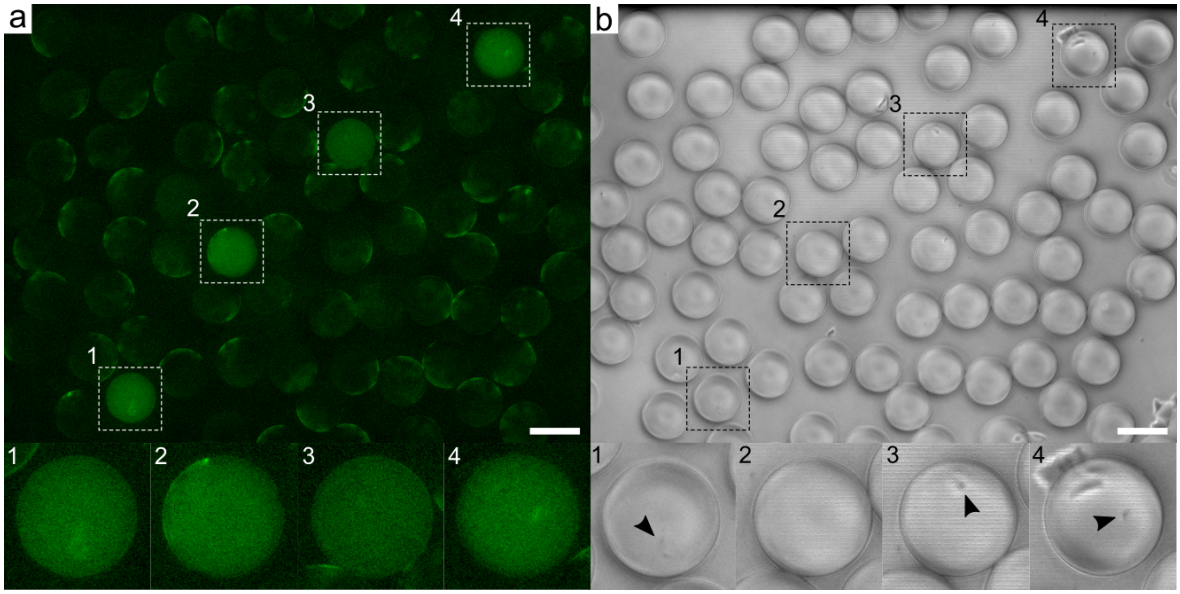

Figure 4.15: Fluorescence microscopy of drops. (**a**) FITC phase fluorescent image of droplets after 20 hours of incubation through a 10× objective. Micrographs showing close ups of the most fluorescent droplets. (**b**) Phase contrast of the same droplets as seen in (**a**). Micrographs showing close ups of the most fluorescent droplets. Black arrows indicate the presence of cells or cell fragments. Scale bars are 80 µm.

Despite difficulties in fluorescence microscopy and the large variation from laser measurements, I do detect fluorescent droplets emphasizing the presence of protease. When directly comparing the normalized means of our active drops with the standard curve of 37°C, I get a rough estimate of the amount of protease secreted from a single cell (Fig. 4.16). Note that the SD for the cells on the graph are from the variation between the means of the triplicates where the actual SD are a much larger for each of the individual replicates (Table 4.3, 4.4 and 4.5).

At four hours of incubation the measured activity is roughly equivalent to the activity of 1 µg mL^{-1} of trypsin. After 8 hours of incubation it increases an equivalent of 3 µg mL^{-1} of trypsin. At 24 hours most of the cells are dead, and the high activity we observe are likely a mix of secreted protease before cell death and intracellular protease released after cell death. We know from the protocol of the protease kit and our own previous controls (Fig. 4.10b), that the protease substrate have an undefined continuous increase in fluorescence over time and do not reach the plateau we normally would expect from enzyme kinetics. It is therefore difficult to conclude on the distribution of fluorescence caused from secreted protease vs. intracellular protease after 24 hours of incubation. When looking at the two last replicates (Table 4.4 and Fig. A.6; Table 4.5

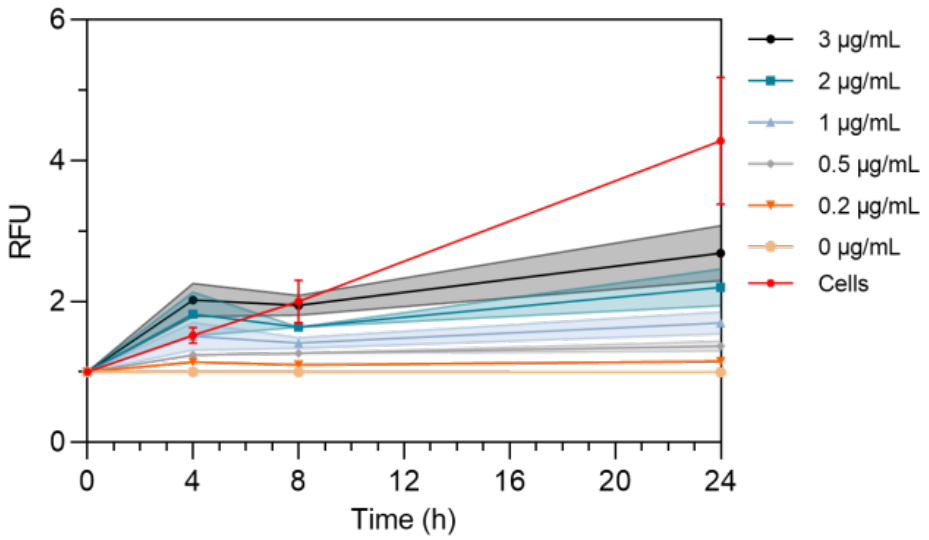

Figure 4.16: Estimation of cell secreted protease. Mean RFU values detected from encapsulated cells plotted together with the standard curve incubated at 37°.

and Fig. A.7) we in general see less number of active drops compared to the occupation we have. We want to be believe that this is due to cells being less stressed and thereby secrete less protease. However, the activity I do measure might only come from drops containing dead cells. Nevertheless, in the first replicate the death rate during the first eight hours is very low and we here see a high fraction of active drops. In this case it is more likely that the detected active drops are linked to drops containing living cells and not dead.

Though all these data only give us loose estimates of the amount of secreted protease from single cells, it does not change the fact that we were able to detect activity on a single-cell level. To ensure that the fluorescence I measure is derived from protease and not some malfunction of the kit or any unexpected events, I am in the next section trying to validate the source of the activity.

4.4 Protease activity validation by inhibition

To confirm that the measured activity is in fact from protease, I use a protease inhibitor kit. The commercialized kit is targeting five different protease classes; aspartic protease, cysteine protease, serine protease, metalloproteases and aminopeptidases. The inhibitor mix is used in concentrations of 0.1X, 0.5X and 1X and tested in bulk with 2 and 10 µg mL^{-1} trypsin. The kit is tested in the same conditions as used for cell secretion, to ensure compatibility between the kit and the secretion assay (Fig. 4.17). With 10 µg mL^{-1} trypsin, we observe a strong inhibition effect using both 1X and 0.5X,

and less inhibition when using 0.1X. For 2 µg mL^{-1} trypsin, we observe a strong inhibition effect for all the different concentrations of inhibitors with 0.1X being slightly less efficient.

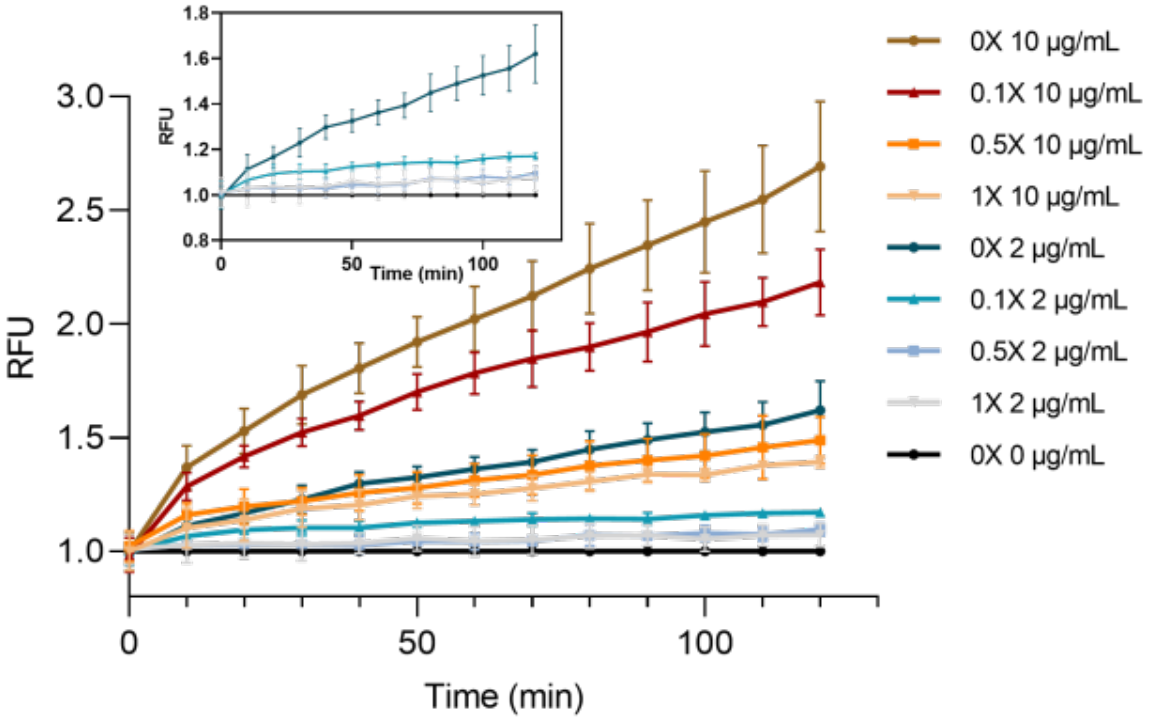

Figure 4.17: Control of protease inhibitors. The effect of 0X, 0.1X, 0.5X and 1X inhibitor mix tested on 2 and 10 µg mL^{-1} of trypsin. Insert: Close-up of 2 µg mL^{-1} alone.

A final concentration of 1X protease inhibitor is together with protease substrate emulsified with *T. b. brucei* under the same conditions as described in the cell secretion section. Droplets with and without protease inhibitors are collected and incubated for four, eight and 24 hours, where fluorescence is measured and cell survival is estimated (Fig. 4.18; Table 4.6). In Fig. 4.18a I present and compare the active drops detected from laser measurements with and without the use of protease inhibitors over time. The active populations are defined as described for Fig. 4.14. I present the RFU values laying above the threshold line visualized as the gray line in the histograms and the content of the gray box in the heat maps. In the presence of protease inhibitor (black dots) we observe a clear effect on detected fluorescence compared to the drops without inhibitor (blue dots). The average RFU mean and SD values of the droplet population with inhibitors are lower and only increase slightly over time, where the mean and SD values of the population without inhibitors distinctly increase. We further observe that using protease inhibitors do not affect the survival and growth of the cells (Fig. 4.18b,c). This indicates that the difference I detect in fluorescence between drops with and without inhibitors are indeed caused from inhibition of protease activity and

not from a change in the fitness of the cells. In two additional replicates we observe a similar difference between the drops with and without protease inhibitors (Fig. A.9; Table A.1). The survival and occupation data for all the replicates are presented in Fig. 4.18b,c.

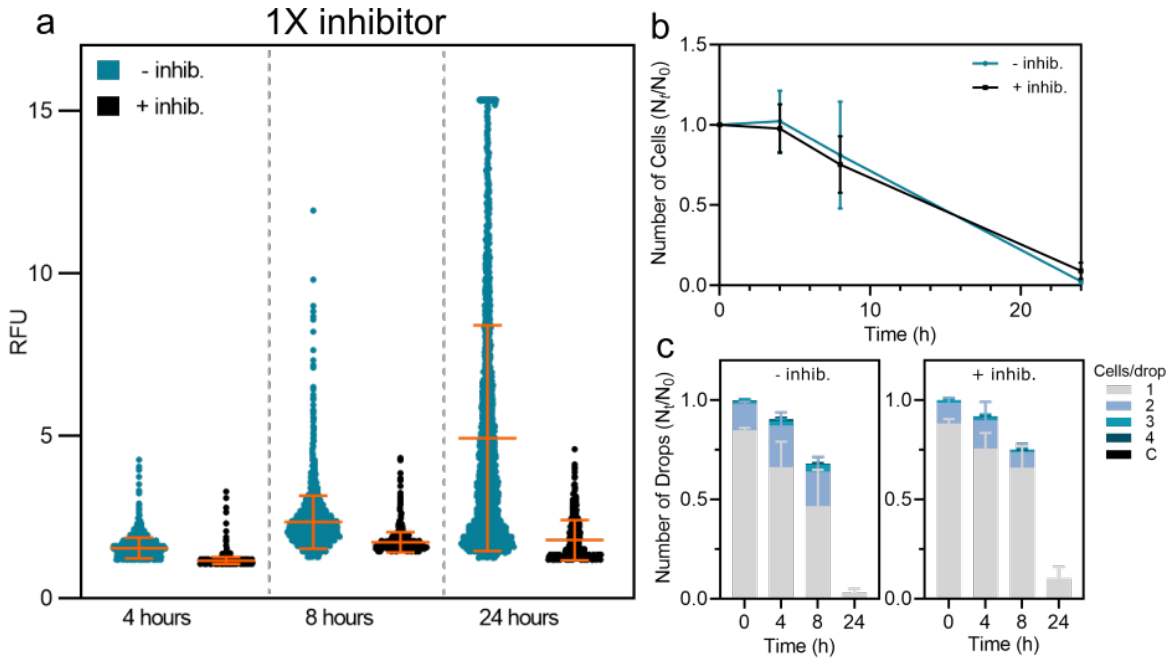

Figure 4.18: 1X protease inhibition on single cells in drops. Comparison of detected fluorescence in presence of (black) or without (blue) 1X protease inhibitor over time of 1. replicate (**a**). Survival (**b**) and cell occupation (**c**) in presence of or without protease inhibitor over time for all replicates.

I further test the protease secretion assay using a concentration of 0.5X (Fig. 4.19 and Table 4.6) and 0.1X (Fig. 4.20 and Table 4.6) protease inhibitors. We here observe an overall similar inhibition pattern as for 1X with no significant difference between the three concentrations of protease inhibitors. The inhibition tests with 0.5X and 0.1X inhibition are likewise made as triplicates, where the two additional replicates are presented in Fig. A.10 and Table A.2 for 0.5X and in Fig. A.11 and Table A.3 for 0.1X. The similar inhibition pattern we observe between the different concentrations is in accordance with the inhibition I measured from the in bulk trypsin controls (Fig. 4.17: insert), assuming the secreted protease concentration in drops is equal to 1-3 $\mu g\,mL^{-1}$ of trypsin (Fig. 4.16). Here, a trypsin concentration of 2 $\mu g\,mL^{-1}$ did not result in a significant difference between using 0.1X, 0.5X or 1X of inhibitors.

The similar inhibition pattern we observe between the three different inhibitor concentrations supports our assumption of a secreted protease concentration in drops in the range of 1-3 $\mu g\,mL^{-1}$ (Fig. 4.16). Higher protease concentrations would likely cause

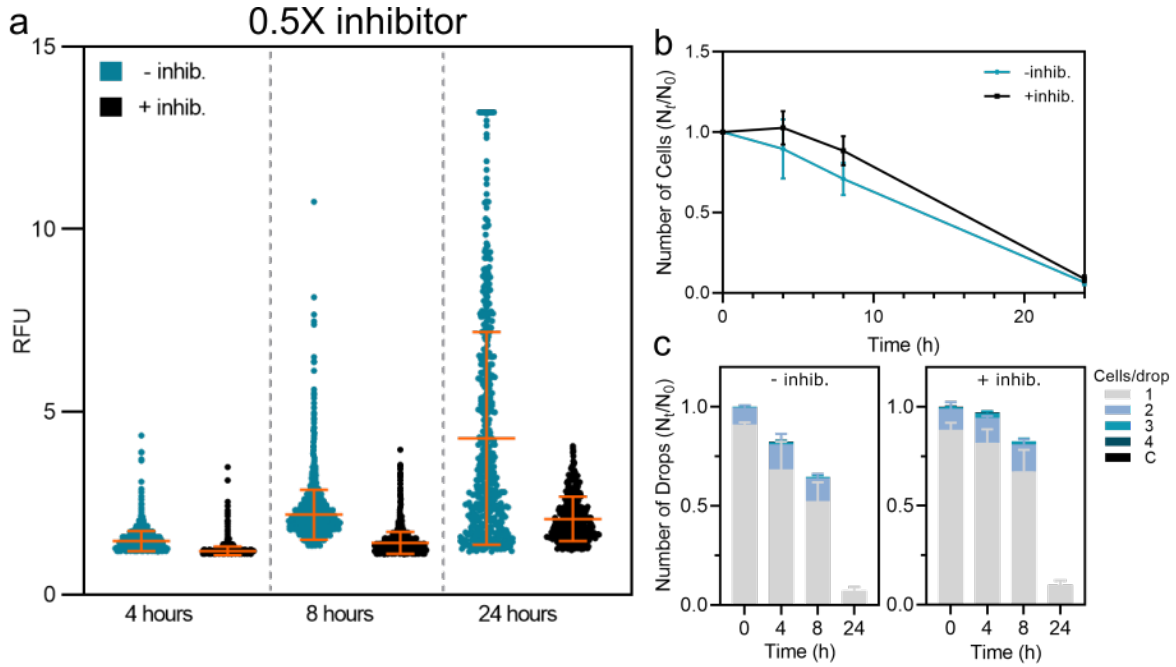

Figure 4.19: 0.5X protease inhibition on single cells in drops. Comparison of detected fluorescence in presence of (black) or without (blue) 0.5X protease inhibitor over time of 1. replicate (**a**). Survival (**b**) and cell occupation (**c**) in presence of or without protease inhibitor over time for all replicates.

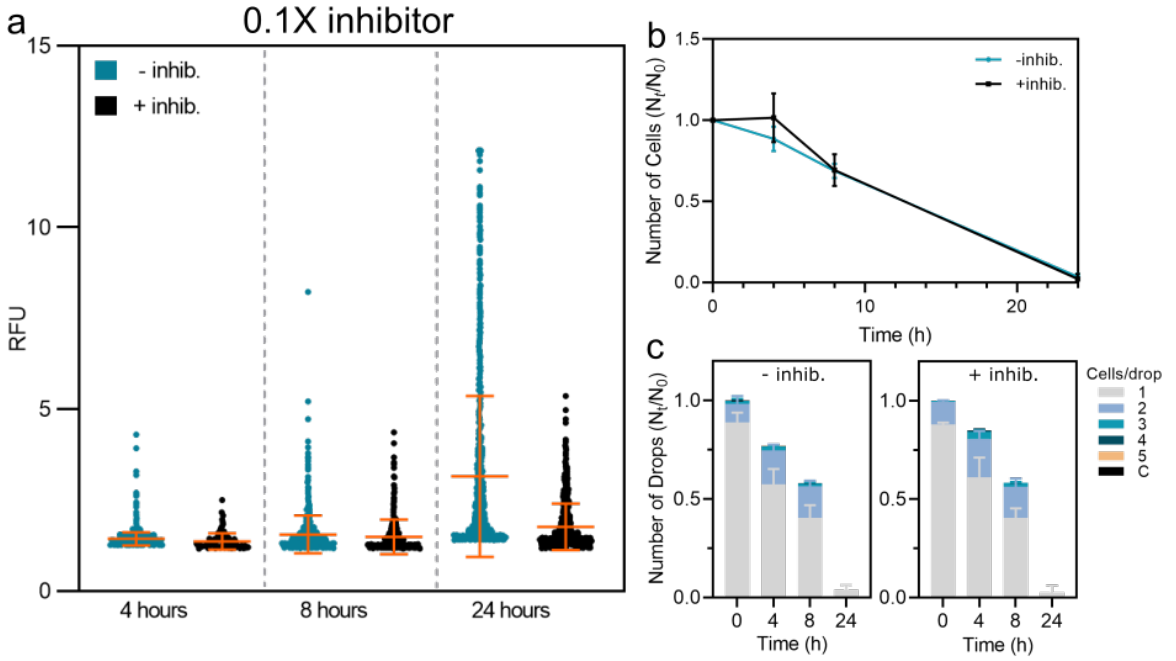

Figure 4.20: 0.1X protease inhibition on single cells in drops. Comparison of detected fluorescence in presence of (black) or without (blue) 0.1X protease inhibitor over time of 1. replicate (**a**). Survival (**b**) and cell occupation (**c**) in presence of or without protease inhibitor over time for all replicates.

Table 4.6: Overview of 1X, 0.5X and 0.1X inhibition of encapsulated *T. b. brucei*. Mean RFU values±SD of detected fluorescence in presence of or without protease inhibitors and the respective fractions of active drops and cell occupation for each condition over time.

1X inhibitor

	Start	4 hours	8 hours	24 hours
- Inhib. (RFU±SD)	1.00±0.03	1.56±0.31	2.35±0.79	4.91±3.47
Active drops (%)	-	15.89	18.03	22.41
Cell occupation (%)	17.72	18.94	16.51	0.40
+Inhib. (RFU±SD)	1.00±0.03	1.16±0.11	1.39±0.28	1.84±0.62
Active drops (%)	-	18.48	17.59	7.61
Cell occupation (%)	23.25	20.16	14.09	1.07

0.5X inhibitor

	Start	4 hours	8 hours	24 hours
- Inhib. (RFU±SD)	1.00±0.03	1.47±0.28	2.20±0.66	4.40±3.00
Active drops (%)	-	9.49	12.84	11.83
Cell occupation (%)	13.40	13.10	9.62	0.87
+Inhib. (RFU±SD)	1.00±0.03	1.20±0.12	1.42±0.30	2.11±0.62
Active drops (%)	-	15.74	21.46	14.20
Cell occupation (%)	25.50	22.87	22.38	1.85

0.1X inhibitor

	Start	4 hours	8 hours	24 hours
- Inhib. (RFU±SD)	1.00±0.03	1.39±0.18	1.56±0.47	3.22±2.25
Active drops (%)	-	8.65	4.46	8.00
Cell occupation (%)	19.73	14.03	10.82	0.50
+Inhib. (RFU±SD)	1.00±0.03	1.37±0.23	1.50±0.47	1.79±0.64
Active drops (%)	-	0.71	3.70	14.79
Cell occupation (%)	20.43	20.38	13.83	1.03

less inhibition with the 0.1X inhibitor like we observe for 10 µg mL^{-1} trypsin in bulk (Fig. 4.17). Regardless of inhibitor concentrations we do observe a difference in activity with and without inhibitors over time. This proves that the activity I detected in the drops were indeed protease derived. Though the substrate used in this work did provide insightful information of single-cell protease secretion, the exact amounts of secreted protease are still to be investigated. The detected fluorescence variance from the protease was too large when encapsulated on-chip using a single known protease concentration (Fig. 4.11; Fig. A.1-A3). In addition, the rather big difference we observe between the standard curves when incubated at either room temperate or at 37°C, indicates an instability or negative effect on the kit at higher temperatures. This is an issue when working with cells like *T. b. brucei* which needs to be handled at a constant temperature of 37°C. For deeper analysis of protease secretion and a possible variability at a single cell level, new and more sensitive methods are required.

The simplest solution is to find other green fluorometric enzyme activity kits directly compatible with our setup as it is (laser ex. = 473 nm). The search in finding the perfect activity kit can further be expanded by considering different colored fluorometric assays. This would require a few corrections of the setup as changing the laser and PMT for correct measurement and detection of other wavelengths. Other approaches can involve self-designed substrates targeting our desired enzymes. One example is filling vesicles with high concentrations of self-quenching dye like calcein [189]. The vesicles can be created to compose specific lipids or proteins being direct targets for the enzyme we wish to investigate. The vesicles can then be co-encapsulated in drops together with our cells. Cell-secreted enzymes will attack the vesicles resulting in membrane disruption and release of fluorescent dye detectable by our setup. Similar procedures have previously been done in microfluidic systems for visualization of vesicles after filling of calcein [190, 191].

4.5 Conclusion

In this section, I investigated the protease secretion of *T. b. brucei* at a single-cell level. By encapsulating a protease substrate together with *T. b. brucei*, I was able to detect a sub-population of drops over time with higher fluorescence. By comparing the mean fluorescence detected from the encapsulated cells with a trypsin standard curve, I could roughly propose an estimate of secreted protease equivalent to 1-3 µg mL^{-1} trypsin. These results emphasize the promising use of a droplet-based microfluidic

system to investigate enzyme secretion from single cell trypanosomes. A future prospect for analysis are to develop more sensitive assays to enable detection of the possible variability in enzyme activity between the encapsulated cells.

4.6 Material and methods

4.6.1 Cell preparation

Cells were cultivated using standard cultivation protocols [85]. In brief, monomorphic *T. b. brucei* 427 90-13 BSF strain blocked from entering the stumpy cell cycle arrested stage, were grown in IMDM (Life Technologies) supplemented with 10% (v/v) heat-inactivated fetal calf serum (FCS), 0.2 mM β -mercaptoethanol, 36 mM $NaHCO_3$, 1 mM hypoxanthine, 0.16 mM thymidine, 1 mM sodium pyruvate, 0.05 mM bathocuprone, 1.5 mM L-cysteine, 40 µg mL^{-1} streptomycin and 40 U mL^{-1} penicillin (IMDM+). *T. b. brucei* BSF were maintained as one-mL cultures in 24-well Nunc^{TM} plates (Thermo Fischer Scientific) at 37°C with 5% CO_2. Every two or three days, cultures were sub-cultured with a 1.000 or 10.000 fold dilution, respectively.

4.6.2 EnzChek's activity assays

EnzChek^{TM} enzyme activity kits for phospholipase PLA2, PLC and protease detection were used for leakage test in droplets. For phospholipase tests I used the enzyme provided by the kit. For all protease controls I used the commercialized Gibco®Trypsin (Thermo Fisher Scientific) as control enzyme. For leakage tests by laser measurements the EnzChek^{TM} protease substrate and trypsin were handled as recommended by the manufacture's protocol. For the observation tests in incubation chamber, the trypsin and protease substrate were used in the same conditions used for the single-cell secretion tests. Trypsin was diluted in Trypanosome Dilution Buffer (20 mM Na2HPO4, 2 mM NaH2PO4, 80 mM NaCl, 5 mM KCl, 1 mM MgSO4, 20 mM glucose, pH 7.4) (TDB) and the protease substrate was diluted in IMDM serum free medium (IMDM-) [188].

Endpoint enzyme reactions were emulsified in parallel with a negative control in dual production devices with a channel depth of 66 µm and a nozzle width 50 µm. Q_{aq} for both positive and negative sample inlets were 100 µL h^{-1} and the joined Q_{oil} was 800 µL h^{-1}, resulting in 0.5 nL droplets with individual droplet frequencies f_1 and f_2 of 60 Hz and a total droplet frequency, f, of 120 Hz. Drops were collected in a 2D-collection device for fluorescence microscopy and in a 3D-collection device for laser

measurements and incubated at 37°C until further use.

4.6.3 In bulk activity measurements

For protease activity measurements I adapted the protocol for protease secretion from Proto *et al.* (2011) [188]. *T. b. brucei* were grown in 75 mL IMDM+ to a concentration of 1.5-2 $\times$ 10^6 cells mL^{-1} (mid-log phase). $1{\cdot}10^8$ cells were washed in TDB (centrifugation at 2000 rpm for 4 minutes) and incubated in a secretion medium composed of TDB and IMDM- in 50:50 ratio for 2.5 hours. Hereafter, samples were centrifuged at 1500 g for 15 min for removal of cells. Half of the supernatant was saved for direct use while half was run in slow passage through a 0.2 µm syringe filter and concentrated 30-fold using a VivaSpin 20 with a 10.000 molecular weight cut-off filter unit.

Trypsin used for the standard curves was likewise diluted in secretion medium to final concentrations of 0-3 µg mL^{-1}. In prior to activity detection, protease substrate was mixed in a 96-well microtiter plate (mtp) with all samples in a 50:50 ratio to final concentrations of 20 µg mL^{-1} substrate and final volumes of 100 µL. Fluorescence was detected with a 5 minute interval for 2 hours in a FLUOstar® Omega plate reader (BMG LABTECH). All samples were made as technical triplicates and two different samples of cell secretion medium as concentrated and none concentrated.

For endpoint protease activity measurements *T. b. brucei* were grown for two days in 10 mL IMDM+ in a Nunc^{TM} 25 cm^2 flask (Thermo Fischer Scientific) to a concentration of 1.5-2 $\times$ 10^6 cells mL^{-1}. Hereafter cells were washed in TDB by centrifugation (2000 rpm for 4 minutes) and mixed with protease substrate diluted in IMDM- in a 50:50 ratio. The samples were distributed in 96-mtp wells in final concentrations of 1.5 $\times$ 10^6 cells mL^{-1} and 20 µg mL^{-1} substrate in a total volume of 100 µL. Immediately after mixing fluorescence was measured in a FLUOstar® Omega plate reader (BMG LABTECH). The mtp was then incubated at 37°C with 5% CO_2 until the following measurements at four, eight and 24 hours. The bulk endpoint measurements were made as biological triplicates each consisting of technical triplicates.

4.6.4 Protease assay for emulsification

Cells were grown two days prior of the experiment start in 10 mL IMDM+ to a concentration of 2.47 $\times$ 10^6 cells mL^{-1} (SD = 0.6). Cells were hereafter adjusted to a starting concentration of 3 $\times$ 10^6 cells mL^{-1} by concentrating the cells and 2$\times$ washing in pre-heated TDB by centrifugation (2000 rpm for 4 minutes). Protease substrate from

EnzChek Protease Assay kit were diluted in preheated IMDM- to a concentration of $40\,\mu g\,mL^{-1}$.

Cells and substrate were loaded separately in 1 mL syringes (Braun) with 0.4×19 mm needle tips (Terumo®) and polyethene tubing (Adtech) (0.3 mm inner diameter and 0.76 mm outer diameter). Tubings were connected to a co-flow production device with a channel depth of 60 µm and a nozzle width 30 µm. Cells and substrate were mixed in a 50:50 ratio on-chip to final concentrations of 1.5×10^6 cells mL^{-1} and $20\,\mu g\,mL^{-1}$ substrate just before emulsification. Flow rates of the cell and substrate suspensions Q_{aq} were both $150\,\mu L\,h^{-1}$ and $Q_{oil} = 760 \pm 20\,\mu L\,h^{-1}$ resulting in 0.2 nL droplets at a frequency of 400 Hz. Drops were collected for 20-25 minutes in a 3D-collection vial and incubated at 37°C until further use.

For validation of protease activity we used the commercialized Protease Inhibitor Cocktail Set II 100X (Calbiochem®, MERCK) targeting five protease classes; aspartic protease, cysteine protease, serine protease, metalloproteases and aminopeptidases. The inhibitors were mixed in IMDM- together with the EnzChek^{TM} substrate to final concentrations of 1X, 0.5X or 0.1X. From here the same procedure were followed as described above. All experiments were performed as triplicates. For each replicate, one assay with and without inhibitors were made from the same preparation of cells and encapsulated in series starting with the assay without inhibitors. For all controls and standard curves in drops, we used trypsin in final concentrations of 0-3 $\mu g\,mL^{-1}$ diluted in TDB following the same protocol as for cell measurements.

4.6.5 Droplet fluorescence measurements

Fluorescence imaging of droplets incubated in a 2D-collection device were performed by an Axioplan 2 (Zeiss) fluorescence microscope with observation through a 10x Fluar objective. All images were processed with the software ImageJ processing program [192]. For laser measurements the drops were reinjected in a classic production device with a channel depth of 63 µm and a nozzle width 30 µm for 0.2 nL drops, and a channel depth of 85 µm and a nozzle width 50 µm for 0.5 nL drops. Flow rates for reinjection were $Q_{drops} = 200\,\mu L\,h^{-1}$ and $Q_{oil} = 100\,\mu L\,h^{-1}$ for spacing the drops. Fluorescence was measured for around 120 seconds for each condition. All raw data were processed and presented by Scilab 6.1.0 (ESI Group) (`https://www.scilab.org/`) and GNU octave (`https://www.gnu.org/software/octave/doc/interpreter/`) or GraphPad Prism 8.0.0 for Windows, GraphPad Software (`https://www.graphpad.com/`).

4.7 Summary

In this chapter, I have designed a protease activity assay in a droplet-based microfluidic format for measuring secreted enzyme at a single cell level. The protease activity was detected as a result of a fluorescent end-product by laser measurements.

- At first I evaluated the compatibility of three commercialized enzymatic activity kits with a droplet format.
- I performed a series of control tests with the chosen enzyme kit by mimicking the cell encapsulation procedure to validate fluorescence detection with our setup.
- By encapsulating protease substrate and *T. b. brucei* I was able to detect protease activity at a single cell level.
- I finally validated the measured activity to derive from protease by including protease inhibitors in our assay.

5 Single-cell analysis in droplet microfluidics

This chapter presents a series of preliminary yet promising tests for two different experiments involving single-cell analysis of *T. b. brucei*. In Chapter 3 I investigated the growth dynamics upon droplet encapsulation. In the first part of this chapter I expand the investigation of growth dynamics and analyse the differentiation from slender forms to stumpy forms in glycerol conditions. Where I in Chapter 4 analysed single-cell enzyme secretion, the second part of this chapter is dedicated to analysing the direct host interaction between RBCs and *T. b. brucei* in a droplet format.

5.1 Stumpy differentiation and adaptation to glycerol

5.1.1 Introduction

Transmission between mammal hosts through an insect vector leads to numerous physiological and metabolic changes in the parasitic life cycle. In order to survive in both mammals and insects, trypanosomes are adapting their metabolism to the carbon sources available in their surroundings. The PCF (procyclic forms) inside the tsetse fly consume proline, where the BSF (bloodstream forms) in the mammal host mainly rely on glucose [193]. The BSFs have for a long time been believed to exclusively rely on glucose as a carbon source, however, glycerol have recently been reported to support growth in lack of glucose [194, 195]. These observations support the late discovery of BSFs colonizing extravascular compartments as skin [68] and adipose tissue [23] containing high concentrations of glycerol [196, 197]. In addition, in adipose tissue BSFs were observed both as slender dividing forms and also stumpy non-dividing forms [23]. Differentiation into stumpy forms are normally density dependent and triggered

by accumulation of the stumpy induction factor, SIF [73]. However, the presence of stumpy forms in adipose tissue suggests that glycerol plays a role in differentiation, which we later have observed in the lab. When differentiated into stumpy forms a protein associated with differentiation (PAD1) is highly expressed and used as a molecular marker for stumpy forms [198]. In the lab, we used a modified *T. b. brucei* reporter cell line to observe a correlation between growth arrest from stumpy differentiation and the expression of PAD1 in glycerol medium (unpublished) (Fig. 5.1). The reporter cell line GFP::PAD1$_{utr}$ is AnTat *T. b. brucei* with a GFP gene with nuclear localization followed by the 3'UTR of PAD1. Emitted fluorescence from the nuclear region by GFP::PAD1$_{utr}$ thereby reflects the expression of PAD1 [23, 199, 200]. Cultivation of the reporter cell line in glucose rich medium promoted steady growth (Fig. 5.1a) with no or little expression of GFP (Fig. 5.1b) indicating a population dominated by dividing slender forms. Cultivation in glycerol rich medium contrary promoted slow growth and increasing expression of GFP, indicating that the population have started to differentiate into the non-dividing stumpy forms. After approximately 10 days in glycerol, the GFP levels start to decrease while the growth rates increase indicating an adaptation to glycerol (Fig. 5.1). However, after adaptation a constant level of GFP expression of around 10% is still kept. The specific dynamics of the cell adaptation to glycerol is not fully understood. We believe that single-cell analysis here can contribute to insightful information. Our goal is to investigate the adaptation phase and try to understand why GFP and thereby PAD1 is continuously expressed. I here use our droplet-based microfluidic system to investigate the dynamics of the PAD1 expression in presence of glycerol at a single cell level.

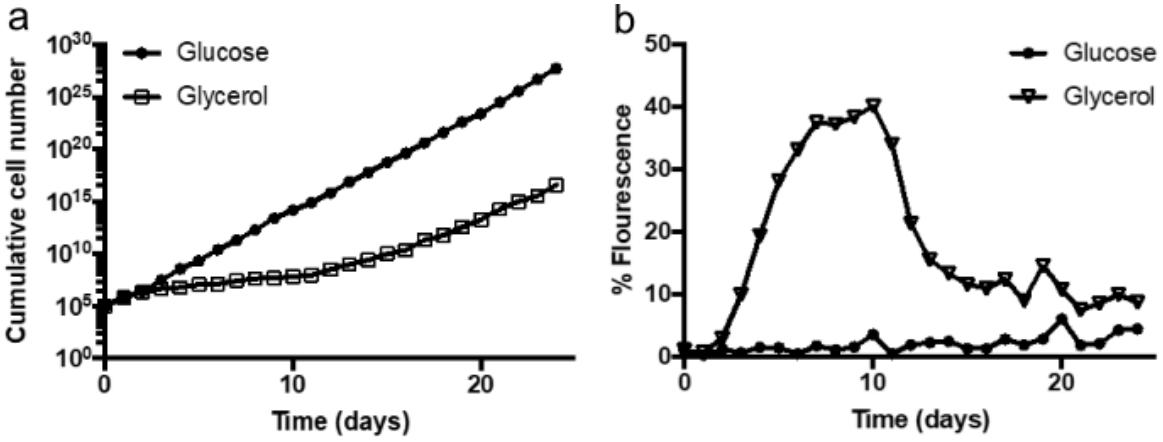

Figure 5.1: GFP:PAD1$_{utr}$ expression and adaption in glycerol. (**a**) Growth of AnTat GFP::PAD1$_{utr}$ in glucose vs. glycerol as cumulative cell numbers over 24 days. (**b**) GFP:PAD1$_{utr}$ expression in glucose vs. glycerol as percentage of fluorescent cells over time. Experiments and data are performed by Erika Pineda within the team.

5.1.2 Results and discussion

I here use the *T. b. brucei* reporter cell line AnTat GFP::PAD1$_{utr}$ to study the correlation of PAD1 expression and growth in presence of glycerol. In chapter 3, I revealed the average growth rates in drops to be slower than those in bulk. Furthermore, we here learn that glycerol cultivation also result in slow growth (Fig. 5.1). Since we are investigating growth dynamics, we have to make sure that the cells are going through at least a few cycles of division during encapsulation. I therefore test three different droplet sizes, to find the one promoting most growth. *T. b. brucei* grown in glucose are encapsulated in 0.5 nL, 0.75 nL or 2 nL drops, collected in a 2D-incubation chamber and counted after four, eight and 24 hours (Fig. 5.2). We here observe that cultivation in 0.75 nL drops results in highest growth for all the time points and choose this size for the following experimenters.

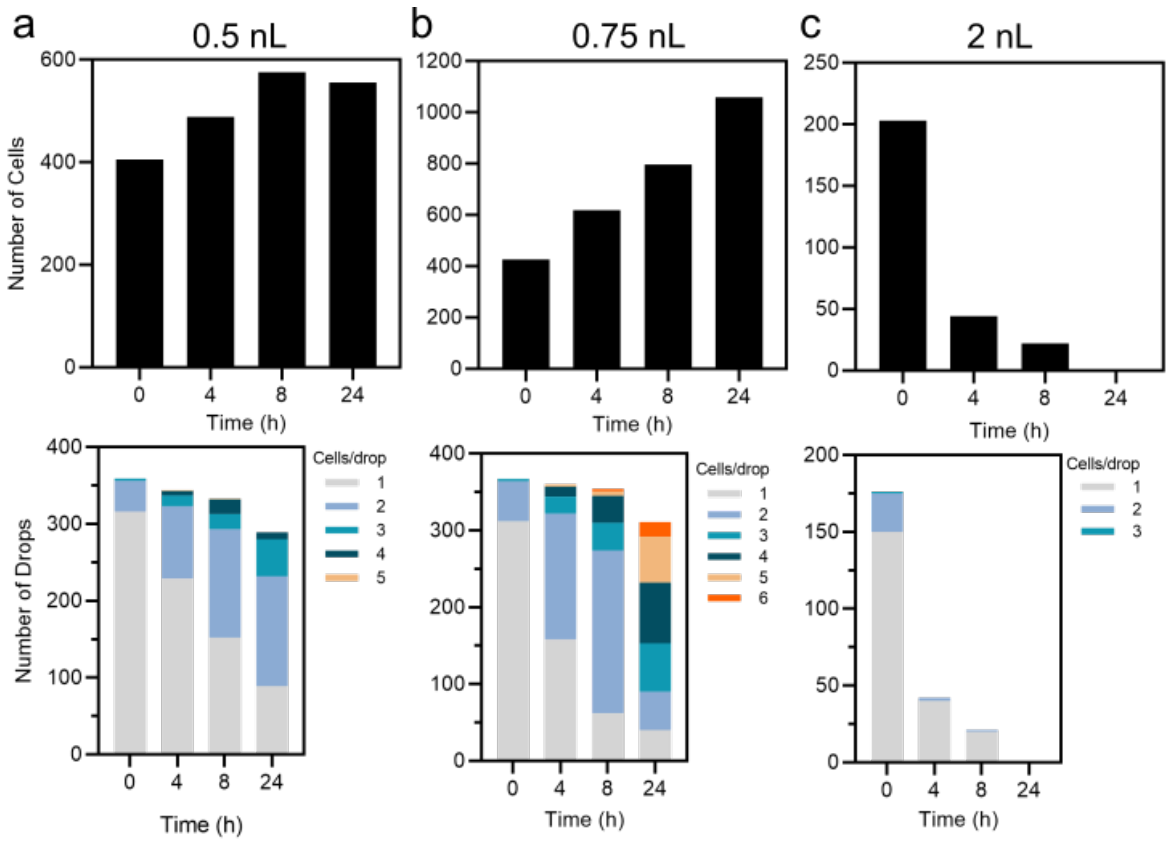

Figure 5.2: Survival and growth in different droplet sizes. Survival (top) and growth (bottom) of GFP::PAD1$_{utr}$ reporter cells grown in glucose by single-cell encapsulation in droplet sizes of 0.5 nL (**a**), 0.75 nL (**b**) and 2 nL (**c**).

To keep high growth and still analyse the effect of glycerol, we start an in bulk cultivation in a 50:50 mix of glucose and glycerol (Fig. A.12a-orange). The cells are then encapsulated with an occupation factor of $\lambda = 0.3$ and collected in a 2D incubation

chamber. The cells are counted every four hour for three days (Fig. 5.3). The data from drops containing two cells or more from the beginning of encapsulation have been removed to focus only on single cell behaviour. When grown in a mix of glucose and glycerol the cells still survive for sufficient time to undergo a few cycles of cell division. From 24 to 32 hours of incubation the majority of the drops contain living cells with a third of the population containing growing cells. The large amount of non-growing cells are related to the increasing amount of differentiating cells, since we here are operating in the beginning of the growth curve (Fig. A.12a,b-orange).

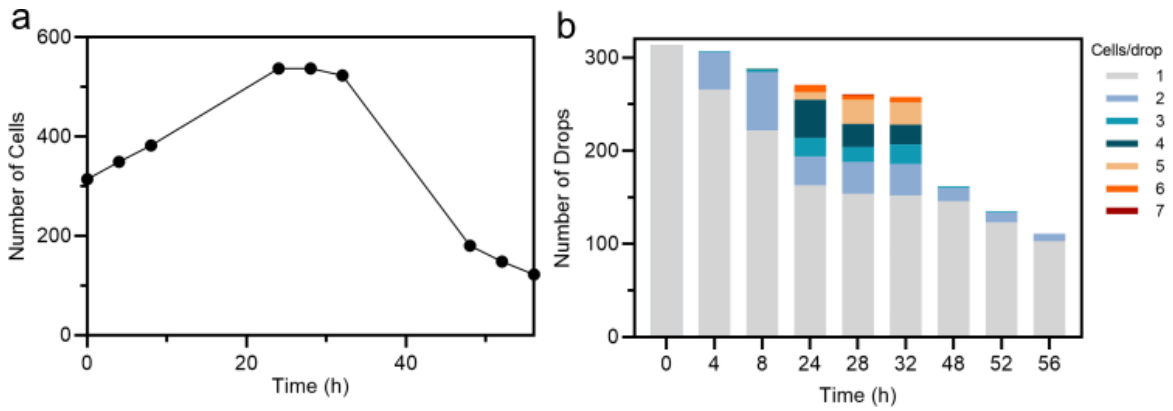

Figure 5.3: Survival and growth by droplet encapsulation. (**a**) Survival of GFP::PAD1$_{utr}$ reporter cells from single-cell encapsulation in a 50:50 mix of glucose and glycerol as total cell number over time. (**b**) Growth of GFP::PAD1$_{utr}$ reporter cells as number of drops containing a given number of cells over time.

To investigate the proportion of the stumpy GFP::PAD1$_{utr}$ expressing cells, we want to count the cells using fluorescence microscopy in the beginning and the end of incubation. However, when droplets are trapped in a 2D-incubation chamber and exposed to blue LED light, the cells quickly died within the next hour. Different fluorescence microscopes were tested with various settings of the LED intensity. During all the tests, the cells directly exposed to the lighted area died shortly after. I therefore choose to only count the fluorescence after 24 hours on incubation, which is sufficient time for dividing cells to go through a few cell cycles. The cell population grown in 50:50 glucose and glycerol are encapsulated in drops after reaching the adaptation phase (Fig. A.12b-orange, circle 1). The droplets are collected and counted every fourth hour where fluorescence microscopy is used for the last counting at 24 hours (Fig. 5.4a and Table 5.1 top). We first observe that the majority of the drops contain growing cells. Out of the 233 total drops with living cells, 15 drops contain fluorescent cells. 13 of these drops contain only single cells where 2 of the drops contain two cells both being fluorescent. The low percentage of drops containing fluorescent cells (6.44%) is similar

to the total percentage observed in the bulk population from the time the cells were taken (∼5%). This supports the non-dividing nature of the GFP-expressing cells. The two drops containing two fluorescent cells could have been at an intermediate stage between dividing slenders and non-dividing stumpys during the encapsulation process. At this stage, cells are already committed to differentiation but are still able to go trough a few cycles of division before full transformation [201].

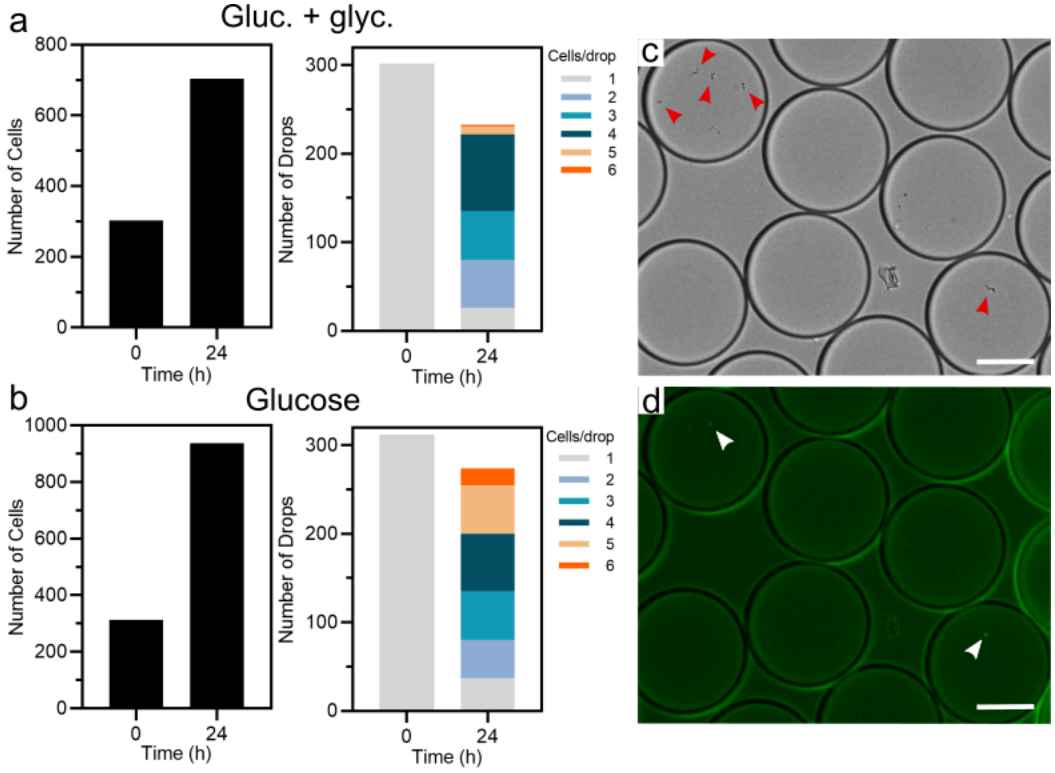

Figure 5.4: Survival and growth for fluorescence counting. Survival and growth of the GFP::PAD1$_{utr}$ reporter cell from single-cell encapsulation in glucose and glycerol (**a**) or glucose alone (**b**) after 24 hours of incubation. (**c**) Example of cells grown in glucose (red arrows) after 24 hours of incubation and fluorescence imaging (**d**) showing the expression of GFP:PAD1$_{utr}$ (with arrows) through a 20× objective. Scale bars are 50 µm.

As a control for background fluorescence, I encapsulate cells from a population only grown in glucose (Fig. A.12a,b-black, circle 2). As expected, we observe a higher total number of cells and more drops containing high growth compared to a mixed cultivation (Fig. 5.4b and Table 5.1 bottom). When grown in glucose, we obtain a higher fraction of the drops containing fluorescent cells (20%). About half of the fluorescent cells are found in drops without growth indicating a differentiated state prior to encapsulation. Since the cells are grown without glycerol the drops containing growing and fluorescent cells, could be a result of high cell densities (Fig. 5.4c,d). Here, confinement in a small volume could result in higher concentrations of the released differentiation factor SIF than compared to in bulk cultivation.

Table 5.1: Distribution of fluorescent cells. Overview of droplet numbers, growth and fluorescent cells when grown in a 50:50 mix of glucose and glycerol (top) or glucose alone (bottom). These data belong to Fig. 5.4.

Glucose and glycerol

n cells pr. drop	Number of drops with n cells	% (n) of drops with fluorescent cells	Number of drops with no growth (fluorescent)
1	26	50% (13)	26 (13)
2	54	3.70% (2)	-
3-6	153	-	-
Total	233	6.44% (15)	

Glucose control

n cells pr. drop	Number of drops with n cells	% (n) of drops with fluorescent cells	Number of drops with no growth (fluorescent)
1	37	89.19% (33)	31 (28)
2	43	41.86% (18)	-
3-6	191	1.57% (3)	-
Total	274	19.71% (54)	

Although cultivation in glycerol promotes slow growth (Fig. 5.1 and Fig. A.12a), we still want to test this condition in droplets, since glycerol trigger more differentiation and GFP expression than the mix (A.12b-blue)). We start a new cell culture with cells cultivated only with glycerol (Fig. A.12c,d-blue). Cells are taken from the decreasing phase and diluted in glucose to stimulate growth of the non-differentiated cells (Fig. A.12c,d-blue, circle 3). When encapsulated with glucose we observe a very low survival (Fig. 5.5a). Only 28 drops contain living cells, 18 of these contain fluorescent single cells (Table 5.2 top). While still being in the wanted phase of decreasing fluorescence, I repeat the encapsulation process but test encapsulation with glycerol instead (Fig. A.12c,d-blue, circle 4). Here we observe better survival and growth than when encapsulated with glucose, but less compared to a cultivation in mixed glucose and glycerol or glucose alone, as expected (Fig. 5.5b and Table 5.2 bottom). When grown in glycerol we notice a very high fraction of 77% drops containing fluorescent cells. 84 of the fluorescent cells belong to drops with no growth, where the rest (32 cells) are from drops with growth. Since fluorescence is coupled to non-dividing stumpy forms, we did not expect such a high number of drops containing growing and fluorescent cells. From monitoring the growth curve of the bulk population, we however observe that the percentage of fluorescent cells start to increase again in the following days from where we took the cells (Fig. A.12d). This means that the cells have not yet

reached the adapted phase and are still triggered by the presence of glycerol to initiate differentiation. The high amount of fluorescent cells we observe in the growing drops are therefore likely to be derived from the continuous exposure to glycerol after slender forms have divided.

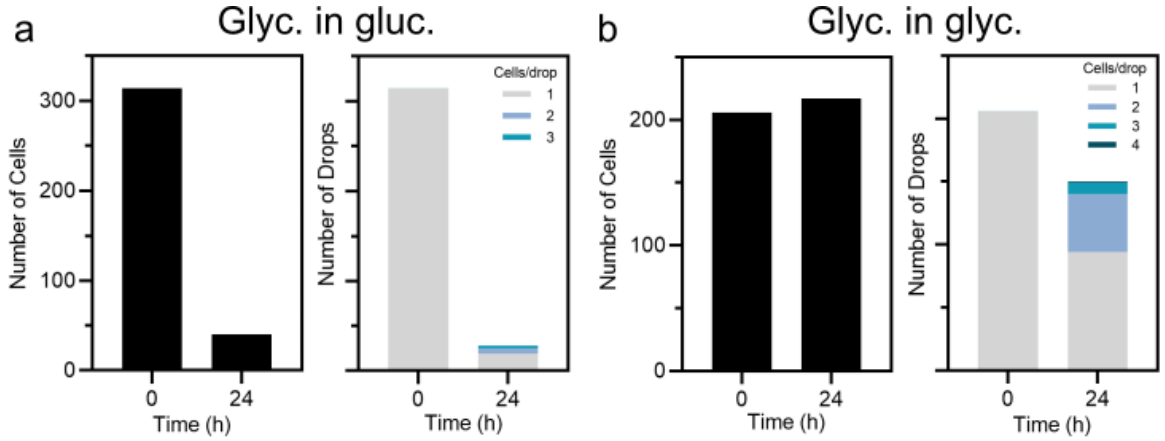

Figure 5.5: Survival and growth in glycerol. Survival and growth of AnTat GFP::PAD1$_{utr}$ reporter cells single-cell encapsulation when grown in glycerol and encapsulated with glucose (**a**) or with glycerol (**b**). Survival and growth are presented respectively as total cell number and number of drops containing a given number of cells at start 0 and 24 hours of incubation.

We further observe a few cases of dividing cells where the two new cell bodies are still attached and where both express the GFP:PAD1$_{utr}$ (Fig. 5.6b). Although PAD1 is a marker of non-dividing stumpy forms, this observation could be related to an intermediate or committed form as suggested previously [24, 23]. A committed slender form, still able to complete a few division cycles, starts to express PAD1 mRNA before turning into a non-dividing intermediate form. The expression of PAD1 then starts upon full differentiation into the stumpy form [24, 201]. The expression of GFP:PAD1$_{utr}$ while still dividing in intermediate cells might play a role in the maintenance of the constant level of fluorescence we observed after adaptation to glycerol (Fig. 5.1b). Another explanation recently suggested by Schuster *et al.*, is the ability of the cells to skip the stumpy stage. They observed slender BSF forms expressing GFP:PAD1$_{utr}$ dividing in the insect vector, and propose that slender BSF could be taken up by the fly and directly differentiate into PCFs [25]. The intermediate stages previously described might be related to these PAD1-expressing slender forms. All these observations indicate high heterogeneity within a population with small sub-populations neither being stumpy nor slender. In order to draw any specific conclusions of the PAD1 dynamics related to growing cells, we need more information of GFP:PAD1$_{utr}$ expression from single cells. It would here be extremely relevant to monitor the GFP:PAD1$_{utr}$ expres-

Table 5.2: Distribution of fluorescent cells in glycerol. Overview of droplet numbers, growth and fluorescent cells when grown in glycerol and diluted in glucose (top) or glycerol medium (bottom).

Glyc. in gluc.

n cells pr. drop	Number of drops with n cells	% (n) of drops with fluorescent cells	Number of drops with no growth (fluorescent)
1	19	84.21% (16)	15 (14)
2	6	33.33% (2)	-
3-6	3	-	-
Total	28	64.29% (18)	

Glyc. in glyc.

n cells pr. drop	Number of drops with n cells	% (n) of drops with fluorescent cells	Number of drops with no growth (fluorescent)
1	94	91.49% (86)	88 (84)
2	46	60.87% (28)	-
3-6	10	20% (2)	-
Total	150	77.33% (116)	

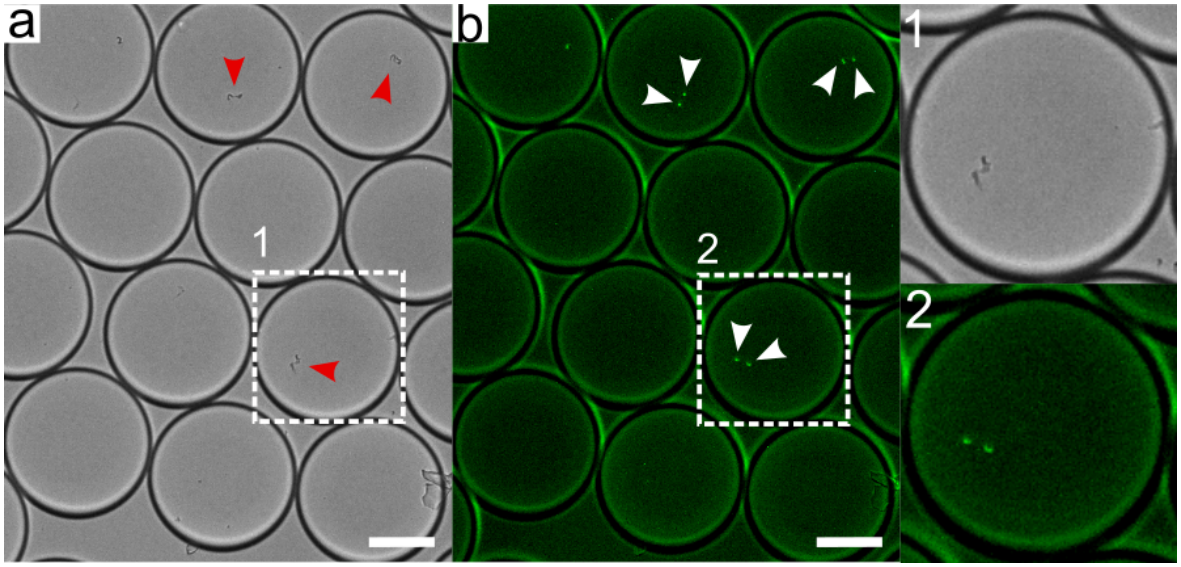

Figure 5.6: Expression of PAD1 in growing cells. (**a**) Example of growing cells (red arrows) in glycerol with both cell bodies expressing GFP:PAD1 (**b**) (white arrows) by fluorescence microscopy through a 20× objective. Micrograph 1 and 2 are showing close-ups from (**a**) and (**b**) respectively. Scale bars are 50 µm.

sion from the beginning of drop encapsulation. Since the cells died from excitation of blue light during counting, we should consider different approaches like using FACS prior to encapsulation. This will give us the certainty of PAD1:GFP$_{utr}$ expression in all the cells from start of the experiment and thereby give us a more clear insight to the growth dynamics of the PAD1 expressing cells.

5.1.3 Conclusion

I here investigated the correlation between growth and PAD1 expression in presence of glycerol at a single-cell level. Using a GFP::PAD1$_{utr}$ reporter cell line allowed us to analyse the correlation between growth and PAD1 expression when cultivated in drops. When grown in glycerol, I identified dividing cells still attached expressing the GFP::PAD1$_{utr}$. This observation supported previous studies observing intermediate and special slender forms expressing PAD1 while still dividing. All these findings are strongly indicating a higher cell-to-cell heterogeneity within a trypanosome population than originally assumed. Further investigation of the existence of such special forms are of highest interest since they will change the perception of the trypanosome life cycle as we know it today. For further investigation of the GFP::PAD1$_{utr}$ expression in drops, a crucial step is the improvement of imaging techniques allowing us to see the specific stage of the cell cycle and to avoid cell death during fluorescence microscopy.

5.1.4 Material and methods

5.1.4.1 Cell preparation

A *T. b. brucei* AnTat GFP::PAD1$_{utr}$ BSF reporter cell-line identifying stumpy forms, kindly provided by Luisa Figueiredo [23], were grown in Creek's minimal medium [202] supplemented with 5 µg mL^{-1} hygromycin B, 2.5 µg mL^{-1} neomycin, 5 µg mL^{-1} blasticidine, and either 10 mM glucose, 10 mM glycerol or a 50:50 mix of both. The cells were maintained as 2×2-mL cultures in 6-well Nunc^{TM} plates (Thermo Fischer Scientific) at 37°C with 5% CO_2. The cells were counted and sub-cultured everyday to a starting concentration of 10^5 cells mL^{-1} while fluorescence were measured in a Guava® easyCyte^{TM} Flow cytometer. The in bulk cell culturing were maintained in collaboration with Erika Pineda within the team.

5.1.4.2 Droplet encapsulation

Cells were taken from the desired phase of the bulk cultures, washed and adjusted to a final concentration of 4×10^5 cells mL^{-1} in glucose or glycerol supplemented IMDM-giving a theoretical occupation of 30% ($\lambda = 0.3$). Cell suspensions were loaded in 1 mL syringes (Braun) with 0.4×19 mm needle tips (Terumo®) and polyethene tubing (Adtech) (0.3 mm inner diameter and 0.76 mm outer diameter) and connected to a classic production device. For droplet sizes of 0.5 nL and 0.75 nL, channel depths were 85 µm and nozzle widths were 50 µm. For 2 nL drops the channel depth was 95 µm and the nozzle widths 100 µm. The flow rates used for creation of 0.5 nL drops were $Q_{aq} = 250\,\mu\mathrm{L\,h}^{-1}$ and $Q_{oil} = 870\,\mu\mathrm{L\,h}^{-1}$. For 0.75 nL drops $Q_{aq} = 550 \pm 5\,\mu\mathrm{L\,h}^{-1}$ and $Q_{oil} = 740 \pm 10\,\mu\mathrm{L\,h}^{-1}$. For 2 nL drops $Q_{aq} = 230\,\mu\mathrm{L\,h}^{-1}$ and $Q_{oil} = 800\,\mu\mathrm{L\,h}^{-1}$. All drops were collected in a 2D-incubation chamber and incubated at 37°C and 5% CO_2 until further use.

5.1.4.3 Fluorescence microscopy

The encapsulated cells were counted by eye at the beginning of encapsulation and after four, eight and 24 hours of incubation using our microfluidic setup. For fluorescent counting I used an EVOS inverted digital microscope (AMG) using a blue LED light. All counting and imaging were done through a 20x objective. Fluorescence imaging was furthermore tested with an Axioplan 2 (Zeiss) fluorescence microscope, with observation through a 10x Fluar objective, and an automated microscope system (Leica DMI6000 B, Leica microsystems) with adaptive focus control connected to an Orca-Flash 4.0 LT digital camera (Hamamatsu) using blue LED (lumencor®) through a 40x objective. All images were processed with the software ImageJ processing program [192]. All graphs are made with GraphPad Prism 8.0.0 for Windows, GraphPad Software, San Diego, California USA (`https://www.graphpad.com/`).

5.2 Measurements of RBC and *T. b. brucei* interaction

5.2.1 Introduction

One of the main symptoms of trypanosome infection is anemia caused by hemolysis [203, 17]. The trypanosome secretome has been described to contain a variety of enzymes including different classes of phospholipase and protease which are believed to contribute to the hemolytic effect of RBC [204, 20, 21, 22]. The recent emergence of strong analytical tools for single cell studies, like microfluidics, provides interesting opportunities for deeper investigation of direct host interaction between RBC and trypanosomes at a single cell level. Where I in Chapter 4 investigated single-cell enzyme secretion, I here attempt to investigate the direct interaction with RBCs. I create a droplet-based assay for analysing trypanosome interaction with RBCs at a single cell resolution. We wish to study the hemolytic effect of trypanosomes on RBC possibly by secretion of enzymes. To measure RBC hemolysis in a droplet format I use a commercialized kit based on fluorescent proteins binding to the membrane of RBC. When co-encapsulated with trypanosomes a destruction of RBC will indicate an interaction from the parasites either by secreted enzymes or other virulence factors. Ideally, the rupture of RBC will lead to a homogeneous distribution of fluorescent compounds with a detectable difference of fluorescence from before and after hemolysis. I here use RBCs from sheep in a series of experiments to demonstrate the detectability of hemolysis in a droplet-microfluidic platform.

5.2.2 Results and discussion

In order to detect hemolysis in a droplet format, I first find an ideal approach for controlling hemolysis of RBC. I here measure osmotic hemolysis using various NaCl dilutions in water. The osmotic tolerance of the RBC membrane is tested using NaCl solutions of 0.025, 0.05, 0.075, 0.1, 0.15, 0.2 and 0.3%. NaCl dilutions are added to RBCs and incubated for one hour. After incubation, absorbance is measured and plotted as a function of NaCl concentrations (Fig. 5.7). Simultaneously, I mix $10\,\mu g\,mL^{-1}$ trypsin and $3\,\mu M$ phospholipase separately with the RBC.

From the osmotic hemolysis assay we observe an EC50 around 0.087% $\pm$0.015 NaCl. From the measurements of osmotic hemolysis with $10\,\mu g\,mL^{-1}$ trypsin and $3\,\mu M$ phospholipase we do not observe any indications of hemolysis with absorbance values

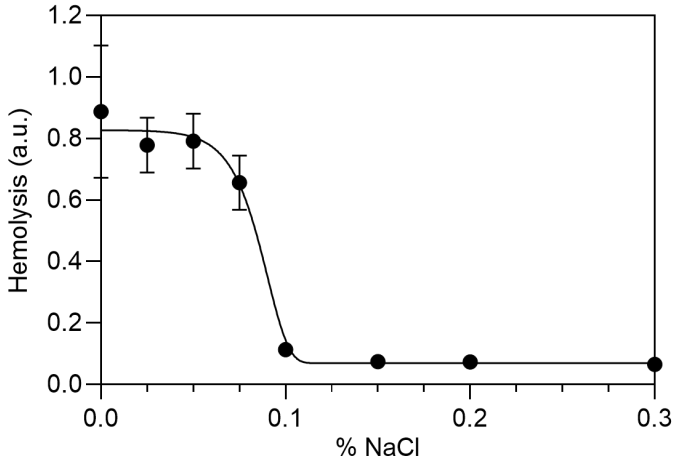

Figure 5.7: Hemolysis by osmotic stress. RBC hemolysis is measured in bulk as absorbance (540 nm) as a function of NaCl concentrations ranging from 0 to 0.3%. The osmotic hemolysis assay was performed as technical triplicates.

of 0.067 and 0.056 respectively. I further encapsulate trypsin with RBC in drops to see if any visible difference occurred. After 24 hours of incubation we still do not observe any changes (Fig. A.13).

The composition of lipids and proteins in the RBC membrane are varying between animals resulting in some species having a higher tolerance against membrane rupture than others [26, 27, 28]. Previous studies have tested the osmotic tolerance with NaCl between different species. Among the tested mammals (including humans) camels had the highest tolerance with an EC50 around 0.2% and goats had the lowest EC50 around 0.6% [205, 206]. The EC50 we observe here at 0.087% NaCl is lower compared to the previous studies, indicating a high osmotic tolerance of the RBC I use in this study. In addition, a study have shown difference in hemolysis between different animal species treated with phospholipase [204]. We have already concluded that our RBC have a high tolerance towards osmotic pressure. The membrane composition of our RBC could furthermore result in high tolerance towards enzymatic activities as well. This could explain why we did not observe any hemolytic effects using enzymes even after 24 hours of incubation.

To test the hemolysis assay in a droplet-microfluidic format, I first make the RBC fluorescent in order to visualize hemolysis. RBCs are covered with $70\,\mu g\,mL^{-1}$ of fluorescent lectin proteins from a commercialized kit (Fig. 5.8) [207]. Lectins bind to sugar groups as glycoproteins and glycolipids which are present in the RBC membrane. At first, the fluorescent RBCs are co-encapsulated with a NaCl concentration of 0.25% being higher than our EC50 (0.087%) to visualize RBC before hemolysis. However,

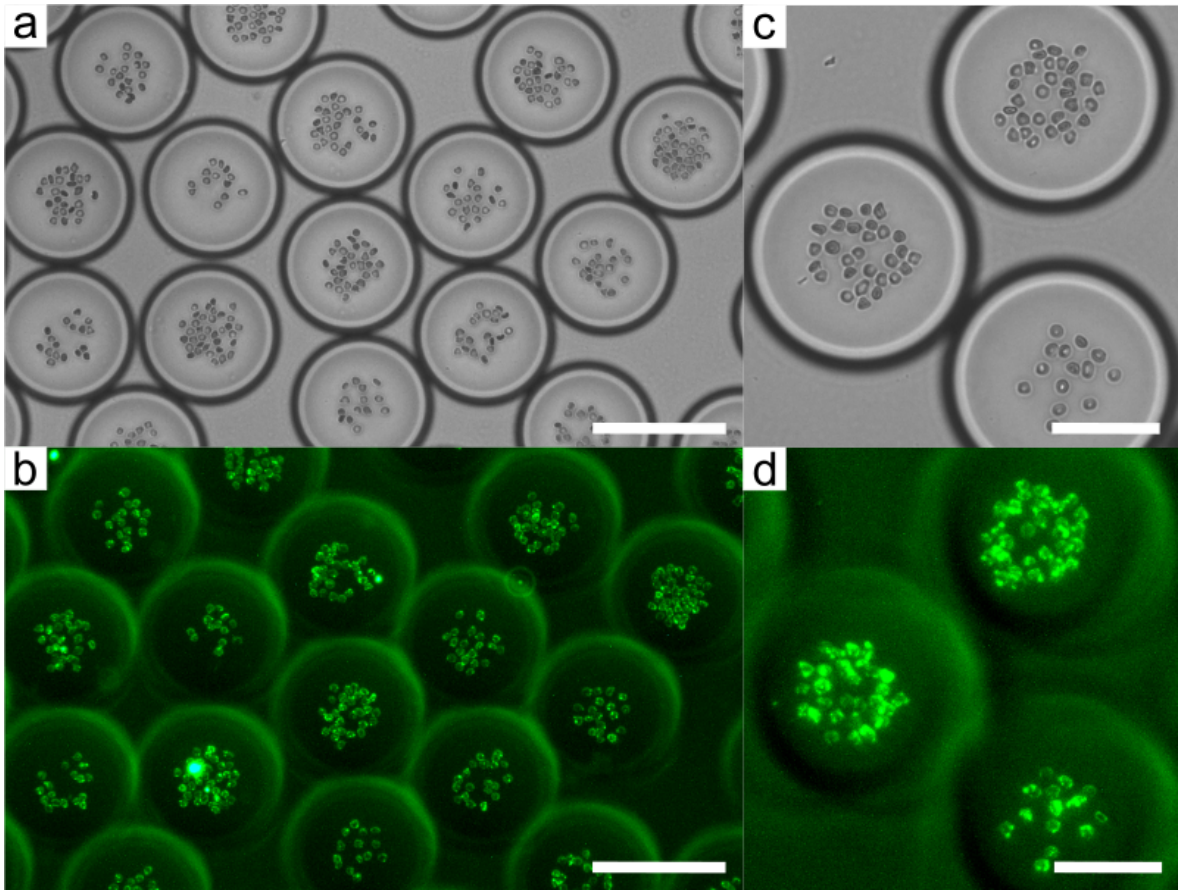

Figure 5.8: Fluorescent RBC before hemolysis. RBCs coated with fluorescent lectin proteins incubated with 0.25 mg mL^{-1} NaCl. Microscopic images at phase contrast through a 20× objective (**a**) and a 40× objective (**c**). Correlated fluorescent images showing the coated RBC through a 20× objective (**b**) and a 40× objective (**d**). Scale bars are respectively 80 µm and 40 µm for the 20× (**a,b**) and 40× (**c,d**) objective images.

when using a co-flow encapsulation device the RBCs are highly sticking to each other and do not lead to equal distribution of cells between the drops (Fig. A.14). Therefore, the fluorescent RBC and NaCl were then mixed off-chip prior to encapsulation in a classic drop-making device to obtain a more homogeneous distribution. The droplets are collected in a 2D-incubation chamber and a 3D-collection vial and incubated for 30 min.

We foremost observe a homogeneous distribution of RBCs in the drops compared to using the co-flow device. We clearly recognize intact RBCs in contrast phase imaging (Fig. 5.8a,c) and clear fluorescence of each cell using fluorescence microscopy (Fig. 5.8b,d). Clumping of some RBCs are still observed but in less extent than the previous encapsulation approach (Fig. A.15). The clumping could be the result of the strong binding lectin proteins and might be avoided by using a lower concentration.

Fluorescent RBCs are moreover encapsulated with a NaCl concentration of 0.075%

being on the low side of the EC50, to visualize RBC after hemolysis. The drops are collected in a 3D-collection vial and incubated for 30 min. After incubation the drops are reinjected in a 2D-incubation chamber and fluorescence is observed (Fig. 5.9).

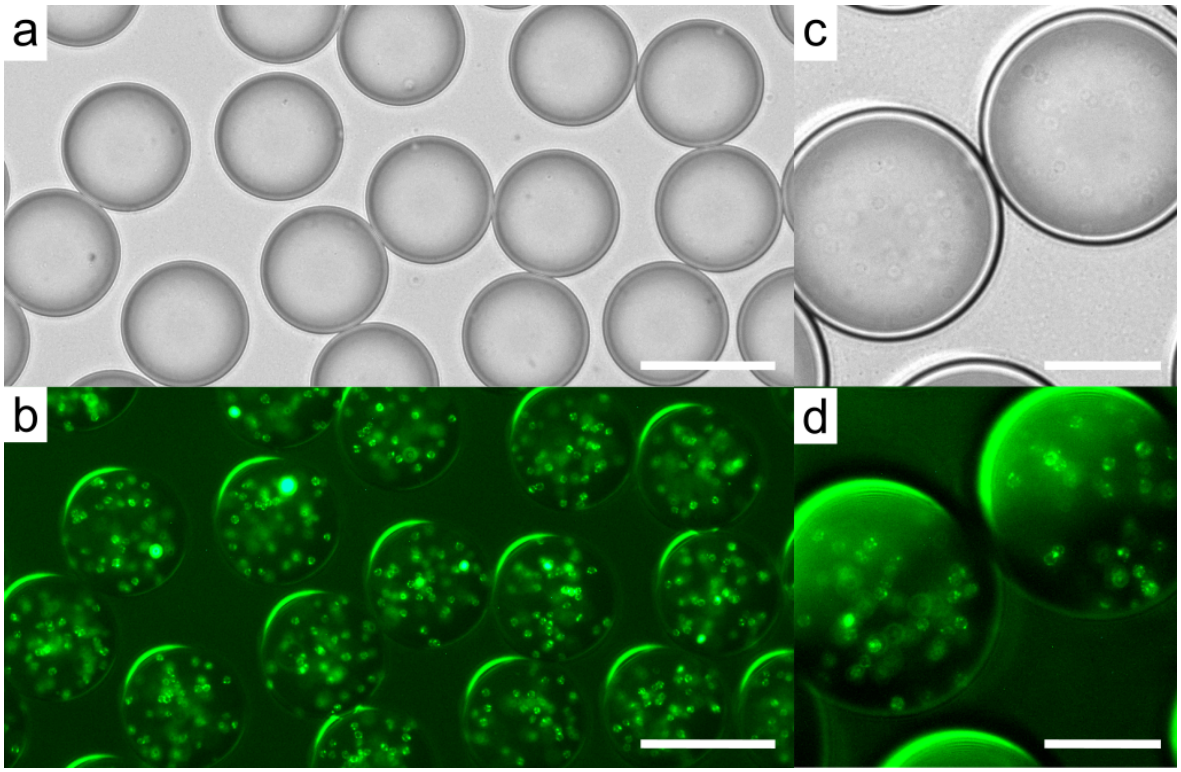

Figure 5.9: Fluorescent RBC after hemolysis. RBCs coated with fluorescent lectin proteins incubated with 0.075 mg mL^{-1} NaCl. Microscopic images at phase contrast through a 20× objective (**a**) and a 40× objective (**c**). Correlated fluorescent images showing the coated RBC through a 20× objective (**b**) and a 40× objective (**d**). Scale bars are respectively 80 µm and 40 µm for the 20× (**a,b**) and 40× (**c,d**) objective images..

At a first look, we do not observe any intact RBCs by phase contrast imaging indicating hemolysis of the RBCs (Fig. 5.9a,c). However, by fluorescent microscopy the RBCs still appear intact (Fig. 5.9b,d). With phase contrast imaging at a higher magnification we discover vague silhouettes of empty RBCs (Fig. 5.9c). This phenomena known as ghost cells indicate that the cells have undergone hemolysis but still kept their membranes intact at some extent [208]. I further measure the droplet fluorescence with and without hemolysis by laser measurements to check for differences not seen by eye. The droplets collected in the 3D-collection vial are reinjected and the fluorescence is measured by laser (Fig. 5.10). Before hemolysis we observe fluorescent RBCs as high thin peaks within the main droplet peak (Fig. 5.10a). Before hemolysis we detect a total mean RFU at 2.65 ±0.86. After hemolysis we do not observe any difference with similar looking peaks representing the fluorescent ghost RBCs with initact membranes (Fig. 5.10c). After hemolysis the total mean RFU is 3.12 ±0.98.

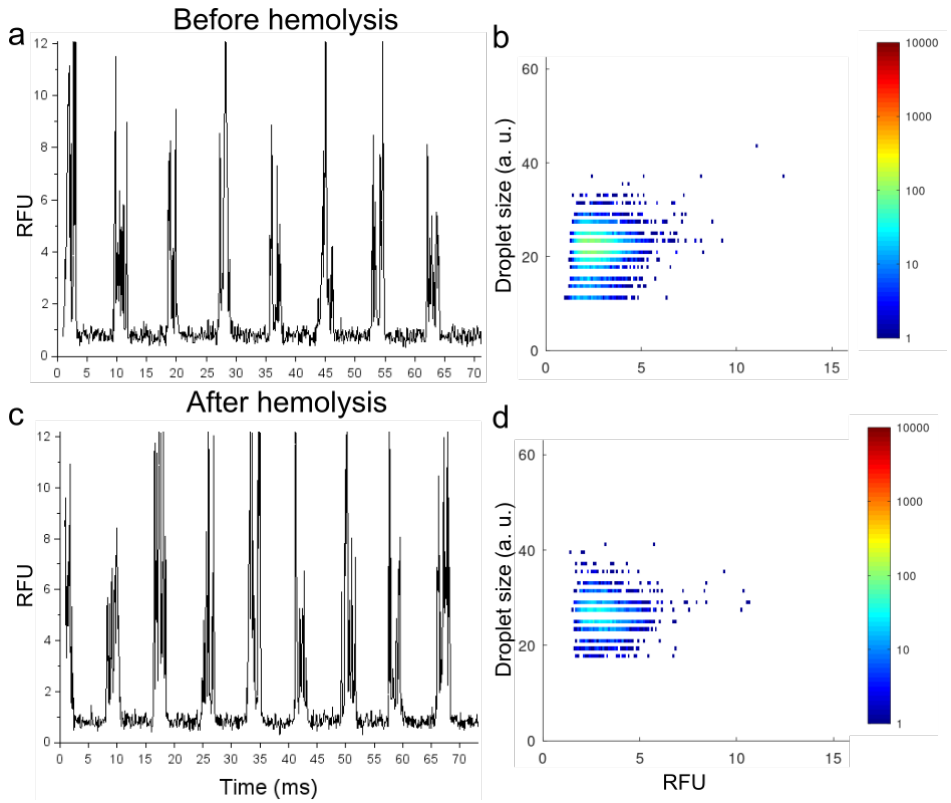

Figure 5.10: Laser measurements of hemolysis. Detected RFU in RBC-containing droplets before hemolysis (**a**) and after hemolysis (**c**) with the correlating heat maps (**b,d**) showing the mean RFU values.

The fluorescent RBC assay I used here did not workout as expected with osmotic hemolysis leading to full rupture of the RBCs and thereby a homogeneous distribution of fluorescence inside the drops. This assay however still holds the opportunity for testing hemolysis by trypanosome secreted enzymes. The visual change from before and after hemolysis seen by phase contrast imaging gives the opportunity of using image analysis without the need of fluorescence microscopy. The ratio of ghost and normal RBCs in and between the drops can be used to estimate hemolysis. To continue this assay, the first step will be the encapsulation of protease and phospholipase instead of NaCl, at higher concentrations than used before. Meanwhile, other procedures can involve the encapsulation of RBCs from different species with a known lower membrane tolerance. We additionally observed a relatively fast precipitation of RBC in the drops and in the loading systems. This led to a fast decrease of RBC concentration inside the drops. In future tests a precise control of the RBC concentration might be needed for co-encapsulation with trypanosomes. This matter could cause problems but can be solved by adding a small magnetic stirring bar inside the syringe during encapsulation.

For future tests of hemolysis by secreted enzymes we first need to investigate the direct interaction between trypanosomes and RBCs at a single cell level. I here test

the compatibility of *T. b. brucei* and RBCs co-encapsulation in droplets. *T. b. brucei* and RBCs are washed and diluted in secretion medium to final concentrations of 2×10^6 cells mL^{-1} and around 6.25-12.5 $\times$ 10^8 cells mL^{-1} respectively. The cells are co-emulsified in 0.2 nL drops and collected in a 2D-collection chamber and incubated at 37°C until further use (Fig. 5.11a). The *T. b. brucei* cells are counted at start and after four, eight and 24 hours of incubation (Fig. 5.11b).

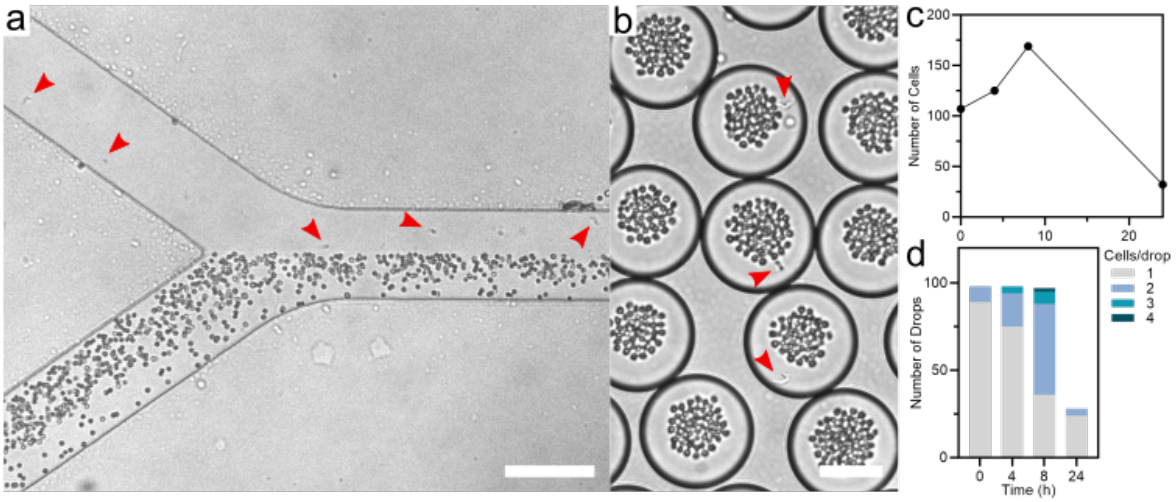

Figure 5.11: Co-encapsulation of *T. b. brucei* and RBC. (**a**) Encapsulation process of RBC and trypanosomes (red arrows) in a co-flow device. Scale bar is 100 µm. (**b**) Encapsulated RBC and trypanosomes (red arrows) in 0.2 nL drops imaged through a 20× objective. Scale bare is 80 µm. Survival, as number of cells over time (**c**), and growth, as number of occupied drops over time (**d**), of *T. b. brucei* encapsulated with RBC after four, eighth and 24 hours of incubation.

After eight hours of incubation together with RBCs almost no cells have died and more than half of the cells have gone through one cell division. After 24 hours, the cells have started to die with a cell occupation of around 25% of the drops containing living cells. We do not observe any changes in the RBCs structure or cell numbers during these incubation times. If observations of interactions are needed for longer periods of time, we can here play with the droplet volumes in order to extent survival of the trypanosomes. Furthermore, the specific number of RBCs is a controlling parameter which easily can be modified. For future experiments we should therefore consider changing the ratio of RBCs vs. *T. b. brucei* to optimize the observation of cell interactions. When the perfect droplet size and cell ratio is found, the next step is to encapsulate the *T. b. brucei* with the fluorescent RBC assay to study hemolysis based on trypanosome interaction at a single cell level. The most important step is first to find the best procedure to measure hemolysis in our droplet format. Though this approach needs some refinement it holds promising opportunities for studying host interaction

between RBC and *T. b. brucei* and to further reveal heterogeneous mechanisms.

5.2.3 Conclusion

I here aimed to investigate the interaction of RBCs with *T. b. brucei* in a droplet-microfluidic format. I first analysed the hemolytic properties of the RBC used in this work to osmotic pressure. I discovered a high membrane tolerance compared to other mammal species. I then coated the membranes of our RBCs with a fluorescent protein enabling easy visualisation in the drops. Incubating fluorescent RBCs in a NaCl solution lower than the EC50, resulted in ghost cells; full hemolysis but with intact cell membranes. Lastly, preliminary tests showed a good compatibility of co-encapsulating *T. b. brucei* and RBCs for incubation times up to 24 hours. I have here shown droplet-based microfluidics as a promising tool to measure hemolysis for further analysis of the interaction between RBCs and trypanosomes. In future experiments we most importantly need to find the best approach for measuring hemolysis in a droplet format. Only after, we should integrate the encapsulation with *T. b. brucei* to investigate the direct effect of cell interaction and enzyme secretion.

5.2.4 Material and methods

5.2.4.1 RBC preparation

For all RBC experiments I used 50% sheep erythrocytes in alsever buffer (Boehringer Ingelheim Therapeutics GmbH). For testing osmotic hemolysis, RBC were diluted 10 times in PBS. Volumes of 200 µL RBC were distributed in 1.5 mL Eppendorf tubes. The tubes were centrifuged at 3000 rpm for 3 min and PBS were removed. 200 µL of NaCl solutions in water were added to the RBC in concentrations of 0, 0.025, 0.05, 0.075, 0.1, 0.15, 0.2 and 0.3%. The RBCs with NaCl were incubated at 37°C for one hour and mixed every 15 minute. Absorbance was measured in 96 micro-well plate in a FLUOstar® Omega plate reader (BMG LABTECH) at 540 nm. Each concentration was made as technical triplicates. 3 µM PLA2 phospholipase and 10 µg mL^{-1} trypsin were diluted in PBS and tested in parallel. Data are presented by GraphPad Prism 8.0.0 for Windows, GraphPad Software (`https://www.graphpad.com/`).

5.2.4.2 Fluorescent labeling of RBC

Fluorescent RBCs were made by coating of fluorescent lectin proteins from the Alexa Fluor® 488 conjugate kit (invitrogen). The fluorescent protein solution was briefly cen-

trifuged and supernatant was collected to eliminate protein aggregations. 70 µg mL^{-1} fluorescent protein was mixed with 6.25-12.5 × 10^8 cells mL^{-1} RBC and incubated for one hour. After incubation, fluorescent RBC were washed three times in PBS prior to emulsification with NaCl.

5.2.4.3 Cell encapsulation

For on-chip mixing, fluorescent RBC and NaCl were loaded separately in 1 mL syringes (Braun) with 0.4×19 mm needle tips (Terumo®) and polyethene tubing (Adtech) (0.3 mm inner diameter and 0.76 mm outer diameter). Tubings were connected to a co-flow production device with a channel depth of 60 µm and a nozzle width 30 µm. RBC and NaCl were mixed in a 50:50 ration with Q_{aq1} and Q_{aq2} = 150 µL h^{-1} and Q_{oil} = 750 resulting in 0.18 nL drops. For off-chip mixing, RBC and NaCl were mixed just prior to emulsification in a classic production device with a channel depth of 50 µm and a nozzle width 30 µm and with Q_{aq} = 200 µL h^{-1} and Q_{oil} = 700 µL h^{-1} resulting in 0.23 nL drops. This gave a final drop occupation of roughly 60 to 125 RBCs per drop. Droplets were collected in a 2D-incubation chamber and 3D-collection vial a until further use.

5.2.4.4 Fluorescence detection

Fluorescence imaging was done in a 2D-incubation chamber with an EVOS inverted digital microscope (AMG) using a blue LED light. All images were acquired through a 20× or 40× objective. Droplet fluorescence was further detected by laser measurements. The drops were reinjected in a classic production device with a channel depth of 63 µm and a nozzle width 30 µm. Flow rates for reinjection were Q_{drops} = 200 µL h^{-1} and Q_{oil} = 100 µL h^{-1} for spacing the drops. All raw data were processed and presented by Scilab 6.1.0 (ESI Group) (`https://www.scilab.org/`) and GNU octave (`https://www.gnu.org/software/octave/doc/interpreter/`).

5.2.4.5 *T. b. brucei* and RBC encapsulation

For RBC and *T. b. brucei* co-encapsulation, *T. b. brucei* cells were grown two days prior of the experiment start in 10 mL IMDM+ to a concentration of 1.5-2.5 × 10^6 cells mL^{-1}. Cells were adjusted to a starting concentration of 2 × 10^6 cells mL^{-1} by concentrating the cells and washed twice in preheated TDB by centrifugation (2000 rpm for 4 minutes). RBC were washed and diluted in IMDM- to a concentration of approximately 6.25-12.5 × 10^8 cells mL^{-1}. RBC and *T. b. brucei* were loaded separately

in 1 mL syringes (Braun) with 0.4×19 mm needle tips (Terumo®) and polyethene tubing (Adtech) (0.3 mm inner diameter and 0.76 mm outer diameter). Tubings were connected to a co-flow production device with a channel depth of 60 µm and a nozzle width 30 µm. The cells were emulsified in 50:50 ratio with Q_{aq1} and $Q_{aq2} = 300\,\mu L\,h^{-1}$ and $Q_{oil} = 750\,\mu L\,h^{-1}$ resulting in 0.21 nL drops. This equals a theoretical final droplet occupation of 20% drops containing trypanosomes ($\lambda = 0.2$) and approximately 62-125 RBCs per drop. Droplets were collected in a 2D-incubation chamber and incubated at 37°C until further use. Data are presented by GraphPad Prism 8.0.0 for Windows, GraphPad Software (`https://www.graphpad.com/`).

5.3 Summary

The first part of this chapter describes the analysis of the correlation between growth and stumpy differentiation in glycerol conditions. I here used a GFP:PAD1$_{utr}$ reporter cell line expressing GFP when cells are differentiated to a non-dividing stumpy form.

- I tested the survival and growth dynamics of the reporter cell line in three different droplet sizes and found 0.75 nL the optimal size for growth.
- I analysed growth and GFP expression levels when cultivated in glucose, glycerol and a 50:50 mix of them both.
- When grown in glycerol I observed dividing cells still expressing GFP, supporting the existence of an intermediate or special form as suggested in previous studies.

In the second part of this chapter I have tested the use of droplet-based microfluidics for analysing interactions between RBC and *T. b. brucei*.

- At first I tested the membrane tolerance for osmotic hemolysis and discovered a high tolerance for the RBCs use in this work.
- I then used a commercialized kit to coat RBCs with fluorescent proteins to visualise hemolysis in a droplet format.
- Lastly, I tested the compatibility of co-encapsulating RBC and *T. b. brucei*, resulting in survival and growth in 0.2 nL drops for minimum 8 hours of incubation.

6 General conclusion and perspectives

In this thesis, I explored the compartmentalization, cultivation and analysis of single cell *T. b. brucei* using droplet-based microfluidics. At first, I described the configuration of a home build optical setup used for performing droplet-based microfluidics allowing high-throughput analysis of single cells. By encapsulating *T. b. brucei* in drops I showed survival of the cells from several hours to days where multiple cycles of division were observed. The droplet sizes influenced the survival and division of the cells with longest survival in the largest drops, but highest cell densities (cells per volume) in the smallest droplets. Here, our data revealed an heterogeneous growth pattern between the cells in a population, with some variants dividing more efficiently than the average and others more slowly. An interesting continuation, is the selection of the drops with highly dividing variants. Implementation to the setup of a screening module selecting high biomass, will allow us to collect the highest dividing variants. Several rounds of re-cultivation, drop encapsulation and selection will allow us to investigate specific dynamics of special variants on a population level. Droplet cultivation further led to higher cell densities among fast dividing variants compared to standard cultivation techniques. This designates droplet-cultivation promising for *in vitro* growth experiments where high densities of *T. b. brucei* is needed. In this work, the highest cell densities were reached in 0.2 nL drops with a cell maximum at eight hours, whereafter cell death started. For longer study intervals, one could explore the specific reasons for cell death and find ways to extend survival. Furthermore, an optimization of the system could be considered by automatizing the imaging process for faster data collection. Here, the development of image processing algorithms would be needed for detecting specific cell numbers and identifying living cells over dead. Other systems could be implemented to identify the different cell cycle stages.

Pairing single-cell encapsulation with an enzymatic substrate enabled us to investigate *T. b. brucei* protease secretion. I showed the capability of detecting protease

activity based on fluorescence and roughly estimated the concentration of secreted protease by comparing with activities of known protease concentrations. The substrate used here, had a large range for detection of multiple protease classes. Studying the *T. b. brucei* secretome would allow us to find the most abundant protease classes. By creating knock-out strains of different protease, one could further investigate if the detected activity belongs to one or several classes. Complications with our substrate made it challenging to further investigate variability between the secreted protease. This leaves an obvious continuation of finding different approaches to detect protease activities in drops, enabling to study variability. In addition, other strategies for detecting variability at a single cell level should be investigated. This could include studying the swimming pattern of individual cells or monitoring other secreted compounds or metabolites.

I also investigated the correlation between the expression of the protein associated with differentiation, PAD1, and growth arrest on a single-cell level. Single-cell encapsulation of a GFP::PAD1$_{utr}$ reporter cell line enabled preliminary analysis of growth behaviour and PAD1 expression in presence of different carbon sources. Our observations supported those of bulk cultivation with an inverse correlation between growth rates and PAD1 expression, with glycerol enhancing the PAD1 expression and glucose enhancing growth. The identification of dividing cells still expressing PAD1, emphasized the need for deeper analysis of growth and differentiation dynamics in presence of glycerol. These possible intermediate forms could play crucial roles in invasion of different tissues or transfer between hosts.

Finally, I tested an approach for analysing the direct interaction between RBC and trypanosomes based on hemolysis. The preliminary results showed the possibility of labeling RBCs with fluorescent proteins for direct observation. I further showed a good compatibility of co-encapsulating *T. b. brucei* and RBCs at incubation times up to 24 hours. This approach showed promising for future analysis of trypanosome interaction with RBCs and for further measuring secreted enzyme activity at a single cell level.

In this thesis, I have shown droplet-based microfluidics to be an efficient tool for single cell encapsulation and analysis of *T. b. brucei*. This system holds great opportunity to establish a high-throughput analytical platform for quantitative measurements of isolated trypanosomes. Such single-cell technologies are of high interest for numerous applications advancing the exploration of cell-to-cell heterogeneity. This will foremost provide a deeper understanding of the complex dynamics of trypanosomes and can further lead to identification of new drug targets against the disease.

A Appendix

A.1 Enzyme secretion by single-cell *T. b. brucei*

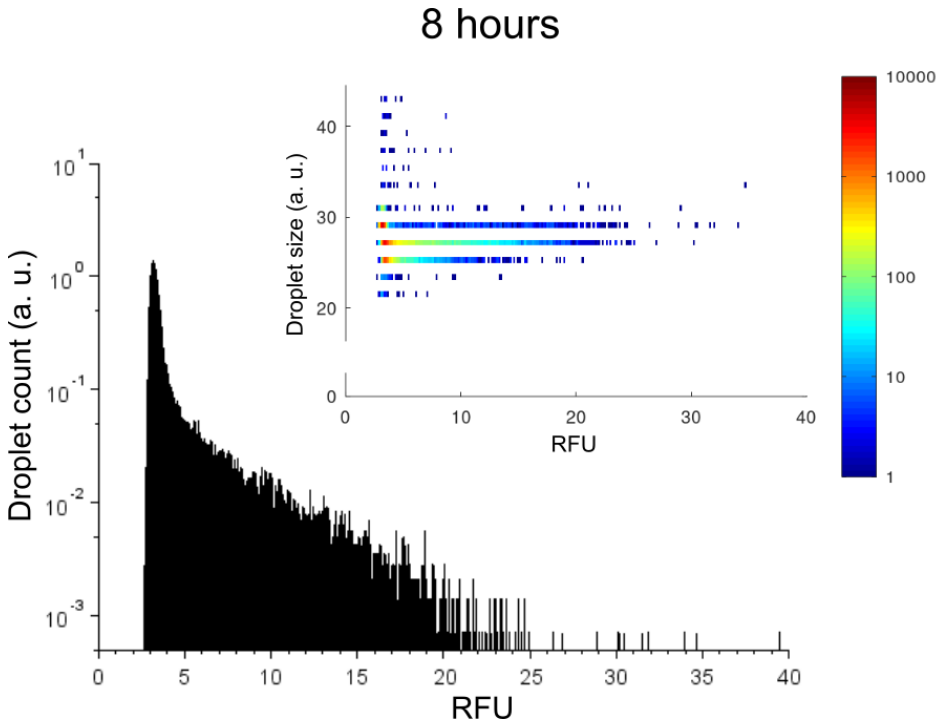

Figure A.1: Positive control with empty drops. Reinjection of two droplet population with 2 and 0 µg mL^{-1} trypsin and 20 µg mL^{-1} substrate after eight hours of incubation. Insert: Heatmap of droplet size vs RFU.

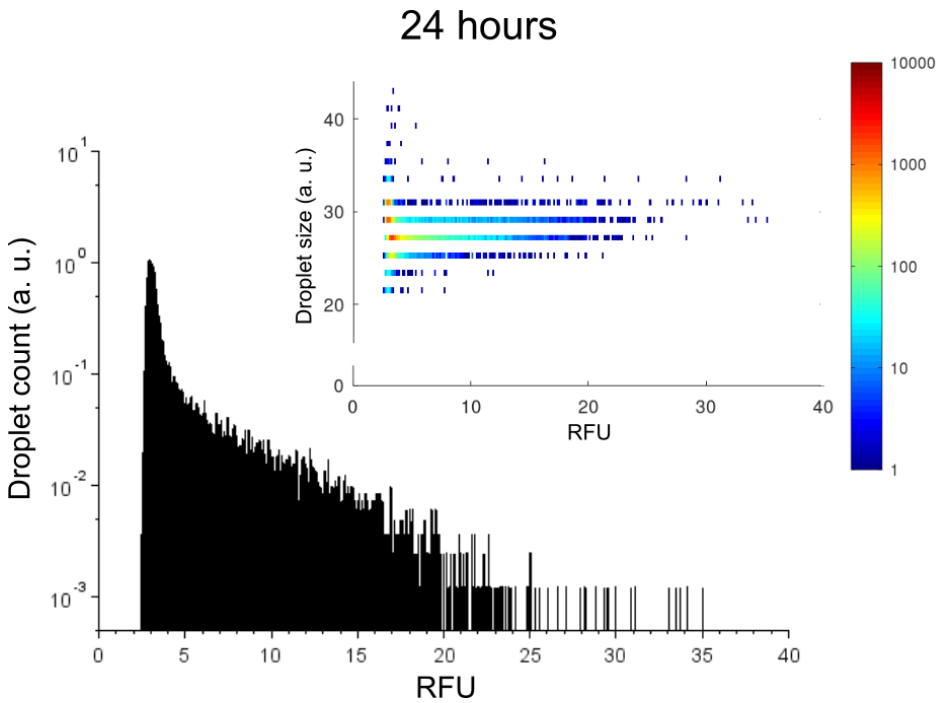

Figure A.2: Positive control with empty drops. Reinjection of two droplet population with 2 and 0 µg mL^{-1} trypsin and 20 µg mL^{-1} substrate after 24 hours of incubation. Insert: Heatmap of droplet size vs RFU.

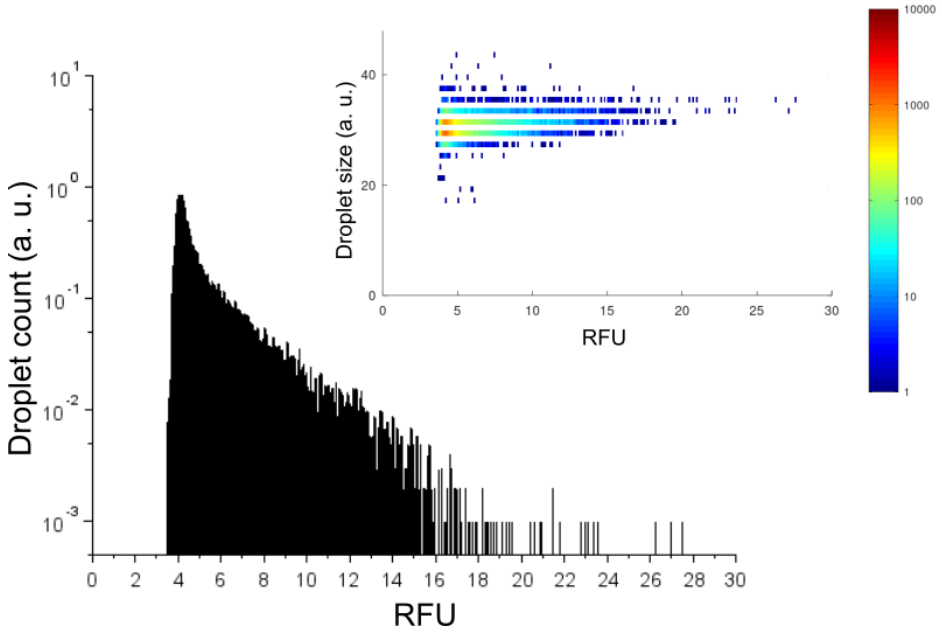

Figure A.3: Positive control without empty drops. Reinjection of one droplet population with 2 µg mL^{-1} trypsin and 20 µg mL^{-1} substrate after four hours of incubation. Insert: Heatmap of droplet size vs RFU.

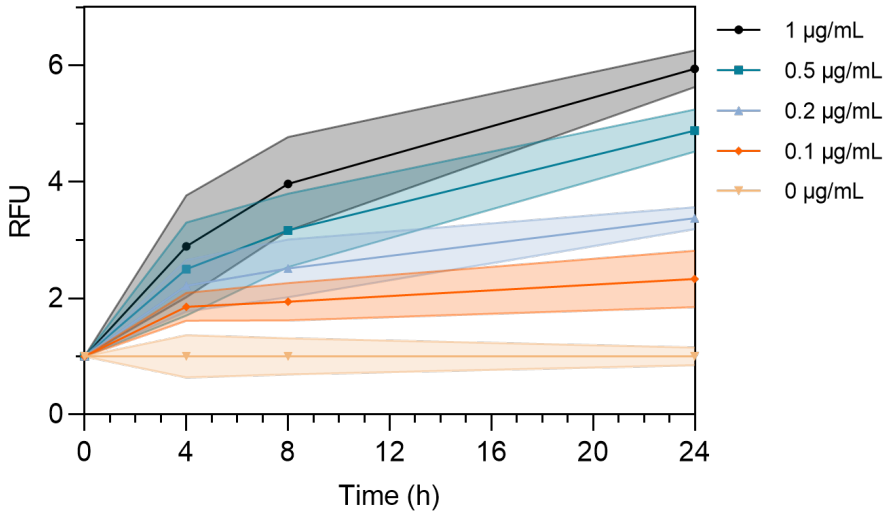

Figure A.4: Trypsin standard curve at room temperature. Droplet measurements of 0-3 µg mL^{-1} of trypsin and 20 µg mL^{-1} protease substrate incubated in bulk at room temperature and.

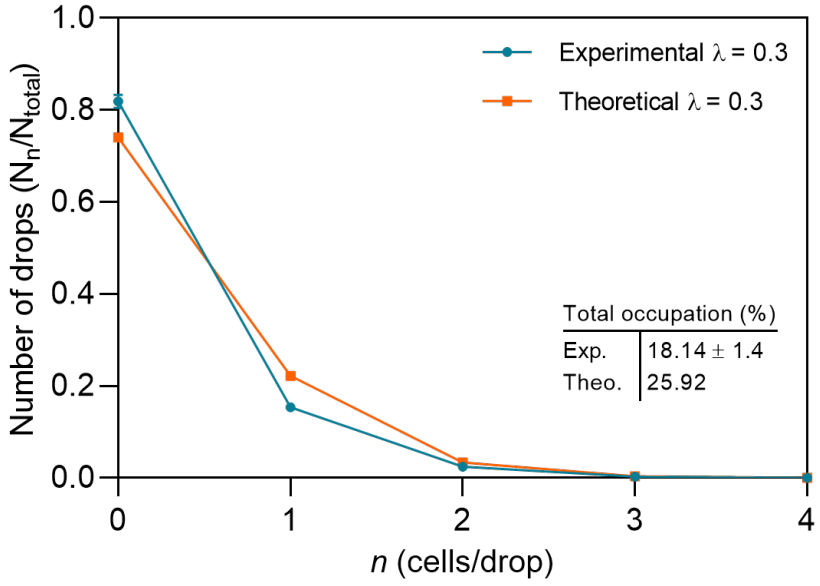

Figure A.5: Poisson distribution of encapsulated cells. Comparison of the experimental cell distribution (blue) with the theoretical Poisson distribution (orange) for $\lambda = 0.3$. Insert: Table presenting the total occupation number regardless of cell number.

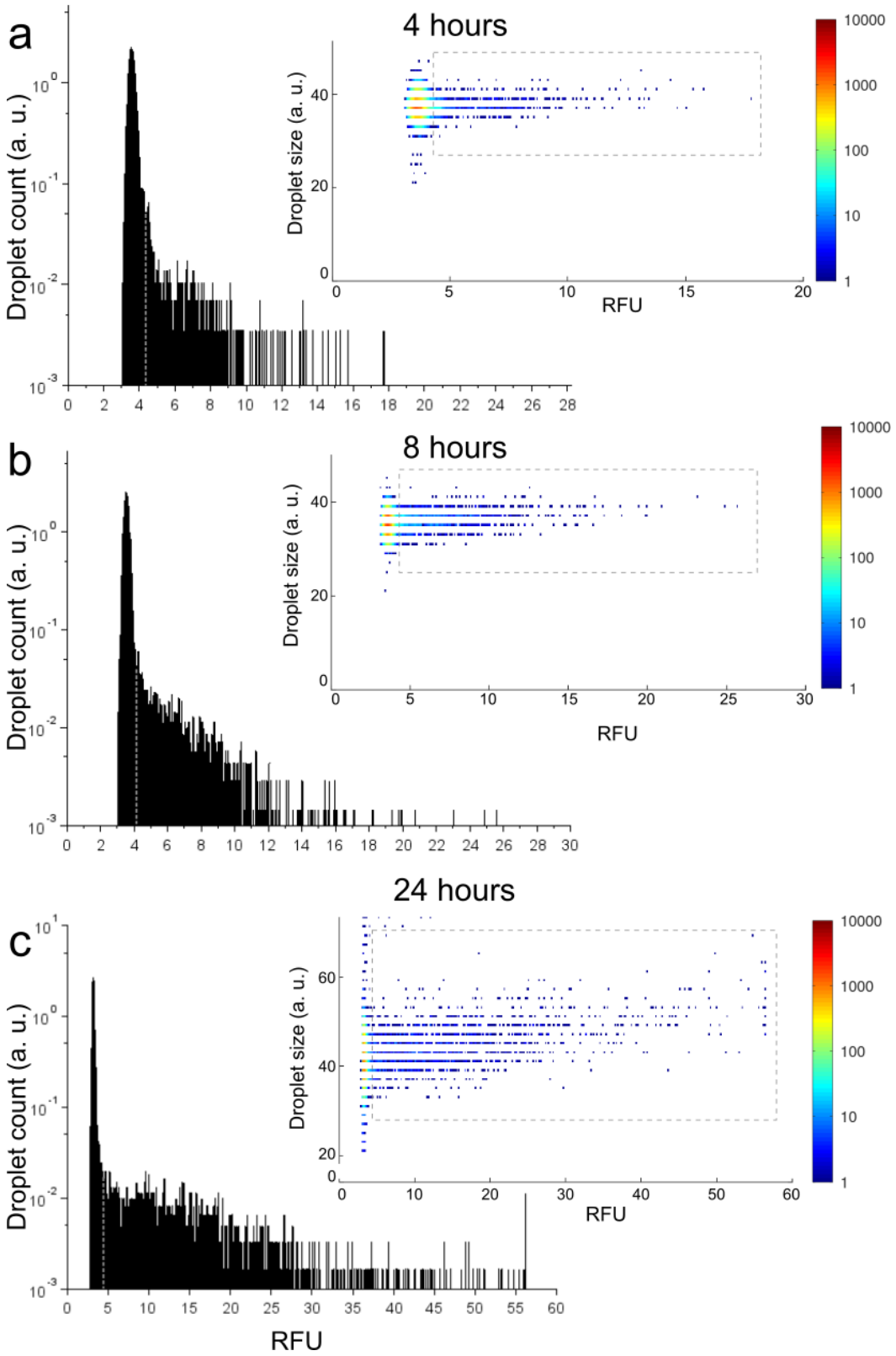

Figure A.6: 2. replicate - Fluorescence of encapsulated *T. b. brucei*. Fluorescence measurements of reinjected *T. b. brucei* encapsulated with protease substrate after four hours (**a**), eight hours (**b**) and 24 hours (**c**) of incubation, presented as droplet numbers at different RFU values. Inserts: Heat maps of droplet size vs. RFU for the respective reinjections.

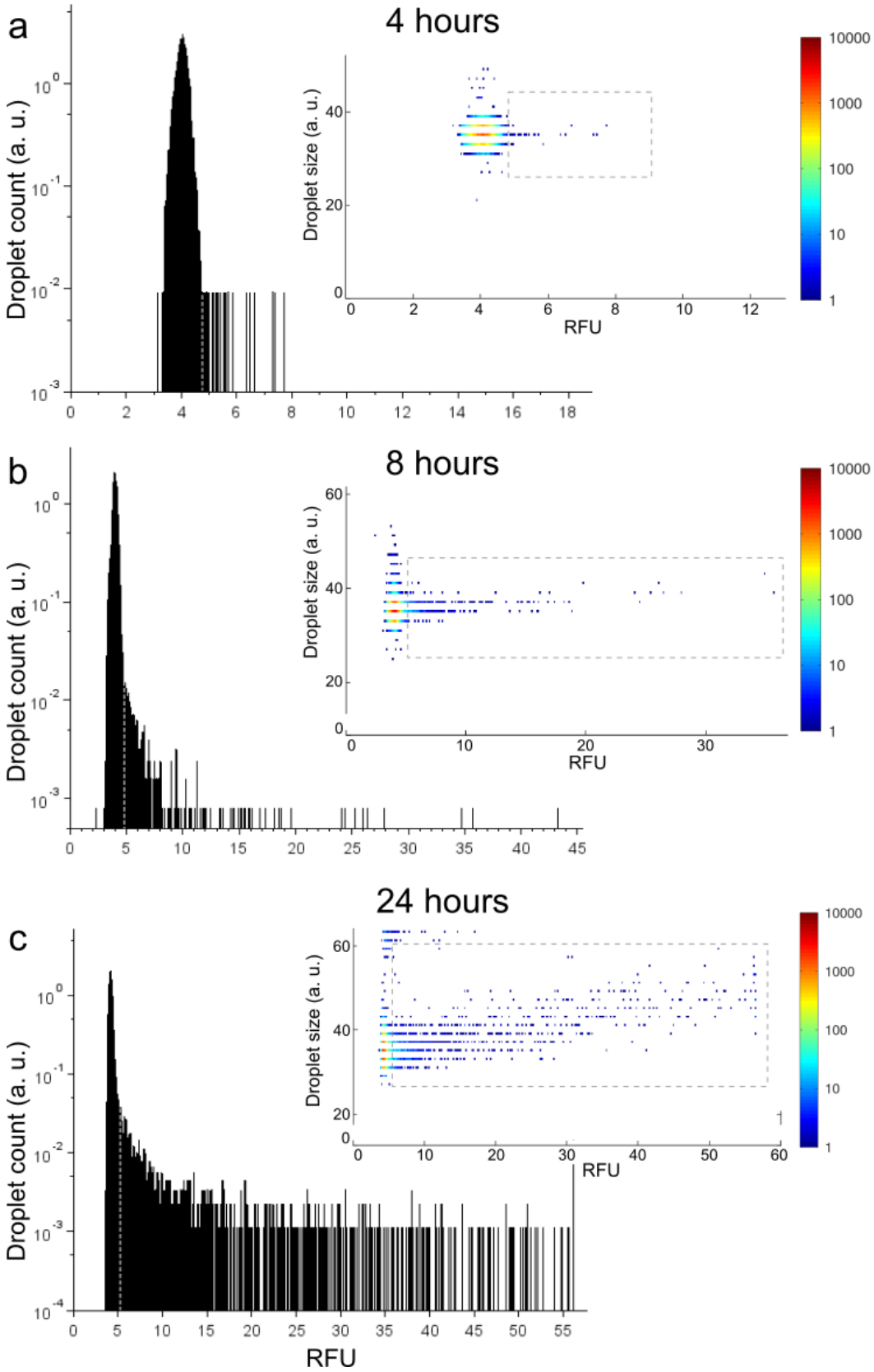

Figure A.7: 3. replicate - Fluorescence of encapsulated *T. b. brucei*. Fluorescence measurements of reinjected *T. b. brucei* encapsulated with protease substrate after four hours (**a**), eight hours (**b**) and 24 hours (**c**) of incubation, presented as droplet numbers at different RFU values. Inserts: Heat maps of droplet size vs. RFU for the respective reinjections.

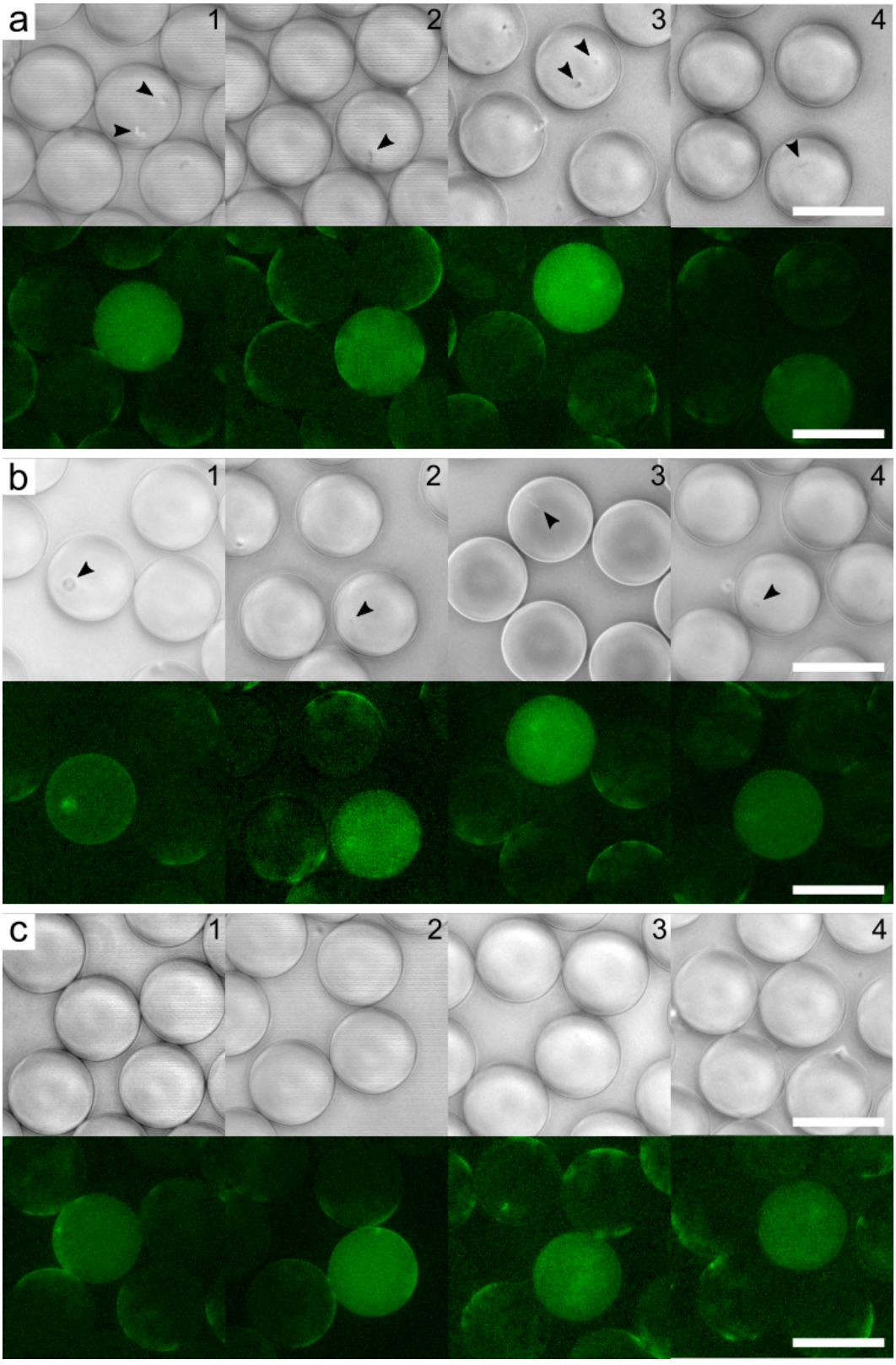

Figure A.8: Fluorescence microscopy of drops. FITC phase fluorescent images and phase contrast of droplets after 20 hours of incubation through a 10× objective. (**a**) Examples of easy detectable fluorescent drops containing cells. (**b**) Fluorescent drops containing fragments which questionable can be from cells. (**c**) Fluorescent drops seemingly being empty. Black arrows indicate the presence of cells or cell fragments. Scale bars are 80 µm.

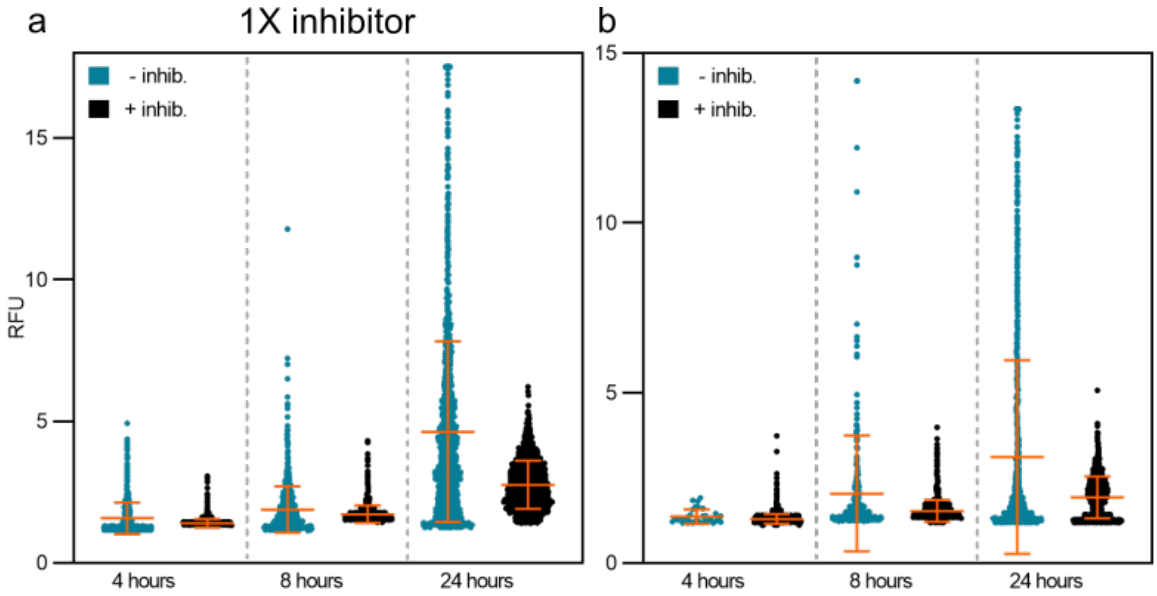

Figure A.9: 1X protease inhibition on single cells in drops. Comparison of detected fluorescence in presence of (black) or without (blue) 1X protease inhibitor over time of 2. replicate (**a**) and 3. replicate (**b**).

Table A.1: Overview of 1X inhibition of encapsulated *T. b. brucei*. Mean RFU values±SD of detected fluorescence in presence of or without 1X protease inhibitors and the respective fractions of active drops and cell occupation for each condition over time of 2. and 3. replicate.

		2. Replica		
	Start	4 hours	8 hours	24 hours
- Inhib. (RFU±SD)	1.00±0.03	1.61±0.57	1.83±0.77	4.69±3.21
Active drops (%)	-	4.47	8.02	13.87
Cell occupation (%)	19.71	15.61	8.60	0.99
+Inhib. (RFU±SD)	1.00±0.03	1.41±0.16	1.74±0.32	2.76±0.85
Active drops (%)	-	8.41	10.44	18.38
Cell occupation (%)	21.07	20.96	18.75	3.40

		3. Replica		
	Start	4 hours	8 hours	24 hours
- Inhib. (RFU±SD)	1.00±0.03	1.39±0.21	1.83±1.00	3.25±3.04
Active drops (%)	-	0.12	1.63	7.80
Cell occupation (%)	17.00	14.44	11.43	0.27
+Inhib. (RFU±SD)	1.00±0.04	1.30±0.14	1.54±0.31	1.94±0.62
Active drops (%)	-	17.04	16.26	14.97
Cell occupation (%)	18.32	16.38	13.78	1.81

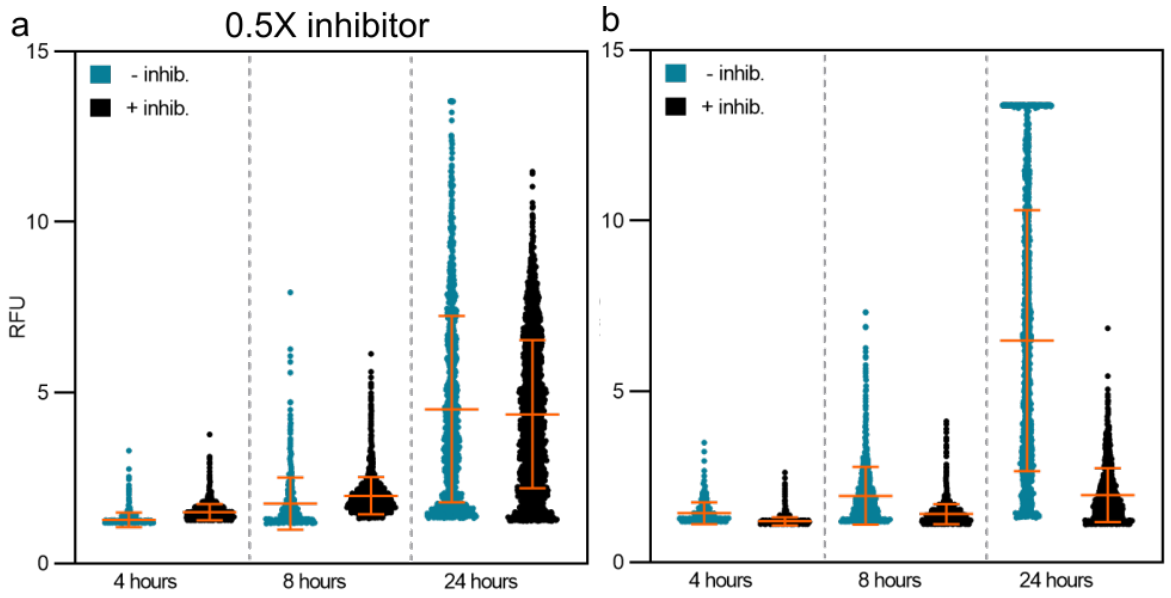

Figure A.10: 0.5X protease inhibition on single cells in drops. Comparison of detected fluorescence in presence of (black) or without (blue) 0.5X protease inhibitor over time of 2. replicate (**a**) and 3. replicate (**b**).

Table A.2: Overview of 0.5X inhibition of encapsulated *T. b. brucei*. Mean RFU values±SD of detected fluorescence in presence of or without 0.5X protease inhibitors and the respective fractions of active drops and cell occupation for each condition over time of 2. and 3. replicate.

	2. Replica			
	Start	4 hours	8 hours	24 hours
- Inhib. (RFU±SD)	1.00±0.04	1.47±0.32	1.95±0.84	6.43±3.84
Active drops (%)	-	2.46	8.32	10.94
Cell occupation (%)	12.38	10.45	8.62	1.14
+Inhib. (RFU±SD)	1.00±0.02	1.21±0.12	1.43±0.29	2.04±0.82
Active drops (%)	-	15.95	18.15	15.71
Cell occupation (%)	20.40	19.92	18.31	2.34

	3. Replica			
	Start	4 hours	8 hours	24 hours
- Inhib. (RFU±SD)	1.00±0.03	1.28±0.21	1.75±0.72	4.92±2.77
Active drops (%)	-	3.15	3.44	9.62
Cell occupation (%)	14.15	9.29	7.48	0.84
+Inhib. (RFU±SD)	1.00±0.03	1.55±0.26	1.99±0.54	4.38±2.20
Active drops (%)	-	13.30	15.59	15.49
Cell occupation (%)	16.24	16.90	11.44	1.79

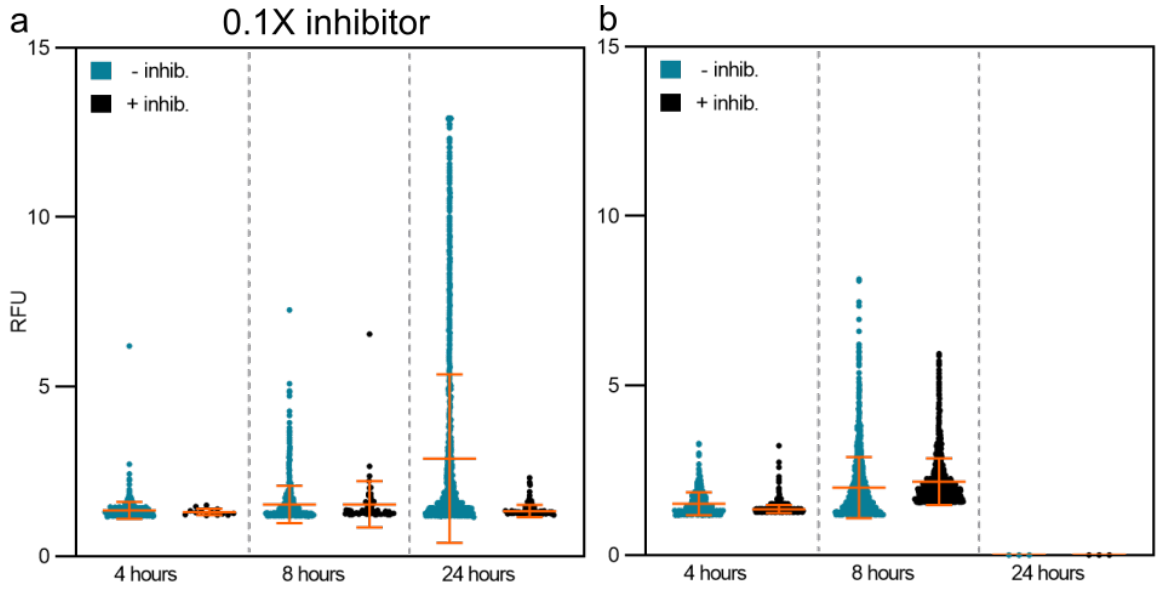

Figure A.11: 0.1X protease inhibition on single cells in drops. Comparison of detected fluorescence in presence of (black) or without (blue) 0.1X protease inhibitor over time of 2. replicate (**a**) and 3. replicate (**b**).

Table A.3: Overview of 0.1X inhibition of encapsulated *T. b. brucei*. Mean RFU values±SD of detected fluorescence in presence of or without 0.1X protease inhibitors and the respective fractions of active drops and cell occupation for each condition over time of 2. and 3. replicate.

		2. Replica		
	Start	4 hours	8 hours	24 hours
- Inhib. (RFU±SD)	1.00±0.03	1.35±0.17	1.54±0.54	2.90±2.50
Active drops (%)	-	3.86	6.28	18.87
Cell occupation (%)	24.15	18.87	13.80	1.36
+Inhib. (RFU±SD)	1.00±0.03	1.30±0.10	1.47±0.31	1.34±0.18
Active drops (%)	-	0.08	0.35	1.50
Cell occupation (%)	24.75	20.73	13.67	0

		3. Replica		
	Start	4 hours	8 hours	24 hours
- Inhib. (RFU±SD)	1.00±0.03	1.52±0.34	2.03±0.91	-
Active drops (%)	-	2.17	9.92	-
Cell occupation (%)	14.61	11.96	9.07	-
+Inhib. (RFU±SD)	1.00±0.03	1.36±0.12	2.18±0.69	-
Active drops (%)	-	11.18	10.54	-
Cell occupation (%)	19.11	13.69	9.93	-

A.2 Single-cell analysis of *T. b. brucei*

A.2.1 Correlation of PAD1 expression and growth arrest

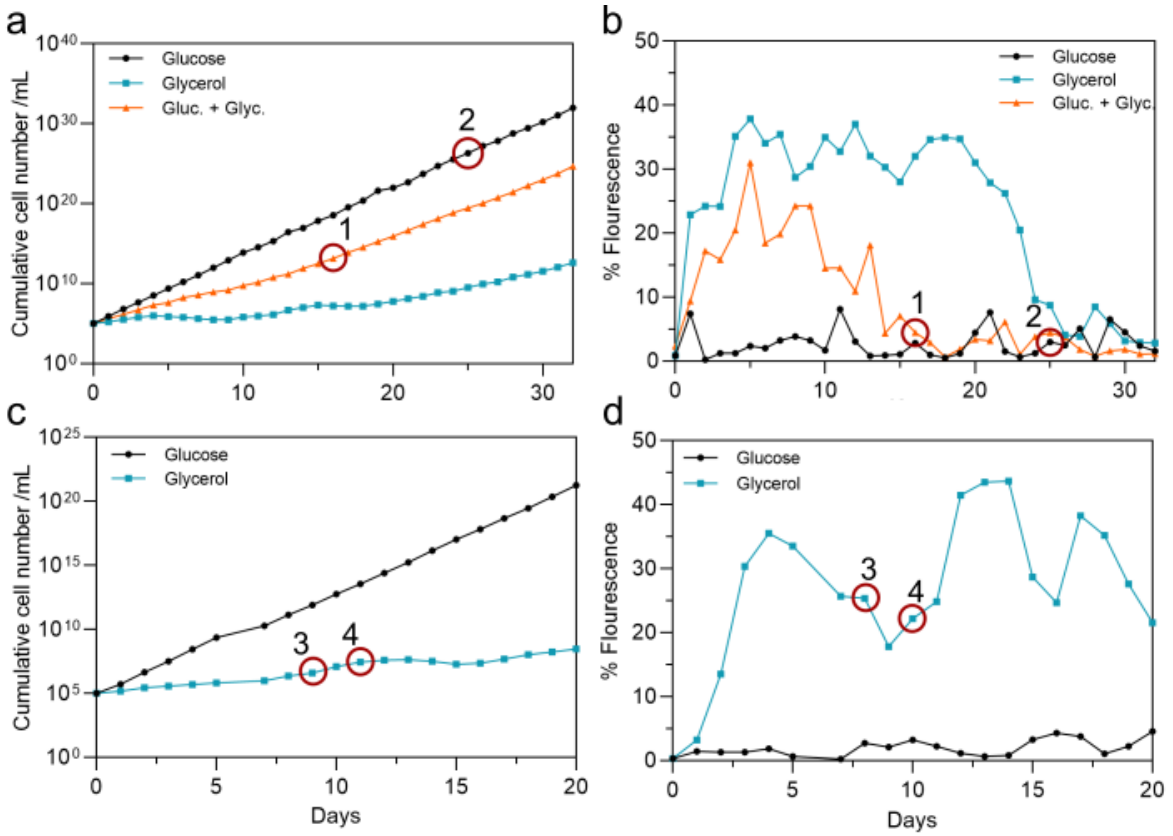

Figure A.12: Growth and PAD1 expression in bulk. (**a**) Growth of AnTat GFP::PAD1$_{utr}$ in glucose, glycerol or Gluc. + glyc. as cumulative cell numbers over time. (**b**) GFP:PAD1 expression in glucose, glycerol or Gluc. + glyc. as percentage of fluorescence over time. (**b**) New cell culture with growth of AnTat GFP::PAD1$_{utr}$ in glucose or glycerol as cumulative cell numbers over time. (**b**) GFP:PAD1 expression in glucose or glycerol as percentage of fluorescence over time. Red circles and numbers are indicating from where the cells were used for single-cell encapsulation.

A.2.2 Red blood cells as an enzymatic substrate

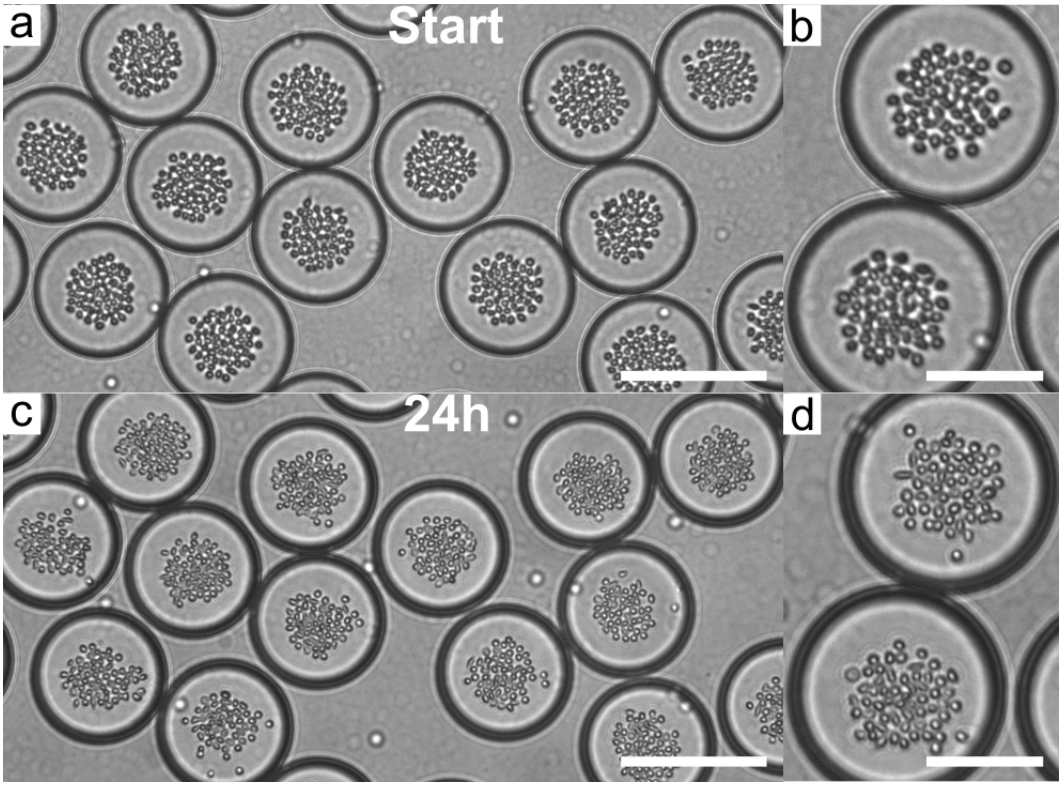

Figure A.13: Effect of protease. RBCs encapsulated with $10\,\mu g\,mL^{-1}$ of trypsin (**a,b**) and incubated for 24 hours (**c,d**) observed through a 20× objective. Scale bars are 80 and 40 µm.

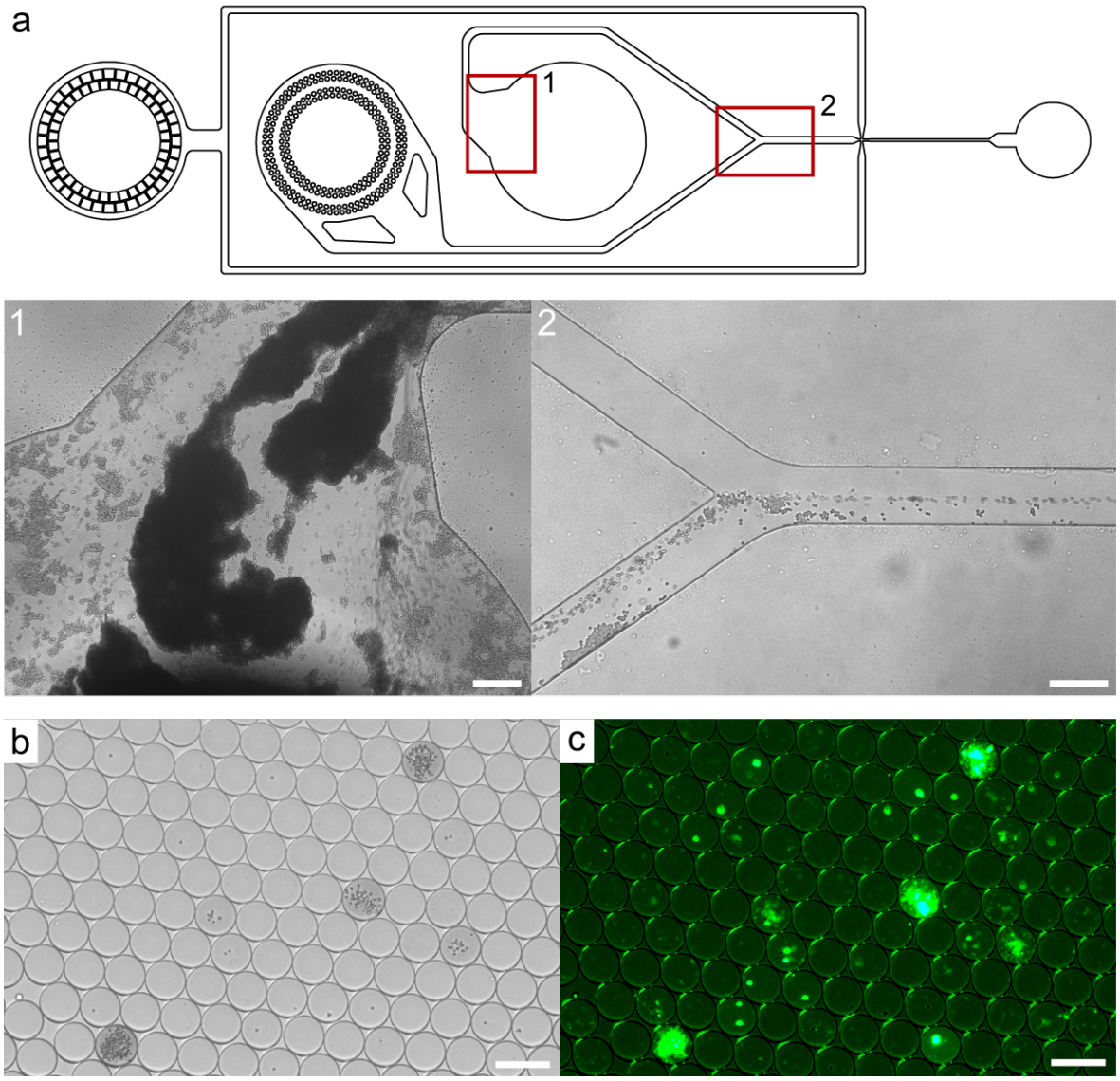

Figure A.14: Encapsulation of fluorescent RBC in co-flow device. (**a**) CAD file of co-flow device with images showing massive RBC clumping at the inlet (1) and minor clumping and the y-junction (2). (**b**) The result of RBC encapsulation in coflow device with few drops of high RBC concentration and many empty. (**c**) Fluorescence imaging showing clumping and high concentrations of the fluorescent proteins on the RBC. Images are taken through a 10× objective with scale bars at 100 µm.

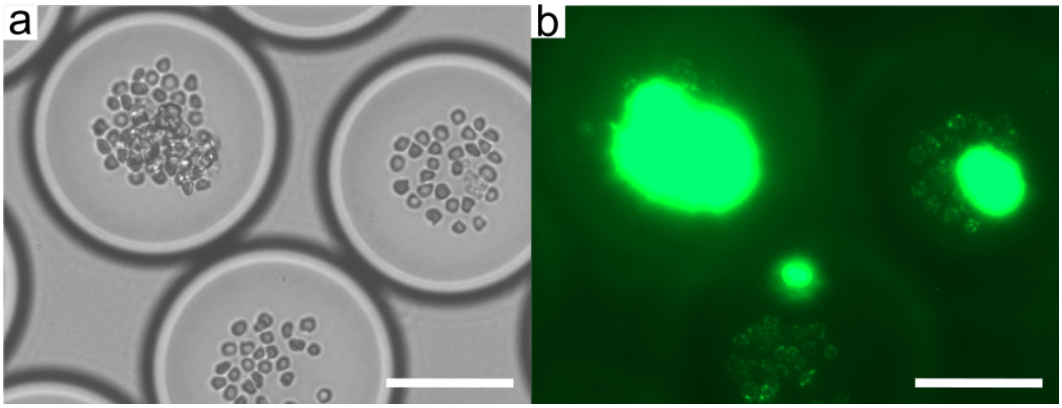

Figure A.15: Clumping of fluorescent lectin. Example of RBC clumps (**a**) from high concentrations of the fluorescent lectin protein through a 40× objective (**a**). Scale bars are 40 µm.

References

[1] Büscher, P., Cecchi, G., Jamonneau, V. & Priotto, G. Human African trypanosomiasis. *Lancet* **390**, 2397–2409 (2017). 21, 35

[2] Giordani, F., Morrison, L. J., Rowan, T. G., DE Koning, H. P. & Barrett, M. P. The animal trypanosomiases and their chemotherapy: a review. *Parasitology* **143**, 1862–1889 (2016). 21, 34, 35

[3] Ulienberg, G. A field guide for THE DIAGNOSIS, TREATMENT AND PREVENTION OF AFRICAN ANIMAL TRYPANOSOMOSIS (1998). URL `http://www.fao.org/3/x0413e/x0413e00.htm`. 21, 34, 35, 36

[4] Rico, E. *et al.* Bloodstream form pre-adaptation to the tsetse fly in Trypanosoma brucei. *Front Cell Infect Microbiol* **3** (2013). URL `https://www.ncbi.nlm.nih.gov/pmc/articles/PMC3827541/`. 21, 29, 38

[5] David Barry, J. & McCulloch, R. Antigenic variation in trypanosomes: Enhanced phenotypic variation in a eukaryotic parasite. In *Advances in Parasitology*, vol. 49, 1–70 (Academic Press, 2001). URL `http://www.sciencedirect.com/science/article/pii/S0065308X01490373`. 21, 29, 38

[6] Blum, M. L. *et al.* A structural motif in the variant surface glycoproteins of Trypanosoma brucei. *Nature* **362**, 603–609 (1993). URL `http://www.nature.com/articles/362603a0`. 21, 38

[7] Whitesides, G. M. The origins and the future of microfluidics. *Nature* **442**, 368–373 (2006). URL `http://www.nature.com/articles/nature05058`. 21, 41, 47

[8] Baret, J.-C., Beck, Y., Billas-Massobrio, I., Moras, D. & Griffiths, A. D. Quantitative cell-based reporter gene assays using droplet-based microfluidics. *Chem. Biol.* **17**, 528–536 (2010). 21, 53

[9] Yin, H. & Marshall, D. Microfluidics for single cell analysis. *Current Opinion in Biotechnology* **23**, 110–119 (2012). URL https://linkinghub.elsevier.com/retrieve/pii/S0958166911007130. 21, 41, 55

[10] Seah, Y. F. S., Hu, H. & Merten, C. A. Microfluidic single-cell technology in immunology and antibody screening. *Mol. Aspects Med.* **59**, 47–61 (2018). 21

[11] Svensson, C.-M. *et al.* Coding of Experimental Conditions in Microfluidic Droplet Assays Using Colored Beads and Machine Learning Supported Image Analysis. *Small* **15**, 1802384 (2019). URL https://onlinelibrary.wiley.com/doi/abs/10.1002/smll.201802384. 21

[12] Kulesa, A., Kehe, J., Hurtado, J. E., Tawde, P. & Blainey, P. C. Combinatorial drug discovery in nanoliter droplets. *PNAS* **115**, 6685–6690 (2018). URL https://www.pnas.org/content/115/26/6685. 21

[13] Stellamanns, E. *et al.* Optical trapping reveals propulsion forces, power generation and motility efficiency of the unicellular parasites Trypanosoma brucei brucei. *Sci Rep* **4** (2014). URL https://www.ncbi.nlm.nih.gov/pmc/articles/PMC4180810/. 22, 41, 44

[14] Hochstetter, A. *et al.* Microfluidics-based single cell analysis reveals drug-dependent motility changes in trypanosomes. *Lab on a Chip* **15**, 1961–1968 (2015). URL http://xlink.rsc.org/?DOI=C5LC00124B. 22, 41, 44, 45

[15] Voyton, C. M. *et al.* A Microfluidic-Based Microscopy Platform for Continuous Interrogation of *Trypanosoma brucei* during Environmental Perturbation. *Biochemistry* **58**, 875–882 (2019). URL https://pubs.acs.org/doi/10.1021/acs.biochem.8b01269. 22

[16] Vigneron, A. *et al.* Single-cell RNA sequencing of Trypanosoma brucei from tsetse salivary glands unveils metacyclogenesis and identifies potential transmission blocking antigens. *Proceedings of the National Academy of Sciences* **117**, 2613–2621 (2020). URL https://www.pnas.org/content/117/5/2613. 22, 46, 56

[17] Tizard, I., Nielsen, K. H., Seed, J. R. & Hall, J. E. Biologically active products from African Trypanosomes. *Microbiol Rev* **42**, 664–681 (1978). URL https://www.ncbi.nlm.nih.gov/pmc/articles/PMC281451/. 24, 99, 137

[18] Opperdoes, F. R. & van Roy, J. The phospholipases of Trypanosoma brucei bloodstream forms and cultured procyclics. *Mol Biochem Parasitol* **5**, 309–319 (1982). 24, 99

[19] Okenu, D. M., Opara, K. N., Nwuba, R. I. & Nwagwu, M. Purification and characterisation of an extracellularly released protease of Trypanosoma brucei. *Parasitol Res* **85**, 424–428 (1999). 24, 99

[20] Nikolskaia, O. V. *et al.* Blood-brain barrier traversal by African trypanosomes requires calcium signaling induced by parasite cysteine protease. *J Clin Invest* **116**, 2739–2747 (2006). URL `https://www.ncbi.nlm.nih.gov/pmc/articles/PMC1570376/`. 24, 99, 137

[21] Geiger, A. *et al.* Exocytosis and protein secretion in Trypanosoma. *BMC Microbiol.* **10**, 20 (2010). 24, 99, 137

[22] Bastos, I. M. D. *et al.* Prolyl oligopeptidase of Trypanosoma brucei hydrolyzes native collagen, peptide hormones and is active in the plasma of infected mice. *Microbes Infect* **12**, 457–466 (2010). 24, 99, 137

[23] Trindade, S. *et al.* Trypanosoma brucei Parasites Occupy and Functionally Adapt to the Adipose Tissue in Mice. *Cell Host Microbe* **19**, 837–848 (2016). 25, 29, 37, 127, 128, 133, 135

[24] MacGregor, P., Savill, N. J., Hall, D. & Matthews, K. R. Transmission Stages Dominate Trypanosome Within-Host Dynamics during Chronic Infections. *Cell Host & Microbe* **9**, 310–318 (2011). URL `https://www.ncbi.nlm.nih.gov/pmc/articles/PMC3094754/`. 25, 133

[25] Schuster, S. *et al.* Unexpected plasticity in the life cycle of Trypanosoma brucei. *eLife* **10**, e66028 (2021). 25, 133

[26] Nelson, G. J. Lipid composition of erythrocytes in various mammalian species. *Biochimica et Biophysica Acta (BBA) - Lipids and Lipid Metabolism* **144**, 221–232 (1967). URL `https://www.sciencedirect.com/science/article/pii/000527606790152X`. 25, 138

[27] Aldrich, K. J., Saunders, D. K., Sievert, L. M. & Sievert, G. Comparison of Erythrocyte Osmotic Fragility among Amphibians, Reptiles, Birds and Mammals. *Transactions of the Kansas Academy of Science (1903-)* **109**, 149–158 (2006). URL `https://www.jstor.org/stable/20476266`. 25, 138

[28] Troiano, J. C., Gould, E. G. & Gould, I. Hemolitic action of Naja naja atra cardiotoxin on erythrocytes from different animals. *Journal of Venomous Animals and Toxins including Tropical Diseases* **12**, 44–58 (2006). URL `http://www.scielo.br/j/jvatitd/a/d745sStz9RR48FvFqh8sDks/?lang=en`. 25, 138

[29] Balázsi, G., van Oudenaarden, A. & Collins, J. J. Cellular decision making and biological noise: from microbes to mammals. *Cell* **144**, 910–925 (2011). 29

[30] Strovas, T. J., Sauter, L. M., Guo, X. & Lidstrom, M. E. Cell-to-Cell Heterogeneity in Growth Rate and Gene Expression in Methylobacterium extorquens AM1. *Journal of Bacteriology* **189**, 7127–7133 (2007). URL `https://journals.asm.org/doi/10.1128/JB.00746-07`. 29, 54

[31] Acar, M., Mettetal, J. T. & van Oudenaarden, A. Stochastic switching as a survival strategy in fluctuating environments. *Nat. Genet.* **40**, 471–475 (2008). 29

[32] Newman, J. R. S. *et al.* Single-cell proteomic analysis of S. cerevisiae reveals the architecture of biological noise. *Nature* **441**, 840–846 (2006). URL `https://www.nature.com/articles/nature04785`. 29, 54

[33] Luzak, V., López-Escobar, L., Siegel, T. N. & Figueiredo, L. M. Cell-to-Cell Heterogeneity in Trypanosomes. *Annual Review of Microbiology* (2021). 29, 39

[34] Joensson, H. N. & Andersson Svahn, H. Droplet Microfluidics—A Tool for Single-Cell Analysis. *Angewandte Chemie International Edition* **51**, 12176–12192 (2012). URL `https://onlinelibrary.wiley.com/doi/abs/10.1002/anie.201200460`. 29, 48, 55

[35] Sánchez Barea, J., Lee, J. & Kang, D.-K. Recent Advances in Droplet-based Microfluidic Technologies for Biochemistry and Molecular Biology. *Micromachines (Basel)* **10** (2019). 29, 48

[36] Shapiro, T. A. & Englund, P. T. The structure and replication of kinetoplast DNA. *Annu Rev Microbiol* **49**, 117–143 (1995). 33, 39

[37] Moreira, D., López-García, P. & Vickerman, K. An updated view of kinetoplastid phylogeny using environmental sequences and a closer outgroup: proposal for a new classification of the class Kinetoplastea. *International Journal of Systematic and Evolutionary Microbiology* **54**, 1861–1875 (2004). 33

[38] Deschamps, P. *et al.* Phylogenomic analysis of kinetoplastids supports that trypanosomatids arose from within bodonids. *Molecular Biology and Evolution* **28**, 53–58 (2011). 33

[39] Simpson, A. G. B., Stevens, J. R. & Lukes, J. The evolution and diversity of kinetoplastid flagellates. *Trends in Parasitology* **22**, 168–174 (2006). 33, 34

[40] Lukeš, J., Skalický, T., Týč, J., Votýpka, J. & Yurchenko, V. Evolution of parasitism in kinetoplastid flagellates. *Molecular and Biochemical Parasitology* **195**, 115–122 (2014). 33

[41] World Health Organization. *WHO interim guidelines for the treatment of gambiense human African trypanosomiasis.* (World Health Organization, 2019). URL `https://www.ncbi.nlm.nih.gov/books/NBK545514/`. 33, 34, 35, 36

[42] Hughes, A. L. & Piontkivska, H. Phylogeny of Trypanosomatidae and Bodonidae (Kinetoplastida) Based on 18S rRNA: Evidence for Paraphyly of Trypanosoma and Six Other Genera. *Molecular Biology and Evolution* **20**, 644–652 (2003). URL `https://doi.org/10.1093/molbev/msg062`. 33

[43] Simarro, P. P. *et al.* The Atlas of human African trypanosomiasis: a contribution to global mapping of neglected tropical diseases. *International Journal of Health Geographics* **9**, 57 (2010). URL `https://doi.org/10.1186/1476-072X-9-57`. 34

[44] Baral, T. N. Immunobiology of African trypanosomes: need of alternative interventions. *J Biomed Biotechnol* **2010**, 389153 (2010). 34

[45] Kennedy, P. G. Clinical features, diagnosis, and treatment of human African trypanosomiasis (sleeping sickness). *The Lancet Neurology* **12**, 186–194 (2013). URL `https://www.thelancet.com/journals/laneur/article/PIIS1474-4422(12)70296-X/abstract`. 34, 37

[46] Büscher, P. *et al.* Sensitivity and specificity of HAT Sero-K-SeT, a rapid diagnostic test for serodiagnosis of sleeping sickness caused by Trypanosoma brucei gambiense: a case-control study. *The Lancet Global Health* **2**, e359–e363 (2014). URL `https://www.thelancet.com/journals/langlo/article/PIIS2214-109X(14)70203-7/abstract`. 35

[47] Lumbala, C. *et al.* Prospective evaluation of a rapid diagnostic test for Trypanosoma brucei gambiense infection developed using recombinant antigens. *PLOS Neglected Tropical Diseases* **12**, e0006386 (2018). URL https://journals.plos.org/plosntds/article?id=10.1371/journal.pntd.0006386. 35

[48] Legros, D. *et al.* Treatment of human African trypanosomiasis—present situation and needs for research and development. *The Lancet Infectious Diseases* **2**, 437–440 (2002). URL https://linkinghub.elsevier.com/retrieve/pii/S1473309902003213. 35

[49] Torreele, E. *et al.* Fexinidazole–a new oral nitroimidazole drug candidate entering clinical development for the treatment of sleeping sickness. *PLoS neglected tropical diseases* **4**, e923 (2010). 35

[50] Mesu, V. K. B. K. *et al.* Oral fexinidazole for late-stage African Trypanosoma brucei gambiense trypanosomiasis: a pivotal multicentre, randomised, non-inferiority trial. *The Lancet* **391**, 144–154 (2018). URL https://www.thelancet.com/journals/lancet/article/PIIS0140-6736(17)32758-7/abstract. 35

[51] Fairlamb, A. H. & Horn, D. Melarsoprol Resistance in African Trypanosomiasis. *Trends in Parasitology* **34**, 481–492 (2018). URL https://www.cell.com/trends/parasitology/abstract/S1471-4922(18)30067-9. 35

[52] Sokolova, A. Y. *et al.* Cross-resistance to nitro drugs and implications for treatment of human African trypanosomiasis. *Antimicrobial Agents and Chemotherapy* **54**, 2893–2900 (2010). 35

[53] Franco, J. R. *et al.* Monitoring the elimination of human African trypanosomiasis at continental and country level: Update to 2018. *PLOS Neglected Tropical Diseases* **14**, e0008261 (2020). URL https://journals.plos.org/plosntds/article?id=10.1371/journal.pntd.0008261. 35, 36

[54] Jones, T. W. & Dávila, A. M. Trypanosoma vivax–out of Africa. *Trends in Parasitology* **17**, 99–101 (2001). 35

[55] Truc, P. *et al.* Atypical human infections by animal trypanosomes. *PLoS neglected tropical diseases* **7**, e2256 (2013). 35

[56] Hager, K. M. *et al.* Endocytosis of a cytotoxic human high density lipoprotein results in disruption of acidic intracellular vesicles and subsequent killing of African trypanosomes. *The Journal of Cell Biology* **126**, 155–167 (1994). 35

[57] Pays, E. *et al.* The trypanolytic factor of human serum. *Nature Reviews. Microbiology* **4**, 477–486 (2006). 35

[58] Lai, D.-H., Hashimi, H., Lun, Z.-R., Ayala, F. J. & Lukeš, J. Adaptations of Trypanosoma brucei to gradual loss of kinetoplast DNA: Trypanosoma equiperdum and Trypanosoma evansi are petite mutants of T. brucei. *Proceedings of the National Academy of Sciences of the United States of America* **105**, 1999–2004 (2008). URL `https://www.ncbi.nlm.nih.gov/pmc/articles/PMC2538871/`. 36

[59] Delespaux, V., Geysen, D., Bossche, P. V. d. & Geerts, S. Molecular tools for the rapid detection of drug resistance in animal trypanosomes. *Trends in Parasitology* **24**, 236–242 (2008). URL `https://www.cell.com/trends/parasitology/abstract/S1471-4922(08)00087-1`. 36

[60] Chitanga, S. *et al.* High Prevalence of Drug Resistance in Animal Trypanosomes without a History of Drug Exposure. *PLOS Neglected Tropical Diseases* **5**, e1454 (2011). URL `https://journals.plos.org/plosntds/article?id=10.1371/journal.pntd.0001454`. 36

[61] Holmes, P. Tsetse-transmitted trypanosomes–their biology, disease impact and control. *Journal of invertebrate pathology* **112 Suppl**, S11–4 (2013). URL `https://doi.org/10.1016/j.jip.2012.07.014`. 37

[62] Kristjanson, P., Swallow, B., Rowlands, G., Kruska, R. & de Leeuw, P. Measuring the costs of African animal trypanosomosis, the potential benefits of control and returns to research. *Agricultural Systems* **59**, 79–98 (1999). URL `https://linkinghub.elsevier.com/retrieve/pii/S0308521X98000869`. 37

[63] Swallow, B. M. Impacts of trypanosomiasis on African agriculture. *PAAT Technical and Scientific Series* **ISSN 1020-7163** (2000). URL `https://www.cabdirect.org/cabdirect/abstract/20003010139`. 37

[64] Langousis, G. & Hill, K. L. Motility and more: the flagellum of Trypanosoma brucei. *Nat. Rev. Microbiol.* **12**, 505–518 (2014). 37, 38, 39

[65] Vickerman, K. Developmental cycles and biology of pathogenic trypanosomes. *British Medical Bulletin* **41**, 105–114 (1985). 37, 38

[66] Gibson, W. & Bailey, M. The development of Trypanosoma brucei within the tsetse fly midgut observed using green fluorescent trypanosomes. *Kinetoplastid Biol Dis* **2**, 1 (2003). URL `https://www.ncbi.nlm.nih.gov/pmc/articles/PMC156611/`. 37

[67] Walshe, D. P., Ooi, C. P., Lehane, M. J. & Haines, L. R. Chapter 3 The Enemy Within: Interactions Between Tsetse, Trypanosomes and Symbionts. In *Advances in Insect Physiology*, vol. 37 of *Advances in Insect Physiology*, 119–175 (Academic Press, 2009). URL `https://www.sciencedirect.com/science/article/pii/S0065280609370034`. 37

[68] Capewell, P. *et al.* The skin is a significant but overlooked anatomical reservoir for vector-borne African trypanosomes. *eLife* **5** (2016). 37, 127

[69] Kennedy, P. G. E. Human African trypanosomiasis of the CNS: current issues and challenges. *J Clin Invest* **113**, 496–504 (2004). 37

[70] Mogk, S. *et al.* African trypanosomes and brain infection - the unsolved question. *Biological Reviews of the Cambridge Philosophical Society* **92**, 1675–1687 (2017). 37

[71] Cross, G. A. M., Kim, H.-S. & Wickstead, B. Capturing the variant surface glycoprotein repertoire (the VSGnome) of Trypanosoma brucei Lister 427. *Molecular and Biochemical Parasitology* **195**, 59–73 (2014). URL `https://www.sciencedirect.com/science/article/pii/S0166685114000772`. 38

[72] Horn, D. Antigenic variation in African trypanosomes. *Molecular and Biochemical Parasitology* **195**, 123–129 (2014). URL `https://www.sciencedirect.com/science/article/pii/S0166685114000590`. 38, 39

[73] Vassella, E., Reuner, B., Yutzy, B. & Boshart, M. Differentiation of African trypanosomes is controlled by a density sensing mechanism which signals cell cycle arrest via the cAMP pathway. *Journal of Cell Science* **110**, 2661–2671 (1997). URL `https://jcs.biologists.org/content/110/21/2661`. 38, 128

[74] Rojas, F. *et al.* Oligopeptide Signaling through TbGPR89 Drives Trypanosome Quorum Sensing. *Cell* **176**, 306–317.e16 (2019). 38

[75] Gibson, W. Kinetoplastea. In Archibald, J. M. *et al.* (eds.) *Handbook of the Protists*, 1–50 (Springer International Publishing, Cham, 2016). URL https://doi.org/10.1007/978-3-319-32669-6_7-1. 39

[76] Engstler, M. *et al.* Hydrodynamic Flow-Mediated Protein Sorting on the Cell Surface of Trypanosomes. *Cell* **131**, 505–515 (2007). URL https://www.cell.com/cell/abstract/S0092-8674(07)01144-0. 39

[77] Grünfelder, C. G. *et al.* Endocytosis of a Glycosylphosphatidylinositol-anchored Protein via Clathrin-coated Vesicles, Sorting by Default in Endosomes, and Exocytosis via RAB11-positive Carriers. *Mol Biol Cell* **14**, 2029–2040 (2003). URL https://www.ncbi.nlm.nih.gov/pmc/articles/PMC165095/. 39, 40

[78] Engstler, M. *et al.* Kinetics of endocytosis and recycling of the GPI-anchored variant surface glycoprotein in Trypanosoma brucei. *J Cell Sci* **117**, 1105–1115 (2004). 39

[79] Field, M. C. & Carrington, M. The trypanosome flagellar pocket. *Nat Rev Microbiol* **7**, 775–786 (2009). URL https://www.nature.com/articles/nrmicro2221. 39

[80] Lacomble, S. *et al.* Three-dimensional cellular architecture of the flagellar pocket and associated cytoskeleton in trypanosomes revealed by electron microscope tomography. *Journal of Cell Science* **122**, 1081–1090 (2009). URL https://doi.org/10.1242/jcs.045740. 39

[81] Michels, P. A. M., Bringaud, F., Herman, M. & Hannaert, V. Metabolic functions of glycosomes in trypanosomatids. *Biochim Biophys Acta* **1763**, 1463–1477 (2006). 40

[82] Hemphill, A., Lawson, D. & Seebeck, T. The Cytoskeletal Architecture of Trypanosoma brucei. *The Journal of Parasitology* **77**, 603–612 (1991). URL https://www.jstor.org/stable/3283167. 40

[83] Vassella, E. *et al.* Major Surface Glycoproteins of Insect Forms of Trypanosoma brucei Are Not Essential for Cyclical Transmission by Tsetse. *PLOS ONE* **4**, e4493 (2009). URL https://journals.plos.org/plosone/article?id=10.1371/journal.pone.0004493. 40

[84] Brun, R. & Schönenberger, M. Cultivation and in vitro cloning or procyclic culture forms of Trypanosoma brucei in a semi-defined medium. Short communication. *Acta Trop.* **36**, 289–292 (1979). 40

[85] Hirumi, H. & Hirumi, K. Continuous cultivation of Trypanosoma brucei blood stream forms in a medium containing a low concentration of serum protein without feeder cell layers. *J. Parasitol.* **75**, 985–989 (1989). 40, 122

[86] Black, S. J. *et al.* Regulation of parasitaemia in mice infected with Trypanosoma brucei. *Curr. Top. Microbiol. Immunol.* **117**, 93–118 (1985). 40

[87] Van Den Abbeele, J., Claes, Y., van Bockstaele, D., Le Ray, D. & Coosemans, M. Trypanosoma brucei spp. development in the tsetse fly: characterization of the post-mesocyclic stages in the foregut and proboscis. *Parasitology* **118 (Pt 5)**, 469–478 (1999). 40

[88] Meissner, M., Agop-Nersesian, C. & Sullivan, W. J. Molecular tools for analysis of gene function in parasitic microorganisms. *Appl Microbiol Biotechnol* **75**, 963–975 (2007). 40

[89] Vasquez, J.-J., Wedel, C., Cosentino, R. O. & Siegel, T. N. Exploiting CRISPR–Cas9 technology to investigate individual histone modifications. *Nucleic Acids Research* **46**, e106 (2018). URL `https://doi.org/10.1093/nar/gky517`. 40

[90] Rico, E., Jeacock, L., Kovářová, J. & Horn, D. Inducible high-efficiency CRISPR-Cas9-targeted gene editing and precision base editing in African trypanosomes. *Sci Rep* **8**, 7960 (2018). URL `https://www.nature.com/articles/s41598-018-26303-w`. 40

[91] Vassella, E., Straesser, K. & Boshart, M. A mitochondrion-specific dye for multicolour fluorescent imaging of Trypanosoma brucei. *Mol Biochem Parasitol* **90**, 381–385 (1997). 40

[92] Woods, A. *et al.* Definition of individual components within the cytoskeleton of Trypanosoma brucei by a library of monoclonal antibodies. *J Cell Sci* **93 (Pt 3)**, 491–500 (1989). 40

[93] Dean, S. *et al.* A toolkit enabling efficient, scalable and reproducible gene tagging in trypanosomatids. *Open Biol* **5**, 140197 (2015). 40

[94] Krüger, T., Maus, K., Kreß, V., Meyer-Natus, E. & Engstler, M. Single-cell motile behaviour of *Trypanosoma brucei* in thin-layered fluid collectives. *Eur. Phys. J. E* **44**, 37 (2021). URL https://doi.org/10.1140/epje/s10189-021-00052-7. 40

[95] Valadares, H. M. S. *et al.* Unequivocal identification of subpopulations in putative multiclonal Trypanosoma cruzi strains by FACs single cell sorting and genotyping. *PLoS Negl Trop Dis* **6**, e1722 (2012). 41

[96] Müller, L. S. M. *et al.* Genome organization and DNA accessibility control antigenic variation in trypanosomes. *Nature* **563**, 121–125 (2018). 41

[97] Baret, J.-C. *et al.* Fluorescence-activated droplet sorting (FADS): efficient microfluidic cell sorting based on enzymatic activity. *Lab Chip* **9**, 1850–1858 (2009). URL https://pubs.rsc.org/en/content/articlelanding/2009/lc/b902504a. 41, 53, 55, 56

[98] Lalanne-Aulet, D. *et al.* Multiscale study of bacterial growth: Experiments and model to understand the impact of gas exchange on global growth. *Phys. Rev. E* **92**, 052706 (2015). URL https://link.aps.org/doi/10.1103/PhysRevE.92.052706. 41

[99] Woronoff, G. *et al.* Metabolic cost of rapid adaptation of single yeast cells. *PNAS* **117**, 10660–10666 (2020). URL https://www.pnas.org/content/117/20/10660. 41, 55

[100] Chronis, N., Zimmer, M. & Bargmann, C. I. Microfluidics for in vivo imaging of neuronal and behavioral activity in Caenorhabditis elegans. *Nature Methods* **4**, 727–731 (2007). 41

[101] Clausell-Tormos, J. *et al.* Droplet-Based Microfluidic Platforms for the Encapsulation and Screening of Mammalian Cells and Multicellular Organisms. *Chemistry & Biology* **15**, 427–437 (2008). URL http://www.sciencedirect.com/science/article/pii/S1074552108001506. 41, 55

[102] Park, T.-E. *et al.* Hypoxia-enhanced Blood-Brain Barrier Chip recapitulates human barrier function and shuttling of drugs and antibodies. *Nature Communications* **10**, 2621 (2019). 41

[103] Brouzes, E. *et al.* Droplet microfluidic technology for single-cell high-throughput screening. *Proc. Natl. Acad. Sci. U.S.A.* **106**, 14195–14200 (2009). 41, 53, 55

[104] Heddergott, N. *et al.* Trypanosome Motion Represents an Adaptation to the Crowded Environment of the Vertebrate Bloodstream. *PLoS Pathogens* **8**, e1003023 (2012). URL http://dx.plos.org/10.1371/journal.ppat.1003023. 41, 42

[105] Bargul, J. L. *et al.* Species-Specific Adaptations of Trypanosome Morphology and Motility to the Mammalian Host. *PLOS Pathogens* **12**, e1005448 (2016). URL https://journals.plos.org/plospathogens/article?id=10.1371/journal.ppat.1005448. 41, 42

[106] Uppaluri, S. *et al.* Flow Loading Induces Oscillatory Trajectories in a Bloodstream Parasite. *Biophysical Journal* **103**, 1162–1169 (2012). URL http://www.sciencedirect.com/science/article/pii/S0006349512009095. 42

[107] Sun, S. Y. *et al.* Flagellum couples cell shape to motility in Trypanosoma brucei. *Proc Natl Acad Sci U S A* **115**, E5916–E5925 (2018). URL https://www.ncbi.nlm.nih.gov/pmc/articles/PMC6042131/. 42, 43

[108] Thomaz, A. A. d. *et al.* Optical tweezers for studying taxis in parasites. *J. Opt.* **13**, 044015 (2011). 44

[109] Ashkin, A. & Dziedzic, J. M. Optical trapping and manipulation of viruses and bacteria. *Science* **235**, 1517–1520 (1987). URL https://science.sciencemag.org/content/235/4795/1517. 44

[110] Voyton, C. M. *et al.* A microfluidic-based microscopy platform for continuous interrogation of Trypanosoma brucei during environmental perturbation. *Biochemistry* (2019). URL https://doi.org/10.1021/acs.biochem.8b01269. 44, 46

[111] Zilionis, R. *et al.* Single-cell barcoding and sequencing using droplet microfluidics. *Nature Protocols* **12**, 44–73 (2017). 46, 47

[112] Zheng, G. X. Y. *et al.* Massively parallel digital transcriptional profiling of single cells. *Nature Communications* **8**, 14049 (2017). URL https://www.nature.com/articles/ncomms14049. 46, 56

[113] Hutchinson, S. *et al.* The establishment of variant surface glycoprotein monoallelic expression revealed by single-cell RNA-seq of Trypanosoma brucei in the tsetse fly salivary glands. *bioRxiv* 2021.03.01.433049 (2021). URL https://www.biorxiv.org/content/10.1101/2021.03.01.433049v1. 46

[114] Briggs, E. M., McCulloch, R., Matthews, K. R. & Otto, T. D. Single cell transcriptomic analysis of bloodstream form Trypanosoma brucei reconstructs cell cycle progression and differentiation via quorum sensing. *bioRxiv* 2020.12.11.420976 (2020). URL `https://www.biorxiv.org/content/10.1101/2020.12.11.420976v1`. 47

[115] Thorsen, T., Roberts, R. W., Arnold, F. H. & Quake, S. R. Dynamic pattern formation in a vesicle-generating microfluidic device. *Physical Review Letters* **86**, 4163–4166 (2001). 47, 48, 50

[116] Christopher, G. F. & Anna, S. L. Microfluidic methods for generating continuous droplet streams. *Journal of Physics D: Applied Physics* **40**, R319–R336 (2007). URL `https://doi.org/10.1088/0022-3727/40/19/r01`. 47, 48, 50, 51

[117] Shang, L., Cheng, Y. & Zhao, Y. Emerging Droplet Microfluidics. *Chemical Reviews* **117**, 7964–8040 (2017). 47, 48, 51

[118] Theberge, A. B. *et al.* Microdroplets in microfluidics: an evolving platform for discoveries in chemistry and biology. *Angewandte Chemie (International Ed. in English)* **49**, 5846–5868 (2010). 48

[119] Baroud, C. N., Gallaire, F. & Dangla, R. Dynamics of microfluidic droplets. *Lab Chip* **10**, 2032–2045 (2010). URL `https://pubs.rsc.org/en/content/articlelanding/2010/lc/c001191f`. 48, 49

[120] Zhu, P. & Wang, L. Passive and active droplet generation with microfluidics: a review. *Lab on a Chip* **17**, 34–75 (2016). URL `https://pubs.rsc.org/en/content/articlelanding/2017/lc/c6lc01018k`. 48, 49, 50, 51

[121] Anna, S. L. & Mayer, H. C. Microscale tipstreaming in a microfluidic flow focusing device. *Physics of Fluids* **18**, 121512 (2006). URL `https://aip.scitation.org/doi/10.1063/1.2397023`. 49

[122] Atencia, J. & Beebe, D. J. Controlled microfluidic interfaces. *Nature* **437**, 648–655 (2005). 49

[123] Baret, J.-C., Kleinschmidt, F., El Harrak, A. & Griffiths, A. D. Kinetic aspects of emulsion stabilization by surfactants: a microfluidic analysis. *Langmuir: the ACS journal of surfaces and colloids* **25**, 6088–6093 (2009). 49

[124] Umbanhowar, P. B., Prasad, V. & Weitz, D. A. Monodisperse Emulsion Generation via Drop Break Off in a Coflowing Stream. *Langmuir* **16**, 347–351 (2000). URL https://doi.org/10.1021/la990101e. 51

[125] Cramer, C., Fischer, P. & Windhab, E. J. Drop formation in a co-flowing ambient fluid. *Chemical Engineering Science* **59**, 3045–3058 (2004). URL https://www.sciencedirect.com/science/article/pii/S0009250904002088. 51

[126] Anna, S. L., Bontoux, N. & Stone, H. A. Formation of dispersions using "flow focusing" in microchannels. *Applied Physics Letters* **82**, 364–366 (2003). URL https://aip.scitation.org/doi/10.1063/1.1537519. 51

[127] Sesen, M., Alan, T. & Neild, A. Droplet control technologies for microfluidic high throughput screening (μHTS). *Lab on a Chip* **17**, 2372–2394 (2017). URL https://pubs.rsc.org/en/content/articlelanding/2017/lc/c7lc00005g. 51

[128] Bremond, N., Thiam, A. R. & Bibette, J. Decompressing Emulsion Droplets Favors Coalescence. *Physical Review Letters* **100**, 024501 (2008). URL https://link.aps.org/doi/10.1103/PhysRevLett.100.024501. 51, 52

[129] Niu, X., Gulati, S., Edel, J. B. & deMello, A. J. Pillar-induced droplet merging in microfluidic circuits. *Lab on a Chip* **8**, 1837–1841 (2008). URL https://pubs.rsc.org/en/content/articlelanding/2008/lc/b813325e. 51

[130] Ahn, K., Agresti, J., Chong, H., Marquez, M. & Weitz, D. A. Electrocoalescence of drops synchronized by size-dependent flow in microfluidic channels. *Applied Physics Letters* **88**, 264105 (2006). 51

[131] Mazutis, L. *et al.* Multi-step microfluidic droplet processing: kinetic analysis of an in vitro translated enzyme. *Lab on a Chip* **9**, 2902–2908 (2009). URL https://pubs.rsc.org/en/content/articlelanding/2009/lc/b907753g. 51, 52

[132] Gu, H., Murade, C. U., Duits, M. H. G. & Mugele, F. A microfluidic platform for on-demand formation and merging of microdroplets using electric control. *Biomicrofluidics* **5**, 011101 (2011). URL https://www.ncbi.nlm.nih.gov/pmc/articles/PMC3082336/. 51

[133] Baroud, C. N., Vincent, M. R. d. S. & Delville, J.-P. An optical toolbox for total control of droplet microfluidics. *Lab on a Chip* **7**, 1029–1033 (2007). URL https://pubs.rsc.org/en/content/articlelanding/2007/lc/b702472j. 51

[134] Sun, J. *et al.* On-chip thermo-triggered coalescence of controllable Pickering emulsion droplet pairs. *RSC Advances* **6**, 64182–64192 (2016). URL https://pubs.rsc.org/en/content/articlelanding/2016/ra/c6ra12594h. 51

[135] Abate, A. R., Hung, T., Mary, P., Agresti, J. J. & Weitz, D. A. High-throughput injection with microfluidics using picoinjectors. *Proc Natl Acad Sci U S A* **107**, 19163–19166 (2010). URL https://www.ncbi.nlm.nih.gov/pmc/articles/PMC2984161/. 51, 52

[136] Tan, Y.-C., Fisher, J. S., Lee, A. I., Cristini, V. & Lee, A. P. Design of microfluidic channel geometries for the control of droplet volume, chemical concentration, and sorting. *Lab on a Chip* **4**, 292–298 (2004). 52

[137] Link, D. R., Anna, S. L., Weitz, D. A. & Stone, H. A. Geometrically mediated breakup of drops in microfluidic devices. *Physical Review Letters* **92**, 054503 (2004). 52, 53

[138] Adamson, D. N., Mustafi, D., Zhang, J. X. J., Zheng, B. & Ismagilov, R. F. Production of arrays of chemically distinct nanolitre plugs via repeated splitting in microfluidic devices. *Lab on a Chip* **6**, 1178–1186 (2006). URL https://pubs.rsc.org/en/content/articlelanding/2006/lc/b604993a. 52

[139] Jung, J. H., Destgeer, G., Ha, B., Park, J. & Sung, H. J. On-demand droplet splitting using surface acoustic waves. *Lab on a Chip* **16**, 3235–3243 (2016). URL https://pubs.rsc.org/en/content/articlelanding/2016/lc/c6lc00648e. 52

[140] Choi, J.-H., Lee, S.-K., Lim, J.-M., Yang, S.-M. & Yi, G.-R. Designed pneumatic valve actuators for controlled droplet breakup and generation. *Lab on a Chip* **10**, 456–461 (2010). 52

[141] Tan, Y.-C. & Lee, A. P. Microfluidic separation of satellite droplets as the basis of a monodispersed micron and submicron emulsification system. *Lab on a Chip* **5**, 1178–1183 (2005). URL https://pubs.rsc.org/en/content/articlelanding/2005/lc/b504497a. 52

[142] Mazutis, L. & Griffiths, A. D. Preparation of monodisperse emulsions by hydrodynamic size fractionation. *Applied Physics Letters* **95**, 204103 (2009). URL https://aip.scitation.org/doi/10.1063/1.3250432. 52

[143] Ahn, K. *et al.* Dielectrophoretic manipulation of drops for high-speed microfluidic sorting devices. *Applied Physics Letters* **88**, 024104 (2006). URL https://aip.scitation.org/doi/full/10.1063/1.2164911. 52

[144] Mazutis, L. *et al.* Single-cell analysis and sorting using droplet-based microfluidics. *Nat Protoc* **8**, 870–891 (2013). URL http://www.nature.com/articles/nprot.2013.046. 53, 56, 100

[145] Zang, E. *et al.* Real-time image processing for label-free enrichment of Actinobacteria cultivated in picolitre droplets. *Lab Chip* **13**, 3707–3713 (2013). URL https://pubs.rsc.org/en/content/articlelanding/2013/lc/c3lc50572c. 53

[146] Liu, X. *et al.* High-throughput screening of antibiotic-resistant bacteria in picodroplets. *Lab Chip* **16**, 1636–1643 (2016). URL https://pubs.rsc.org/en/content/articlelanding/2016/lc/c6lc00180g. 53

[147] Huebner, A. *et al.* Quantitative detection of protein expression in single cells using droplet microfluidics. *Chem. Commun. (Camb.)* 1218–1220 (2007). 53, 54, 56

[148] Frenz, L., Blank, K., Brouzes, E. & Griffiths, A. D. Reliable microfluidic on-chip incubation of droplets in delay-lines. *Lab on a Chip* **9**, 1344–1348 (2009). URL https://pubs.rsc.org/en/content/articlelanding/2009/lc/b816049j. 53, 54

[149] Agresti, J. J. *et al.* Ultrahigh-throughput screening in drop-based microfluidics for directed evolution. *PNAS* **107**, 4004–4009 (2010). URL https://www.pnas.org/content/107/9/4004. 53, 56

[150] Miller, O. J. *et al.* High-resolution dose–response screening using droplet-based microfluidics. *Proc Natl Acad Sci U S A* **109**, 378–383 (2012). URL https://www.ncbi.nlm.nih.gov/pmc/articles/PMC3258639/. 53

[151] Konry, T., Dominguez-Villar, M., Baecher-Allan, C., Hafler, D. A. & Yarmush, M. L. Droplet-based microfluidic platforms for single T cell secretion analysis of IL-10 cytokine. *Biosens Bioelectron* **26**, 2707–2710 (2011). 53, 56, 100

[152] Beneyton, T. *et al.* Out-of-equilibrium microcompartments for the bottom-up integration of metabolic functions. *Nature Communications* **9**, 2391 (2018). URL https://www.nature.com/articles/s41467-018-04825-1. 53

[153] Mahler, L. *et al.* Enhanced and homogeneous oxygen availability during incubation of microfluidic droplets. *RSC Adv.* **5**, 101871–101878 (2015). URL https://pubs.rsc.org/en/content/articlelanding/2015/ra/c5ra20118g. 53, 54

[154] Eyer, K. *et al.* Single-cell deep phenotyping of IgG-secreting cells for high-resolution immune monitoring. *Nature Biotechnology* **35**, 977–982 (2017). URL http://www.nature.com/doifinder/10.1038/nbt.3964. 54, 68, 100

[155] Walling, M. A. & Shepard, J. R. E. Cellular heterogeneity and live cell arrays. *Chem Soc Rev* **40**, 4049–4076 (2011). 54

[156] Spencer, S. L., Gaudet, S., Albeck, J. G., Burke, J. M. & Sorger, P. K. Non-genetic origins of cell-to-cell variability in TRAIL-induced apoptosis. *Nature* **459**, 428–432 (2009). URL https://www.nature.com/articles/nature08012. 54

[157] Balaban, N. Q., Merrin, J., Chait, R., Kowalik, L. & Leibler, S. Bacterial persistence as a phenotypic switch. *Science* **305**, 1622–1625 (2004). 54

[158] Collins, D. J., Neild, A., deMello, A., Liu, A.-Q. & Ai, Y. The Poisson distribution and beyond: methods for microfluidic droplet production and single cell encapsulation. *Lab on a Chip* **15**, 3439–3459 (2015). URL https://pubs.rsc.org/en/content/articlelanding/2015/lc/c5lc00614g. 55

[159] Köster, S. *et al.* Drop-based microfluidic devices for encapsulation of single cells. *Lab Chip* **8**, 1110–1115 (2008). 55, 100

[160] Edd, J. F. *et al.* Controlled encapsulation of single-cells into monodisperse picolitre drops. *Lab on a Chip* **8**, 1262–1264 (2008). 55

[161] Kemna, E. W. M. *et al.* High-yield cell ordering and deterministic cell-in-droplet encapsulation using Dean flow in a curved microchannel. *Lab on a Chip* **12**, 2881–2887 (2012). URL https://pubs.rsc.org/en/content/articlelanding/2012/lc/c2lc00013j. 55

[162] Cao, Z. *et al.* Droplet sorting based on the number of encapsulated particles using a solenoid valve. *Lab Chip* **13**, 171–178 (2012). URL https://pubs.rsc.org/en/content/articlelanding/2013/lc/c2lc40950j. 55

[163] Pan, J. *et al.* Quantitative tracking of the growth of individual algal cells in microdroplet compartments. *Integrative Biology* **3**, 1043–1051 (2011). URL https://doi.org/10.1039/c1ib00033k. 55, 56

[164] Holtze, C. *et al.* Biocompatible surfactants for water-in-fluorocarbon emulsions. *Lab on a Chip* **8**, 1632–1639 (2008). 56

[165] Shembekar, N., Hu, H., Eustace, D. & Merten, C. A. Single-Cell Droplet Microfluidic Screening for Antibodies Specifically Binding to Target Cells. *Cell Rep* **22**, 2206–2215 (2018). 56, 100

[166] Qiu, L. *et al.* A membrane-anchored aptamer sensor for probing IFNγ secretion by single cells. *Chem. Commun.* **53**, 8066–8069 (2017). URL `https://pubs.rsc.org/en/content/articlelanding/2017/cc/c7cc03576d`. 56, 100

[167] Ng, E. X., Miller, M. A., Jing, T. & Chen, C.-H. Single cell multiplexed assay for proteolytic activity using droplet microfluidics. *Biosensors and Bioelectronics* **81**, 408–414 (2016). URL `https://www.sciencedirect.com/science/article/pii/S0956566316301932`. 56, 100

[168] Sjostrom, S. L. *et al.* High-throughput screening for industrial enzyme production hosts by droplet microfluidics. *Lab on a Chip* **14**, 806–813 (2014). 56, 100

[169] Macosko, E. Z. *et al.* Highly Parallel Genome-wide Expression Profiling of Individual Cells Using Nanoliter Droplets. *Cell* **161**, 1202–1214 (2015). URL `http://www.sciencedirect.com/science/article/pii/S0092867415005498`. 56

[170] Boedicker, J. Q., Vincent, M. E. & Ismagilov, R. F. Microfluidic confinement of single cells of bacteria in small volumes initiates high-density behavior of quorum sensing and growth and reveals its variability. *Angewandte Chemie (International Ed. in English)* **48**, 5908–5911 (2009). 56, 57

[171] Del Ben, F. *et al.* A Method for Detecting Circulating Tumor Cells Based on the Measurement of Single-Cell Metabolism in Droplet-Based Microfluidics. *Angew Chem Int Ed Engl* **55**, 8581–8584 (2016). 56, 57

[172] Duffy, D. C., McDonald, J. C., Schueller, O. J. A. & Whitesides, G. M. Rapid Prototyping of Microfluidic Systems in Poly(dimethylsiloxane). *Anal. Chem.* **70**, 4974–4984 (1998). URL `https://doi.org/10.1021/ac980656z`. 64

[173] Xia, Y. & Whitesides, G. M. Soft Lithography. *Angewandte Chemie International Edition* **37**, 550–575 (1998). 64

[174] Whitesides, G. M., Ostuni, E., Takayama, S., Jiang, X. & Ingber, D. E. Soft lithography in biology and biochemistry. *Annual Review of Biomedical Engineering* **3**, 335–373 (2001). 64

[175] McDonald, J. C. *et al.* Fabrication of microfluidic systems in poly(dimethylsiloxane). *Electrophoresis* **21**, 27–40 (2000). 64

[176] Sollier, E., Murray, C., Maoddi, P. & Carlo, D. D. Rapid prototyping polymers for microfluidic devices and high pressure injections. *Lab on a Chip* **11**, 3752–3765 (2011). URL `https://pubs.rsc.org/en/content/articlelanding/2011/lc/c1lc20514e`. 64

[177] Baret, J.-C. Surfactants in droplet-based microfluidics. *Lab Chip* **12**, 422–433 (2012). 69

[178] Lowe, K. C., Davey, M. R. & Power, J. B. Perfluorochemicals: their applications and benefits to cell culture. *Trends Biotechnol.* **16**, 272–277 (1998). 70

[179] Lee, J. N., Park, C. & Whitesides, G. M. Solvent compatibility of poly(dimethylsiloxane)-based microfluidic devices. *Analytical Chemistry* **75**, 6544–6554 (2003). 70

[180] Hedges, L. V. Estimation of effect size from a series of independent experiments. *PSYCHOL.BULL.* **92**, 490–499 (1982). URL `https://www.scholars.northwestern.edu/en/publications/estimation-of-effect-size-from-a-series-of-independent-experiment`. 97

[181] Lonsdale-Eccles, J. D. & Grab, D. J. Trypanosome hydrolases and the blood-brain barrier. *Trends Parasitol* **18**, 17–19 (2002). 99

[182] Alsford, S., Currier, R. B., Guerra-Assunção, J. A., Clark, T. G. & Horn, D. Cathepsin-L Can Resist Lysis by Human Serum in Trypanosoma brucei brucei. *PLoS Pathog* **10**, e1004130 (2014). URL `https://www.ncbi.nlm.nih.gov/pmc/articles/PMC4022737/`. 99

[183] Arolas, J. L., Vendrell, J., Aviles, F. X. & Fricker, L. D. Metallocarboxypeptidases: emerging drug targets in biomedicine. *Curr Pharm Des* **13**, 349–366 (2007). 99

[184] Wimmers, F. *et al.* Single-cell analysis reveals that stochasticity and paracrine signaling control interferon-alpha production by plasmacytoid dendritic cells. *Nat Commun* **9**, 3317 (2018). 100

[185] Huang, M. *et al.* Microfluidic screening and whole-genome sequencing identifies mutations associated with improved protein secretion by yeast. *Proc Natl Acad Sci U S A* **112**, E4689–4696 (2015). 100

[186] Woronoff, G. *et al.* New generation of amino coumarin methyl sulfonate-based fluorogenic substrates for amidase assays in droplet-based microfluidic applications. *Analytical Chemistry* **83**, 2852–2857 (2011). 104

[187] Gruner, P. *et al.* Controlling molecular transport in minimal emulsions. *Nature Communications* **7** (2016). URL `http://www.nature.com/articles/ncomms10392`. 104

[188] Proto, W. R. *et al.* Trypanosoma brucei metacaspase 4 is a pseudopeptidase and a virulence factor. *J Biol Chem* **286**, 39914–39925 (2011). 107, 122, 123

[189] Patel, H., Tscheka, C. & Heerklotz, H. Characterizing vesicle leakage by fluorescence lifetime measurements. *Soft Matter* **5**, 2849–2851 (2009). URL `https://pubs.rsc.org/en/content/articlelanding/2009/sm/b908524f`. 121

[190] Robinson, T., Kuhn, P., Eyer, K. & Dittrich, P. S. Microfluidic trapping of giant unilamellar vesicles to study transport through a membrane pore. *Biomicrofluidics* **7**, 044105 (2013). URL `https://www.ncbi.nlm.nih.gov/pmc/articles/PMC3739824/`. 121

[191] Yandrapalli, N., Petit, J., Bäumchen, O. & Robinson, T. Surfactant-free production of biomimetic giant unilamellar vesicles using PDMS-based microfluidics. *Communications Chemistry* **4** (2021). URL `https://www.nature.com/articles/s42004-021-00530-1`. 121

[192] Schneider, C. A., Rasband, W. S. & Eliceiri, K. W. NIH Image to ImageJ: 25 years of image analysis. *Nature Methods* **9** (2012). URL `https://www.nature.com/articles/nmeth.2089`. 124, 136

[193] Smith, T. K., Bringaud, F., Nolan, D. P. & Figueiredo, L. M. Metabolic reprogramming during the Trypanosoma brucei life cycle. *F1000Research* **6**, F1000 Faculty Rev–683 (2017). URL `https://www.ncbi.nlm.nih.gov/pmc/articles/PMC5461901/`. 127

[194] Pineda, E. *et al.* Glycerol supports growth of the Trypanosoma brucei bloodstream forms in the absence of glucose: Analysis of metabolic adaptations on glycerol-rich conditions. *PLoS Pathog.* **14**, e1007412 (2018). 127

[195] Kovářová, J. *et al.* Gluconeogenesis using glycerol as a substrate in bloodstream-form Trypanosoma brucei. *PLoS pathogens* **14**, e1007475 (2018). 127

[196] Maggs, D. G. *et al.* Interstitial fluid concentrations of glycerol, glucose, and amino acids in human quadricep muscle and adipose tissue. Evidence for significant lipolysis in skeletal muscle. *The Journal of Clinical Investigation* **96**, 370–377 (1995). URL `https://www.jci.org/articles/view/118043`. 127

[197] Rotondo, F. *et al.* Glycerol is synthesized and secreted by adipocytes to dispose of excess glucose, via glycerogenesis and increased acyl-glycerol turnover. *Scientific Reports* **7**, 8983 (2017). URL `https://www.nature.com/articles/s41598-017-09450-4`. 127

[198] Dean, S., Marchetti, R., Kirk, K. & Matthews, K. R. A surface transporter family conveys the trypanosome differentiation signal. *Nature* **459**, 213–217 (2009). URL `https://www.nature.com/articles/nature07997`. 128

[199] MacGregor, P. & Matthews, K. R. Identification of the regulatory elements controlling the transmission stage-specific gene expression of PAD1 in Trypanosoma brucei. *Nucleic Acids Research* **40**, 7705–7717 (2012). 128

[200] Zimmermann, H. *et al.* A quorum sensing-independent path to stumpy development in Trypanosoma brucei. *PLoS Pathog* **13**, e1006324 (2017). 128

[201] MacGregor, P., Szöoõr, B., Savill, N. J. & Matthews, K. R. Trypanosomal immune evasion, chronicity and transmission: an elegant balancing act. *Nat Rev Microbiol* **10** (2012). URL `https://www.ncbi.nlm.nih.gov/pmc/articles/PMC3834543/`. 131, 133

[202] Creek, D. J. *et al.* Metabolomics Guides Rational Development of a Simplified Cell Culture Medium for Drug Screening against Trypanosoma brucei. *Antimicrobial Agents and Chemotherapy* **57**, 2768–2779 (2013). URL `https://journals.asm.org/doi/10.1128/AAC.00044-13`. 135

[203] Murray, M. & Dexter, T. M. Anaemia in bovine African trypanosomiasis. A review. *Acta Trop* **45**, 389–432 (1988). 137

[204] Nok, A. J., Esievo, K. A., Ibrahim, S., Ukoha, A. I. & Ikediobi, C. O. Phospholipase A2 from Trypanosoma congolense: characterization and haematological properties. *Cell Biochemistry and Function* **11**, 125–130 (1993). 137, 138

[205] Oyewale, J. *et al.* Alterations in the osmotic fragility of camel and donkey erythrocytes caused by temperature, pH and blood storage. *Veterinarski arhiv* **81**, 459–470 (2011). URL `https://hrcak.srce.hr/index.php?show=clanak&id_clanak_jezik=105582`. 138

[206] Singh, S., Ponnappan, N., Verma, A. & Mittal, A. Osmotic tolerance of avian erythrocytes to complete hemolysis in solute free water. *Scientific Reports* **9**, 7976 (2019). URL `https://www.nature.com/articles/s41598-019-44487-7`. 138

[207] Gunther, G. R., Wang, J. L., Yahara, I., Cunningham, B. A. & Edelman, G. M. Concanavalin A Derivatives with Altered Biological Activities. *Proceedings of the National Academy of Sciences of the United States of America* **70**, 1012–1016 (1973). URL `https://www.ncbi.nlm.nih.gov/pmc/articles/PMC433414/`. 138

[208] Hoffman, J. F. Biconcave shape of human red-blood-cell ghosts relies on density differences between the rim and dimple of the ghost's plasma membrane. *Proceedings of the National Academy of Sciences* **113**, 14847–14851 (2016). URL `https://www.pnas.org/content/113/51/14847`. 140